



TECHNICAL UNIVERSITY OF CRETE
SCHOOL OF ENVIRONMENTAL ENGINEERING

**IMPACT OF CLIMATE CHANGE ON THE HYDROLOGY AND
GEOCHEMISTRY OF CRETE AND ESTIMATION OF UNCERTAINTY**

Sofia D. Nerantzaki

This research is co-financed by Greece and the European Union (European Social Fund- ESF) through the Operational Programme «Human Resources Development, Education and Lifelong Learning» in the context of the project “Strengthening Human Resources Research Potential via Doctorate Research” (MIS-5000432), implemented by the State Scholarships Foundation (IKY)



Operational Programme
Human Resources Development,
Education and Lifelong Learning
Co-financed by Greece and the European Union



Chania, February 2020



ΠΟΛΥΤΕΧΝΕΙΟ ΚΡΗΤΗΣ
ΣΧΟΛΗ ΜΗΧΑΝΙΚΩΝ ΠΕΡΙΒΑΛΛΟΝΤΟΣ

**ΕΠΙΠΤΩΣΕΙΣ ΤΗΣ ΚΛΙΜΑΤΙΚΗΣ ΑΛΛΑΓΗΣ ΣΤΗΝ ΥΔΡΟΛΟΓΙΑ ΚΑΙ
ΓΕΩΧΗΜΕΙΑ ΤΗΣ ΚΡΗΤΗΣ ΚΑΙ ΑΞΙΟΛΟΓΗΣΗ ΤΗΣ ΑΒΕΒΑΙΟΤΗΤΑΣ
ΤΩΝ ΠΡΟΒΛΕΨΕΩΝ**

Σοφία Δ. Νεραντζάκη

Το έργο συγχρηματοδοτείται από την Ελλάδα και την Ευρωπαϊκή Ένωση (Ευρωπαϊκό Κοινωνικό Ταμείο) μέσω του Επιχειρησιακού Προγράμματος «Ανάπτυξη Ανθρώπινου Δυναμικού, Εκπαίδευση και Διά Βίου Μάθηση», στο πλαίσιο της Πράξης «Ενίσχυση του ανθρώπινου ερευνητικού δυναμικού μέσω της υλοποίησης διδακτορικής έρευνας» (MIS-5000432), που υλοποιεί το Ίδρυμα Κρατικών Υποτροφιών (ΙΚΥ)



Ευρωπαϊκή Ένωση
Ευρωπαϊκό Κοινωνικό Ταμείο

Επιχειρησιακό Πρόγραμμα
Ανάπτυξη Ανθρώπινου Δυναμικού,
Εκπαίδευση και Διά Βίου Μάθηση

Με τη συγχρηματοδότηση της Ελλάδας και της Ευρωπαϊκής Ένωσης



ανάπτυξη - εργασία - αλληλεγγύη

Χανιά, Φεβρουάριος 2020

Impact of climate change on the hydrology and geochemistry of Crete and estimation of uncertainty

Sofia D. Nerantzaki

Thesis Committee

Thesis supervisor

Nikolaos P. Nikolaidis

Advisory Committee

Nikolaos P. Nikolaidis

George P. Karatzas

Dionissios T. Hristopoulos

Evaluation Committee

Nikolaos P. Nikolaidis

George P. Karatzas

Dionissios T. Hristopoulos

Simon Michael Papalexiou

Andreas Panagopoulos

Ioannis A. Sibetheros

Ierotheos Zacharias

ACKNOWLEDGEMENTS

Upon completion of my Ph.D. thesis, I would like to thank all the people who contributed to its realization.

First and foremost, I would like to express my sincere gratitude to my supervisor Professor Nikolaos P. Nikolaidis, for the continuous support on my study and research, for his patience, motivation, enthusiasm, and immense knowledge. He entrusted me by giving me the opportunity to deal with a subject of great interest, since the beginning of my Postgraduate studies. The thesis would not have been possible without his ideas and inspiration and I would like to thank him for his intellectual, scientific, moral and financial support. I am honored to be a member of this laboratory and a PhD student under his supervision.

I would also like to express my sincere gratitude to Professor Dionissios T. Hristopulos, member of my Advisory Committee, for the hours he spent answering queries, providing knowledge and expertise, as well as assisting me in the making of our journal publication. I would like to thank him for the valuable scientific advice and sincere interest in the course of this thesis.

In addition, I would like to thank the member of the Advisory Committee, Professor Georgios P. Karatzas, for patiently attending my preliminary presentation, and benevolently providing thoughtful and insightful comments regarding the structure and content of the Thesis.

Very special thanks to Assistant Professor Simon Michael Papalexiou, member of the Evaluation Committee, for his continuous and priceless support, guidance and cooperation since my Undergraduate studies. I feel very honored and lucky that he chooses to collaborate with me.

I would also like to thank the members of the Advisory Committee, Professor Ioannis Sibetheros, Professor Ierotheos Zacharias and Research Director Andreas Panagopoulos, for their immediate consent and enthusiasm to be members of the Evaluation Committee, as well as their willingness to take time out of their busy schedules and attend my Ph.D. defense, providing helpful suggestions.

Furthermore, I would like to thank Dr. Manolis Grillakis for his contribution to the bias correction of the climate dataset used in this article. I would also like to thank the members of the Herslab: Maria Lilli for giving me helpful advice and guidance for the completion of the Thesis, as well as Dionissis Efstathiou for the help he provided me with computer software and hardware along with his insightful suggestions. Special thanks to MSc Christos Goumas who achieved a last minute recovery of my data.

My sincere thanks to my colleagues and friends Drs. Irene Vozinaki and Elina Yiantzi who were always there listening to my problems, advising me and suggesting improvements to my dissertation.

Last but not least, I would like to thank my family, for their patience and support through all these years.

SPECIAL ACKNOWLEDGEMENTS

This research is co-financed by Greece and the European Union (European Social Fund-ESF) through the Operational Program «Human Resources Development, Education and Lifelong Learning» in the context of the project “Strengthening Human Resources Research Potential via Doctorate Research” (MIS-5000432), implemented by the State Scholarships Foundation (IKY).



Abstract

The Mediterranean region has been identified as a “climate change hot-spot”. The specific region is projected to undergo the most significant drying among 26 regions across the world, by the end of the 21st century. Karstic springs are the exclusive source of water during dry months for most Mediterranean regions. The impact of climate change on the hydrology and water quality of karstic springs has not received proper attention in the scientific literature. In addition, uncertainty assessment of the hydrologic projections for karstic watersheds has not been studied and may reveal possible water deficits that cannot otherwise be taken into account.

This study aims to (1) estimate the impact of climate change on the flow and water quality predictions of Mediterranean karstic watersheds (2) quantify the uncertainty of these predictions and (3) evaluate the response of different Mediterranean karstic springs to the present-day and forecasted meteorological droughts. The methodology developed for this threefold aim is organized in three sections.

The first section entitled “Estimation of the uncertainty of hydrologic predictions in a karstic Mediterranean watershed”, addresses the issues of the estimation of the impact of climate change on the hydrologic projections of a karstic Mediterranean watershed (i.e. the Koiliaris River Basin) and the assessment of the uncertainty which accompanies these projections. Specifically, the study focuses on the uncertainties stemming from model parameter uncertainty, internal variability of rainfall input and climate change scenario. To this end, the Soil Water Assessment Tool (SWAT) along with a karstic model (Karst-SWAT) is used to assess the composite spring and surface flow. The parameter uncertainty of both the surface and karstic flow models are estimated by combining the SUFI2 interface and the @RISK by PALISADE software. Input to the hydrologic models is provided by eleven combinations of five Regional Climate Models (RCMs) and three Representative Concentration Pathways (RCPs) of the EURO-CORDEX ensemble. Representative rainfall time series for certain of these scenarios are stochastically modeled with the LARS weather generator. Monte Carlo simulations are used to investigate the effect of input internal variability on the flow output. The uncertainty of karstic flow due to the parameter uncertainty of the SWAT and Karst-SWAT models is estimated at 10.0% (expressed as the Coefficient of Variation), which is comparable to the estimated uncertainty due to climate change scenarios (10.1%) until 2059. The combined uncertainty for the total flow at the basin exit due to both models’ parameter uncertainty is 6.6%, comparable to the uncertainty due to the internal variability (5.6%). The total uncertainty of karstic flow, combining model parameter uncertainty and the internal variability of the climate scenarios is 11.0%. The total uncertainty estimate is used in conjunction with the lowest karstic flow projection to assess the most adverse scenario for the future mean karstic flow.

The second section, with the title: “Evaluation of the uncertainty of the impact of climate change on flow, sediment and nitrate predictions at the Koiliaris Critical Zone Observatory”, uses a similar methodology as the previous section, this time focusing on the climate change impact and the uncertainty assessment on the water quality projections of the karstic Mediterranean watershed of Koiliaris. Specifically, the study focuses on the nitrate nitrogen mass and suspended sediment mass transferred by the karstic and surface flow. Results suggest that, after 2059, climate change scenario uncertainty for projections of nitrate nitrogen mass is equivalent to the one of flow projections (25.5%, expressed as the Coefficient of Variation) but it is higher for the case of sediment mass (41.6%). The uncertainty due to internal variability of the sediment mass is also higher (18.5%) than the one of the nitrate nitrogen mass (6.9%), due to the complexity of the erosion process. The combined uncertainty due to hydrologic model parameters and internal variability for the nitrate nitrogen mass is 40.1%, which is greater than the uncertainty due to climate change model. Even when considering all these uncertainties, it is forecasted that the Koiliaris River will not have nitrate nitrogen concentrations higher than the limits suggested by the Water Framework Directive.

The third section, or “The response of three Mediterranean karstic springs to drought and the impact of climate change”, translates the meteorological drought of the present-day and future periods, into hydrological drought for three Mediterranean karstic springs with different properties. Specifically, the springs under study are the Stilos spring (Koiliaris River Basin), the Meskla spring and the Agia spring (Keritis River Basin). The springs discharge the broad karstic system of the White Mountains Range, located at the north of Chania, Crete. The Karst-SWAT model is used to quantify the hydrologic response of the karstic springs, which are characterized by different systems and water detention times. The above mentioned set of climate change scenarios is used to assess the climate change impact on the springs and surface flow for the period 2019-2098. A non-parametric drought index is modified to estimate the future frequency, duration and intensity of meteorological and hydrological droughts in comparison to the reference period. The progress of the lowest and the highest flows in the future is analyzed. Drought frequency, duration and intensity of karstic flows are expected to increase for all scenarios and karstic springs. As the water detention time of the spring increases, the duration and intensity of the droughts are likely to increase significantly. Depending on the spring, after 2059, the mean annual karstic flow decreases from 14.2% to 25.1%, the mean number of drought events ranges from a decrease of 8.1% to an increase of 77.5%, the duration of drought events increases from 36.8% to 533% and the mean monthly water deficit (intensity of drought) increases from 27.3% to 83.6%. Both low and high flows will increase, with the former occurring even during wet months.

The methodology proposed here combines the advantages of climate change impact analysis with those of a fully integrated hydrologic model. The integration of surface and subsurface flow in the same model provides more realistic simulations of water cycle and

improved representation of the dominant hydrologic process of groundwater recharge interaction, which is important for impact assessment on groundwater resources. This is the first time, to our knowledge, that a combined assessment of surface and karstic flow model parameter uncertainty and internal variability is applied to a karstic Mediterranean watershed. Analysis shows that the parameter uncertainty of the hydrologic model and the internal variability of the climate change scenarios should be considered in planning water resources adaptation and mitigation measures that aim to alleviate climate change impacts in watersheds of semi-arid or arid climates, especially for the 2019-2058 period. After 2059, the climate change scenario is the most important uncertainty factor. Even under this large uncertainty, the drought status is anticipated to deteriorate after 2059, regardless of the scenario realized for all springs. The results of this study can be used as a guide for competent authorities to adapt their management practices for the prevention of the negative repercussions of karstic spring droughts. A 40-year period is offered for adaptation measures to be prepared and planned for the improved management of the springs' water resources. The study provides a benchmark for comparative studies in other similar regions of the globe, where water needs during the summer are exclusively covered by the flow originating from karstic springs.

Εκτεταμένη Περίληψη

Εισαγωγή

Η περιοχή της Μεσογείου είναι μία από τις πιο επιρρεπείς περιοχές στις επιπτώσεις της κλιματικής αλλαγής, βάσει των αποτελεσμάτων των σεναρίων για την παγκόσμια κλιματική αλλαγή (IPCC, 2013). Η Ελλάδα είναι μία από τις χώρες της Μεσογείου για την οποία οι ξηρές περίοδοι θα είναι όλο και συχνότερες κατά τη διάρκεια του 21ου αιώνα. Δεκάδες ελληνικά νησιά του Αιγαίου έχουν πληγεί από την ξηρασία με την Κρήτη να είναι η πιο ευάλωτη περιοχή, έχοντας απόσταση μόλις 500 χλμ. από την έρημο Σαχάρα και 1500 χλμ. από τη Γη της Επαγγελίας, η οποία έχει ερημοποιηθεί. Το νησί της Κρήτης χαρακτηρίζεται από άνιση χωρική και χρονική κατανομή βροχόπτωσης, η οποία σε συνδυασμό με την εντατική γεωργική δραστηριότητα και τον ανεπτυγμένο τουρισμό το έχουν καταστήσει ως μια από τις πιο επιρρεπείς σε ξηρασία περιοχές της Ελλάδας. Οι μόνιμες παροχές νερού στο νησί προέρχονται κυρίως από τις καρστικές πηγές, που παρέχουν χαμηλές παροχές σε όλη τη διάρκεια του χρόνου. Τα κλιματικά σενάρια, που προβλέπουν αύξηση της θερμοκρασίας και επερχόμενη μείωση της παροχής, είναι ικανά να δώσουν σημαντικές πληροφορίες, ιδιαίτερα για αυτές τις χαμηλές παροχές και για τη διατήρηση των ποσοτήτων νερού στην περιοχή για τα επόμενα έτη. Ταυτόχρονα, η ενδεχόμενη μείωση της ποσότητας των επιφανειακών απορροών, αναμένεται να προκαλέσει αύξηση της συγκέντρωσης των ρύπων στα υδάτινα σώματα. Είναι επιτακτική λοιπόν η ανάγκη καλής προσομοίωσης του σύνθετου συστήματος των καρστικών πηγών ώστε να είναι γνωστές ανά πάσα στιγμή οι μεταβολές στην παροχή και την ποιότητα των υδάτων τους για την περίοδο που διανύουμε αλλά και για το μέλλον, με στόχο τη λήψη μέτρων σωστής διαχείρισης. Η αβεβαιότητα όμως που υφίσταται τόσο στις χρονοσειρές των κλιματικών σεναρίων όσο και στις μεταβλητές των υδρολογικών μοντέλων που χρησιμοποιούνται για προσομοίωση μπορούν να επηρεάσουν σημαντικά τα αποτελέσματα σε βαθμό που να μην είναι αξιόπιστα.

Στόχος

Στόχος της διατριβής αυτής είναι η εκτίμηση των προβλέψεων των κλιματικών σεναρίων και της αβεβαιότητάς τους στην υδρολογία και τη γεωχημεία στην Κρήτη. Συγκεκριμένα, στο πλαίσιο αυτής της διατριβής (1) εκτιμώνται οι επιπτώσεις της κλιματικής αλλαγής στις προβλέψεις της παροχής και της ποιότητας των υδάτων σε χαρακτηριστική καρστική πηγή της Μεσογείου, (2) ποσοτικοποιείται η αβεβαιότητα αυτών των προβλέψεων και (3) αξιολογείται η απόκριση διαφόρων καρστικών πηγών της Μεσογείου στην μετεωρολογική ξηρασία που προβλέπουν τα κλιματικά σενάρια. Η μεθοδολογία που αναπτύχθηκε για αυτόν τον τριπλό στόχο οργανώνεται σε τρία τμήματα που περιγράφονται παρακάτω.

Ποσοτικοποίηση Αβεβαιότητας Υδρολογικών Προβλέψεων

Μεθοδολογία

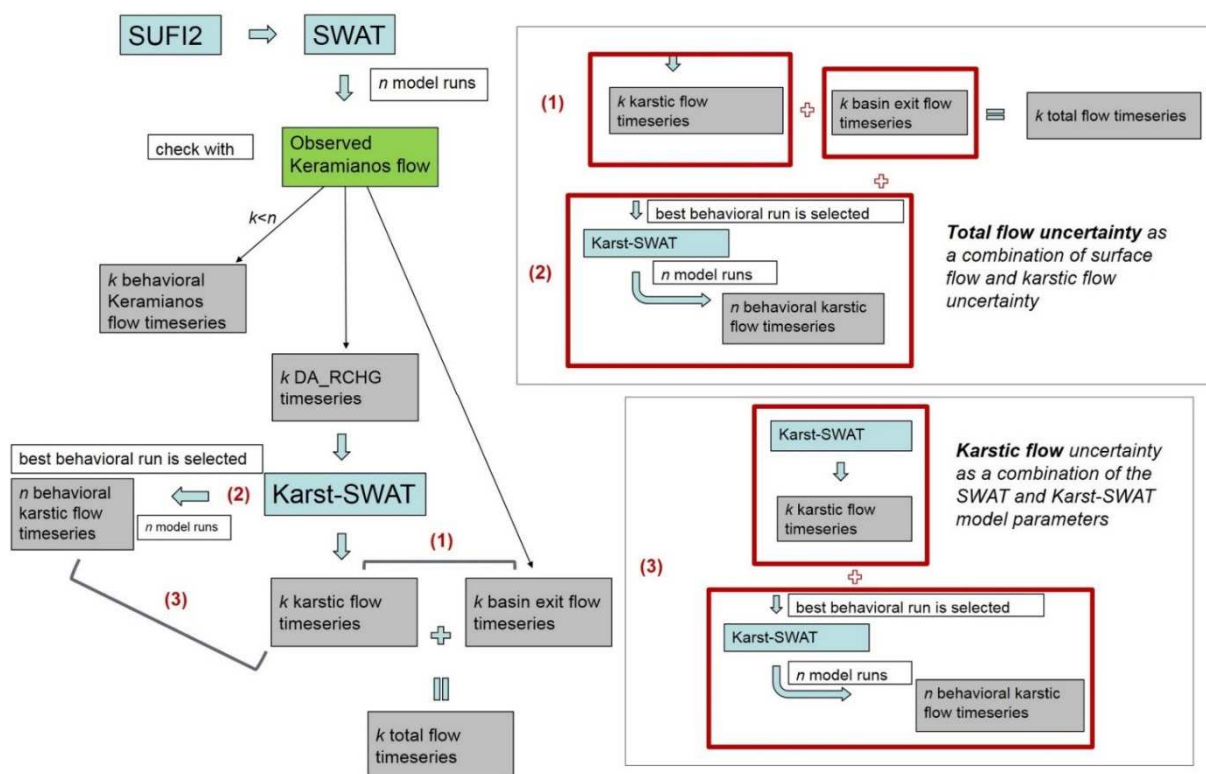
Το πρώτο τμήμα της μελέτης εξετάζει το θέμα της εκτίμησης των επιπτώσεων της κλιματικής αλλαγής στις υδρολογικές προβλέψεις μιας καρστικής μεσογειακής λεκάνης απορροής, αυτής του ποταμού Κοιλιάρη και αξιολογεί τις αβεβαιότητες που τις συνοδεύουν. Συγκεκριμένα, η μελέτη αυτή εστιάζει στις αβεβαιότητες της παροχής που προκύπτουν από την αβεβαιότητα των παραμέτρων του υδρολογικού μοντέλου, την εσωτερική μεταβλητότητα των δεδομένων εισόδου (βροχοπτώσεων) και την αβεβαιότητα λόγω του σεναρίου της κλιματικής αλλαγής.

Για τον σκοπό αυτό, χρησιμοποιείται το Εργαλείο Αξιολόγησης Εδάφους και Υδάτων (SWAT) μαζί με ένα καρστικό μοντέλο (Karst-SWAT, Nikolaidis et al., 2013) με στόχο την εκτίμηση της σύνθετης παροχής, λόγω επιφανειακής παροχής και παροχής της πηγής.

Η αβεβαιότητα των παραμέτρων τόσο του μοντέλου SWAT όσο και του Karst-SWAT υπολογίζεται συνδυάζοντας τα προγράμματα SUFI2 (Abbaspour, 2011) και @RISK της PALISADE (Palisade Corporation, 2010). Το πρώτο χρησιμοποιείται για την ποσοτικοποίηση της αβεβαιότητας των παραμέτρων που ορίζουν την επιφανειακή παροχή (13 βασικές παράμετροι, βάσει ανάλυσης αβεβαιότητας) και το δεύτερο για την ποσοτικοποίηση της αβεβαιότητας των παραμέτρων που ορίζουν την καρστική παροχή (4 παράμετροι όπως ορίζονται στο Nikolaidis et al., 2013). Καθώς βάσει της βιβλιογραφίας δεν έχει πραγματοποιηθεί μελέτη εκτίμησης αβεβαιότητας σε υδρολογικό σύστημα με σύνθετη παροχή (καρστική και επιφανειακή), στο πλαίσιο της μελέτης αυτής παρουσιάζεται για πρώτη φορά ένα μεθοδολογικό πλαίσιο για τον υπολογισμό αυτής της αβεβαιότητας. Η μεθοδολογία παρουσιάζεται στο Σχήμα ΕΠ1. Αφού πραγματοποιηθεί ο υπολογισμός της αβεβαιότητας της επιφανειακής και της καρστικής παροχής ξεχωριστά, οι δύο αβεβαιότητες συνδυάζονται με τη χρήση της Εξίσωσης ΕΠ1 (Σχήμα ΕΠ1, δεξιά)

$$\sigma_x = \sqrt{(\sigma_1)^2 + (\sigma_2)^2}. \quad (\text{ΕΠ1})$$

Τα δεδομένα εισόδου στα υδρολογικά μοντέλα παρέχονται από έντεκα συνδυασμούς πέντε «Περιφερειακών Κλιματικών Μοντέλων» (Regional Climate Models - RCMs) και τριών «Αντιπροσωπευτικών Μονοπατιών Συγκέντρωσης» (Representative Concentration Pathways - RCPs) του ευρωπαϊκού κλάδου του κλιματικού πειράματος CORDEX, EURO-CORDEX (<http://euro-cordex.net/>, <https://euro-cordex.net/060378/index.php.en>, EUR-11). Τα αποτελέσματα του υδρολογικού μοντέλου για τα έντεκα σενάρια αναλύονται και εκτιμάται η σχετική αλλαγή στην μέση ολική, καρστική και επιφανειακή παροχή σε σχέση με την περίοδο αναφοράς (1974-2018) καθώς και το εύρος των αποτελεσμάτων (αβεβαιότητα) λόγω των κλιματικών μοντέλων.



Σχήμα ΕΠ1. Διάγραμμα ροής του μεθοδολογικού πλαισίου για την εκτίμηση της επίδρασης της αβεβαιότητας των παραμέτρων υδρολογικού μοντέλου στην σύνθετη παροχή μιας καρστικής λεκάνης απορροής.

Οι χρονοσειρές βροχόπτωσης του αντιπροσωπευτικού σεναρίου «REMO» (<https://www.remo-rcm.de/059966/index.php/en>), υπό τα RCP2.6, 4.5 και 8.5 (που καλύπτουν το φάσμα της αβεβαιότητας λόγω κλιματικών σεναρίων) προσομοιώνονται στοχαστικά με τη γεννήτρια καιρού LARS (Racsko et al., 1991; Semenov and Stratonovitch, 2010). Τριάντα προσομοιώσεις Monte Carlo για κάθε RCP χρησιμοποιούνται για να ερευνήσουν την επίδραση της εσωτερικής μεταβλητότητας των δεδομένων εισόδου στην παροχή εξόδου του μοντέλου (επιφανειακή, καρστική και ολική). Η μελλοντική περίοδος χωρίζεται σε δυο 40ετείς υπο-περιόδους για να διευκολυνθεί η σύγκριση με την περίοδο αναφοράς (1974-2018).

Αποτελέσματα

Τα βασικότερα αποτελέσματα συνοψίζονται στον Πίνακα ΕΠ1, που παρουσιάζει τα εύρη της αβεβαιότητας των παροχών λόγω των εξεταζόμενων πηγών αβεβαιότητας. Η αβεβαιότητα της ολικής παροχής στην έξοδο της λεκάνης λόγω των παραμέτρων του συνδυασμού των υδρολογικών μοντέλων SWAT και Karst-SWAT εκτιμάται σε 6.6% (Συντελεστής Μεταβλητότητας - CV). Συγκεκριμένα, η αβεβαιότητα της επιφανειακής παροχής είναι 17.1% και της καρστικής παροχής 10.0% (CV). Η αβεβαιότητα των παραμέτρων του υδρολογικού μοντέλου δεν μπορεί να αγνοηθεί. Το εύρος της αβεβαιότητας της καρστικής παροχής λόγω των παραμέτρων του μοντέλου (10.0%)

είναι εξίσου σημαντικό με το εύρος της καρστικής παροχής λόγω των κλιματικών σεναρίων (10.1%) για την περίοδο 2019-2058. Ωστόσο, το τελευταίο υπερδιπλασιάζεται μετά το 2059 (23,5%).

Η μέση ετήσια αβεβαιότητα λόγω εσωτερικής μεταβλητότητας της βροχόπτωσης είναι κατά μέσο όρο 3.9% για τη βροχόπτωση, 5.6% για τη συνολική παροχή, 4.9% για την καρστική παροχή και 7.1% για την επιφανειακή (CV). Το εύρος αβεβαιότητας της βροχόπτωσης είναι πάντοτε χαμηλότερο σε σχέση με το εύρος αβεβαιότητας της συνολικής και της επιφανειακής παροχής, ενώ το εύρος αβεβαιότητας της καρστικής παροχής είναι πάντα χαμηλότερο από αυτό της επιφανειακής, λόγω της μεγαλύτερης σταθερότητας του καρστικού συστήματος. Η αβεβαιότητα που οφείλεται στην εσωτερική μεταβλητότητα της συνολικής παροχής (5.6%) είναι παρόμοια με την αβεβαιότητα που οφείλεται στις παραμέτρους του υδρολογικού μοντέλου (6.6%). Τα αποτελέσματα της μελέτης δείχνουν ότι μεταβολές μέχρι $\pm 11.1\%$ της μέσης ολικής παροχής και μεταβολές μέχρι $\pm 15.4\%$ της μέσης επιφανειακής παροχής επισκιάζονται από την αβεβαιότητα λόγω της εσωτερικής μεταβλητότητας και δεν μπορούν να εξακριβωθούν.

Η σύγκριση των μελλοντικών 40ετών μέσων για όλα τα σενάρια αποκαλύπτει ότι η περίοδος 2019-2058 είναι μια μεταβατική περίοδος, κατά την οποία τα αποτελέσματα διαφορετικών κλιματικών σεναρίων αλληλεπικαλύπτονται λόγω του κυρίαρχου ρόλου της εσωτερικής μεταβλητότητας. Επιπλέον, κατά τη διάρκεια αυτής της περιόδου, οι μεταβολές στην παροχή δεν είναι τόσο σημαντικές όσο εκείνες που προβλέπονται μετά το 2060, όταν το κλιματικό σενάριο γίνεται η βασική πηγή αβεβαιότητας.

Το σύνολο των κλιματικών αλλαγών προβλέπει σημαντική μείωση της μέσης ετήσιας συνολικής και καρστικής παροχής μετά το 2059. Το χειρότερο σενάριο (REMO RCP8.5) προβλέπει ότι η μέση καρστική παροχή θα είναι ίση με 347.7 mm/yr (μείωση 37.9%). Επιπλέον, λαμβάνοντας υπόψη τις αβεβαιότητες λόγω των παραμέτρων του μοντέλου και της εσωτερικής μεταβλητότητας, η προβλεπόμενη μέση ετήσια καρστική παροχή ενδέχεται να φτάσει και τα 271.5 mm/yr (μείωση 51.5%).

Πίνακας ΕΠ1. Συμβολή της αβεβαιότητας λόγω παραμέτρων του υδρολογικού μοντέλου, της εσωτερικής μεταβλητότητας (βροχοπτώσης) και του κλιματικού σεναρίου στην αβεβαιότητα της ολικής παροχής, καρστικής παροχής και επιφανειακής παροχής. Η αβεβαιότητα εκφράζεται μέσω του Συντελεστής Μεταβλητότητας (CV) (%). Η ολική αβεβαιότητα εκφράζει το άθροισμα των αβεβαιοτήτων λόγω παραμέτρων και εσωτερικής μεταβλητότητας, χρησιμοποιώντας την Εξίσωση ΕΠ1.

μεταβλητή	Αβεβαιότητα λόγω παραμέτρων (%)	Αβεβαιότητα λόγω εσωτερικής μεταβλητότητας (%)	Ολική αβεβαιότητα (%)	Αβεβαιότητα λόγω κλιματικού σεναρίου 2019-2058 (%)	Αβεβαιότητα λόγω κλιματικού σεναρίου 2059-2098 (%)
ολική παροχή	6.6	5.6	8.7	12.5	28.1
καρστική παροχή	10.0	4.6	11.0	10.1	23.5
επιφανειακή παροχή	17.1	7.1	18.5	17.3	36.7

Ποσοτικοποίηση Αβεβαιότητας Παραμέτρων Ποιότητας Νερού

Μεθοδολογία

Το δεύτερο τμήμα της μελέτης εξετάζει το θέμα της εκτίμησης των επιπτώσεων της κλιματικής αλλαγής στις προβλέψεις της μάζας (και συγκέντρωσης) του νιτρικού αζώτου και των αιωρούμενων στερεών της καρστικής μεσογειακής λεκάνης απορροής του ποταμού Κοιλιάρη και την αξιολόγηση της αβεβαιότητας που τις συνοδεύει. Και σε αυτή την περίπτωση, η μελέτη εστιάζει στα εύρη των μαζών που προκύπτουν από την αβεβαιότητα των παραμέτρων του μοντέλου, την εσωτερική μεταβλητότητα των δεδομένων εισόδου (βροχοπτώσεων) και την αβεβαιότητα λόγω του σεναρίου της κλιματικής αλλαγής.

Η ενότητα αυτή ακολουθεί την ίδια μεθοδολογία που αναπτύχθηκε στην προηγούμενη. Χρησιμοποιούνται τα ίδια κλιματικά σενάρια – δεδομένα εισόδου καθώς και ο συνδυασμός μοντέλων SWAT και Karst-SWAT. Τα δεδομένα εξόδου των μοντέλων σε αυτή την περίπτωση είναι η μάζα του νιτρικού αζώτου και των αιωρούμενων στερεών που μεταφέρονται τόσο μέσω της καρστικής όσο και της επιφανειακής παροχής. Ο τρόπος μοντελοποίησης του νιτρικού αζώτου και των αιωρούμενων στερεών έχει περιγραφεί από τους Nikolaidis et al. (2013) και Nerantzaki et al. (2015) αντίστοιχα. Το μεθοδολογικό πλαίσιο που αναπτύχθηκε στην προηγούμενη ενότητα για την ποσοτικοποίηση του εύρους των μεταβλητών εξόδου του μοντέλου λόγω της αβεβαιότητας των παραμέτρων εφαρμόζεται και σε αυτή την ενότητα. Το τελευταίο εφαρμόστηκε μόνο για την περίπτωση της μεταβλητής της μάζας του νιτρικού αζώτου,

καθώς δεν υπάρχουν επαρκή δεδομένα αιωρούμενων στερεών για την πραγματοποίηση μιας ικανοποιητικής ανάλυσης.

Αποτελέσματα

Οι παράμετροι των υδρολογικών μοντέλων SWAT και Karst-SWAT προκαλούν ένα εύρος της μέσης ετήσιας μάζας ολικού νιτρικού αζώτου στην έξοδο της λεκάνης ίσο με 40.1% (113.6 tn/yr).

Όσον αφορά την επίδραση της εσωτερικής μεταβλητότητας, τα ποσοστά αβεβαιότητας για την παροχή και τη μάζα των νιτρικών είναι παρόμοια (5.6% και 6.9% αντίστοιχα), ωστόσο το ποσοστό αυτό είναι σημαντικά υψηλότερο για την περίπτωση της μάζας των αιωρούμενων στερεών (18.5%), λόγω της πολυπλοκότητας της διαδικασίας διάβρωσης. Η διάβρωση των ιζημάτων και η μεταφορά τους επηρεάζονται από έναν μεγαλύτερο αριθμό παραγόντων, όπως η διάρκεια των ξηρών περιόδων οι οποίες καθιστούν το ίζημα διαβρώσιμο και επομένως εύκολα μεταφέσιμο κατά την επόμενη υγρή περίοδο.

Συγκρίνοντας τις μελλοντικές ετήσιες μέσες τιμές των μεταβλητών βάσει των έντεκα σεναρίων, η συνολική μάζα νιτρικών αυξάνεται κατά την περίοδο 2019-2058 (12.2%) και μειώνεται μετά το 2059 (23.7%). Η μάζα νιτρικών που μεταφέρεται από την επιφανειακή παροχή αυξάνεται (10.1%) κατά την περίοδο 2059-2098. Αντιστρόφως, η μάζα νιτρικών που μεταφέρεται μέσω της πηγής μειώνεται σημαντικά μετά το 2059 (37.5%). Αυτό συμβαίνει λόγω του γεγονότος ότι οι πλημμύρες αναμένεται να αυξηθούν, ευνοώντας έτσι την έκπλυση των νιτρικών.

Η ανάλυση του ανώτατου 10% της κατανομής της συγκέντρωσης νιτρικών στην επιφανειακή και ολική παροχή, αποκάλυψε ότι η μέση ετήσια συγκέντρωση νιτρικού αζώτου στην περίοδο αναφοράς και τις μελλοντικές περιόδους είναι πολύ χαμηλή σε σύγκριση με το όριο που έχει τεθεί από την Οδηγία Πλαίσιο για τα ύδατα (91/676 / ΕΟΚ - οδηγία για τη νιτρορρύπανση) και τον Παγκόσμιο Οργανισμό Υγείας για το πόσιμο νερό και την καλή χημική κατάσταση σε επιφανειακά και υπόγεια ύδατα (11.3 mg/L). Όσον αφορά τις ημερήσιες συγκεντρώσεις ολικού νιτρικού αζώτου στην έξοδο της λεκάνης, αυτές υπερβαίνουν το προαναφερθέν όριο με συχνότητα 0.05% κατά την 40ετή περίοδο αναφοράς (1979-2018) και κατά μέσο όρο (με βάση τα έντεκα σενάρια κλιματικών μεταβολών) με συχνότητα 0.24% κατά την περίοδο 2059-2098.

Η ολική μάζα των στερεών μειώνεται μέχρι το 2059 (28.3%) και είναι σταθερή μετά το 2059. Για την περίπτωση των στερεών, η μάζα που παρέχεται από την πηγή αυξάνεται σημαντικά μετά το 2059 (740.6%), ενώ η μάζα των ιζημάτων της επιφανειακής παροχής μειώνεται (38.2%), οδηγώντας σε σταθερή ολική μάζα ιζημάτων στην έξοδο της λεκάνης.

Η περίοδος 2019-2058 αναμένεται να είναι μια μεταβατική περίοδος, κατά την οποία τα αποτελέσματα των διαφορετικών κλιματικών σεναρίων αλληλεπικαλύπτονται λόγω της κυριαρχίας της εσωτερικής μεταβλητότητας και οι αλλαγές στη μάζα των νιτρικών δεν είναι τόσο σημαντικές όσο αυτές που προβλέπονται μετά το 2059, όταν η επιλογή του σεναρίου εκπομπών καθίσταται πιο σημαντική. Για την περίπτωση των στερεών, η

αβεβαιότητα λόγω της εσωτερικής μεταβλητότητας είναι υψηλότερη και ακόμη και μετά το 2059 τα αποτελέσματα των σεναρίων επικαλύπτονται.

Η συνδυασμένη αβεβαιότητα της συνολικής εξαγόμενης μάζας νιτρικού αζώτου λόγω τόσο των παραμέτρων του υδρολογικού μοντέλου όσο και της εσωτερικής μεταβλητότητας υπολογίζεται σε 115.3 tn/yr (CV 40.7%) (Εξίσωση ΕΠ1). Αυτή η αβεβαιότητα συνδυασμένων παραμέτρων είναι μεγαλύτερη από την αβεβαιότητα λόγω κλιματικού σεναρίου, ακόμη και μετά το 2059 (23.7%). Η μεγάλη αυτή αβεβαιότητα οφείλεται κατά κύριο λόγο στον περιορισμένο αριθμό παρατηρήσεων νιτρικού αζώτου. Το εύρος αβεβαιότητας στις μέσες ετήσιες προβλέψεις της μάζας νιτρικού αζώτου είναι πολύ υψηλό, καθώς κυμαίνεται από σημαντική μείωση (69.2%) σε μεγάλη αύξηση (77.5%) σε σύγκριση με την τιμή της περιόδου αναφοράς. Ακόμα και όταν λαμβάνονται υπόψη όλες οι αβεβαιότητες, η συγκέντρωση των νιτρικών στη λεκάνη του ποταμού Κοιλιάρη δεν πρόκειται να ξεπεράσει το ανώτατο επιτρεπτό όριο.

Επιπτώσεις της Κλιματικής Αλλαγής στην Παροχή και Ξηρασία των Καρστικών Πηγών.

Μεθοδολογία

Η τρίτη ενότητα της διατριβής επικεντρώνεται στη μοντελοποίηση και εκτίμηση των επιπτώσεων της κλιματικής αλλαγής σε τρεις καρστικές πηγές της Κρήτης με διαφορετικές ιδιότητες, δίνοντας έμφαση στην απόκριση των πηγών στην μετεωρολογική ξηρασία. Η καρστική πηγή του Στύλου (λεκάνη απορροής Κοιλιάρη) εμφανίζει σχετικά γρήγορη απόκριση, με χρόνο παραμονής νερού ίσο με 15 ημέρες και βραδύτερη απόκριση με χρόνο παραμονής 100 ημερών. Η μέση ετήσια καρστική εκφόρτιση είναι περίπου 120hm³. Οι άλλες δύο υπό μελέτη πηγές είναι αυτές των Μεσκλών και της Αγυιάς (λεκάνη απορροής Κερίτη). Η πηγή των Μεσκλών έχει σχετικά γρήγορη απόκριση με χρόνο παραμονής 50 ημερών και αργή απόκριση 833 ημερών (2.28 έτη). Η πηγή της Αγυιάς έχει γρήγορη απόκριση 5 ημερών και αργή απόκριση 2500 ημερών (6.84 έτη). Η μέση ετήσια παροχή της πηγής της Αγυιάς είναι 69hm³ και η μέση ετήσια παροχή της πηγής των Μεσκλών είναι 30hm³.

Χρησιμοποιούνται τα ίδια κλιματικά σενάρια – δεδομένα εισόδου καθώς και ο συνδυασμός μοντέλων SWAT και Karst-SWAT με τις άλλες δύο ενότητες. Το μοντέλο Karst-SWAT προσαρμόζεται στη σύνθετη παροχή του διπλού υπόγειου συστήματος Μεσκλών-Αγυιάς. Η «Τυποποιημένη Εργαλειοθήκη για την Ανάλυση της Ξηρασίας» (SDAT, Farahmand και AghaKouchak, 2015) χρησιμοποιείται για την εξαγωγή μη παραμετρικών τυποποιημένων δεικτών ξηρασίας για βροχοπτώσεις και παροχές. Ο δείκτης εφαρμόζεται για περίοδο συσσώρευσης 6 μηνών. Ορίζονται τρεις βαθμίδες ξηρασίας με βάση τους McKee et al. (1993) "μέτρια", "σοβαρή" και "ακραία" ξηρασία, ανάλογα με τις τιμές που παίρνει ο δείκτης για τους εκάστοτε συνεχόμενους 6 μήνες. Οι συνήθως χρησιμοποιούμενοι δείκτες, όπως και ο προαναφερθείς, εξετάζουν κάθε

συμβάν ξηρασίας της υπό μελέτη χρονοσειράς με βάση τον κλιματολογικό μέσο του συνόλου της χρονοσειράς. Καθώς θεωρούμε πιο σημαντικό να διερευνηθεί η σχετική αλλαγή της μελλοντικής ξηρασίας σε σχέση με την περίοδο αναφοράς, στο πλαίσιο αυτής της διατριβής ο μη παραμετρικός δείκτης ξηρασίας τροποποιείται με αυτόν τον στόχο. Η κύρια διαφορά του νέου δείκτη είναι ότι η κανονικοποίηση γίνεται μόνο στις τιμές (βροχοπτώσης ή παροχής) της περιόδου αναφοράς (1979-2018) και όχι σε όλη την εξεταζόμενη χρονοσειρά (1979-2098). Σε κάθε τιμή του δείκτη για τις μελλοντικές περιόδους αποδίδεται ένας πρότυπος βαθμός Z από την κανονική κατανομή της περιόδου αναφοράς.

Επιπλέον, πραγματοποιείται ανάλυση των ακραίων παροχών (χαμηλές και υψηλές παροχές πηγών και επιφανειακών υδάτων). Για τις χαμηλές παροχές αναλύουμε το κατώτατο 10% της κατανομής των παροχών των καρστικών πηγών. Για τις υψηλές επιφανειακές και καρστικές παροχές (και τις βροχοπτώσεις) διεξάγουμε ανάλυση στο ανώτερο 10% των κατανομών των μεταβλητών, χρησιμοποιώντας τη «Συνάρτηση Μέσης Υπέρβασης» (Mean Excess Function (Nerantzaki and Papalexiou, 2019)).

Αποτελέσματα

Βάσει της μελέτης των επιπτώσεων της κλιματικής αλλαγής, παρατηρούνται εντονότερες μεταβολές στην καρστική παροχή μετά το 2059, όταν μια ήπια μείωση της μέσης ετήσιας βροχοπτώσης (με βάση τα έντεκα υπό μελέτη σενάρια) οδηγεί σε σημαντική μείωση της μέσης ετήσιας καρστικής παροχής. Συγκεκριμένα, η πηγή του Στύλου αναμένεται να μειωθεί σημαντικά μετά το 2059 (25.1%) και η μείωση είναι σημαντική αλλά λιγότερο έντονη για την καρστική παροχή των Μεσκλών (18.7%) και της Αγυιάς (14.2%). Ο υψηλός χρόνος παραμονής του νερού σε μια πηγή εξασφαλίζει αποτελεσματικότερη αποθήκευση νερού και καλύτερη απόκριση στην κλιματική αλλαγή. Η μέση ετήσια επιφανειακή παροχή παρουσιάζει μικρή αύξηση μετά το 2059 (0.4% για τη λεκάνη απορροής του Κουλιάρη και 8.0% για του Κερίτη), λόγω της αύξησης της συχνότητας ακραίων βροχοπτώσεων. Οι βροχοπτώσεις υψηλής έντασης ευνοούν τη δημιουργία επιφανειακής απορροής σε βάρος της καρστικής παροχής, καθώς η ένταση της βροχοπτώσης υπερβαίνει την ταχύτητα διείσδυσης στο υπέδαφος.

Η πηγή της Αγυιάς, η οποία αποτελεί την κύρια πηγή ύδρευσης και άρδευσης για την πόλη των Χανίων, προβλέπεται να έχει χαμηλότερες παροχές μετά το 2059, αλλά η πηγή θα είναι σε θέση να καλύψει τις τρέχουσες ανάγκες ύδρευσης της περιοχής ακόμη και για το χειρότερο σενάριο (αν και οριακά). Αυτές οι ανάγκες νερού αναμένεται να αυξηθούν στο μέλλον και οι τοπικές αρχές έχουν ήδη αρχίσει να συζητούν και να προτείνουν δράσεις για περισσότερο εντατική εκμετάλλευση της πηγής (Αποκεντρωμένη Διοίκηση Κρήτης, 2017). Υπό το πρίσμα αυτών των νέων δεδομένων και της εκτίμησης της μελλοντικής υδρολογικής κατάστασης στην παρούσα μελέτη, οι δράσεις διαχείρισης του νερού για την περιοχή θα πρέπει να σχεδιαστούν προσεκτικά.

Η επίδραση του χρόνου παραμονής νερού των πηγών είναι επίσης εμφανής στην ανάλυση της ξηρασίας. Η συχνότητα των μελλοντικών γεγονότων ξηρασίας είναι υψηλότερη σε καρστικές πηγές με χαμηλότερο χρόνο κράτησης νερού (Στύλος) και χαμηλότερη σε καρστικές πηγές με υψηλότερο χρόνο κράτησης (Αγυιά). Αντίθετα, η διάρκεια των μεμονωμένων γεγονότων ξηρασίας είναι υψηλότερη για τις καρστικές πηγές με υψηλό χρόνο παραμονής νερού. Επίσης, ο συσχετισμός μεταξύ του δείκτη μετεωρολογικής και υδρολογικής ξηρασίας μειώνεται καθώς ο χρόνος παραμονής της πηγής αυξάνεται.

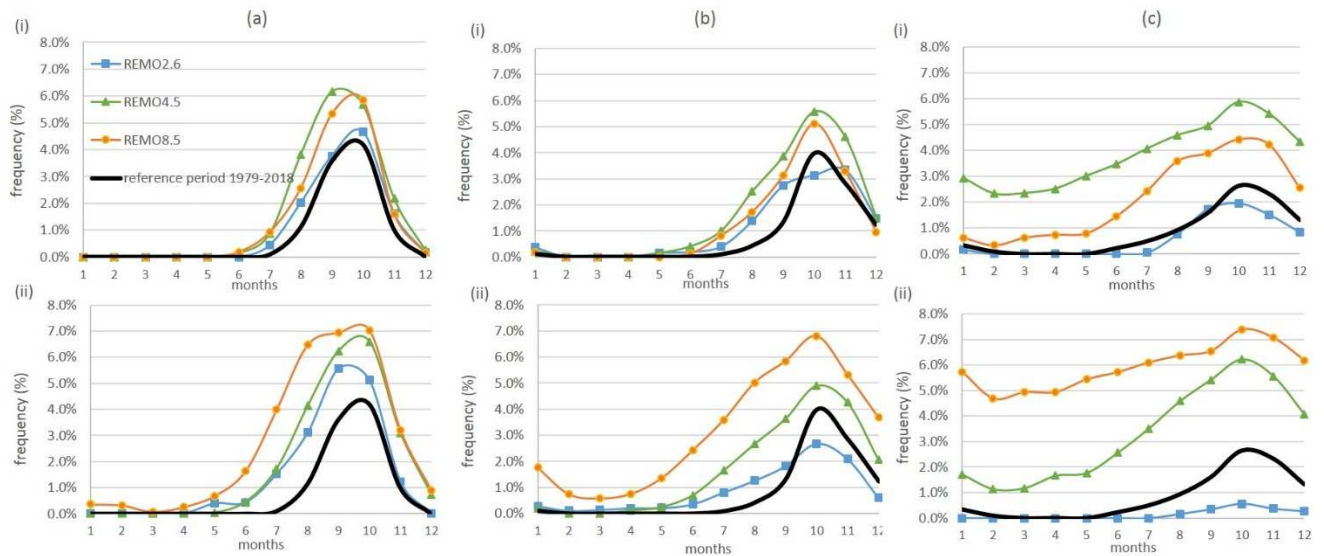
Μετά το 2059, βάσει των αποτελεσμάτων της πρώτης ενότητας, η μεταβλητότητα λόγω του σεναρίου κλιματικής αλλαγής είναι πολύ μεγάλη και το σενάριο της κλιματικής αλλαγής καθίσταται ο κύριος παράγοντας αβεβαιότητας. Ακόμη και με αυτά τα υψηλά ποσοστά αβεβαιότητας (23.5%), οι δυσμενέστερες επιπτώσεις στις υδρολογικές-καρστικές ξηρασίες αναμένεται να πραγματοποιηθούν μετά το 2059, ανεξάρτητα από το σενάριο κλιματικής αλλαγής που θα επικρατήσει. Αναλυτικά, οι αλλαγές στη διάρκεια, ένταση και συχνότητα των επεισοδίων ξηρασίας στο μέλλον σε σχέση με την περίοδο επαναφορά φαίνονται στον Πίνακα ΕΠ2. Ο μέσος όρος του λόγου του ελλείμματος προς τη μέση μηνιαία παροχή αυξάνεται για όλες τις πηγές, ειδικά για την πηγή της Αγυιάς, για την οποία διπλασιάζεται. Επιπλέον, για όλες τις πηγές, προβλέπονται πολυετείς ξηρασίες μετά το 2059, βάσει κάθε σεναρίου που μελετήθηκε.

Πίνακας ΕΠ2. Ποσοστά μεταβολής της συχνότητας, της διάρκειας και της έντασης (μέση μηνιαία ένταση) των επεισοδίων ξηρασίας στις δύο μελλοντικές περιόδους (2019-2058 και 2059-2098) σε σύγκριση με την περίοδο αναφοράς (1979-2018)

2019-2058 compared to 1979-2018			
variable	Frequency	Duration	Intensity
rainfall	16.7 %	0.2 %	14.9 %
Stilos flow	65.8 %	20.4 %	8.6 %
Meskla flow	15.2 %	20.2 %	20.5 %
Agia flow	4.0 %	83.0 %	20.0 %
2059-2098 compared to 1979-2018			
variable	Frequency	Duration	Intensity
rainfall	47.3 %	6.7 %	22.9 %
Stilos flow	77.5 %	45.0 %	27.3 %
Meskla flow	35.9 %	36.8 %	38.6 %
Agia flow	-8.1 %	533 %	83.6 %

Η ανάλυση των ακραίων (χαμηλών και υψηλών) επιφανειακών παροχών και παροχών πηγών υποδεικνύει ότι θα αυξηθεί η μεταβλητότητα των τιμών παροχής, αφού

αυξάνονται τόσο οι υψηλές όσο και οι χαμηλές παροχές σε συχνότητα και ένταση. Οι μελλοντικές κατανομές των (υψηλών) ακραίων βροχοπτώσεων δεν διευκολύνουν την αποθήκευση νερού στις πηγές και η αυξανόμενη συχνότητα μετεωρολογικής ξηρασίας οδηγεί σε αύξηση των χαμηλών παροχών καθ' όλη τη διάρκεια του έτους και ιδιαίτερα κατά τους ξηρούς μήνες, επιδεινώνοντας μια ήδη δύσκολη κατάσταση (Σχήμα ΕΠ2).



Σχήμα ΕΠ2. Συχνότητα χαμηλών ημερήσιων καρστικών παροχών των πηγών (α) Στύλος (β) Μεσκλά και (γ) Αγιά που αντιστοιχούν σε κάθε μήνα του χρόνου για την περίοδο αναφοράς (1979-2018) και τις δύο μελλοντικές περιόδους: (i) 2019-2058 και (ii) 2059-2098, υπό το σενάριο REMO και τα RCP2.6, 4.5 και 8.5.

Αυτά τα αποτελέσματα παρέχουν μια απεικόνιση των συνθηκών που αναμένεται να επικρατήσουν για τις μεσογειακές καρστικές πηγές στο μέλλον. Η κατάσταση της ξηρασίας αναμένεται να επιδεινωθεί, ιδίως μετά το 2059, ανεξάρτητα από το σενάριο που θα πραγματοποιηθεί, για όλες τις πηγές. Τα αποτελέσματα αυτής της μελέτης μπορούν να χρησιμοποιηθούν ως οδηγός από τους αρμόδιους φορείς για την προσαρμογή των πρακτικών διαχείρισης για την πρόληψη των αρνητικών επιπτώσεων της ξηρασίας των καρστικών πηγών. Προβλέπεται ότι η επόμενη 40ετής περίοδος μπορεί να χρησιμοποιηθεί για την προετοιμασία και τον προγραμματισμό μέτρων προσαρμογής για τη βελτίωση της διαχείρισης των υδάτινων πόρων των πηγών.

Αναφορές

IPCC, 2013: Climate Change 2013: The Physical Science Basis. Contribution of Working Group I to the Fifth Assessment Report of the Intergovernmental Panel on Climate Change [Stocker, T.F., D. Qin, G.-K. Plattner, M. Tignor, S.K. Allen, J. Boschung, A. Nauels, Y. Xia, V. Bex and P.M. Midgley (eds.)]. Cambridge University Press, Cambridge, United Kingdom

and New York, NY, USA, 1535 pp

Nikolaidis, N.P., Bouraoui, F., Bidoglio, G., 2013. Hydrologic and geochemical modeling of a karstic Mediterranean watershed. *J. Hydrol.* 477, 129–138. doi:10.1016/J.JHYDROL.2012.11.018

Abbaspour, K.C., 2011. SWAT Calibration and Uncertainty Programs: A User Manual. Dübendorf, Switzerland.

Palisade Corporation, 2010. Risk Analysis and Simulation Add-In for Microsoft® Excel. Ithaca, NY USA.

Racsko, P., Szeidl, L., Semenov, M., 1991. A serial approach to local stochastic weather models. *Ecol. Modell.* 57, 27–41. doi:10.1016/0304-3800(91)90053-4

Semenov, M., Stratonovitch, P., 2010. Use of multi-model ensembles from global climate models for assessment of climate change impacts. *Clim. Res.* 41, 1–14. doi:10.3354/cr00836

Nerantzaki, S.D., Giannakis, G.V., Efstathiou, D., Nikolaidis, N.P., Sibetheros, I.A., Karatzas, G.P., Zacharias, I., 2016. Modeling suspended sediment transport and assessing the impacts of climate change in a karstic Mediterranean watershed. *Sci. Total Environ.* 538, 288–297. doi:10.1016/J.SCITOTENV.2015.07.092

Farahmand, A., AghaKouchak, A., 2015. A generalized framework for deriving nonparametric standardized drought indicators. *Adv. Water Resour.* 76, 140–145. doi:10.1016/J.ADVWATRES.2014.11.012

Nerantzaki, S.D., Papalexiou, S.M., 2019. Tails of extremes: Advancing a graphical method and harnessing big data to assess precipitation extremes. *Adv. Water Resour.* 134, 103448. doi:10.1016/J.ADVWATRES.2019.103448

Table of Contents

Chapter 1	Introduction	1
1.1	Motivation	1
1.2	Study sites	3
1.3	Brief Literature Review	3
1.3.1	Droughts	3
1.3.2	Uncertainties	4
1.3.3	Innovation points	6
1.4	Outline	7
	References	8
Chapter 2	Estimation of the uncertainty of hydrologic predictions in a karstic Mediterranean watershed	13
2.1	Abstract	14
2.2	Introduction	15
2.3	Materials and Methods	17
2.3.1	Study Area and Data	17
2.3.2	Climate Change Scenarios	20
2.3.3	The SWAT and Karst-SWAT model	22
2.3.4	SWAT and Karst-SWAT Parameter Uncertainty Assessment	24
2.3.5	Assessment of Internal Variability	27
2.3.6	Simulation of Model Input	28
2.4	Results	30
2.4.1	Flow Variability due to Model Parameter Uncertainty	30
2.4.2	Flow Variability due to Climate Change Scenario	35
2.4.3	Flow Variability due to Internal Variability of Rainfall	36
2.4.4	Combined Flow Variability due to Model Parameter Uncertainty and Internal Variability of Rainfall	40
2.5	Discussion	41
2.6	Conclusions	44
	References	46
Chapter 3	Evaluation of the uncertainty of the impact of climate change on flow, sediment and nitrate predictions at the Koiliaris Critical Zone Observatory	53
3.1	Abstract	54

3.2 Introduction	55
3.3 Materials and methods	56
3.3.1 Case study and Data.....	56
3.3.2 The Karst-SWAT model.....	58
3.3.3 Model Calibration and Parameter Uncertainty Framework.....	60
3.3.4 Climate Change Scenarios.....	62
3.3.5 Rainfall Simulation	62
3.3.6 Assessment of Internal Variability.....	63
3.3.7 Monte Carlo Simulations.....	64
3.4 Results	65
3.4.1 Hydrologic Model Goodness of Fit	65
3.4.2 Variability due to Hydrologic Model Parameters.....	66
3.4.3 Variability due to Climate Change Scenarios	68
3.4.4 Uncertainty due to the Internal Variability of Rainfall.....	71
3.4.5 Combining the Uncertainties of Nitrate Mass.....	75
3.5 Discussion and Conclusions	76
References.....	78
Chapter 4 The response of three Mediterranean karstic springs to drought and the impact of climate change.....	81
4.1 Abstract.....	82
4.2 Introduction	83
4.3 Materials and Methods	85
4.3.1 Study Area and Data	85
4.3.2 Climate Change Scenarios.....	88
4.3.3 The Karst-SWAT model	89
4.3.4 Methods used for the Analysis of the Results	89
4.4 Results	92
4.4.1 Evaluation of Hydrologic and Climate Change Models.	92
4.4.2 Impact of Climate Change on the Annual and Monthly Rainfall and Flow	94
4.4.3 Impact of Climate Change on the Meteorological and Hydrological Drought Frequency, Intensity and Duration.....	100
4.4.4 Impact of Climate Change on the Flow Extremes.....	106

4.5 Discussion and Conclusions	110
References	113
Chapter 5 Summary and Conclusions	117
5.1 Summary of aims and methodology	117
5.2 Conclusions.....	118
5.2.1 On the quantification of hydrologic predictions uncertainty of karstic Mediterranean watersheds.....	118
5.2.2 On the quantification of nitrate (and sediment) fluxes predictions uncertainty in karstic Mediterranean watersheds.....	119
5.2.3 On the estimation of the impact of climate change on three karstic springs with different properties.....	120
5.3 General Remarks	122
Publications	125
Publications in Scientific Journals based on the Thesis.....	125
Publication in Conference Proceedings based on the Thesis	125
Conference Presentations based on the Thesis	125
Publications in Scientific Journals related to the Thesis	125
Appendix A.....	127
A1 Tables and Figures	127
A2 Simulation of minimum and maximum temperature using the Box-Jenkins methodology.....	129
A3 Adjustment of LARS-WG	132
References.....	140
Appendix B.....	141
B.1 Karst-SWAT equations.....	141
Stilos spring.....	141
Meskla and Agia springs.....	142
B.2 Tables and Figures.....	143

Chapter 1 Introduction

1.1 Motivation

Karstic regions describe landscapes containing caves and often extensive groundwater systems developed on soluble rocks (i.e. limestone, marble and gypsum). Usual hydrologic formations in these areas are sinking streams, caves, enclosed depressions and large springs. Karstic landscapes occupy approximately 20% of the planet's dry ice-free land and offer the partial or entire drinking supply of about one fourth of the global population (Ford and Williams, 2007; Maupin and Barber, 2005).

Karstic systems account for around 75% of the freshwater input into the Mediterranean Sea (Wang and Polcher, 2019). These water bodies will play a major role in water management for the Mediterranean region in the future, as they relate to water availability for potable water and agriculture (i.e. food security issues). The Mediterranean basin has been the cradle of karstic studies since ancient times (Ford and Williams, 2007) and it is estimated that at least 15% of the Mediterranean surface is covered by carbonate outcrops and that karstic aquifers supply at least 25% of domestic water supply, without taking industry, agricultural and tourism withdrawals under consideration (Bakalowicz, 2015). It should be noted that 75% of the total Mediterranean agricultural land is irrigated and this accounts for more than 60% of the total water abstractions (e.g. Spain 64%, Greece 88%, Portugal 80%) (Wriedt et al., 2009).

The IPCC model projections of anthropogenic impacts have identified the Mediterranean region as a "climate change hot-spot" (Giorgi, 2006; Hoerling et al., 2012). The specific region is projected to undergo the most significant drying (as a percentage of climatological rainfall) among 26 regions across the world, by the end of the 21st century (Giorgi, 2006). Water scarcity and depleting groundwater resources are threatening the sustainability of the natural ecosystem and human activities (van Beek et al., 2011).

The island of Crete is a Mediterranean, semi-arid, karst-dominated region, characterized by high rainfall variability, with long periods of drought and infrequent but high-intensity rainfall (Agou et al., 2019). Water needs rise during dry months and are almost exclusively covered by karstic springs distributed in the region along with some operational dams (Nerantzaki et al., 2019). The concurrence of low karstic flows in combination with the increased demands may result to substantial water stress. In water management practice, the evaluation of low flows is essential for a range of goals, such as water supply, irrigation, habitat protection, and water quality management (Risva et al., 2018). Due to the projected changes in air temperature and rainfall, the mobility and dilution of contaminants will be influenced due to the decrease in river flows, but the relationships are not straightforward to capture. Relatively little is known about the changes in water quality due to climate change in the Mediterranean region and even

fewer studies have dealt with the ways that climate change affects water quality of karstic aquifers. Both the quality and availability of water resources in the Mediterranean region are expected to change significantly according to the Intergovernmental Panel on Climate Change (IPCC) Synthesis Report (Pachauri et al., 2014).

The socio-economic impacts of climate change have already been witnessed in Syria, located at the southeast Mediterranean region, just 1300 km away from Crete. The Syrian drought had a catalytic effect, leading Syria and the greater Fertile Crescent to experience the worst 3-year drought ever recorded (Trigo et al., 2010). The already tense water conditions were exacerbated, leading to agricultural production failure along with livestock mortality. The most important effect was the migration of 1.5 million people (Kelley et al., 2015) or more (Gleick, 2014; Selby et al., 2017) from rural farming to urban regions, contributing to the social instability of the area. These events are a precursor of the imminent conditions that may prevail for the rest of the Mediterranean region in the near future.

It is, therefore, imperative to properly simulate the complex system of the Mediterranean karstic springs, so that changes in the water resources are known at all times (current and future periods). Climate change impact assessment results must have high reliability, especially for such regions. The first step for reliable predictions of both surface and karstic flow (and water quality) is the robust hydrologic (and geochemical) modeling of the watershed of interest, using operational models which can thoroughly describe the complex hydrological conditions of karstic watersheds. Hydrological (and geochemical) modeling still introduces a variety of uncertainties associated, for example, with internal climate system variability and hydrological model parameters, which can significantly affect model outputs and our confidence in the results. The uncertainties are more critical when modeling the (low) flows of Mediterranean regions, since water depletion may hide behind the uncertainty range of the flow outcomes. Few studies have addressed hydrological projections uncertainty over the Mediterranean region, and, to our knowledge, none have over Mediterranean regions with karstic formations.

Taking the above mentioned topics under consideration, the fundamental questions this study addresses are:

- What is the climate change impact on the Mediterranean karstic flow and how does climate change affect the drought frequency, intensity and duration of droughts?
- How can the uncertainty of the hydrologic predictions for a karstic Mediterranean watershed be quantified and which is the most important source of uncertainty?
- Accordingly, how can the uncertainty of the geochemical predictions for a karstic Mediterranean watershed be quantified?

Each of these questions will be examined and answered in the next chapters.

1.2 Study sites

The author has already performed a study concerning the climate change impact on the hydrological budget of Crete using data from 22 streamflow gauging stations and 47 spring gauging stations (Nerantzaki et al., 2019). Having performed a thorough examination of the hydrology of the island, the author selected two major karstic watersheds for the implementation of the methodology presented here, based on the availability of observed flow and nitrate concentration data, the apprehension of the watershed's hydrologic processes and the significance of the watersheds in terms of water resources. The selected watersheds are the Koiliaris River Basin and the Keritis River Basin, both located in Chania. These watersheds include karstic springs which discharge the broad karstic system of the White Mountains Range, and they are the main contributors of water for the region of Chania.

The Koiliaris River Basin is a Critical Zone Observatory. The watershed is about 130 km², and includes two episodic streams (Keramianos and Anavreti) and the karstic spring of Stilos, which provides permanent flows throughout the year. The karstic spring of Stilos is fed from the karstic regions inside the basin but also from an area located outside of the watershed, i.e. the extended karstic are. The spring displays a relatively fast response with a detention time equal to 15 days and a slower response with a detention time of 100 days. The average annual karstic discharge is about 120hm³. The Stilos spring has high ecological value since it is the only spring in Crete which forms a permanent river flow.

The Keritis River Basin (210km²) encompasses the springs of Agia and Meskla, which, together with the intermittent surface runoff, form the Keritis River. The springs are fed by karstic regions within the watershed. The karstic system of the particular watershed is more complex, as the underground reservoir of Meskla connects with the one of Agia, transferring large volumes of water. The Meskla spring has a relatively fast response with detention time of 50 days and a slow response of 833 days (2.28 years). The Agia spring has a fast response of 5 days and a significant slow response of 2500 days (6.84 years). The mean annual flow of the Agia spring is 69hm³ and the mean annual flow of the Meskla spring is 30hm³. Agia spring has low variability and is dried up during summer months due to intensive water pumping.

1.3 Brief Literature Review

1.3.1 Droughts

According to literature, droughts can be categorized as meteorological, hydrological and agricultural (Wilhite and Glantz, 1985). Meteorological droughts refer to decrease in precipitation, hydrological droughts to deficit in surface water and agricultural droughts to drop in soil moisture. Orłowsky and Seneviratne (2012) found enhanced dryness (meteorological drought) on the annual time scale in the Mediterranean using the CMIP3

models. Lu et al. (2019) recently found statistically significant annual drying over the Mediterranean region (agricultural drought), with stronger drying as the strength of forcing increases, using the CMIP5 models.

Large scale hydrological drought studies do not take under consideration the effects of non-linearity in smaller scales, which is a result of many hydrologic processes. An extensive bibliography of climate change assessment studies on several (regional scale) Mediterranean regions exists, however, the climate change impact research for karstic watersheds (Mediterranean or other), is limited. For example, Hartmann et al. (2012) used a multi-model approach to assess future water availability at a large Eastern Mediterranean karst spring, and suggested that in the remote future (2068–2098), when variability of climate change decreases, a decrease of water availability of 15% to 30% is forecasted. Another example is the study of Nerantzaki et al. (2019), who used a combination of CMIP5 models to estimate the future hydrological budget of a karst-dominated Mediterranean island (i.e. Crete) and found an average decrease of 16.5% for spring flow. This gap in literature needs to be filled, considering that water needs in the arid and semi-arid regions of the Mediterranean are exclusively covered by karstic springs and groundwater resources during the summer months, when there is no surface runoff. Several questions arise for Mediterranean karstic watersheds, such as whether climate change scenarios predictions suggest satisfactory available water supplies and what impact the multi-year droughts will have on the springs' water provision. It is crucial to acknowledge the importance of karstic springs, estimate the present and future response for these regions and plan water resources management accordingly.

1.3.2 Uncertainties

There are different classifications concerning the sources of uncertainty; historically, the three most common sources considered in hydrologic modeling are input data, model structure, and parameterization (Beven and Freer, 2001; Refsgaard et al., 2006; Xue et al., 2014; Yen et al., 2014). Parameterization uncertainty has received the highest attention according to previous studies. In rainfall-runoff modeling, uncertainty in rainfall inputs also compromises model predictions and subsequently water management decisions (Fatichi et al., 2014). Uncertainties in temperature input data can also have a significant impact in the flow output of Snowmelt–Rainfall-Driven Watershed models for the snow-melting period (Zhang et al., 2016). Model structure uncertainty is caused by the lack of the ability to perfectly model real-world processes, since hydrologic models are simplifications resulting from incomplete representation of reality (Gupta and Govindaraju, 2019). According to Mockler et al. (2016), the uncertainty sources for flow simulations vary and depend on the catchment area, the model selected and the data employed, along with implementation decisions.

The contribution of parameter uncertainty to the hydrologic model output is high, as different parameter sets can result in annual streamflow changes in opposite directions (Zhang et al., 2019). The issue of model parameter uncertainty has led the hydrological community to develop several techniques for its quantification. These include the Parameter Solution (ParaSol) (van Griensven and Meixner, 2006), the Sequential Uncertainty Fitting algorithm (SUFI2) (Abbaspour, 2011), and the Generalized Likelihood Uncertainty Estimation (GLUE) (Beven and Binley, 1992). These techniques have been proven robust for parameter sensitivity and uncertainty analysis in the hydrological simulation, with the SUFI2 technique exhibiting higher skill in predicting the parameter uncertainty (Zhao et al., 2018; Xue et al., 2014; Yang et al., 2008). The estimation of hydrologic model parameter uncertainty has also been addressed for certain areas in the Mediterranean region (Sellami et al., 2016; Sellami et al., 2013; Malagò et al., 2016; Garambois et al., 2013), but studies concerning parameter uncertainty in karstic regions of the world are limited (Moussu et al., 2011; Hartmann et al., 2015).

Uncertainty in future climate change scenarios stems from three main sources: forcing, model response, and internal variability or stochastic uncertainty (Deser et al., 2012; Hawkins and Sutton, 2011). Forcing uncertainty stems from external factors influencing the climate system, such as future trajectories of anthropogenic emissions of greenhouse gases, stratospheric ozone concentrations, land use change, etc. (Deser et al., 2010). Model response uncertainty occurs because different models may yield different responses with the same external forcing. The term “internal” or “stochastic” uncertainty (or “climate noise”) describes the natural variability of the input data (i.e. rainfall, temperature etc.) which is due to the natural processes in the atmosphere (non-linear dynamic processes intrinsic to the atmosphere with long-time scale variability), the ocean, and the coupled ocean-atmosphere system (low-frequency variability from the thermodynamic coupling between the atmosphere and upper ocean mixed layer which produces slow climate fluctuations). Internal variability occurs independently of external forcing. It is critical to quantify internal variability, because it provides the outcome range for a given forced response and is thus necessary for the robust detection of climate change effects and for practical decision making purposes (Steinschneider et al., 2015; Liu et al., 2013). There are different studies concerning the quantification of internal variability in rainfall including “signal-to-noise”, “time of emergence”, and “multimodel or initial conditions” approaches (see Schindler et al., 2015 for references).

In this context, few studies have addressed the parameter uncertainty and internal variability problem over the Mediterranean region, where observational data foreshadow a substantial change towards higher temperatures and lower rainfall rates (Intergovernmental Panel on Climate Change, 2014; Seager et al., 2014). The area has been identified as a climate change hot-spot (Diffenbaugh and Giorgi, 2012; Giorgi, 2006). These changes are expected to lead to lower river flows and the quantification of their range would provide useful feedback on the possible water deficit, which is a big

impediment for these arid areas. Climate change affects both recharge and discharge rates and changes in quantity and quality of water in aquifers due to groundwater variation (Panwar and Chakrapani, 2013). Groundwater resources response to climate change is slower in comparison to the surface water (Kløve et al., 2011; Ertürk et al., 2014). Previous approaches for climate change impact and uncertainty assessments for future water availability in the Mediterranean region do not incorporate karst processes, with few exceptions (i.e. Hartmann et al., 2012, who used a multi-model approach to estimate water availability at a Mediterranean karstic spring).

1.3.3 Innovation points

The methodology presented here combines the advantages of climate change impact analysis with those of a fully integrated hydrologic model. The integration of surface and subsurface flow in the same model provides more realistic simulations of the water cycle and improved representation of the dominant hydrologic process of groundwater recharge interaction, which is important for impact assessment on groundwater resources.

This is the first time, to our knowledge, that a combined assessment of surface and karstic flow model parameter uncertainty and internal variability is applied to a karstic Mediterranean watershed.

Our analysis shows that the parameter uncertainty of the hydrologic model and the internal variability of the climate change scenarios should be considered in planning water resources adaptation and mitigation measures that aim to alleviate climate change impacts in karstic watersheds of semi-arid or arid climates, especially for the 2019-2058 period. After 2059, the climate change scenario is the most important uncertainty factor. The case of the Koiliaris River Basin provides a benchmark for comparative studies in other similar regions of the globe, where water needs during the summer are exclusively covered by the flow originating from karstic springs.

An extensive bibliography of climate change assessment studies on several (regional scale) Mediterranean regions exists, however, the climate change impact research for karstic watersheds (Mediterranean or other), is limited. To this day, there are no studies examining the way the hydrologic droughts of karstic springs will respond to the imminent meteorological droughts. Here, for the first time, three karstic springs with different hydrologic properties are modeled and their response to climate change and to future meteorological droughts is studied at the same time.

Finally, the commonly used drought indices have the limitation that they can give an indication of a time series drought relative to the hydrological (or meteorological) average of the time period for which they are examined. By simply modifying a non-parametric indicator, it was possible to compare future droughts with respect to the

hydrological (or meteorological) average of the reference period, thus acquiring a more useful index.

1.4 Outline

The thesis includes an Introductory Chapter (Chapter 1), followed by three Chapters, each one of which constitutes a journal or a conference publication and reports on one of the three main objectives of the study.

Chapter 2 is entitled “Estimation of the uncertainty of hydrologic predictions in a karstic Mediterranean watershed” and describes the modeling framework developed for the estimation of the hydrologic predictions and the quantification of the associated uncertainties in a karstic Mediterranean basin (i.e. Kiliaris River Basin). This study (1) evaluates the Karst-SWAT model parameter uncertainty, differentiating between surface runoff and karstic flow parameters, (2) evaluates the significance of rainfall input uncertainty (internal variability) on the mean annual values of flow outcomes in a Mediterranean karstic watershed, and (3) compares the above mentioned uncertainties with the uncertainty stemming from climate change scenario.

Chapter 3 is entitled “Evaluation of the uncertainty of the impact of climate change on flow, sediment and nitrate predictions at the Kiliaris Critical Zone Observatory” and discusses the application of the framework detailed in Chapter 2, on the nitrate nitrogen and suspended sediment masses transferred through surface and karstic water in a karstic Mediterranean watershed.

Chapter 4 is entitled “The response of three Mediterranean karstic springs to drought and the impact of climate change” and explores the climate change impact on the water resources of three karstic springs with different hydrologic properties, emphasizing on the frequency, duration and intensity of their hydrologic droughts.

Chapter 5 completes the thesis with a synthesis of the main results.

References

- Abbaspour, K.C., 2011. SWAT Calibration and Uncertainty Programs: A User Manual. Dübendorf, Switzerland.
- Agou, V.D., Varouchakis, E.A., Hristopulos, D.T., 2019. Geostatistical analysis of precipitation in the island of Crete (Greece) based on a sparse monitoring network. *Environ. Monit. Assess.* 191, 353. doi:10.1007/s10661-019-7462-8
- Bakalowicz, M., 2015. Karst and karst groundwater resources in the Mediterranean. *Environ. Earth Sci.* 74, 5–14. doi:10.1007/s12665-015-4239-4
- Beven, K., Binley, A., 1992. The future of distributed models: Model calibration and uncertainty prediction. *Hydrol. Process.* 6, 279–298. doi:10.1002/hyp.3360060305
- Beven, K., Freer, J., 2001. Equifinality, data assimilation, and uncertainty estimation in mechanistic modelling of complex environmental systems using the GLUE methodology. *J. Hydrol.* 249, 11–29. doi:10.1016/S0022-1694(01)00421-8
- Deser, C., Alexander, M.A., Xie, S.-P., Phillips, A.S., 2010. Sea Surface Temperature Variability: Patterns and Mechanisms. *Ann. Rev. Mar. Sci.* 2, 115–143. doi:10.1146/annurev-marine-120408-151453
- Deser, C., Phillips, A., Bourdette, V., Teng, H., 2012. Uncertainty in climate change projections: the role of internal variability. *Clim. Dyn.* 38, 527–546. doi:10.1007/s00382-010-0977-x
- Diffenbaugh, N.S., Giorgi, F., 2012. Climate change hotspots in the CMIP5 global climate model ensemble. *Clim. Change* 114, 813–822. doi:10.1007/s10584-012-0570-x
- Ertürk, A., Ekdal, A., Gürel, M., Karakaya, N., Guzel, C., Gönenç, E., 2014. Evaluating the impact of climate change on groundwater resources in a small Mediterranean watershed. *Sci. Total Environ.* 499, 437–447. doi:10.1016/J.SCITOTENV.2014.07.001
- Fatichi, S., Rimkus, S., Burlando, P., Bordoy, R., 2014. Does internal climate variability overwhelm climate change signals in streamflow? The upper Po and Rhone basin case studies. *Sci. Total Environ.* 493, 1171–1182. doi:10.1016/J.SCITOTENV.2013.12.014
- Ford, D. (Derek C., Williams, P.W. (Paul W., 2007. Karst hydrogeology and geomorphology. John Wiley & Sons.
- Garambois, P.A., Roux, H., Larnier, K., Castaings, W., Dartus, D., 2013. Characterization of process-oriented hydrologic model behavior with temporal sensitivity analysis for flash floods in Mediterranean catchments. *Hydrol. Earth Syst. Sci.* 17, 2305–2322. doi:10.5194/hess-17-2305-2013
- Giorgi, F., 2006. Climate change hot-spots. *Geophys. Res. Lett.* 33, L08707. doi:10.1029/2006GL025734
- Gupta, A., Govindaraju, R.S., 2019. Propagation of structural uncertainty in watershed hydrologic models. *J. Hydrol.* 575, 66–81. doi:10.1016/J.JHYDROL.2019.05.026
- Hartmann, A., Gleeson, T., Rosolem, R., Pianosi, F., Wada, Y., Wagener, T., 2015. A large-scale simulation model to assess karstic groundwater recharge over Europe and the Mediterranean. *Geosci. Model Dev.* 8, 1729–1746. doi:10.5194/gmd-8-1729-2015
- Hartmann, A., Lange, J., Vivó Aguado, À., Mizyed, N., Smiatek, G., Kunstmann, H., 2012. A multi-model approach for improved simulations of future water availability at a large

- Eastern Mediterranean karst spring. *J. Hydrol.* 468, 130–138. doi:10.1016/j.jhydrol.2012.08.024
- Hawkins, E., Sutton, R., 2011. The potential to narrow uncertainty in projections of regional precipitation change. *Clim. Dyn.* 37, 407–418. doi:10.1007/s00382-010-0810-6
- Intergovernmental Panel on Climate Change (Ed.), 2014. *Climate Change 2013 - The Physical Science Basis*. Cambridge University Press, Cambridge. doi:10.1017/CBO9781107415324
- Kløve, B., Ala-aho, P., Bertrand, G., Boukalova, Z., Ertürk, A., Goldscheider, N., Ilmonen, J., Karakaya, N., Kupfersberger, H., Kværner, J., Lundberg, A., Mileusnić, M., Moszczynska, A., Muotka, T., Preda, E., Rossi, P., Siergieiev, D., Šimek, J., Wachniew, P., Angheluta, V., Widerlund, A., 2011. Groundwater dependent ecosystems. Part I: Hydroecological status and trends. *Environ. Sci. Policy* 14, 770–781. doi:10.1016/J.ENVSCI.2011.04.002
- Liu, Y., Zhang, J., Wang, G., Liu, J., He, R., Wang, H., Liu, C., Jin, J., 2013. Assessing the effect of climate natural variability in water resources evaluation impacted by climate change. *Hydrol. Process.* 27, 1061–1071. doi:10.1002/hyp.9251
- Malagò, A., Efstathiou, D., Bouraoui, F., Nikolaidis, N.P., Franchini, M., Bidoglio, G., Kritsotakis, M., 2016. Regional scale hydrologic modeling of a karst-dominant geomorphology: The case study of the Island of Crete. *J. Hydrol.* 540, 64–81. doi:10.1016/J.JHYDROL.2016.05.061
- Maupin, M.A., Barber, N.L., 2005. Estimated withdrawals from principal aquifers in the United States, 2000, Circular. doi:10.3133/CIR1279
- Mockler, E.M., Chun, K.P., Sapriza-Azuri, G., Bruen, M., Wheeler, H.S., 2016. Assessing the relative importance of parameter and forcing uncertainty and their interactions in conceptual hydrological model simulations. *Adv. Water Resour.* 97, 299–313. doi:10.1016/J.ADVWATRES.2016.10.008
- Moussu, F., Oudin, L., Plagnes, V., Mangin, A., Bendjoudi, H., 2011. A multi-objective calibration framework for rainfall–discharge models applied to karst systems. *J. Hydrol.* 400, 364–376. doi:10.1016/J.JHYDROL.2011.01.047
- Nerantzaki, S.D., Efstathiou, D., Giannakis, G. V., Kritsotakis, M., Grillakis, M.G., Koutroulis, A.G., Tsanis, I.K., Nikolaidis, N.P., 2019. Climate change impact on the hydrological budget of a large Mediterranean island. *Hydrol. Sci. J.* 64, 1190–1203. doi:10.1080/02626667.2019.1630741
- Panwar, S., Chakrapani, G.J., 2013. Climate change and its influence on groundwater resources. *Curr. Sci.* doi:10.2307/24092675
- Refsgaard, J.C., van der Sluijs, J.P., Brown, J., van der Keur, P., 2006. A framework for dealing with uncertainty due to model structure error. *Adv. Water Resour.* 29, 1586–1597. doi:10.1016/J.ADVWATRES.2005.11.013
- Risva, K., Nikolopoulos, D., Efstratiadis, A., Nalbantis, I., 2018. A Framework for Dry Period Low Flow Forecasting in Mediterranean Streams. *Water Resour. Manag.* 32, 4911–4932. doi:10.1007/s11269-018-2060-z
- Schindler, A., Toreti, A., Zampieri, M., Scoccimarro, E., Gualdi, S., Fukutome, S., Xoplaki, E., Luterbacher, J., Schindler, A., Toreti, A., Zampieri, M., Scoccimarro, E., Gualdi, S., Fukutome, S., Xoplaki, E., Luterbacher, J., 2015. On the Internal Variability of Simulated Daily Precipitation. *J. Clim.* 28, 3624–3630. doi:10.1175/JCLI-D-14-00745.1

- Seager, R., Liu, H., Henderson, N., Simpson, I., Kelley, C., Shaw, T., Kushnir, Y., Ting, M., Seager, R., Liu, H., Henderson, N., Simpson, I., Kelley, C., Shaw, T., Kushnir, Y., Ting, M., 2014. Causes of Increasing Aridification of the Mediterranean Region in Response to Rising Greenhouse Gases. *J. Clim.* 27, 4655–4676. doi:10.1175/JCLI-D-13-00446.1
- Sellami, H., Benabdallah, S., La Jeunesse, I., Vanclooster, M., 2016. Quantifying hydrological responses of small Mediterranean catchments under climate change projections. *Sci. Total Environ.* 543, 924–936. doi:10.1016/J.SCITOTENV.2015.07.006
- Sellami, H., La Jeunesse, I., Benabdallah, S., Vanclooster, M., 2013. Parameter and rating curve uncertainty propagation analysis of the SWAT model for two small Mediterranean catchments. *Hydrol. Sci. J.* 58, 1635–1657. doi:10.1080/02626667.2013.837222
- Steinschneider, S., Wi, S., Brown, C., 2015. The integrated effects of climate and hydrologic uncertainty on future flood risk assessments. *Hydrol. Process.* 29, 2823–2839. doi:10.1002/hyp.10409
- van Beek, L.P.H., Wada, Y., Bierkens, M.F.P., 2011. Global monthly water stress: 1. Water balance and water availability. *Water Resour. Res.* 47. doi:10.1029/2010WR009791
- van Griensven, A., Meixner, T., 2006. Methods to quantify and identify the sources of uncertainty for river basin water quality models. *Water Sci. Technol.* 53, 51–59. doi:10.2166/wst.2006.007
- Wang, F., Polcher, J., 2019. Assessing the freshwater flux from the continents to the Mediterranean Sea. *Sci. Rep.* 9, 8024. doi:10.1038/s41598-019-44293-1
- Wilhite, D.A., Glantz, M.H., 1985. Understanding: the Drought Phenomenon: The Role of Definitions. *Water Int.* 10, 111–120. doi:10.1080/02508068508686328
- Wriedt, G., Van der Velde, M., Aloe, A., Bouraoui, F., 2009. Estimating irrigation water requirements in Europe. *J. Hydrol.* 373, 527–544. doi:10.1016/J.JHYDROL.2009.05.018
- Xue, C., Chen, B., Wu, H., 2014. Parameter Uncertainty Analysis of Surface Flow and Sediment Yield in the Huolin Basin, China. *J. Hydrol. Eng.* 19, 1224–1236. doi:10.1061/(ASCE)HE.1943-5584.0000909
- Yang, J., Reichert, P., Abbaspour, K.C., Xia, J., Yang, H., 2008. Comparing uncertainty analysis techniques for a SWAT application to the Chaohe Basin in China. *J. Hydrol.* 358, 1–23. doi:10.1016/j.jhydrol.2008.05.012
- Yen, H., Wang, X., Fontane, D.G., Harmel, R.D., Arabi, M., 2014. A framework for propagation of uncertainty contributed by parameterization, input data, model structure, and calibration/validation data in watershed modeling. *Environ. Model. Softw.* 54, 211–221. doi:10.1016/J.ENVSOF.2014.01.004
- Zhang, J.L., Li, Y.P., Huang, G.H., Wang, C.X., Cheng, G.H., Zhang, J.L., Li, Y.P., Huang, G.H., Wang, C.X., Cheng, G.H., 2016. Evaluation of Uncertainties in Input Data and Parameters of a Hydrological Model Using a Bayesian Framework: A Case Study of a Snowmelt–Precipitation-Driven Watershed. *J. Hydrometeorol.* 17, 2333–2350. doi:10.1175/JHM-D-15-0236.1
- Zhang, R., Corte-Real, J., Moreira, M., Kilsby, C., Birkinshaw, S., Burton, A., Fowler, H.J., Forsythe, N., Nunes, J.P., Sampaio, E., dos Santos, F.L., Mourato, S., 2019. Downscaling climate change of water availability, sediment yield and extreme events: Application to a Mediterranean climate basin. *Int. J. Climatol.* 39, 2947–2963. doi:10.1002/joc.5994

Zhao, F., Wu, Y., Qiu, L., Sun, Y., Sun, L., Li, Q., Niu, J., Wang, G., Zhao, F., Wu, Y., Qiu, L., Sun, Y., Sun, L., Li, Q., Niu, J., Wang, G., 2018. Parameter Uncertainty Analysis of the SWAT Model in a Mountain-Loess Transitional Watershed on the Chinese Loess Plateau. *Water* 10, 690. doi:10.3390/w10060690

Chapter 2 Estimation of the uncertainty of hydrologic predictions in a karstic Mediterranean watershed

Sofia D. Nerantzaki ^{a*}, Nikolaos P. Nikolaidis ^a and Dionissios T. Hristopulos ^b

^a *School of Environmental Engineering, Technical University of Crete, University Campus, 73100 Chania, Greece*

^b *School of Mineral Resources Engineering, Technical University of Crete, University Campus, 73100 Chania, Greece*

**corresponding author, email: sofia_ner@hotmail.com, +306973475458*

Published as: “Nerantzaki, S.D., Hristopulos, D.T., Nikolaidis, N.P. 2020. Estimation of the uncertainty of hydrologic predictions in a karstic Mediterranean watershed, Science of the Total Environment. <https://doi.org/10.1016/j.scitotenv.2020.137131>”

2.1 Abstract

The Koiliaris River basin is a semi-arid Mediterranean karstic watershed where water needs during the summer are exclusively covered by the karstic springs flow. Uncertainty assessment of the hydrologic projections for karstic watersheds may reveal possible water deficits that cannot otherwise be taken into account. The Soil Water Assessment Tool (SWAT) along with a karstic model (Karst-SWAT) are used to assess the composite spring and surface flow. The parameter uncertainty of both the surface and karstic flow models is estimated by combining the SUFI2 interface and the @RISK by PALISADE software. Eleven combinations of five Regional Climate Models (RCMs) and three Representative Concentration Pathways (RCPs) provide input to the hydrologic models. Representative rainfall time series for certain scenarios are stochastically modeled with the LARS weather generator. Monte Carlo simulations are used to investigate the effect of input internal variability on the flow output. The uncertainty of karstic flow due to the parameter uncertainty of the SWAT and Karst-SWAT models is 10.0% (Coefficient of Variation), which is comparable to the estimated uncertainty due to climate change scenarios (10.1%) until 2059. The combined uncertainty for the total flow at the basin exit due to both models' parameter uncertainty is 6.6%, comparable to the uncertainty due to the internal variability (5.6%). The total uncertainty of karstic flow, combining model parameter uncertainty and the internal variability of the climate scenarios is 11.0%. The total uncertainty estimate is used in conjunction with the lowest karstic flow projection to assess the most adverse scenario for the future mean annual karstic flow. This is the first study which estimates the combined uncertainty of surface and karstic flow prediction due to model parameter uncertainty and internal variability. Our study provides a rigorous methodology for uncertainty estimation and analysis which is transferable to other karstic regions of the world.

Keywords: Mediterranean karstic watershed; parameter uncertainty; internal variability; Karst-SWAT; climate change uncertainty; uncertainty partition

2.2 Introduction

The karstic landscape is formed by the dissolution of soluble rocks (limestone, dolomite). More than 25% of the world's population either lives on or obtains its water from karstic aquifers (Maupin and Barber, 2005). Karstic systems account for around 75% of the freshwater input into the Mediterranean Sea (Wang and Polcher, 2019). These water bodies will play a major role in water management as they relate to water availability for potable water and agriculture (i.e. food security issues). The island of Crete is a Mediterranean, semi-arid, karst-dominated region, characterized by high rainfall variability, with long periods of drought and infrequent but high-intensity rainfall (Agou et al., 2019). Water needs rise during summer months and are almost exclusively covered by karstic springs distributed in the region along with some operational dams (Nerantzaki et al., 2019). Hydrologic modeling and climate change analysis along with climate change uncertainty assessment for such watersheds is of utmost importance in view of the impacts of climate change in the Mediterranean region. Water scarcity and depleting groundwater resources are threatening the sustainability of the natural ecosystem and human activities (van Beek et al., 2011), and water depletion may hide behind the uncertainty range of the flow outcomes. For this reason, climate change impact assessment results must have high reliability, especially for such regions.

There are different classifications concerning the sources of uncertainty; historically, the three most common sources considered in hydrologic modeling are input data, model structure, and parameterization (Beven and Freer, 2001; Refsgaard et al., 2006; Xue et al., 2014; Yen et al., 2014). Parameterization uncertainty has received the highest attention according to previous studies. In rainfall-runoff modeling, uncertainty in rainfall inputs also compromises model predictions and subsequently water management decisions (Fatichi et al., 2014). Uncertainties in temperature input data can also have a significant impact in the flow output of Snowmelt-Rainfall-Driven Watershed models for the snow-melting period (Zhang et al., 2016). Model structure uncertainty is caused by the lack of the ability to perfectly model real-world processes, since hydrologic models are simplifications resulting from incomplete representation of reality (Gupta and Govindaraju, 2019). According to Mockler et al. (2016), the uncertainty sources for flow simulations vary and depend on the catchment area, the model selected and the data employed, along with implementation decisions.

The contribution of parameter uncertainty to the hydrologic model output is high, as different parameter sets can result in annual streamflow changes in opposite directions (see for example Zhang et al., 2019). The issue of model parameter uncertainty has led the hydrological community to develop several techniques for its quantification. These include the Parameter Solution (ParaSol) (van Griensven and Meixner, 2006), the Sequential Uncertainty Fitting algorithm (SUFI2) (Abbaspour, 2011), and the Generalized Likelihood Uncertainty Estimation (GLUE) (Beven and Binley, 1992). These techniques have been proven robust for parameter sensitivity and uncertainty analysis in the

hydrological simulation, with the SUFI2 technique exhibiting higher skill in predicting the parameter uncertainty (Zhao et al., 2018; Xue et al., 2014; Yang et al., 2008). The estimation of hydrologic model parameter uncertainty has also been addressed for certain areas in the Mediterranean region (Sellami et al., 2016; Sellami et al., 2013; Malagò et al., 2016; Garambois et al., 2013), but studies concerning parameter uncertainty in karstic regions of the world are limited (Moussu et al., 2011; Hartmann et al., 2015).

Uncertainty in future climate change scenarios stems from three main sources: forcing, model response, and internal variability or stochastic uncertainty (Deser et al., 2012; Hawkins and Sutton, 2011). Forcing uncertainty stems from external factors influencing the climate system, such as future trajectories of anthropogenic emissions of greenhouse gases, stratospheric ozone concentrations, land use change, etc. (Deser et al., 2010). Model response uncertainty occurs because different models may yield different responses with the same external forcing. The term “internal” or “stochastic” uncertainty (or “climate noise”) describes the natural variability of the input data (i.e. rainfall, temperature etc.) which is due to the natural processes in the atmosphere (non-linear dynamic processes intrinsic to the atmosphere with long-time scale variability), the ocean, and the coupled ocean-atmosphere system (low-frequency variability from the thermodynamic coupling between the atmosphere and upper ocean mixed layer which produces slow climate fluctuations). Internal variability occurs independently of external forcing. It is critical to quantify internal variability, because it provides the outcome range for a given forced response and is thus necessary for the robust detection of climate change effects and for practical decision making purposes (Steinschneider et al., 2015; Liu et al., 2013). There are different studies concerning the quantification of internal variability in rainfall including “signal-to-noise”, “time of emergence”, and “multimodel or initial conditions” approaches (see Schindler et al., 2015 for references).

In this context, few studies have addressed the parameter uncertainty and internal variability problem over the Mediterranean region, where observational data foreshadow a substantial change towards higher temperatures and lower rainfall rates (Intergovernmental Panel on Climate Change, 2014; Seager et al., 2014). The area has been identified as a climate change hot-spot (Diffenbaugh and Giorgi, 2012; Giorgi, 2006). These changes are expected to lead to lower river flows and the quantification of their range would provide useful feedback on the possible water deficit, which is a big impediment for these arid areas. Climate change affects both recharge and discharge rates and changes in quantity and quality of water in aquifers due to groundwater variation (Panwar and Chakrapani, 2013). Groundwater resources response to climate change is slower in comparison to the surface water (Kløve et al., 2011; Ertürk et al., 2014). Previous approaches for climate change impact and uncertainty assessments for future water availability in the Mediterranean region do not incorporate karst processes, with few exceptions (i.e. Hartmann et al., 2012, who used a multi-model approach to estimate water availability at a Mediterranean karstic spring)

The goal of this study is to (1) evaluate the Karst-SWAT model parameter uncertainty, differentiating between surface flow and karstic flow parameters, (2) evaluate the significance of rainfall input uncertainty (internal variability) on the mean annual values of flow outcomes in a Mediterranean karstic watershed, and (3) compare the above mentioned uncertainties with the uncertainty stemming from climate change scenario. To this end, the Soil Water Assessment Tool (SWAT) in combination with a karstic model (Karst-SWAT) is used to assess the total flow at the Koiliaris River basin. The SWAT model is selected because it provides a Deep Aquifer Recharge output which is used as input to the Karst-SWAT model, developed by Nikolaidis et al. The SUFI2 algorithm (Sequential Uncertainty Fitting Version 2) in the SWAT-CUP software is used to assess uncertainty due to the surface model (SWAT) parameters, while the risk analysis software @RISK by PALISADE is used to conduct uncertainty analysis due to the karstic model parameters. For the assessment of climate change variability, eleven combinations of five Regional Climate Models (RCMs) and three Representative Concentration Pathways (RCPs) are used. The Long Ashton Research Station Weather Generator (LARS-WG) (Racsko et al., 1991; Semenov and Stratonovitch, 2010) with a daily time step under both current and future climate conditions is used to generate realizations of rainfall time series with the same statistical characteristics (monthly and daily mean, standard deviation, 95-th percentile, minimum and maximum) as the original observed and forecasted (based on the climate change scenarios) time series. The generated time series realizations are used as input in the SWAT and karst-SWAT model, for the simulation of flow at Koiliaris River Basin. This approach allows investigating the impact of the internal variability on the surface and karstic flow predictions. The overall flow uncertainty due to both model parameter uncertainty and internal variability is finally estimated. The study presents a methodology for estimating and partitioning sources of uncertainty in a karstic watershed with composite flow and we expect that the Koiliaris river basin will represent a benchmark for comparative studies in other similar regions of the globe.

2.3 Materials and Methods

2.3.1 Study Area and Data

The Koiliaris River basin is a Critical Zone Observatory that represents severely degraded soils due to heavy agricultural impacts, such as grazing, over many centuries. It is situated in the island of Crete, Greece, 15 km east of the city of Chania. The catchment area is about 130 km², and altitudes range between 0 and 2120 m (above mean sea level). Soils are thin and poorly developed. The dominant geologic formations are Plattenkalk limestones and dolomites, Tripolis and Trypali series, calcaric marls and marly limestones, quaternary alluvial deposits and crystalline schists (Nikolaidis et al., 2013). The karstic formations in the basin, which correspond to the Plattenkalk limestones of Figure 2.1, in combination with a fault that extends from the northeast to the southwest, direct water from an extended karstic watershed area towards Stylos springs (Figure 2.1) (Moraetis et al.,

2010, Nikolaidis et al., 2013), thus supplying the permanent flow of the Koiliaris river. The overall recharge area of the springs extends outside the watershed boundaries, beyond the area of the 130 km² (Nikolaidis et al., 2013) to an area of about 80 km² in the southeast of the watershed boundary (Figure 2.1).

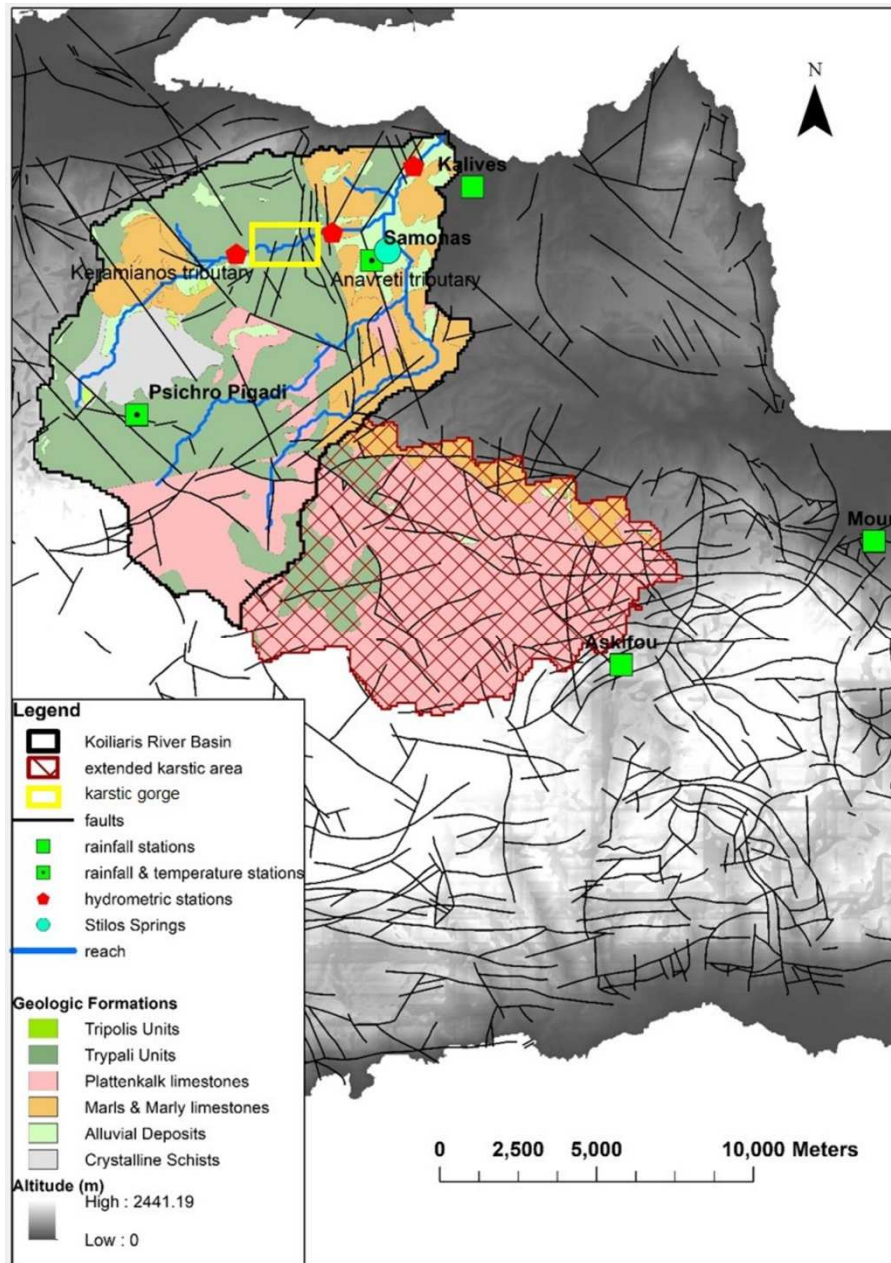


Figure 2.1. Map of Koiliaris Critical Zone Observatory (Crete, Greece) showing the location of the five rainfall and temperature measurement stations (green squares), the locations of three hydrometric stations (red hexagons), and the modelled extended karstic area (shown with a hatched pattern).

In addition to the permanent Stylos spring discharge, a temporary tributary called Keramianos, a temporary spring called Anavreti, and two episodic tributaries (upstream of Anavreti, Figure 2.1), contribute to the Koiliaris main river flow. The Keramianos tributary merges with the Anavreti and Stylos flows after it enters and later exits a karstic gorge, i.e. the Diktamos gorge (Figure 2.1). According to field measurements covering the 2004-2018 period, the total flow at the basin exit is estimated to be about 812 mm/yr, ranging from 406 to 1747 mm/yr (annual standard deviation equal to 430 mm/yr). The karstic flow originating from Stylos springs contributes the most to the total annual flow, while the contribution of the surface runoff (mainly Keramianos and Anavreti tributaries) to the total river flow is lower (20%-30%) (Nerantzaki et al., 2015). In the Koiliaris river basin, rangeland covers 58% of the total area, while cultivated areas, forests, urban areas, and aquatic areas account for 29.4%, 8.5%, 2.8%, and 0.6% respectively. Intensive cultivation and livestock grazing has led to significant deterioration of the soil quality and land fertility. Water is pumped from the springs for irrigation and drinking, while the surface flow is also used for irrigation.

Rainfall data used to generate rainfall scenarios are provided by five meteorological stations, two of which are located within the watershed boundaries. These stations (at Samonas and Psichro Pigadi, see Figure 2.1) are managed by the “Laboratory of Hydrochemical Engineering and Remediation of Soil” of the Technical University of Crete. These stations record rainfall intensity (mm) as well as minimum and maximum temperature data (°C) every 5 minutes since 2007. The remaining three rainfall stations located outside the basin, i.e. Askifu, Kalives and Mouri, are managed by the Region of Crete and record daily rainfall intensity data since 1973. The Koiliaris River Basin, as part of the Island of Crete, is characterized by a dry semi-humid Mediterranean climate with dry and warm summers and humid and relatively cold winters. Annual rainfall varies spatially ranging between 700 mm in coastal areas (i.e. Kalives station, Figure 2.1) and 1330 mm in high altitudes (i.e. Psichro Pigadi station, Figure 2.1). In general, mean annual rainfall increases with altitude (Malagò et al., 2016). However, some of the higher values (2200 mm) are recorded in Askifou plateau station which does not have the highest altitude. The mean annual temperature ranges from 14°C (Psichro Pigadi station, 1000 m altitude) to 18°C (Samonas station, 385 m altitude). Water level data from three hydrometric stations (see Figure 2.1) with a 10-minute time step are used to calibrate the SWAT model. These include a hydrometric station located near the exit of the basin towards the sea (covering the 2004-2018 period) and two hydrometric stations along the Keramianos river bed (2013-2017). More specifically, three stage-discharge rating curves have been set up using the level logger data and simultaneous flow measurements at the three hydrometric stations. Using the stage-discharge curves and the level data we obtain continuous flow time series with a 10-minute time step.

2.3.2 Climate Change Scenarios

A sub-set of simulations is selected from the recent high resolution (12.5 km) EURO-CORDEX (EUR-11) climate model ensemble (Jacob et al., 2014). The General Circulation Models (GCMs) simulations of EURO-CORDEX have been conducted within the Coupled Model Intercomparison Project Phase 5 (CMIP5) and represent various scenarios of greenhouse gas emission pathways. The regional simulations (Regional Climate Models - RCMs) downscale the global climate projections of CMIP5 (Taylor et al., 2012) and the Representative Concentration Pathways (RCPs) (Moss et al., 2010; van Vuuren et al., 2007). The sub-sampling technique used in Jacob et al. (2018) to assess the cross-sectoral impacts of 1.5°C of global warming at a pan-European scale is also used in this study. Five EUR-11 models were selected based on three criteria: (a) the range of driving global climate models (GCMs), (b) the variety of institutions which develop the RCMs (different model genealogy), and (c) the range of climate change signals in terms of wet/dry and cold/warm responses. Based on these criteria and the methodology developed by Mendlik and Gobiet (2016), we use the same set of models as in the study of Nerantzaki et al. (2019), which assessed the climate change impact on the hydrological budget of Crete. The RCMs used in this study are presented in Table A1 of Appendix A.

RCP scenarios assume pathways to different target radiative forcing by 2100. The RCP2.6 emission pathway storyline leads to very low greenhouse gas concentration levels. It is described as a peak and decline scenario in which the radiative forcing level initially reaches a value of 3.1 W/m² (by mid-century) and then declines to 2.6 W/m² (by 2100) (van Vuuren et al., 2007). The RCP4.5 represents a stabilization scenario in which the radiative forcing is stabilized just after 2100, without overshooting the long-run radiative forcing target level (Wise et al., 2009). Finally, RCP8.5 represents an increasing greenhouse gas emissions scenario over time (Riahi et al., 2007).

The RCM simulated temperature and rainfall data (for each emission pathway) are adjusted for biases against a thirty-year period between 1980 and 2009 that served as reference for the correction. The quantile mapping methodology known as multi-segment statistical bias correction (MSBC) is used (Grillakis et al., 2013). The method considers discrete segments of the cumulative probability function and applies quantile mapping correction separately to each segment.

The downscaled time series of rainfall and temperature from the 11 scenarios are used as input to the combined SWAT and Karst-SWAT model and the flow outputs are evaluated (karstic, surface, and total flow). For further analysis, uncertainty originating from (a) RCM and (b) RCP can be assessed separately by varying the modelling component in focus, while holding the other constant. For example, in order to assess uncertainty related to the RCM, the five RCMs are varied while the RCP4.5 is held constant, or the four RCMs are varied while RCP8.5 is kept constant. Respectively, uncertainty related to the RCP can be estimated by varying the three RCPs for the same RCM (we only perform this

for GCM-RCMs of EC-EARTH-r12_SMHI-RCA4 and MPI-ESM-LR-r1_CSC-REMO, which include three RCPs).

From the 11 RCMs of the ensemble we focus our analysis of internal variability on the MPI-ESM-LR-r1_CSC-REMO (hereafter REMO). The selection of the REMO model is motivated by the fact that REMO includes the highest (RCP2.6) and the lowest (RCP8.5) rainfall projections among the selected 11 models; therefore, it is representative of the entire range of rainfall for the ensemble. In addition, REMO shows the highest skill scores for temperature in the European, Mediterranean and North American domain, and for rainfall in the Mediterranean, African and West Asian regions (Jacob et al., 2012). REMO is run for a range of Representative Concentration Pathways (RCPs), i.e. RCP2.6, RCP4.5, and RCP8.5 (Moss et al., 2010; O'Neill et al., 2014).

Based on the analysis of the rainfall and temperature data for both reference (1974-2018) and projected periods (2019-2098), the projected period is divided into two non-overlapping segments which correspond to the intervals 2019-2058 and 2059-2098. This segmentation is driven by two factors. Firstly, the intensity of the rainfall and the duration of wet and dry periods change significantly around 2059 (as discussed in Section 2.4.2, and evidenced later in Figure 2.7). The cumulative rainfall of the RCP8.5 scenario shows that after 2060 there is a significant change in slope (Figure A1, Appendix A). Secondly, at least 40 years of observed data are required to reliably calibrate the LARS-WG generator; this is accomplished with the proposed segmentation. Following this segmentation, we have one rainfall time series for the reference period and six rainfall time series for the projected time period (2019-2098), i.e., two per each RCP studied. All six rainfall time series are used as input for the LARS-WG. The mean annual values of the downscaled time series of rainfall and temperature for the reference period are presented in Table 2.1 in terms of water height (mm/yr) and degrees Celsius (°C) respectively. Table 2.1 also shows the relative change of rainfall and the absolute change in temperature for each of the two projection periods compared to the reference period (1974-2018).

Table 2.1. Average changes in temperatures (\pm oC) and average relative changes in rainfall (%) compared to the average values during the reference period (1974-2018) for the three downscaled RCPs per time window.

variables	2019-2058			2059-2098		
	RCP2.6	RCP4.5	RCP8.5	RCP2.6	RCP4.5	RCP8.5
rainfall (%)	+0.2%	-9.6%	+1.9%	+4.6%	-8.4%	-23.7%
temperature (\pm oC)	+0.9	+1.4	+1.4	+0.85	+2.6	+3.6
Reference period (1974-2019)						
rainfall (mm/yr)	1460.3					
temperature (oC)	17.3					

2.3.3 The SWAT and Karst-SWAT model

The SWAT model (Soil and Water Assessment Tool) is a well-known and widely used deterministic, watershed to river-basin scale, hydrological model, which operates on a daily time step. SWAT can assess the quality and quantity of surface and ground water and predict the environmental impacts of land use, land management practices, and climate change (Arnold et al., 1998; Neitsch et al., 2009). In the model, the watershed is divided into smaller sub-basins in order to separate the tributaries; these are further divided into hydrologic response units (HRUs) which constitute unique combinations of soil type, land use and slope value within the watershed. The land use classes for the Koiliaris basin were obtained by Corine Land Use (2000), the soil types were defined using the European Soil Database (v2 Raster Library 1kmx1km), and the slopes were extracted from a Digital Elevation Model with 25 m pixel size (Bashfield and Keim, 2011), obtained from a Pan-European elevation data at 1 arc-second (EU-DEM).

To simulate the karstic springs flow, we use the methodology developed in (Moraetis et al., 2010) to define the spatial extent of the karst area, based on fault analysis and other available data and observations, and its volume by means of mass balance modeling. In order to account for the variability of the spring discharge, SWAT is augmented by connecting (in series) a modified version of the karst flow model described by Tzoraki and Nikolaidis (2007) which considers a two-reservoir underground model. The SWAT model uses the rainfall as input and simulates the surface hydrologic processes (snow accumulation and melt, surface runoff, infiltration to shallow groundwater and evapotranspiration) over the karstic HRUs (total of 46 HRUs with karstic soils). The

surface water is then directed to the subsurface of the karstic area thus creating the deep groundwater discharge which feeds the spring flow. The discharge is aggregated on a daily step and provides the input to the two-part reservoir karst model (Nikolaidis et al., 2013). The model equations describing the karst component include the upper reservoir mass balance, i.e.

$$\frac{dV_1}{dt} = Q_{in,1} - Q_2, \quad (2.1)$$

and the lower reservoir mass balance, i.e.,

$$\frac{dV_2}{dt} = Q_{in,2} - Q_2, \quad (2.2)$$

where

$$Q_{in,1} = a_1 * Q_{in,deepGW}, \quad (2.3)$$

$$Q_{in,2} = (1 - a_1) * Q_{in,deepGW} + a_2 * Q_1 \quad (2.4)$$

$$Q_1 = k_u * V_1 \quad (2.5)$$

$$Q_2 = k_l * V_2, \quad (2.6)$$

and $Q_{in,deepGW}$ is the deep groundwater discharge from SWAT (the corresponding variable from SWAT is DA_RCHG, or deep aquifer recharge), a_1 is the fraction of flow entering the upper reservoir, a_2 is the fraction of flow from the upper reservoir discharge entering the lower reservoir and k_u and k_l are recession constants (in units of 1/day) for the upper and lower reservoir. For constant $Q_{in,1}$ and $Q_{in,2}$ the analytical solutions of (2.1) and (2.2) are:

$$Q_1 = Q_{1,0}e^{-k_u t} + Q_{in,1}(1 - e^{-k_u t}), \quad (2.7)$$

$$Q_2 = Q_{2,0}e^{-k_l t} + Q_{in,2}(1 - e^{-k_l t}). \quad (2.8)$$

The total karstic flow is then calculated as

$$Q_{karstic} = (1 - a_2) * Q_1 + Q_2 \quad (2.9)$$

The karst model parameters are calibrated, and the resulting karstic flow time series is used as point source input at the spring location (Equation 2.9). The mass balance equations for the two-part reservoir model are solved analytically (Tzoraki and Nikolaidis, 2007; Nikolaidis et al., 2013).

2.3.4 SWAT and Karst-SWAT Parameter Uncertainty Assessment

In this study the SUFI2 algorithm (Sequential Uncertainty Fitting Version 2) (Abbaspour et al., 2004) in the SWAT-CUP software (Abbaspour, 2011) is used for calibration and uncertainty analysis of the SWAT parameters. SUFI2 has proved superior to other uncertainty assessment techniques by the majority of comparison studies (Uniyal et al., 2015; Yang et al., 2008; Zhao et al., 2018). In SUFI2, the parameters are considered to follow the uniform distribution, and their uncertainty is expressed using respective intervals. The parameter uncertainties propagate through the SWAT model to uncertainties in the output variables. The latter are expressed by means of the respective 95% probability intervals.

The Latin Hypercube sampling (LHS) approach is used to calculate the 2.5% and 97.5% levels of the cumulative distribution of each output variable due to the propagation of the input parameter uncertainties. The resulting interval is referred to as 95% prediction uncertainty or 95PPU (95 percent prediction uncertainty). Two statistics, the P-factor and the R-factor, are used to quantify the fit between the observed data and the simulated probability distributions. The P-factor is the percentage of observed data contained within the 95PPU. The R-factor is the width of the 95PPU interval divided by the standard deviation of the observed data. For streamflow, a value of P-factor at least equal to 0.7 is considered adequate (Abbaspour, 2015). This implies that most of the observed data are within the 95PPU band and that the model has been well calibrated (Zhao et al., 2018). In addition, it is suggested that the R-factor be lower than 1.5 (Abbaspour et al., 2015).

We initialize LHS with large input parameter uncertainty, so that the measured data fall within the 95PPU. The SUFI2 algorithm performs a number of iterations; normally, three to five iterations of 300-1000 simulations (based on LHS) are sufficient for satisfactory results (4 iterations of 1000 simulations were carried out in this study). The input parameter range is reduced after each SUFI2 iteration, leading to a respective reduction of the 95PPU interval of the output variables; consequently, the P-factor and R-factor also decrease. An objective function is used to measure the distance between the observations and the simulations. The objective function that we use in this study is the coefficient of determination, i.e., r^2 , between the observed and the simulated outputs at each simulation. After all the LHS simulations are completed for the specific SUFI2 iteration, SWAT-CUP calculates the objective function and the 95PPU for all the simulated output variables. New input parameter ranges are selected by the program for the next iteration. The iterations terminate when acceptable R-factor and P-factor values are obtained. The input parameters are set to the values which optimize the objective function.

2.4.1 Flow Variability due to SWAT model parameters

The SUFI2 algorithm is initially applied to the SWAT model which estimates the surface runoff. Since the uncertainty analysis requires continuous (without gaps) flow

observations, we need to select the most appropriate hydrometric station. There are three hydrometric stations at the Koiliaris River Basin (Figure 2.1). The hydrometric station at the basin exit records total flow, i.e., the combination of surface and karstic flow. Therefore, the data from this hydrometric station are not the most suitable for assessing the uncertainty due to the SWAT surface flow parameters. The two remaining stations along the Diktamos gorge record exclusively surface flow data. However, the hydrometric station located at the gorge exit is the most representative for the surface flow of the basin due to its location close to the basin exit. The selected station at the gorge exit provides observed daily surface flow for five continuous years (2013-2017), which are used as the observed data for the SUFI2 analysis.

The initial SWAT parameters are based on the trial and error method as reported in Nikolaidis et al., 2013). An initial iteration of 1000 LHS simulations is carried out for 13 hydrologic input parameters. These parameters are selected based on the sensitivity analysis of the SWAT model conducted prior to the calibration process (see Appendix A, Table A2). During this first iteration, the intervals of the input parameters θ_i are set to $[\theta_i^{(0)} - 0.9\theta_i^{(0)}, \theta_i^{(0)} + 0.9\theta_i^{(0)}]$, where $i = 1, \dots, 13$, and $\theta_i^{(0)}$ is the initial value of parameter θ_i . The surface flow at the gorge exit is computed, and the simulations are characterized as behavioral if the coefficient of determination (r^2) is greater than 0.5 (Moriasi et al., 2007). Three additional iterations of 1000 LHS simulations are carried out, resulting to updated input parameters with a progressively narrower range.

The above procedure determines the uncertainty of surface flow at the gorge exit. To further quantify the uncertainty of the other output variables (surface flow at the basin's exit and DA_RCHG from the 46 karstic HRUs), the input parameter range of the final SUFI2 iteration is used to run an additional ensemble of 100 LHS simulations. These allow quantifying the uncertainty range of the surface flow at the gorge exit (where observational data are available), but also the uncertainty range of the surface flow at the basin exit (where only total flow observations are available). In addition, the procedure above quantifies the uncertainty of the DA_RCHG from the 46 karstic HRUs, through which the water enters the deep aquifer, thus providing the input to the Karst-SWAT model.

Fewer (100 instead of 1000) model simulations are used in this stage, as each simulation is time-consuming due to the high number of output variables (49 variables: 46 for the DA_RCHG of the karstic HRUs, two for the surface flow at the gorge exit, and one for the surface flow at the basin exit). The execution time is 1925 min on Intel Core i5-2450 @ 2.50 GHz. Uncertainty assessment is based on those simulations (60 out of 100) that are characterized as behavioral with respect to the surface flow at the gorge exit. The respective simulations of surface flow at the basin exit and the DA_RCHG of the karstic HRUs are also used for uncertainty assessment. The behavioral DA_RCHG time series (more precisely, the time series which correspond to the behavioral simulations of surface flow at the gorge exit), are used as input to the Karst-SWAT model, which then

produces an ensemble of 60 simulated time series for the karstic flow. Then, each behavioral simulation of the surface flow at the basin exit is added to the corresponding simulation of the karstic flow, resulting to 60 simulations of total flow at the basin exit. The range of the total flow for the period 2013–2017 is finally calculated.

2.4.2 Variability due to Karst-SWAT model parameters

In this section we focus on the impact of uncertainty in the Karst-SWAT input parameters to the karstic flow uncertainty. Once the karst model parameters are calibrated (see above), the @RISK program (Palisade Corporation, 2010) is run using four input (karst model) variables which are assumed to follow the uniform distribution. Four iterations of 1000 simulations of Latin Hypercube sampling are carried out to determine the uncertainty of the four model parameters that control karstic flow. The range of the karstic flow for the period 2013–2017 is then calculated.

2.4.3 Variability due to combined SWAT and Karst-SWAT model parameters

The total uncertainty of karstic flow due to the combined SWAT and Karst-SWAT model parameter uncertainty can then be estimated. According to Taylor (1997), a good measurement of the uncertainty δx of variable x is the standard deviation σ_x . If variable x is measured with independent and random uncertainties σ_1, σ_2 , then the uncertainty σ_x is

$$\sigma_x = \sqrt{(\sigma_1)^2 + (\sigma_2)^2}. \quad (2.10)$$

Equation (2.10) can be used to estimate the total flow uncertainty σ_x that results from (1) the uncertainty of surface and karstic flow due to SWAT parameters, and (2) karstic flow uncertainty due to Karst-SWAT parameters. Uncertainty (1) can be calculated from the ensemble of the 60 behavioral LHS simulations resulting from the sum of SWAT surface flow and the corresponding karstic flow from the Karst-SWAT model. Uncertainty (2) can be estimated as described in sub-section 2.4.2. Uncertainties (1) and (2) are independent as they originate from different models and parameter analysis methods. The total uncertainty, due to the parameters from (i) SWAT and (ii) Karst-SWAT for the variable of the karstic flow alone (3), can be also calculated in a similar manner. A graphical representation of the parameter uncertainty for the flow of Koiliaris watershed is given in Figure 2.2.

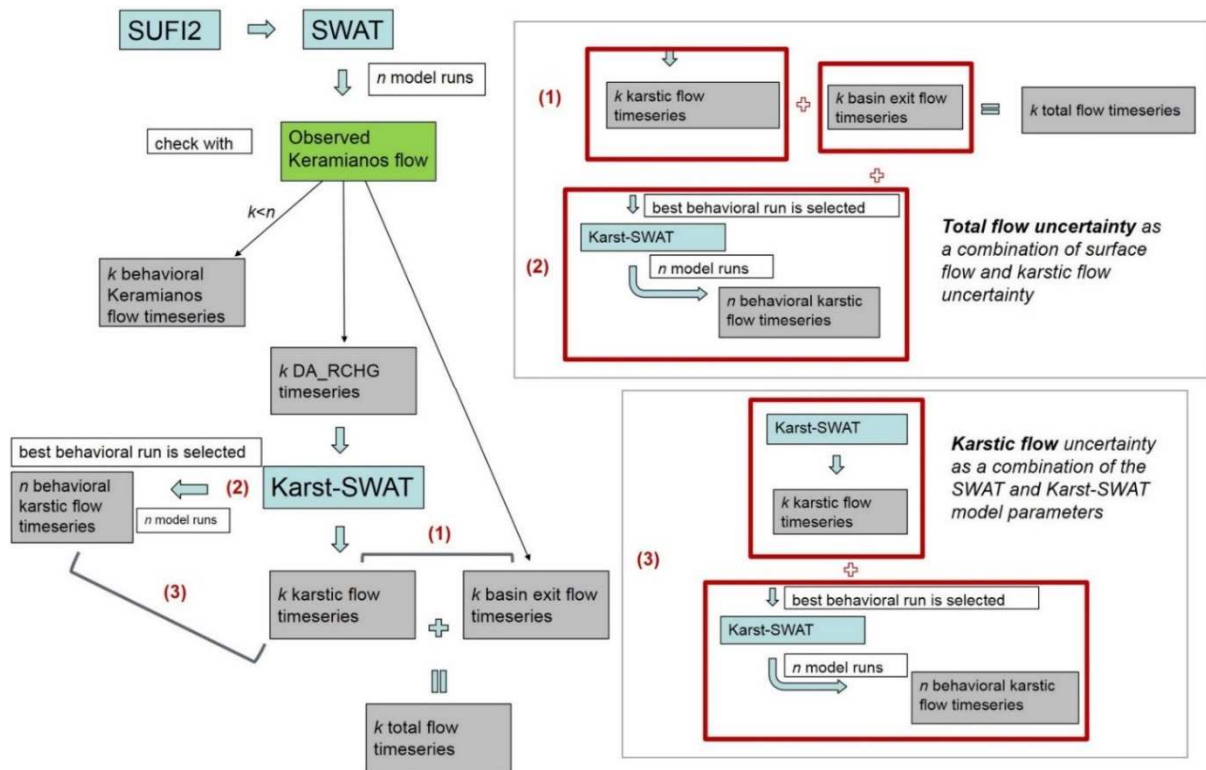


Figure 2.2. Graphical representation of the procedure followed for estimating the uncertainty of the hydrologic model of the Koiliaris River watershed.

2.3.5 Assessment of Internal Variability

A big part of the methodology presented in this study aims to assess the impact of internal variability or stochastic uncertainty of the meteorological input on the flow of a karstic Mediterranean watershed. The input time series consist of the rainfall time series at Mouri station for the reference period (1974-2018) as well as the projected time series for the same station, based on the CSC-REMO (Jacob et al. 2012) Regional Climate Model (RCM) for three Representative Concentration Pathways (RCPs), i.e. RCP2.6, RCP4.5, and RCP8.5. The RCM is based on the MPI-ESM-LR-r1 driving Global Climate Model of the EURO-CORDEX (Jacob et al., 2014) climate model ensemble (section 2.2).

Initially, the input time series of the temperature RCPs are considered as stochastic processes characterized by variable daily means and standard deviations. The Box-Jenkins methodology (Box and Jenkins, 1976) is used to simulate the time series of minimum and maximum temperature at Samonas and Psichro Pigadi Station. Thirty temperature realizations are simulated for each climate scenario, while the rainfall input of the original time series is kept constant for each simulation. Results suggest that the range of the temperature input does not significantly affect the flow output (section 3.3).

Input time series from the rainfall RCPs are imported in the Long Ashton Research Station Weather Generator or LARS-WG, and an ensemble of thirty rainfall time series is generated for every initial time series. The generated time series are then used as input

in the SWAT and Karst-SWAT model. The model outcomes are surface flow (provided by the classic SWAT model) and spring flow (provided by the Karst-SWAT) model. The total flow of the basin is considered as the sum of the spring and karst flow. The methodology is schematically illustrated in Figure 2.3 and the stochastic rainfall generator (LARS-WG) and the Karst-SWAT model are described in the sub-sections 2.3.6 and 2.3.3.

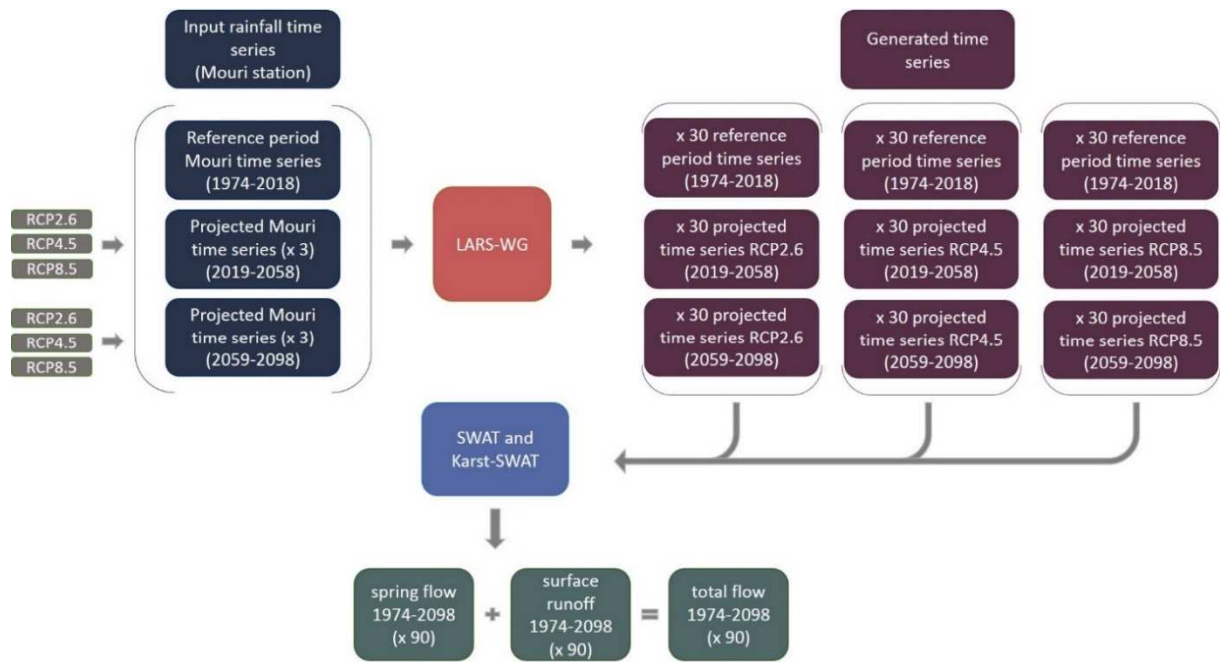


Figure 2.3. Schematic representation of the methodology used to assess the impact of internal rainfall variability (during the reference period and based on climate model projections) to the uncertainty of the Koiliaris river flow (comprising spring flow, surface flow, and total flow).

2.3.6 Simulation of Model Input

The Long Ashton Research Station Weather Generator or LARS weather generator (LARS-WG) is a single-site stochastic weather generator which can simulate rainfall (along with maximum and minimum temperature and solar radiation) under future climate conditions (Racsko et al, 1991; Semenov and Stratonovitch, 2010). The LARS-WG is chosen in order to overcome the limitations of the Markov chain model of rainfall occurrence (Bailey, 1964; Richardson, 1981). The latter considers two rainfall states, wet (non-zero rainfall) and dry (zero rainfall), and transitions based only on the conditions of the preceding day. This is not always sufficient to correctly simulate the maximum dry spell length which is crucial for realistic assessment of water resources in semi-arid regions. The LARS weather generator is selected for its ability to capture long dry spells, which is appropriate for the study site. LARS-WG has been tested at several sites, proving its ability to match the observed data more satisfactorily than the popular WGEN

(Semenov et al., 1998). In addition, LARS-WG has performed well compared to other weather generators in terms of matching the statistical properties of observed rainfall (Mehan et al., 2017). LARS-WG requires tuning more parameters than other generators, which means that a longer series of observed data is required for good parameterization. In addition, it tends to underestimate the inter-annual variance of monthly means, a shortcoming noted in Semenov et al. (1998).

LARS-WG utilizes semi-empirical distributions (defined as the cumulative probability distribution function) for the lengths of wet and dry day time series and for the intensity of daily rainfall. Rainfall occurrence in LARS-WG is modelled as a sequence of alternating wet and dry series. The length of each series is chosen randomly from the wet/dry semi-empirical distribution for the month in which the series begins. The rainfall intensity for wet days is generated from the semi-empirical distribution of rainfall intensity on wet days for the particular month. The intensity value generated for each wet day is independent of the length of the wet series or the amount of rainfall on previous days.

More specifically, the semi-empirical model for the distributions of dry and wet series and for rainfall intensity is defined in terms of a histogram that contains 23 bins, each corresponding to a different event. Histograms are constructed for all seasons in the case of the wet and dry distributions, and for all months in the case of the rainfall intensity distribution. In order to choose random values from the semi-empirical distribution, the generator initially selects one of the histogram bins with a probability that is proportional to the number of events in each bin. Then, it samples a specific value in this bin based on the uniform distribution over the bin values. This empirical distribution is sufficiently flexible to approximate a variety of shapes, as the histogram bins can be adjusted.

Since LARS-WG lacks multivariate capability, it cannot produce correlated time series at multiple locations. Therefore, LARS-WG is applied using the data from Mouri station which has the shortest period (one year) of missing data. Mouri is representative for the permanent springs flow ---although located just outside the karstic watershed--- and is well correlated with the remaining 4 stations. The remaining stations are “simulated” based on Mouri and utilizing their annual correlations. De Silva et al. (2007) suggest that the normal ratio method should be used if any surrounding gauges have a mean annual rainfall which exceeds by at least 10% the mean annual rainfall of the considered gauge with gaps, which in our case is true, as the mean annual rainfall of the stations studied indicates, due to the altitudinal differences of the stations. According to the method, the estimate of the unknown rainfall value is given by:

$$P_X = \frac{N_X}{N_A} P_A \quad (2.11)$$

where P_X and P_A are the daily rainfall values of the missing data station and the station with the available rainfall data respectively, and N_X and N_A are the normal annual rainfall

(mean of 30 years of annual rainfall data) of the missing data station and the station with the available daily data.

Thus, there are five rainfall time series, four of which are generated using the original time series of Mouri. This methodology was initially applied to the available record of daily Mouri data. The SWAT model was run using the Mouri-based rainfall time series. The downscaled and bias corrected time series of the future time series for the Mouri station (period 2019-2098) was also used to generate the future time series of the rest of the stations using the normal ratio methodology.

The number of Monte Carlo realizations (LARS-WG states) was selected by experimenting with different numbers (10, 15, 30, 60, 90, 120, 170, and 220) of rainfall realizations and checking if the range of values of the simulated monthly time series contains at least 95% of the values of the original time series (Gilman, 1968). To reduce the overall computational time, the smallest number of realizations meeting the 95% inclusion criterion is used in the analysis.

The effect of temperature input uncertainty on flow is also tested in this study. Temperature data are available from two stations: Psichro Pigadi and Samonas, which provide daily minimum and maximum temperatures for the period 1974-2018. Daily minimum and maximum temperatures are considered as stochastic processes characterized by variable daily means and standard deviations. The Box-Jenkins methodology (Box and Jenkins, 1970) was used to simulate the time series of minimum and maximum temperature at both stations (Figures A2, A3, Appendix A). Thirty temperature realizations were simulated for each climate scenario while the rainfall input of the original time series was kept constant for each simulation.

In order to investigate the variability of the simulations, box-plots of the standard deviations for each month and all scenarios are constructed. Results suggest that the LARS-WG simulations in certain months do not satisfactorily reproduce the inherent variability of the rainfall. In order to rectify the variability underestimation problem, a linear transformation is applied to those time series that are not adequately simulated by the LARS generator. The transformation generates corrected time series with the same properties (mean and variance) as the original sample (see Appendix A, section A3 for further information).

2.4 Results

2.4.1 Flow Variability due to Model Parameter Uncertainty

The model output vs. the observed daily flow at the basin's exit is shown in Figure 2.4. Three important statistical indices suggested by Moriasi et al. (2007) are calculated. These are the Nash-Sutcliffe Efficiency (NSE) which is the residual variance ("noise") compared to the measured data variance ("information"), the Percent Bias (PBias) which

is the relative (with respect to the true values) model error, and the standard deviation ratio (RSR), which is equal to the root mean square error (RMSE) divided by the standard deviation of the observations. Ultimately, we get: NSE=0.59, PBias=-7.67% and RSR=0.64 for the daily values, and NSE=0.81, PBias=-3.67% and RSR=0.44 for the monthly values. A simulation is considered adequate if $NSE > 0.5$, $|PBias| < 25\%$ and $RSR < 0.7$ (see Moriasi et al., 2007). The satisfactory model indices signify that the selection of the Mouri station for generating the rainfall of the rest of the input stations is suited. The mean annual simulated total flow for the 2004-2018 period is estimated at 833.4 mm/yr (the field data have a mean value of 825.4 mm/yr for the specific period). The flow estimate is converted from cubic meters per second into equivalent runoff depth per year with reference to the area of 211.8 km², which includes the main basin and the extended karstic area

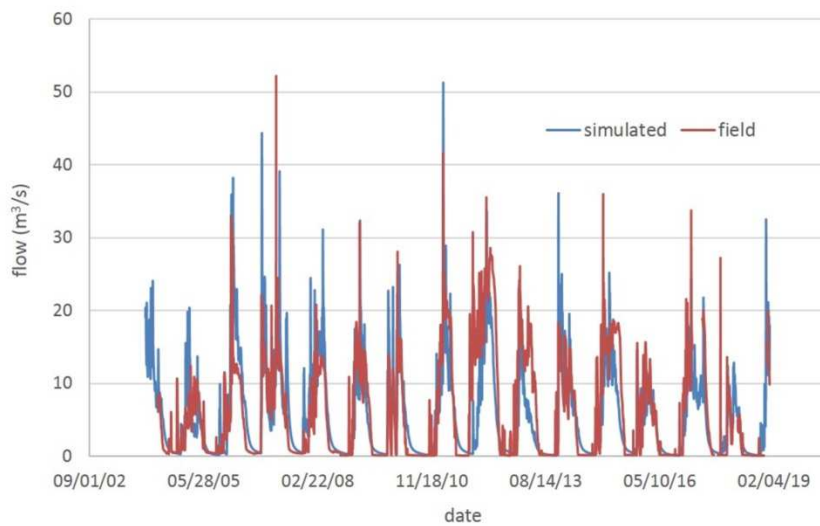


Figure 2.4. Comparison of observed daily flow at the basin's exit with the calibrated daily total flow (i.e., the simulation which gives optimal fit to the data) based on the SWAT model.

2.4.1.1 Variability due to SWAT model parameters

The SUFI2 is used as an uncertainty assessment method for the 2013-2017 period at the station located at the gorge exit. The parameter ranges for the 13 parameters, after the four SUFI2 iterations of 1000 LHS simulations are presented in Table 2.2. The final parameter range varies for each variable and is on average $\pm 38\%$. The P-factor is 94% at the gorge exit, therefore SUFI2 was capable of capturing the majority of the observations, and the algorithm reached a satisfactory R-factor of 0.72. From the final ensemble of the 100 LHS simulations, 60 meet the objective function (r^2 greater than 0.5). The surface flow at the gorge exit is estimated for the 60 behavioral simulations and the standard deviation of the mean annual surface flow at the gorge exit due to the SWAT model parameters is 0.6 mm/yr (Coefficient of Variation (CV) equal to 6.8%) (Figure 2.5). The

standard deviation of the mean annual surface runoff at the basin exit is 46.9 mm/yr (CV equal to 17.1%) for the same simulations. The standard deviation of the weighted mean annual DA_RCHG (sum of mm of water multiplied by the area of the corresponding HRU and divided by the total area of HRUs) due to the SWAT model parameters is 16.1 mm/yr (CV equal to 2.4%, also for the behavioral simulations). It is important to note that the variable “Deep aquifer percolation fraction” (RCHRG_DP) was not included in the list of the 13 variables tested for the uncertainty analysis, since we consider it to take the maximum value (equal to 1) for the karstic HRUs, and zero for the non-karstic HRUs. Therefore, the water quantities entering the deep aquifer are not expected to vary significantly and this justifies the low relative uncertainty range of the DA_RCHG. Each behavioral DA_RCHG time series is used as input into the Karst-SWAT model, providing an equal range of the karstic flow output as the DA_RCHG range (CV equal to 2.4% and standard deviation equal to 2.8 mm/yr). When the surface flow with its uncertainty is added to the karstic flow to form the total flow (we sum the corresponding model runs), the mean annual total flow has a standard deviation of 22.7 mm/yr (CV equal to 2.7%) which is due to the SWAT model parameters alone (Figure 2.6, red dotted lines).

2.4.1.2 Variability due to Karst-SWAT model parameters

For the quantification of the karstic flow uncertainty due to the Karst-SWAT model parameters, four iterations of 1000 simulations are run with the @RISK software. The simulation of the DA_RCHG which corresponds to the best fit simulation of the surface flow at the gorge exit, is used as input to the Karst-SWAT model. We assume that the parameters have a uniform distribution and their values range $\pm 38\%$ of their respective calibrated value. The interval is chosen using the reasoning that the parameters of the two models (SWAT and Karst-SWAT) should vary in the same range for comparison purposes. According to the sensitivity analysis performed with @RISK, the most sensitive parameter is the fraction of the upper reservoir flow to the lower reservoir (a_2), followed by the fraction of inflow to the upper reservoir (a_1), then the recession constant of the lower reservoir (k_l) and finally the recession constant of the upper reservoir (k_u). The resulting standard deviation for the mean annual karstic flow, due to the Karst-SWAT parameters is 49.9 mm/yr (CV is 9.7%) (Figure 2.6, blue dashed lines).

2.4.1.3 Variability due to combined SWAT and Karst-SWAT model parameters

The total uncertainty due to the combination of SWAT and Karst-SWAT model parameters for the total flow can then be estimated. Equation (2.10) gives a total standard deviation of 54.7 mm/yr (CV equal to 6.6%) for the total flow output (using the uncertainties (1) and (2)), stemming from the parameter uncertainty of both models. The total uncertainty due to the combination of SWAT and Karst-SWAT model parameters for the karstic flow can also be estimated by Equation (2.10) using the uncertainty of the karstic flow due to

SWAT parameters (as σ_1) and the uncertainty due to Karst-SWAT parameters (as σ_2). The total uncertainty for the karstic flow is estimated at 49.9 mm/yr (CV equal to 10.0%).

Table 2.2. Definition and estimated range of SWAT model input parameters after four SUFI2 iterations.

Parameter	Definition	Min	Max
r_CN2.mgt	Initial SCS runoff curve number for moisture condition II	-0.95	-0.33
r_SOL_AWC().sol	Available water capacity of the soil layer (mm H ₂ O/mm soil)	1.06	1.97
r_REVAPMN.gw	Groundwater "revap" coefficient	-0.24	0.98
r_CH_N1.sub	Manning's "n" value for the tributary channels.	-0.58	0.48
r_CH_K2.rte	Effective hydraulic conductivity in main channel alluvium (mm/h)	-0.55	0.29
r_ALPHA_BF	Baseflow alpha factor (days)	-2.04	-0.97
r_SURLAG.bsn	Surface runoff lag coefficient.	-0.72	0.11
r_OV_N.hru	Manning's "n" value for overland flow.	-0.67	-0.24
r_CH_K1.sub	Effective hydraulic conductivity in tributary channel alluvium (mm/hr)	0.74	1.59
r_ALPHA_BNK.rte	Baseflow alpha factor for bank storage (days)	-0.24	0.32
r_SOL_Z().sol	Depth from soil surface to bottom of layer	0.56	1.21
r_CH_N2.rte	Manning's "n" value for the main channel	-0.67	0.03
r_SOL_K().sol	Saturated hydraulic conductivity (mm/hr)	-1.44	-0.86

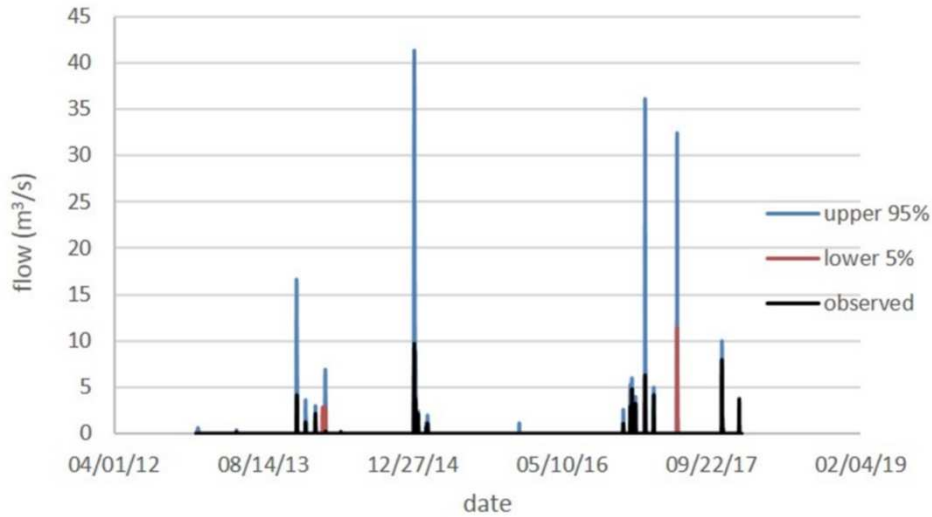


Figure 2.5. Lower 5% (red) and upper 95% (blue) percentiles of the simulated probability distribution of Keramianos river surface flow at the gorge exit versus time and comparison with the observed data (black). The variability of the simulated flow is due to the parameter uncertainty of the SWAT model. Note that the flow at the gorge exit is intermittent.

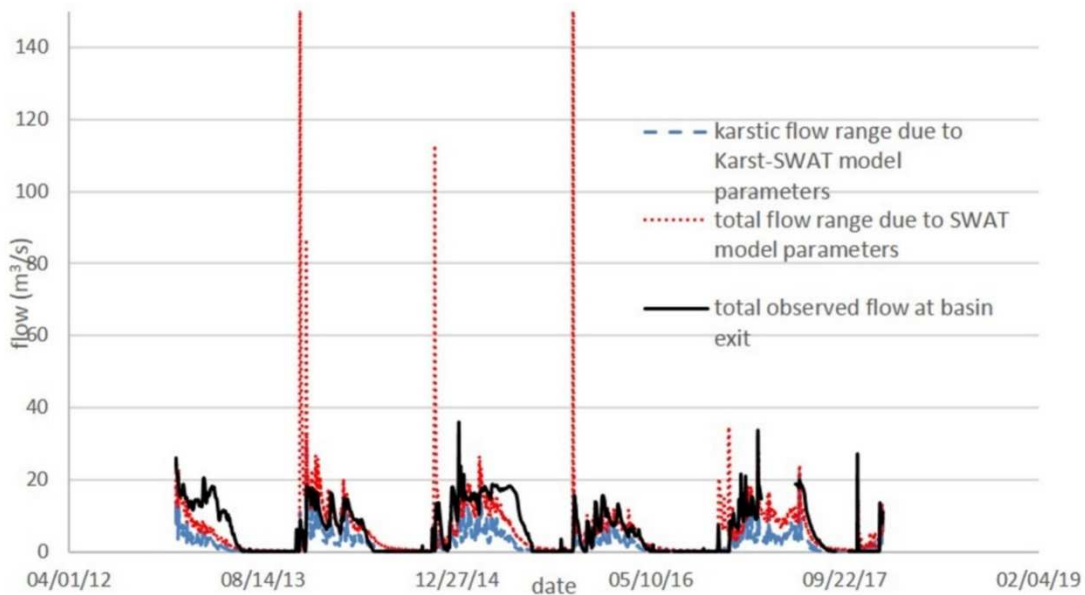


Figure 2.6. Evolution of flow uncertainty over time showing the partition of uncertainty between the SWAT and Karst-SWAT models: red dotted lines mark the total flow uncertainty (based on the 5%-95% percentile range) due to the uncertainty of the SWAT model parameters. Blue dashed lines signify the karstic flow uncertainty due to the Karst-SWAT parameters. The black solid line is the total flow at the basin exit based on the field data.

2.4.2 Flow Variability due to Climate Change Scenario

The time series of rainfall and temperature of the 11 climate scenarios are used as input in the combined SWAT and Karst-SWAT model (calibrated using the optimal parameter set). The mean, range (maximum minus minimum value of mean flow), standard deviation (stdev) and Coefficient of Variation (CV) of the mean annual rainfall, total, karstic and surface flow for the 11 scenarios are presented in Table 2.3 for the two future periods. The mean of the climate change scenarios indicates a slight increase of 3.3% in the period 2019-2058 which leads to an increase of 10.5% in surface flow but a decrease of 2.9% in karstic flow (total flow increases by 1.5%). This is noteworthy, since it means that an increase in rainfall in a karstic region does not necessarily imply increased groundwater resources. When rainfall intensity exceeds the infiltration rate (into the groundwater), the formation of surface runoff in the form of intermittent rivers is favored. This explains the increase in surface flow and decrease in karstic flow. After 2059, the mean of the climate change scenarios indicates a decrease of 7.0% in rainfall, leading to a decrease of 6.1% in surface flow and a decrease of 16.4% in karstic flow (total flow decreases by 13.0%). For this period as well, the impact of climate change is more severe for the groundwater resources.

Rainfall uncertainty propagates through the SWAT model and is amplified in the flow outputs. Uncertainty is higher in surface flow compared to uncertainty in karstic flow. As it is obvious, the climate change envelope increases with time, and the CV in the period 2059-2098 is typically two times higher than the CV during the period 2019-2058. The minimum value of the 2059-2098 period for the karstic flow output over the 11 scenarios, corresponds to the mean annual karstic flow of the RCP8.5 of the REMO model (331.5 mm/yr), while the maximum value corresponds to the mean annual karstic flow of the RCP2.6 of the REMO model (683.1 mm/yr). Thus, the REMO model encompasses the karstic flow ensemble range, which is a critical variable of interest for the specific watershed. Therefore, we use REMO to model the uncertainty due to internal variability. The separate assessment of uncertainty originating from (a) RCM and (b) RCP is quantified using the range to mean ratio (we prefer the range over the standard deviation since the samples are small, i.e. maximum 3 RCPs for each GCM). Results suggest that (i) RCM uncertainties for both karstic and surface flow are always lower than RCP uncertainty and (ii) the divergence between the results of different scenarios increases after 2059, especially for karstic flow. More specifically, for the 2019-2058 period, the RCM uncertainty is 20.4% for karstic and 33.5% for surface flow and the RCP uncertainty is 28.7% for karstic and 46.0% for surface flow (range/mean). For the 2059-2098 period, the RCM uncertainty is 36.6% for karstic and 63.4% for surface flow and the RCP uncertainty is 63.3% for karstic and 91.7% for surface flow.

Table 2.3. Mean, range (maximum minus minimum value of mean annual flow) standard deviation (stdev), coefficient of variation (CV), and ratio to mean (r/m) for rainfall, total, karstic and surface flow for the two future periods (2019-2058 and 2059-2098). The statistics are based on the temperature and rainfall projections according to the 11 selected scenarios (GCM, RCM and RCP combinations) which are used as input in the hydrological models (SWAT and Karst-SWAT with the SUFI2-based calibrated parameters).

variables	2019-2058					2059-2098				
	mean	range	stdev	CV (%)	r/m	mean	range	stdev	CV (%)	r/m
rainfall	1508.9	1309.3-1813.6	139.6	9.3%	0.334	1358.0	1067.9-1897.3	248.9	18.3%	0.611
total flow	845.9	693.4-1032.4	105.7	12.5%	0.401	724.8	480.7-1146.1	203.4	28.1%	0.918
karstic flow	543.4	462.1-622.8	55.1	10.1%	0.269	467.9	331.5-683.1	109.9	23.5%	0.751
surface flow	302.6	231.4-409.6	52.45	17.3%	0.589	256.9	147.1-463.0	94.2	36.7%	1.229
variables	1974-2018									
rainfall	1460.3									
total flow	833.4									
karstic flow	559.8									
surface flow	273.7									

2.4.3 Flow Variability due to Internal Variability of Rainfall

The input time series of rainfall for the SWAT model are simulated as described in section 2.6 for each future sub-period (i.e. 2019-2058 and 2059-2098) and also for the reference period (1974-2018). Results suggest that flow variability resulting from temperature uncertainty is negligible (CV of mean annual flows is less than 0.5% for all scenarios and time periods). Hence, the flow outputs of the Karst-SWAT model are not sensitive to temperature variations. Therefore, for the purpose of assessing the effect of input uncertainties on the hydrological outcome, rainfall is considered as the meteorological key factor that influences the flow output and temperature is not further considered.

For the selection of the number of iterations of rainfall realizations (10, 15, 30, 60, 90, 120, 170, and 220), this range of values of the simulated monthly time series contains 85.6%, 88.8%, 95%, 97.7%, 97.9%, 98.1%, 99.1%, and 99.4% respectively of the values

of the original time series. Therefore, the 30 realizations are selected as the least number of realizations which contain at least 95% of the values of the original time series for all scenarios and for both time windows (2019-2058 and 2059-2098). As far as the total flow simulated by the Karst-SWAT model is concerned, the range of these monthly flow values contains 91.9% to 93% for the 2019-2058 period and 87.7% to 89.4% for the 2059-2098 period, depending on the climate scenario. This indicates the importance of proper rainfall simulation, as the flow output is more sensitive and there is greater uncertainty therein. The results of the model output range stemming from the rainfall uncertainty are depicted in Figure 2.7. The total flow generated from the SWAT model follows the patterns of rainfall (Figure 2.8).

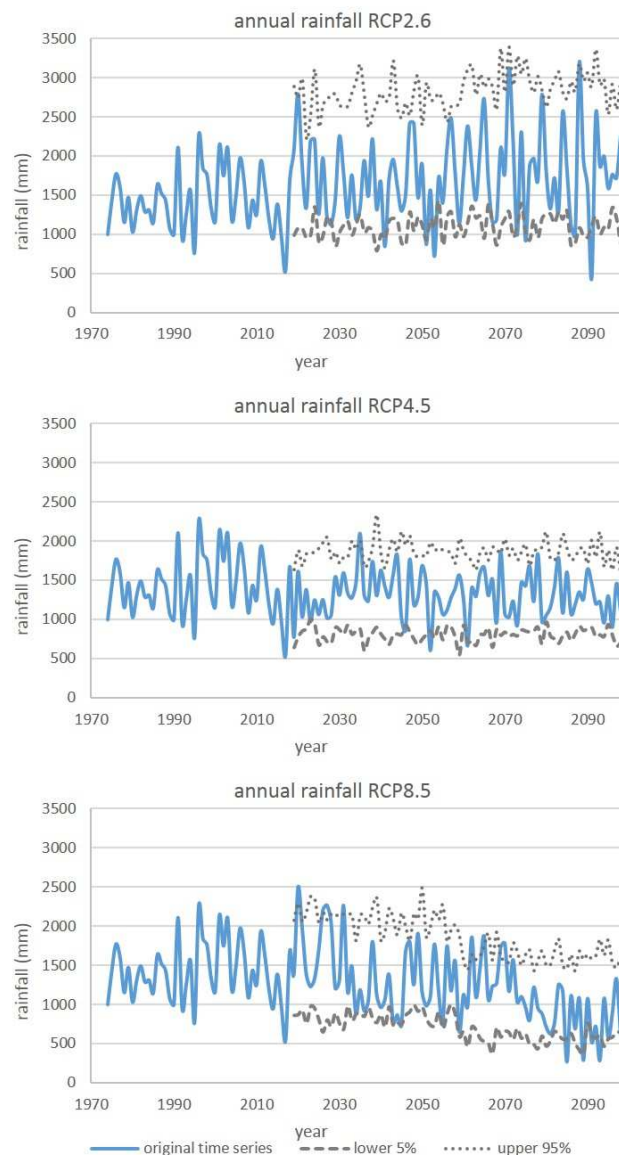


Figure 2.7. Annual rainfall for each climate change scenario: RCP2.6 (top), RCP4.5 (middle) and RCP8.5 (bottom) for the time period 2019 to 2098. The original time series (based on historical data and climate scenario rainfall forecasts) is shown by the blue solid line. The 90% confidence interval of the rainfall values (based on the LARS-WG) is shown by the dashed grey (5% percentile) and dotted grey (95% percentile) lines.

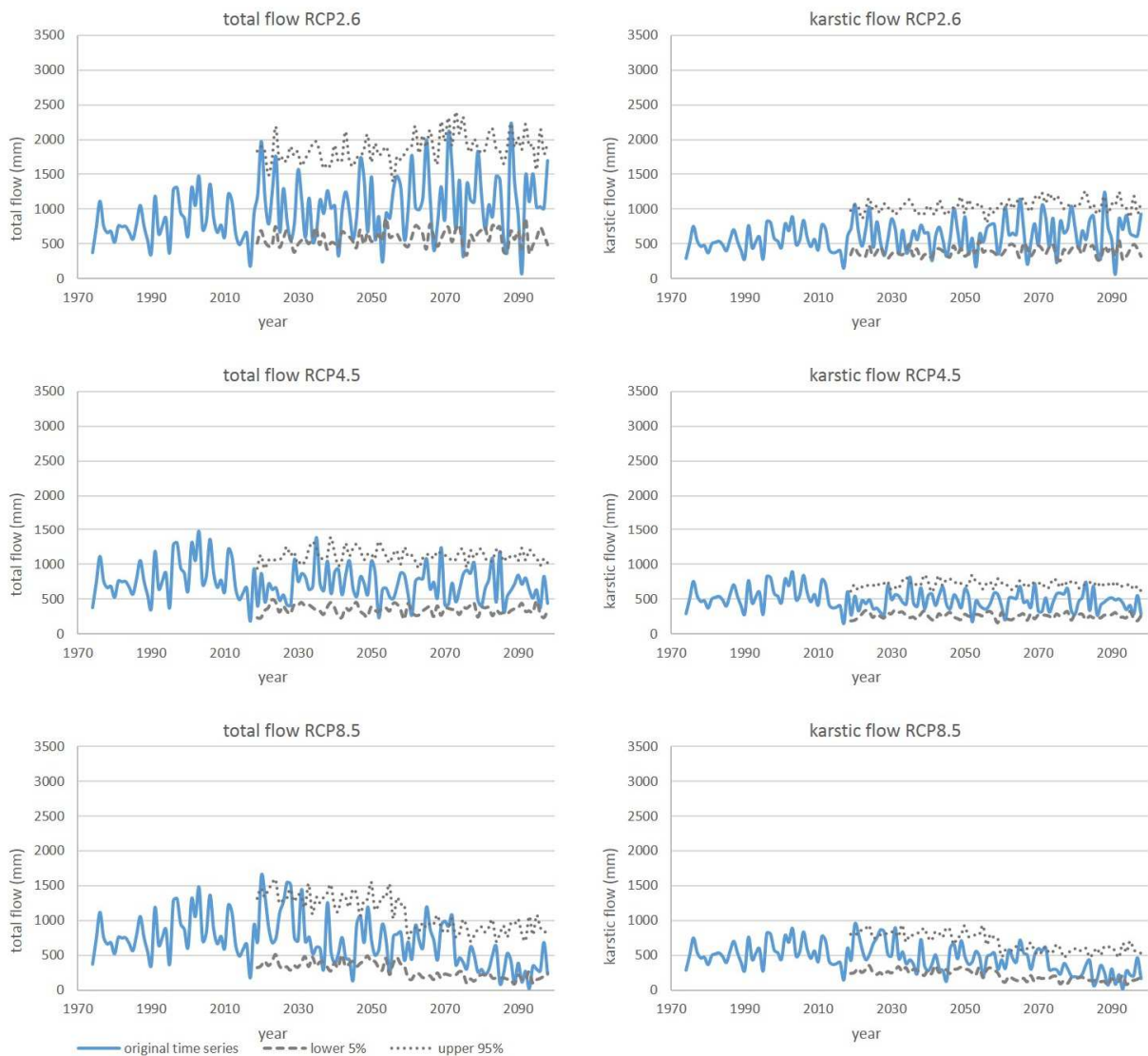


Figure 2.8. Historical data (reference period 1974-2018) and simulations (for the time period 2019 to 2098) of total flow at the Koiliaris basin exit (left) and the respective karstic flow (right). Three different climate change scenarios are used: (top row) RCP2.6, (middle row) RCP4.5 and (bottom row) RCP8.5. The original time series (based on historical data and climate scenario rainfall forecasts) is shown by the blue solid line. The 90% confidence intervals for flow based on the simulated realizations are shown by the dashed (5% percentile) and dotted (95% percentile) lines.

The mean and standard deviation for both the annual total and karstic flow, for the two projected 40-year periods of the three scenarios, RCP2.6, RCP4.5 and RCP8.5, and for the reference period can be summarized in Table 2.4. The mean annual total flow of the reference period based on LARS-WG simulations of the observed rainfall data which are used as input to the SWAT model is 805.4 mm/yr. The RCP8.5 scenario predicts a relatively stable state for the 2019-2058 period compared to the reference period.

However, due to the estimated internal variability, predictions of the mean annual total flow for the RCP8.5 scenario may vary from a decrease of -12.4% to an increase of +5.8%. The RCP4.5, for the 2019-2058 period, respectively, predicts on average a -14.5% decrease with a range of -25.4% to -3.7%. The RCP2.6 scenario predicts an increase ranging from 22.5% to 47.0%. After 2059, the respective changes are as follows: decrease from -46.9% to 32.2% (RCP8.5 scenario), decrease from 26.8% to 8.2% (RCP4.5 scenario), and increase ranging from 27.7% to 63.4% (RCP2.6 scenario). It is noteworthy that the impact of the adverse scenario (RCP8.5) is noticeable after 2059, whereas until then, the intermediate scenario (RCP4.5) has a greater negative influence on flow.

The internal variability of the reference period (1974-2019) expressed as Coefficient of Variation (CV) is 3.7% for the mean annual rainfall, 5.6% for the mean annual total flow, 4.6% for the mean annual karstic flow, and 7.7% for the mean annual surface flow. The internal variability of the emission scenarios, for the future 40-year periods is on average 4.0% for the mean annual rainfall, 5.6% for the mean annual total flow, 5.0% for the mean annual karstic flow and 7.0% for the mean annual surface flow. The internal variability of the future periods is slightly higher than the reference period (with the exception of the RCP8.5 scenario and the 2019-2058 period) and has a small variation between the RCP scenarios. Therefore, the process of analyzing each future period using LARS-WG was useful for the more detailed representation of their internal variability.

We apply the Anderson-Darling test on the annual means of the 30 rainfall samples generated from LARS-WG (for the reference and the future sub-periods and for all three RCPs) and verify that the null hypothesis (normal distribution) cannot be rejected. The same stands for the corresponding SWAT flow outputs (karstic, surface and total flow). The mean and standard deviation of the annual total flow for the reference period (1974-2018) due to the internal variability of rainfall is 805.4 mm/yr and 45.1 mm/yr respectively (CV equal to 5.6%). Considering that the samples follow the Normal Distribution, the range of the distribution can be estimated (the standard deviation of the Normal Distribution corresponds to the 34.1% of the distribution range) and is close to the range of the sample (715.5-895.3 mm/yr). The results imply that, for example, for total flow, climate change signals of up to $\pm 11.1\%$ can be neither identified nor rejected due to internal variability (this percentage is $\pm 15.4\%$ for surface flow and $\pm 9.2\%$ for karstic flow). More specifically, the total flow predictions for the RCP8.5 scenario for the 2019-2058 period, suggest a shift of total flow in the range of -12.4% to +5.8%, and the largest part of this range lies within the $\pm 11.1\%$. This indicates that changes in this period for the RCP8.5 scenario are ambiguous.

Table 2.4. Mean, standard deviation (stdev), and coefficient of variation (within parentheses) for rainfall, total, karstic and surface flow for the two future periods (2019-2058 and 2059-2098) and the reference period (1974-2018). The statistics are based on the simulation of rainfall according to the internal variability for the reference period and the three climate change scenarios. The hydrological models (SWAT and Karst-SWAT) use the SUFI2-based calibrated parameters.

	2019 – 2058			2059 -2098		
variables	RCP 2.6	RCP 4.5	RCP 8.5	RCP 2.6	RCP 4.5	RCP 8.5
	mean/stdev (mm/yr)	mean/stdev (mm/yr)	mean/stdev (mm/yr)	mean/stdev (mm/yr)	mean/stdev (mm/yr)	mean/stdev (mm/yr)
rainfall	1838.0/69.6 (3.8%)	1306.3/57.5 (4.4%)	1424.6/45.8 (3.2%)	1944.2/90.0 (4.6%)	1288.8/50.5 (3.9%)	1068.5/42.7 (4.0%)
total flow	1123.3/51.4 (4.6%)	712.1/45.5 (6.4%)	806.2/38.1 (4.7%)	1212.9/74.8 (6.2%)	687.7/39.0 (5.7%)	503.8/30.8 (6.1%)
karstic flow	675.5/28.5 (4.2%)	473.5/25.5 (5.4%)	518.7/22.2 (4.3%)	719.7/39.2 (5.4%)	459.7/23.6 (5.1%)	347.7/18.9 (5.5%)
surface flow	447.7/23.7 (5.3%)	238.6/20.4 (8.5%)	287.6/16.5 (5.8%)	493.3/36.9 (7.3%)	227.9/16.4 (7.2%)	156.1/12.6 (8.1%)
Reference period (1974-2018)						
rainfall	1446.1/53.3 (3.7%)					
total flow	805.4/45.1 (5.6%)					
karstic flow	543.8/25.3 (4.6%)					
surface flow	261.6/20.2 (7.7%)					

2.4.4 Combined Flow Variability due to Model Parameter Uncertainty and Internal Variability of Rainfall

Considering that the model outputs (karstic, surface and total flow) contain uncertainty due to both parameterization (SWAT and Karst-SWAT) and the internal variability of rainfall, their uncertainties (in terms of standard deviation) can be combined, with the use of Equation (2.10). The results for each output variable are summarized in Table 2.5 (they were computed using the standard deviations of each variable but they are expressed here in terms of Coefficient of Variation). Considering the mean values of Table 2.4 for each variable and time period, and that the standard deviation of the Normal Distribution corresponds to the 34.1% of the distribution range, the estimation of the distribution range of each variable is possible (95% confidence interval). Table 2.6 summarizes the modeled value of each variable for the reference period along with its range (due to both model parameter and internal variability uncertainty) and the ensemble of projections based on all three RCPs used along with their total uncertainty

(stemming from both model parameter uncertainty and rainfall variability). The ranges are based on the lowest 2.5% and the highest 97.5% percentiles of the probability distributions for the three RCPs. It is obvious that the ranges increase after 2059 due to spread of the RCPs (the uncertainty due to parameters is constant, and internal variability does not change significantly among scenarios).

Table 2.5. Contributions of hydrologic model parameter and internal variability (rainfall) uncertainty to the output variable uncertainty (total flow, karstic flow and surface flow). The uncertainty is expressed in terms of the Coefficient of Variation (%). The last column gives the estimate of the total uncertainty.

Variable	Parameter uncertainty (%)	Internal variability (%)	Total uncertainty (%)
total flow	6.6	5.6	8.7
karstic flow	10.0	4.6	11.0
surface flow	17.1	7.1	18.5

Table 2.6. Estimated ranges for the total, karstic and surface flow over the reference period (1974-2018) and the two future periods (2019-2058 and 2059-2098). The range of flows over the reference period and over the future periods takes into account the uncertainty in both the hydrologic model parameters and rainfall. The ranges over the future periods are based on the lowest 5% and the highest 95% percentiles of the probability distributions for the three RCPs.

Variable	Reference period	2019-2058 Range (mm)	2059-2098 Range (mm)
total flow	665.8 – 944.9	588.7 – 1317.9	416.5 – 1423.1
karstic flow	424.7 – 662.9	369.8 – 823.5	271.5 – 877.4
surface flow	165.2 – 358.0	150.7 – 612.7	98.6 – 675.0

2.5 Discussion

This study focuses on estimating the impact of uncertainties on the flow estimates in a karstic Mediterranean watershed with semi-arid climate. We first concentrate on the uncertainties due to model parameters for the reference period. We distinguish between uncertainties that affect the surface flow and are used by the SWAT model and those that define the karstic flow and are used by the Karst-SWAT model. We also estimate their combined effect on karstic and total flow. We then investigate the internal variability of rainfall input time series based on the reference period (during which data are available) and future climate change projections, focusing on the effect of internal variability on surface, karstic and total flow at the watershed’s exit. We derive estimates of the

watershed flow as well as a range of probable values that encompass the impact of uncertainty. We are not concerned with the selection of the optimal climate change model, but rather with assessing the uncertainty of the hydrologic model outputs, given typical climate change model time series. The rainfall generator used (LARS-WG) does not account for the presence of potential trends in the rainfall time series. However, as we are interested in simulating the average statistical features of the 40-year periods and not the temporal evolution, it is not necessary to explicitly model the trend function. Finally, the climate change scenarios do not provide estimates of water needs, due to changes in either population or economic activities (tourism, agriculture/livestock sector) that could affect the hydrologic balance. The analysis of the watershed, therefore, does not at this stage incorporate dynamic socio-economic factors.

This study does not address the uncertainty stemming from hydrologic model selection. However, two other studies have applied two additional models for the quantification of surface and karstic flow at the same region. Kourgialas et al. (2010) used a combination of three models (a karstic model, a GIS-based Energy Budget Snow Melt model, and the Hydrological Simulation Program – FORTRAN model) to assess the surface and karstic flow. Yu et al. (2019) recently developed and applied a coupled surface-subsurface modelling framework (Penn State Integrated Hydrologic Model-PIHM) which is capable of assessing the groundwater flow of a karstic watershed. Both models gave satisfactory goodness of fit with the observed values. Although they were tested for a limited number of years (3 years), the relative error of daily flow values (simulated vs. observed) (3.6% and 2.3% for the calibration period respectively), is equivalent to the daily error of the specific study (3.1%) and similar to that of Nikolaidis et al. (2013) (2.65%), hence the karstic water volume does not differ significantly among the three model setups.

According to our results, the uncertainty of total flow at the basin exit due to hydrological model parameters is estimated at 6.6% (CV), based on the combination of both SWAT and Karst-SWAT model parameters. Specifically, the uncertainty of surface flow is 17.1% and of karstic flow 10.0% (CV). The hydrologic model parameter uncertainty cannot be ignored. Galavi et al. (2019) considered three main sources of uncertainty in an impact study on a basin in Malaysia (Hydrological model parameters, GCMs, and emission scenario uncertainties) and suggested that the hydrological model parameter uncertainty should be included in uncertainty assessment for future periods, although it was the lowest uncertainty contributor in their study. According to Galavi et al. (2019), GCM and emission scenario uncertainties (of RCP4.5 and RCP8.5) increase as time progresses. This observation is also borne out in our study. In our study, however, the relative contribution of RCP uncertainty is higher than that of RCM (in contrast to Galavi et al, 2019, where GCM was higher than RCP uncertainty). This difference is due the fact that we also included the RCP2.6 emission scenario in the analysis.

In their review, Douglas-Mankin et al. (2010) deduce that streamflow parameter uncertainty is higher in regions with high evaporation rates and localized storm patterns,

as well as in arid climate regions compared to humid ones. There are a few studies that investigate the impact of SWAT parameter uncertainty on the estimates of surface flow in Mediterranean watersheds. For example, Sellami et al. (2013), studied the application of SWAT to two watersheds in southern France. The authors conclude that the complexity of the modelled system can affect the uncertainty estimates. Particularly, they found larger prediction uncertainty in the karstic than in the non-karstic catchment. They concluded that SWAT does not rigorously simulate groundwater flow, as most of the unbracketed observations are located in the recession parts of the hydrograph. Our study can enhance parameter uncertainty estimation in karstic watersheds, by analytically assessing the groundwater (karstic) flow and its parameter uncertainty. For the case of karstic flow, the range due to model parameters uncertainty (10.0%) is equally important as the range due to climate change scenario (10.1%); however, the latter more than doubles after 2059 (23.5%)

Our study also quantifies how the internal variability (or stochastic uncertainty) inherent in rainfall time series predicted by climate change time scenarios is propagated to estimates of surface and karstic flows. The mean annual internal variability is on average 3.9% for rainfall, 5.6% for total flow, 4.9% for karstic flow and 7.1% for surface flow (expressed in terms of the coefficient of variation). The rainfall uncertainty range is always lower compared to the uncertainty range of the total and surface flow. The uncertainty range of karstic flow is always lower than that of the surface flow, due to the higher stability of the karstic system. In addition, our analysis includes estimation of the internal variability during the reference and the future periods, although the results would not vary significantly if we had assumed stable variability for the future periods, as in Hawkins and Sutton (2011). This is because the present climate variability is very similar (albeit slightly lower in most cases) to the projections' internal climate variability. The uncertainty due to internal variability for the total flow (5.6%) is similar to the uncertainty due to model parameters in the basin of Koiliaris (6.6%).

A similar study of internal variability was conducted by Fatichi et al. (2014). They used a combination of a stochastic downscaling methodology and the distributed hydrological model Topkapi-ETH, to provide projections of future streamflow (up to year 2050) for two basins, one of which is located in northern Italy (Mediterranean). They also used data from one GCM, i.e., ECHAM5, and two RCMs, i.e., REMO and RegCM3 for the A1B emission scenario combined with two stochastic generators for rainfall and temperature and generated 85 realizations for the future decades. Their results suggest that internal (stochastic) climate variability is a fundamental source of uncertainty, typically comparable or larger than the projected climate change signal. According to their findings, changes up to $\pm 20\%$ of the mean flow cannot be identified. The results of our study suggest that changes up to $\pm 11.1\%$ of the mean total flow and changes up to $\pm 15.4\%$ of the mean surface flow cannot be identified. Liu et al. (2013) demonstrated that in the near future (2021-2051), the effect of climate natural process could dominate over

other uncertainties, whereas in the far future of 2061-2091, climate change owing to greenhouse gas emissions may be the main contributor of total uncertainty. In our study, the comparison of the future 40-year means for all scenarios also reveals that 2019-2058 is a transition period, during which the outcomes of different climate scenarios overlap due to the dominant role of internal variability. In addition, during this period changes in flow are not as significant as those forecasted after 2060, when the particular realization of the emission scenario becomes more important. Northrop and Chandler (2014) also came to a similar conclusion using Bayesian analysis on models obtained from phase 3 of the Coupled Model Intercomparison Project (CMIP3). The projected impact of climate change at the Koiliaris River, and the island of Crete in general, changes significantly as a function of the scenario that will be realized after 2059 [a statement also supported by Joseph et al. (2018)], and ranges from significant flow increases (37.5% for RCP2.6) to significant decreases in flow (42.3% for RCP8.5). The climate change ensemble mean, however, indicates a significant decrease in the mean annual total flow (13.0%) and karstic flow (16.4%) after 2059. The worst case scenario (REMO RCP8.5) predicts a mean karstic flow of 347.7 mm/yr (decrease of 37.9%). Furthermore, by taking the uncertainties of model parameter and internal variability into consideration, the predicted karstic flow can be as low as 271.5 mm/yr (decrease of 51.5%).

2.6 Conclusions

The methodology presented here combines the advantages of climate change impact analysis with those of a fully integrated hydrologic model. The integration of surface and subsurface flow in the same model provides more realistic simulations of water cycle and improved representation of the dominant hydrologic process of groundwater recharge interaction, which is important for impact assessment on groundwater resources. This is the first time, to our knowledge, that a combined assessment of surface and karstic flow model parameter uncertainty and internal variability is applied to a karstic Mediterranean watershed. Our analysis shows that the parameter uncertainty of the hydrologic model and the internal variability of the climate change scenarios should be considered in planning water resources adaptation and mitigation measures that aim to alleviate climate change impacts in watersheds of semi-arid or arid climates, especially for the 2019-2058 period. After 2059, the climate change scenario is the most important uncertainty factor. The methodology presented herein aims to illustrate the range of potential outcomes for flow in karstic watersheds. The case of the Koiliaris River Basin provides a benchmark for comparative studies in other similar regions of the globe, where water needs during the summer are exclusively covered by the flow originating from karstic springs. Accurate estimates of the overall uncertainty are necessary for planning purposes and may reveal possible water deficits that cannot otherwise be identified.

Acknowledgments

This research is co-financed by Greece and the European Union (European Social Fund-ESF) through the Operational Program «Human Resources Development, Education and Lifelong Learning» in the context of the project “Strengthening Human Resources Research Potential via Doctorate Research” (MIS-5000432), implemented by the State Scholarships Foundation (IKY).

The authors would also like to thank Dr. M.G. Grillakis for his contribution to bias correction of the climate dataset used in this article.

References

- Abbaspour, K.C., 2011. SWAT Calibration and Uncertainty Programs: A User Manual. Dübendorf, Switzerland.
- Abbaspour, K.C., Johnson, C.A., van Genuchten, M.T., 2004. Estimating Uncertain Flow and Transport Parameters Using a Sequential Uncertainty Fitting Procedure. *Vadose Zo. J.* 3, 1340–1352. doi:10.2113/3.4.1340
- Abbaspour, K.C., Rouholahnejad, E., Vaghefi, S., Srinivasan, R., Yang, H., Kløve, B., 2015. A continental-scale hydrology and water quality model for Europe: Calibration and uncertainty of a high-resolution large-scale SWAT model. *J. Hydrol.* 524, 733–752. doi:10.1016/J.JHYDROL.2015.03.027
- Agou, V.D., Varouchakis, E.A., Hristopulos, D.T., 2019. Geostatistical analysis of precipitation in the island of Crete (Greece) based on a sparse monitoring network. *Environ. Monit. Assess.* 191, 353. doi:10.1007/s10661-019-7462-8
- Arnold, J.G., Srinivasan, R., Muttiah, R.S., Williams, J.R., 1998. LARGE AREA HYDROLOGIC MODELING AND ASSESSMENT PART I: MODEL DEVELOPMENT. *J. Am. Water Resour. Assoc.* 34, 73–89. doi:10.1111/j.1752-1688.1998.tb05961.x
- Asadieh, B., Krakauer, N.Y., 2017. Global change in streamflow extremes under climate change over the 21st century. *Hydrol. Earth Syst. Sci.* 21, 5863–5874. doi:10.5194/hess-21-5863-2017
- Bailey, N.T.J., 1964. *The elements of stochastic processes, with applications to the natural sciences.* Wiley.
- Bakalowicz, M., 2015. Karst and karst groundwater resources in the Mediterranean. *Environ. Earth Sci.* 74, 5–14. doi:10.1007/s12665-015-4239-4
- Bashfield, A., Keim, A., 2011. Continent-wide DEM creation for the European Union. 34th Int. Symp. Remote Sens. Environ.
- Beven, K., Binley, A., 1992. The future of distributed models: Model calibration and uncertainty prediction. *Hydrol. Process.* 6, 279–298. doi:10.1002/hyp.3360060305
- Beven, K., Freer, J., 2001. Equifinality, data assimilation, and uncertainty estimation in mechanistic modelling of complex environmental systems using the GLUE methodology. *J. Hydrol.* 249, 11–29. doi:10.1016/S0022-1694(01)00421-8
- Box, G.E.P., Jenkins, G.M., 1976. *Time series analysis : forecasting and control.* Holden-Day.
- De Silva, R.P., Dayawansa, N.D.K., Ratnasiri, M.D., 2007. A comparison of methods used in estimating missing rainfall data. *J. Agric. Sci.* 3, 101. doi:10.4038/jas.v3i2.8107
- Deser, C., Alexander, M.A., Xie, S.-P., Phillips, A.S., 2010. Sea Surface Temperature Variability: Patterns and Mechanisms. *Ann. Rev. Mar. Sci.* 2, 115–143. doi:10.1146/annurev-marine-120408-151453
- Deser, C., Phillips, A., Bourdette, V., Teng, H., 2012. Uncertainty in climate change projections: the role of internal variability. *Clim. Dyn.* 38, 527–546. doi:10.1007/s00382-010-0977-x
- Diffenbaugh, N.S., Giorgi, F., 2012. Climate change hotspots in the CMIP5 global climate model ensemble. *Clim. Change* 114, 813–822. doi:10.1007/s10584-012-0570-x
- Douglas-Mankin, K.R., Srinivasan, R., Arnold, J.G., 2010. *Soil and Water Assessment Tool*

- (SWAT) Model: Current Developments and Applications. *Trans. ASABE* 53, 1423–1431. doi:10.13031/2013.34915
- Ertürk, A., Ekdal, A., Gürel, M., Karakaya, N., Guzel, C., Gönenç, E., 2014. Evaluating the impact of climate change on groundwater resources in a small Mediterranean watershed. *Sci. Total Environ.* 499, 437–447. doi:10.1016/J.SCITOTENV.2014.07.001
- Farahmand, A., AghaKouchak, A., 2015. A generalized framework for deriving nonparametric standardized drought indicators. *Adv. Water Resour.* 76, 140–145. doi:10.1016/J.ADVWATRES.2014.11.012
- Fatichi, S., Rimkus, S., Burlando, P., Bordoy, R., 2014. Does internal climate variability overwhelm climate change signals in streamflow? The upper Po and Rhone basin case studies. *Sci. Total Environ.* 493, 1171–1182. doi:10.1016/J.SCITOTENV.2013.12.014
- Ford, D. (Derek C., Williams, P.W. (Paul W., 2007. *Karst hydrogeology and geomorphology*. John Wiley & Sons.
- Galavi, H., Kamal, M.R., Mirzaei, M., Ebrahimian, M., 2019. Assessing the contribution of different uncertainty sources in streamflow projections. *Theor. Appl. Climatol.* 137, 1289–1303. doi:10.1007/s00704-018-2669-0
- Garambois, P.A., Roux, H., Larnier, K., Castaings, W., Dartus, D., 2013. Characterization of process-oriented hydrologic model behavior with temporal sensitivity analysis for flash floods in Mediterranean catchments. *Hydrol. Earth Syst. Sci.* 17, 2305–2322. doi:10.5194/hess-17-2305-2013
- Gilman, J.M., 1968. A brief survey of stopping rules in Monte Carlo simulations. *Proc. Second Conf. Appl. simulations*.
- Giorgi, F., 2006. Climate change hot-spots. *Geophys. Res. Lett.* 33, L08707. doi:10.1029/2006GL025734
- Grillakis, M.G., Koutroulis, A.G., Tsanis, I.K., 2013. Multisegment statistical bias correction of daily GCM precipitation output. *J. Geophys. Res. Atmos.* 118, 3150–3162. doi:10.1002/jgrd.50323
- Gupta, A., Govindaraju, R.S., 2019. Propagation of structural uncertainty in watershed hydrologic models. *J. Hydrol.* 575, 66–81. doi:10.1016/J.JHYDROL.2019.05.026
- Hartmann, A., Gleeson, T., Rosolem, R., Pianosi, F., Wada, Y., Wagener, T., 2015. A large-scale simulation model to assess karstic groundwater recharge over Europe and the Mediterranean. *Geosci. Model Dev.* 8, 1729–1746. doi:10.5194/gmd-8-1729-2015
- Hartmann, A., Lange, J., Vivó Aguado, À., Mizyed, N., Smiatek, G., Kunstmann, H., 2012. A multi-model approach for improved simulations of future water availability at a large Eastern Mediterranean karst spring. *J. Hydrol.* 468, 130–138. doi:10.1016/j.jhydrol.2012.08.024
- Hawkins, E., Sutton, R., 2011. The potential to narrow uncertainty in projections of regional precipitation change. *Clim. Dyn.* 37, 407–418. doi:10.1007/s00382-010-0810-6
- Intergovernmental Panel on Climate Change (Ed.), 2014. *Climate Change 2013 - The Physical Science Basis*. Cambridge University Press, Cambridge. doi:10.1017/CBO9781107415324
- Jacob, D., Kotova, L., Teichmann, C., Sobolowski, S.P., Vautard, R., Donnelly, C., Koutroulis, A.G., Grillakis, M.G., Tsanis, I.K., Damm, A., Sakalli, A., van Vliet, M.T.H., 2018. Climate

Impacts in Europe Under +1.5°C Global Warming. *Earth's Futur.* 6, 264–285. doi:10.1002/2017EF000710

Jacob, D., Petersen, J., Eggert, B., Alias, A., Christensen, O.B., Bouwer, L.M., Braun, A., Colette, A., Déqué, M., Georgievski, G., Georgopoulou, E., Gobiet, A., Menut, L., Nikulin, G., Haensler, A., Hempelmann, N., Jones, C., Keuler, K., Kovats, S., Kröner, N., Kotlarski, S., Kriegsmann, A., Martin, E., van Meijgaard, E., Moseley, C., Pfeifer, S., Preuschmann, S., Radermacher, C., Radtke, K., Rechid, D., Rounsevell, M., Samuelsson, P., Somot, S., Soussana, J.-F., Teichmann, C., Valentini, R., Vautard, R., Weber, B., Yiou, P., 2014. EURO-CORDEX: new high-resolution climate change projections for European impact research. *Reg. Environ. Chang.* 14, 563–578. doi:10.1007/s10113-013-0499-2

Joseph, J., Ghosh, S., Pathak, A., Sahai, A.K., 2018. Hydrologic impacts of climate change: Comparisons between hydrological parameter uncertainty and climate model uncertainty. *J. Hydrol.* 566, 1–22. doi:10.1016/J.JHYDROL.2018.08.080

Kløve, B., Ala-aho, P., Bertrand, G., Boukalova, Z., Ertürk, A., Goldscheider, N., Ilmonen, J., Karakaya, N., Kupfersberger, H., Kværner, J., Lundberg, A., Mileusnić, M., Moszczynska, A., Muotka, T., Preda, E., Rossi, P., Siergieiev, D., Šimek, J., Wachniew, P., Angheluta, V., Widerlund, A., 2011. Groundwater dependent ecosystems. Part I: Hydroecological status and trends. *Environ. Sci. Policy* 14, 770–781. doi:10.1016/J.ENVSCI.2011.04.002

Kourgialas, N.N., Karatzas, G.P., Nikolaidis, N.P., 2010. An integrated framework for the hydrologic simulation of a complex geomorphological river basin. *J. Hydrol.* 381, 308–321. doi:10.1016/j.jhydrol.2009.12.003

Liu, Y., Zhang, J., Wang, G., Liu, J., He, R., Wang, H., Liu, C., Jin, J., 2013. Assessing the effect of climate natural variability in water resources evaluation impacted by climate change. *Hydrol. Process.* 27, 1061–1071. doi:10.1002/hyp.9251

Lu, J., Carbone, G.J., Grego, J.M., 2019. Uncertainty and hotspots in 21st century projections of agricultural drought from CMIP5 models. *Sci. Rep.* 9, 4922. doi:10.1038/s41598-019-41196-z

Malagò, A., Efstathiou, D., Bouraoui, F., Nikolaidis, N.P., Franchini, M., Bidoglio, G., Kritsotakis, M., 2016. Regional scale hydrologic modeling of a karst-dominant geomorphology: The case study of the Island of Crete. *J. Hydrol.* 540, 64–81. doi:10.1016/J.JHYDROL.2016.05.061

Maupin, M.A., Barber, N.L., 2005. Estimated withdrawals from principal aquifers in the United States, 2000, Circular. doi:10.3133/CIR1279

Mckee, T.B., Doesken, N.J., Kleist, J., 1993. THE RELATIONSHIP OF DROUGHT FREQUENCY AND DURATION TO TIME SCALES.

Mehan, S., Guo, T., Gitau, M., Flanagan, D.C., 2017. Comparative Study of Different Stochastic Weather Generators for Long-Term Climate Data Simulation. *Climate* 5, 26. doi:10.3390/cli5020026

Mendlik, T., Gobiet, A., 2016. Selecting climate simulations for impact studies based on multivariate patterns of climate change. *Clim. Change* 135, 381–393. doi:10.1007/s10584-015-1582-0

Mockler, E.M., Chun, K.P., Sapriza-Azuri, G., Bruen, M., Wheeler, H.S., 2016. Assessing the relative importance of parameter and forcing uncertainty and their interactions in conceptual hydrological model simulations. *Adv. Water Resour.* 97, 299–313.

doi:10.1016/J.ADVWATRES.2016.10.008

Moraetis, D., Efstathiou, D., Stamati, F., Tzoraki, O., Nikolaidis, N.P., Schnoor, J.L., Vozinakis, K., 2010. High-frequency monitoring for the identification of hydrological and biogeochemical processes in a Mediterranean river basin. *J. Hydrol.* 389, 127–136. doi:10.1016/j.jhydrol.2010.05.037

Moriasi, D.N., Arnold, J.G., Van Liew, M.W., Bingner, R.L., Harmel, R., Veith, T.L., 2007. Model evaluation guidelines for systematic quantification of accuracy in watershed simulations. *Trans. ASABE* 50, 885–900. doi:10.13031/2013.23153

Moss, R.H., Edmonds, J.A., Hibbard, K.A., Manning, M.R., Rose, S.K., van Vuuren, D.P., Carter, T.R., Emori, S., Kainuma, M., Kram, T., Meehl, G.A., Mitchell, J.F.B., Nakicenovic, N., Riahi, K., Smith, S.J., Stouffer, R.J., Thomson, A.M., Weyant, J.P., Wilbanks, T.J., 2010. The next generation of scenarios for climate change research and assessment. *Nature* 463, 747–756. doi:10.1038/nature08823

Moussu, F., Oudin, L., Plagnes, V., Mangin, A., Bendjoudi, H., 2011. A multi-objective calibration framework for rainfall–discharge models applied to karst systems. *J. Hydrol.* 400, 364–376. doi:10.1016/J.JHYDROL.2011.01.047

Neitsch, S.L., Arnold, J.G., Kiniry, J.R., Williams, J.R., 2009. *Soil and Water Assessment Tool Theoretical Documentation—Version 2009*. Temple.

Nerantzaki, S.D., Efstathiou, D., Giannakis, G. V., Kritsotakis, M., Grillakis, M.G., Koutroulis, A.G., Tsanis, I.K., Nikolaidis, N.P., 2019. Climate change impact on the hydrological budget of a large Mediterranean island. *Hydrol. Sci. J.* 64, 1190–1203. doi:10.1080/02626667.2019.1630741

Nerantzaki, S.D., Giannakis, G.V., Efstathiou, D., Nikolaidis, N.P., Sibetheros, I.A., Karatzas, G.P., Zacharias, I., 2015. Modeling suspended sediment transport and assessing the impacts of climate change in a karstic Mediterranean watershed. *Sci. Total Environ.* 538, 288–297. doi:10.1016/J.SCITOTENV.2015.07.092

Nerantzaki, S.D., Papalexiou, S.M., 2019. Tails of extremes: Advancing a graphical method and harnessing big data to assess precipitation extremes. *Adv. Water Resour.* 134, 103448. doi:10.1016/J.ADVWATRES.2019.103448

Nikolaidis, N.P., Bouraoui, F., Bidoglio, G., 2013. Hydrologic and geochemical modeling of a karstic Mediterranean watershed. *J. Hydrol.* 477, 129–138. doi:10.1016/J.JHYDROL.2012.11.018

Northrop, P.J., Chandler, R.E., Northrop, P.J., Chandler, R.E., 2014. Quantifying Sources of Uncertainty in Projections of Future Climate*. *J. Clim.* 27, 8793–8808. doi:10.1175/JCLI-D-14-00265.1

Orlowsky, B., Seneviratne, S.I., 2012. Global changes in extreme events: regional and seasonal dimension. *Clim. Change* 110, 669–696. doi:10.1007/s10584-011-0122-9

Palisade Corporation, 2010. *Risk Analysis and Simulation Add-In for Microsoft® Excel*. Ithaca, NY USA.

Panwar, S., Chakrapani, G.J., 2013. Climate change and its influence on groundwater resources. *Curr. Sci.* doi:10.2307/24092675

Papalexiou, S.M., Montanari, A., 2019. Global and Regional Increase of Precipitation Extremes under Global Warming. *Water Resour. Res.* 2018WR024067.

doi:10.1029/2018WR024067

Racsko, P., Szeidl, L., Semenov, M., 1991. A serial approach to local stochastic weather models. *Ecol. Modell.* 57, 27–41. doi:10.1016/0304-3800(91)90053-4

Refsgaard, J.C., van der Sluijs, J.P., Brown, J., van der Keur, P., 2006. A framework for dealing with uncertainty due to model structure error. *Adv. Water Resour.* 29, 1586–1597. doi:10.1016/J.ADVWATRES.2005.11.013

Riahi, K., Grübler, A., Nakicenovic, N., 2007. Scenarios of long-term socio-economic and environmental development under climate stabilization. *Technol. Forecast. Soc. Change* 74, 887–935. doi:10.1016/J.TECHFORE.2006.05.026

Richardson, C.W., 1981. Stochastic simulation of daily precipitation, temperature, and solar radiation. *Water Resour. Res.* 17, 182–190. doi:10.1029/WR017i001p00182

Risva, K., Nikolopoulos, D., Efstratiadis, A., Nalbantis, I., 2018. A Framework for Dry Period Low Flow Forecasting in Mediterranean Streams. *Water Resour. Manag.* 32, 4911–4932. doi:10.1007/s11269-018-2060-z

Schindler, A., Toreti, A., Zampieri, M., Scoccimarro, E., Gualdi, S., Fukutome, S., Xoplaki, E., Luterbacher, J., Schindler, A., Toreti, A., Zampieri, M., Scoccimarro, E., Gualdi, S., Fukutome, S., Xoplaki, E., Luterbacher, J., 2015. On the Internal Variability of Simulated Daily Precipitation. *J. Clim.* 28, 3624–3630. doi:10.1175/JCLI-D-14-00745.1

Seager, R., Liu, H., Henderson, N., Simpson, I., Kelley, C., Shaw, T., Kushnir, Y., Ting, M., Seager, R., Liu, H., Henderson, N., Simpson, I., Kelley, C., Shaw, T., Kushnir, Y., Ting, M., 2014. Causes of Increasing Aridification of the Mediterranean Region in Response to Rising Greenhouse Gases. *J. Clim.* 27, 4655–4676. doi:10.1175/JCLI-D-13-00446.1

Sellami, H., Benabdallah, S., La Jeunesse, I., Vanclooster, M., 2016. Quantifying hydrological responses of small Mediterranean catchments under climate change projections. *Sci. Total Environ.* 543, 924–936. doi:10.1016/J.SCITOTENV.2015.07.006

Sellami, H., La Jeunesse, I., Benabdallah, S., Vanclooster, M., 2013. Parameter and rating curve uncertainty propagation analysis of the SWAT model for two small Mediterranean catchments. *Hydrol. Sci. J.* 58, 1635–1657. doi:10.1080/02626667.2013.837222

Semenov, M., Brooks, R., Barrow, E., Richardson, C., 1998. Comparison of the WGEN and LARS-WG stochastic weather generators for diverse climates. *Clim. Res.* 10, 95–107. doi:10.3354/cr010095

Semenov, M., Stratonovitch, P., 2010. Use of multi-model ensembles from global climate models for assessment of climate change impacts. *Clim. Res.* 41, 1–14. doi:10.3354/cr00836

Steinschneider, S., Wi, S., Brown, C., 2015. The integrated effects of climate and hydrologic uncertainty on future flood risk assessments. *Hydrol. Process.* 29, 2823–2839. doi:10.1002/hyp.10409

Taylor, J.R., 1997. *An introduction to error analysis : the study of uncertainties in physical measurements.* University Science Books.

Taylor, K.E., Stouffer, R.J., Meehl, G.A., Taylor, K.E., Stouffer, R.J., Meehl, G.A., 2012. An Overview of CMIP5 and the Experiment Design. *Bull. Am. Meteorol. Soc.* 93, 485–498. doi:10.1175/BAMS-D-11-00094.1

Tzoraki, O., Nikolaidis, N.P., 2007. A generalized framework for modeling the hydrologic

- and biogeochemical response of a Mediterranean temporary river basin. *J. Hydrol.* 346, 112–121. doi:10.1016/j.jhydrol.2007.08.025
- Uniyal, B., Jha, M.K., Verma, A.K., 2015. Parameter identification and uncertainty analysis for simulating streamflow in a river basin of Eastern India. *Hydrol. Process.* 29, 3744–3766. doi:10.1002/hyp.10446
- van Beek, L.P.H., Wada, Y., Bierkens, M.F.P., 2011. Global monthly water stress: 1. Water balance and water availability. *Water Resour. Res.* 47. doi:10.1029/2010WR009791
- van Griensven, A., Meixner, T., 2006. Methods to quantify and identify the sources of uncertainty for river basin water quality models. *Water Sci. Technol.* 53, 51–59. doi:10.2166/wst.2006.007
- van Vuuren, D.P., Lucas, P.L., Hilderink, H., 2007. Downscaling drivers of global environmental change: Enabling use of global SRES scenarios at the national and grid levels. *Glob. Environ. Chang.* 17, 114–130. doi:10.1016/J.GLOENVCHA.2006.04.004
- Wang, F., Polcher, J., 2019. Assessing the freshwater flux from the continents to the Mediterranean Sea. *Sci. Rep.* 9, 8024. doi:10.1038/s41598-019-44293-1
- Wise, M., Calvin, K., Thomson, A., Clarke, L., Bond-Lamberty, B., Sands, R., Smith, S.J., Janetos, A., Edmonds, J., 2009. Implications of limiting CO₂ concentrations for land use and energy. *Science* 324, 1183–6. doi:10.1126/science.1168475
- Wriedt, G., Van der Velde, M., Aloe, A., Bouraoui, F., 2009. Estimating irrigation water requirements in Europe. *J. Hydrol.* 373, 527–544. doi:10.1016/J.JHYDROL.2009.05.018
- Xue, C., Chen, B., Wu, H., 2014. Parameter Uncertainty Analysis of Surface Flow and Sediment Yield in the Huolin Basin, China. *J. Hydrol. Eng.* 19, 1224–1236. doi:10.1061/(ASCE)HE.1943-5584.0000909
- Yang, J., Reichert, P., Abbaspour, K.C., Xia, J., Yang, H., 2008. Comparing uncertainty analysis techniques for a SWAT application to the Chaohe Basin in China. *J. Hydrol.* 358, 1–23. doi:10.1016/j.jhydrol.2008.05.012
- Yen, H., Wang, X., Fontane, D.G., Harmel, R.D., Arabi, M., 2014. A framework for propagation of uncertainty contributed by parameterization, input data, model structure, and calibration/validation data in watershed modeling. *Environ. Model. Softw.* 54, 211–221. doi:10.1016/J.ENVSOFT.2014.01.004
- Yu, X., Moraetis, D., Nikolaidis, N.P., Li, B., Duffy, C., Liu, B., 2019. A coupled surface-subsurface hydrologic model to assess groundwater flood risk spatially and temporally. *Environ. Model. Softw.* 114, 129–139. doi:10.1016/J.ENVSOFT.2019.01.008
- Zhang, J.L., Li, Y.P., Huang, G.H., Wang, C.X., Cheng, G.H., Zhang, J.L., Li, Y.P., Huang, G.H., Wang, C.X., Cheng, G.H., 2016. Evaluation of Uncertainties in Input Data and Parameters of a Hydrological Model Using a Bayesian Framework: A Case Study of a Snowmelt-Precipitation-Driven Watershed. *J. Hydrometeorol.* 17, 2333–2350. doi:10.1175/JHM-D-15-0236.1
- Zhang, R., Corte-Real, J., Moreira, M., Kilsby, C., Birkinshaw, S., Burton, A., Fowler, H.J., Forsythe, N., Nunes, J.P., Sampaio, E., dos Santos, F.L., Mourato, S., 2019. Downscaling climate change of water availability, sediment yield and extreme events: Application to a Mediterranean climate basin. *Int. J. Climatol.* 39, 2947–2963. doi:10.1002/joc.5994
- Zhao, F., Wu, Y., Qiu, L., Sun, Y., Sun, L., Li, Q., Niu, J., Wang, G., Zhao, F., Wu, Y., Qiu, L., Sun,

Y., Sun, L., Li, Q., Niu, J., Wang, G., 2018. Parameter Uncertainty Analysis of the SWAT Model in a Mountain-Loess Transitional Watershed on the Chinese Loess Plateau. *Water* 10, 690. doi:10.3390/w10060690

Chapter 3 Evaluation of the uncertainty of the impact of climate change on flow, sediment and nitrate predictions at the Koiliaris Critical Zone Observatory

Sofia D. Nerantzaki ^{a*}, Nikolaos P. Nikolaidis ^a and Dionissios T. Hristopoulos ^b

^a *School of Environmental Engineering, Technical University of Crete, University Campus, 73100 Chania, Greece*

^b *School of Mineral Resources Engineering, Technical University of Crete, University Campus, 73100 Chania, Greece*

**corresponding author, email: sofia_ner@hotmail.com, +306973475458*

Submitted to the conference: “ADAPTtoCLIMATE Conference, 2019”

Published as: Nerantzaki S.D., Nikolaidis N.P., Hristopoulos D.T., 2019. Evaluation of the uncertainty of the impact of climate change on flow, sediment and nitrate predictions at the Koiliaris Critical Zone Observatory. ADAPTtoCLIMATE Conference Proceedings, June 24-25, Heraklion, Crete.

3.1 Abstract

This study aims to assess the variability in flow and water quality predictions at a Mediterranean karstic watershed due to model parameter uncertainty, internal variability of rainfall input and climate change scenario. To achieve this, we use a modified version of the deterministic Soil Water Assessment Tool (SWAT) which incorporates a model to account for the flow originating from the karstic springs (Karst-SWAT). The SUFI2 algorithm and the @RISK software are used for the quantification of uncertainty due to surface parameters and karstic parameters respectively. A combination of representative climate change models is selected from the EURO-CORDEX climate model ensemble and used for analysis. The rainfall input time series are stochastically modeled using the Long Ashton Research Station Weather Generator (LARS-WG). Monte Carlo simulations for the 2019-2098 time period are used as input to the Karst-SWAT model to assess the uncertainty of the modeled nitrate nitrogen and sediment masses transported through the flow due to internal variability. Results suggest that, after 2059, climate change scenario uncertainty for projections of nitrate nitrogen mass is equivalent to the one of flow projections (25.5%, expressed as the Coefficient of Variation) but it is higher for the case of sediment mass (41.6%). The uncertainty due to internal variability of the sediment mass is also higher (18.5%) than the one of the nitrate nitrogen mass (6.9%), due to the complexity of the erosion process. The combined uncertainty due to hydrologic model parameters and internal variability for the nitrate nitrogen mass is 40.1%, which is greater than the uncertainty due to climate change model. The limited observational data contribute the most to the high parameter uncertainty. Even when considering all these uncertainties, it is forecasted that the Koiliaris River will not have concentrations of nitrate nitrogen higher than the limits suggested by the Water Framework Directive (11.3 mg/L).

Key words: *climate change; parameter uncertainty; internal variability; sediments; nitrates; karstic Mediterranean watershed;*

3.2 Introduction

Climate change impacts on water flow have received a lot of attention but relatively little is known about the respective changes in water quality, especially in the Mediterranean region, regarding sediment transport and erosion (Zhang et al., 2019; Nerantzaki et al., 2016; Nerantzaki et al., 2015; Bussi et al., 2014; Bangash et al., 2013; Maas et al., 2002) or nitrate concentrations (Mas-Pla and Menció, 2019). Even fewer studies have dealt with the ways that climate change affects water quality of karstic aquifers (Hartmann et al., 2014). Both the quality and availability of water resources in the Mediterranean region are expected to change significantly according to the Intergovernmental Panel on Climate Change (IPCC) Synthesis Report (Pachauri et al., 2014). Due to the projected changes in air temperature and rainfall, river flows are expected to be affected and the mobility and dilution of contaminants will also be influenced, but the relationships are not straightforward to capture.

Recent research has also revealed that the water management community has neglected and in many cases underestimated the uncertainties in the projected water quantity and quality, in particular, uncertainties associated with internal climate system variability and hydrologic modelling. The inherent uncertainty that exists in the input time series can significantly affect model outputs and our confidence in the results. In addition, very few studies have addressed the parameter uncertainty quantification issue for the case of sediment simulations (Singh et al., 2014; Sayama et al., 2010) and only recently a couple of studies dealt with the parameter uncertainty assessment of nitrate simulations (Mehdi et al., 2018; Shürz et al., 2019), or both nitrate and sediment simulations (Dakhlalla and Parajuli, 2019). There are no uncertainty assessment studies on water quality simulations, to our knowledge, for the Mediterranean region, where observational data foreshadow a substantial change towards higher temperatures and lower precipitation rates, and lower flows accordingly, and much less over regions with karstic formations.

The aim of this study is to assess the output range in nitrate nitrogen and suspended sediment predictions at a Mediterranean karstic watershed (i.e. the Koiliaris Critical Zone Observatory), due to climate change scenarios, hydrologic model parameters and internal variability of rainfall input. We achieve this by using a modified version of the deterministic Soil Water Assessment Tool (SWAT) which incorporates a karstic model (Karst-SWAT), in combination with a representative set of climate change models. A stochastic rainfall generator (Long Ashton Research Station Weather Generator or LARS-WG), is run under both current and future climate conditions, to generate rainfall time series with the same statistical characteristics as the original (observed and forecasted). The generated time series are used as input in the karst-SWAT model, for the simulation of nitrate nitrogen (hereafter nitrate) and sediment concentrations and masses at the Koiliaris River Basin, in order to explore the uncertainty in present and future predictions. A combination of the SUFI2 algorithm and the @RISK program is used for the parameter

uncertainty assessment of surface and karstic variables respectively. The uncertainties are coupled and the possible range of the variables is assessed.

3.3 Materials and methods

3.3.1 Case study and Data

The Koiliaris Critical Zone Observatory, which represents severely degraded soils due to heavy agricultural impacts such as grazing, over many centuries, represents Mediterranean soils under imminent threat of desertification due to climate change. It is situated in Crete, Greece, 15 km east of the city of Chania. The catchment area is about 130 km². The karstic formations in the basin, which correspond to the Plattenkalk limestones of Figure 3.1, in combination with a fault that extends from the northeast to the southwest, direct water from an extended karstic watershed area towards Stilos springs (Figure 3.1)(Moraetis et al., 2010; Nikolaidis et al., 2013), thus supplying the permanent flow of the Koiliaris river. The overall recharge area of the springs, extends outside the watershed boundaries (Nikolaidis et al., 2013) to the southeast of the watershed boundary, over an area of about 80 km² (Figure 3.1).

In addition to the permanent Stilos spring discharge, there is also a temporary tributary called Keramianos, a temporary spring called Anavreti, and two episodic tributaries (upstream of Anavreti, Figure 3.1), which combine together to compose the Koiliaris river flow system. The total flow at the basin exit is estimated at about 190 hm³/year (Nerantzaki et al., 2015). The Keramianos tributary drains a small sub-catchment that generates surface runoff due to the schist geologic formation of the area. Keramianos stream flows along a karstic gorge (Diktamos gorge) and then over an alluvial plain before joining the Koiliaris river (Figure 3.1). Schist formations are quite friable and in combination with the steep slopes and the adaptation of intensive agricultural practices that are common in the area of Keramianos sub-basin, the top soil becomes extremely brittle and easily erodible. More specifically, due to the abandonment of traditional agricultural practices over the years, tractors now enter and plow the terraces, leading occasionally to their collapse, and exacerbating the erodibility of the soils. In addition, overgrazing leaves the top soil unprotected and vulnerable to surface runoff. Thus, Keramianos is the main tributary responsible for the bulk of the sediment transport in Koiliaris River. On the other hand, waters derived from the karstic springs, have a relatively constant – low – concentration (Nerantzaki et al., 2015).

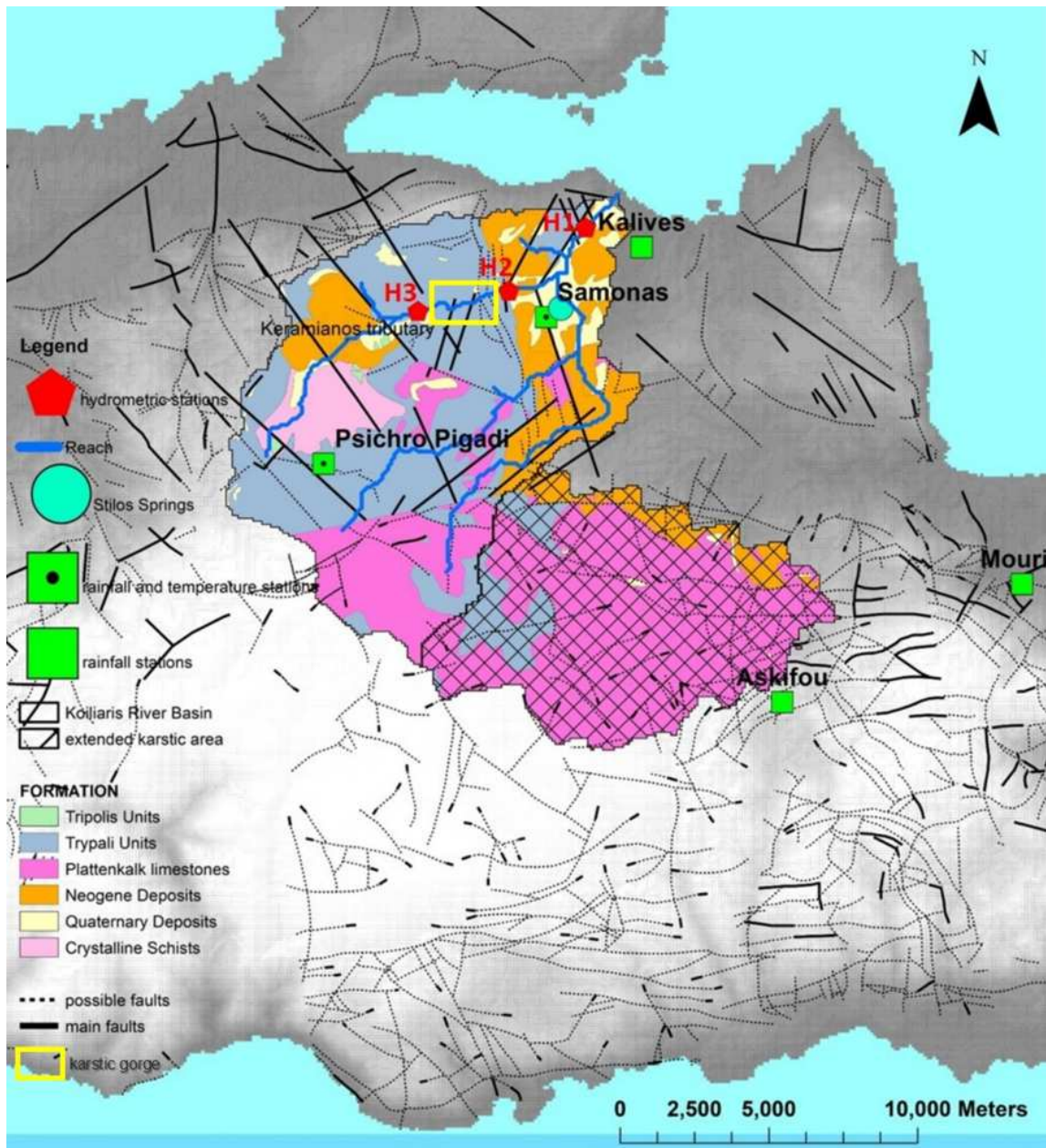


Figure 3.1. Map of Koiliaris River Basin (Crete, Greece) showing precipitation and temperature measurement stations and the modelled extended karstic area

The agricultural land consists of olive groves, citrus groves, vines and vegetables (32.1%) grown with conventional practices such as tilling, irrigation and use of fertilizers. Intensively grazed scrubland/pasture by livestock covers large areas (67.3%) of the watershed at high altitudes and forest (0.6%). The livestock grazing in the watershed and its extended karst numbers 123,987 sheep and goats in 2001. With a grazing area of 16,875 ha, the grazing intensity is 6.8 animals/ha. According to the country's statistics, fertilizer consumption was 405,000 t/year in 2002. Generally, nitrates related pollution is caused through the introduction of excessive amounts of nitrogen to surface and ground waters, mainly as a result of agricultural practices. Intensive cultivation and

livestock grazing have deteriorated significantly soil quality and land fertility. Soils are thin, poorly developed, following the lithology of the area (Nikolaidis et al., 2013).

The data used as input to the SWAT model are provided by five meteorological stations, two of which are located within the watershed boundaries. These stations (at Samonas and Psichro Pigadi, see Figure 3.1) are managed by the “Laboratory of Hydrochemical Engineering and Remediation of Soil” of the Technical University of Crete and record data every 5 minutes. The remaining three precipitation stations at Askifou, Kalives and Mouri are managed by the Region of Crete and are located outside the basin. Data from a telemetric station located near the exit of the basin towards the sea and two hydrometric stations along the Keramianos river bed, recording water level data every 10 minutes, are used to calibrate the SWAT model. In addition to the telemetric data, monthly field campaigns are conducted for both surface and ground water quality measurements at the basin exit nitrate concentration (2004-2010 interrupted time-series) and at station H3, at the gorge entrance (2007-2017). Further details on the monitoring network and data analysis can be found in Moraetis et al., (2010).

Grab samples for the determination of suspended sediment concentration were collected from the Koiliaris River at the hydrometric station H1 (Agios Georgios), on a monthly basis from 2011 to 2014. In addition, samples were also collected after every intense precipitation event in-between December 2013 and February 2014 at the station H3 which is located upstream of the gorge and corresponds to the Keramianos sub-basin.

Data from the meteorological stations are available for the 1979-2018 period (45 years). However, there are periods of missing data for all 5 stations, which are infilled using the normal ratio methodology (as suggested by the American Society of Engineers (1996)) and utilizing monthly correlations between these stations or stations outside the watershed. According to the method, the estimate of the unknown rainfall value is given by: $P_X = \frac{N_X}{N_A} P_A$, where P_X and P_A are the daily rainfall values of the missing data station and the station with the available rainfall data respectively, and N_X and N_A are the normal annual rainfall of the missing data station and the station with the available daily data.

3.3.2 The Karst-SWAT model

The SWAT model (Soil and Water Assessment Tool) is a well-known and widely used deterministic, watershed to river basin-scale, hydrological model, which operates on a daily time step. SWAT can assess the quality and quantity of surface and ground water and predict the environmental impacts of land use, land management practices, and climate change (Arnold et al., 1998; Neitsch et al, 2011). In the model, the watershed is divided into smaller sub-basins in order to separate the tributaries; these are further divided into hydrologic response units (HRUs) which constitute unique combinations of soil type, land use and slope value within the watershed.

Details regarding the methodology followed for the simulation of karstic and surface flow can be found in Nerantzaki et al. (2020). In brief, the SWAT model uses the precipitation as input and simulates the surface hydrologic processes (snow accumulation and melt, surface runoff, infiltration to shallow groundwater and evapotranspiration) over the karst area. The surface water along with the nitrate nitrogen and a percentage of the sediment yield over the karstic areas is then directed to the subsurface. Particularly, we utilize (1) the deep groundwater flow (DA_RCHG in SWAT), (2) the nitrate nitrogen NO₃-N leached past the bottom of the soil profile during the time step (nitrate nitrogen - NO₃L in SWAT), and (3) a percentage of the sediment yield (SYLD in SWAT) from the HRUs located in the karstic areas (see Nerantzaki et al., 2015). We aggregate these variables on a daily step and provide the input to a two-part reservoir karst model (Nikolaidis et al., 2013). The karst model parameters are calibrated, and the resulting flow time series is used as point source input at the spring location. The mass balance equations for the two-part reservoir model are solved analytically for a daily input time step (Nikolaidis et al., 2013). Given that the volume of the two reservoirs reflects the daily volume corresponding to the discharging water from the spring and does not account for the permanent volume of the karst below the spring level, a deep karst factor parameter was introduced in the model equation of the lower reservoir to account for the extra dilution of the incoming chemical loads and in this way provide an estimate of the total volume of the karst.

As far as the sediment transport is concerned, sediment yield from surface erosion is estimated for each HRU with the Modified Universal Soil Loss Equation (MUSLE). Thus, sediment yield is determined by the surface runoff volume, the peak runoff rate, the soil erodibility, the type of land use management and the support practices that are being followed, the slope and the coarse fragment of the soil (Williams, 1975). Sediment routing in the channel consists of two processes operating simultaneously, deposition and degradation. The aforementioned two processes are computed with a simplified version of Bagnold stream power equation. The sediment mass balance of the karst is calculated in a similar manner as the nitrate-N mass balance presented by Nikolaidis et al. (2013). The sampling station H1 is located just downstream of the cross-section where the Keramianos tributary merges with the main river, the latter being fed by the karstic springs. Thus, the sediment and nitrate concentration at the sampling point is assumed to be equal to

$$C_{model} = \frac{Q_{karst} * C_{karst} + Q_{surf} * C_{surf}}{Q_{karst} + Q_{surf}} \quad (3.1)$$

where Q_{karst} and C_{karst} is the flow and concentration (nitrate or suspended sediment) from the karstic springs, Q_{surf} is the surface flow from tributaries and C_{surf} is the concentration of the surface flow. The determination of Q_{karst} is possible through the Karst-SWAT model.

Equations (B10), (B11) (Appendix B) were used for the determination of C_{karst} , while Q_{surf} and C_{surf} are provided from the calibrated SWAT model. The sediment or nitrate concentration from the modified SWAT model given by Equation (3.1) is expected to match the corresponding observed values at station H1.

3.3.3 Model Calibration and Parameter Uncertainty Framework

Nerantzaki et al. (2020) recently established a modeling framework for the assessment of surface and karstic flow variability due to parameter uncertainty. They used the SWAT model with a karstic component (Karst-SWAT) for the surface and karstic flow modeling respectively. For the quantification of the uncertainty stemming from the parameters defining the surface flow and karstic flow, they used the SUFI-2 algorithm with the @RISK software, accordingly. Here we use this framework, adjusted for the nitrate nitrogen mass transferred with the river.

For the case of the nitrate nitrogen simulation, we initially calibrate the SWAT model (manually) by employing the nitrate concentration data at the gorge entrance (station H3). We then calibrate the Karst-SWAT model parameters, using the input (NO3L) by the SWAT model; we use the mixed flow concentration of Equation (3.1) and the observed nitrate concentration data at the basin exit to test the agreement between model and observations.

The next step is to perform the SUFI2 algorithm, using the observed data of nitrate concentration at station H3 for the period 2007–2017. During this period, observational data of the nitrate mass in surface flow are available. These data are limited to 20 measurements of nitrate concentration. The observed concentrations are transformed into nitrate masses by multiplying with the corresponding flows observed at the station H3 during the time of sampling. The SUFI2 algorithm performs 4 iterations of 1000 simulations (based on Latin Hypercube Sampling). We set 10 parameters which affect flow (using the same range as in Nerantzaki et al., 2020) and 6 parameters which affect nitrate concentration, to be altered with every simulation. The parameters are selected based on a sensitivity analysis conducted for numerous variables. It is important to note that the range of the parameters affecting flow is kept constant after each iteration. Nitrate concentration (or mass) is sensitive to both parameters defining flow and parameters defining nitrate generation and transfer, but the flow parameters should not vary beyond the ranges set during the calibration of flow. By keeping the same flow parameters range (as in Nerantzaki et al., 2020), we respect the flow parameters uncertainty and, at the same time, we can examine the nitrate output range based on the parameters which affect the nitrate nitrogen alone. The P-factor and the R-factor are used to quantify the fit between the observed data and the simulated probability distributions. The P-factor is the percentage of observed data contained within the 95PPU. The R-factor is the width of the 95PPU interval divided by the standard deviation of the observed data.

For the simulation of nitrate nitrogen, a value of P-factor at least equal to 0.5 is considered adequate (Abbaspour, 2015). It is also suggested that the R-factor is lower than 1.5 (Abbaspour et al., 2015). The parameters set which gives the best fitted simulation is selected for the calibration of the nitrate mass at station H3.

The above procedure determines the uncertainty of nitrate mass at the gorge entrance (H3). To further quantify the uncertainty of the other output variables (nitrate NO₃-N transported with water at the basin exit (NO₃_OUT), and nitrate nitrogen leached past the bottom of the soil profile (NO₃L) from 46 karstic HRUs), the input parameter range of the final SUFI2 iteration is used to run an additional ensemble of 100 LHS simulations. These allow to quantify the uncertainty range of the surface flow at the basin exit (where no observational data of nitrate concentrations of surface water are available). In addition, this procedure quantifies the uncertainty of the NO₃L from the 46 karstic HRUs, through which the water enters the deep aquifer, thus providing the input range to the Karst-SWAT model.

The next step is the quantification of the uncertainty due to the Karst-SWAT parameters. Once the karst model parameters are calibrated, the @RISK program (Palisade Corporation, 2010) is run using five (karst model) variables which are assumed to follow the uniform distribution. Four of these variables determine the flow and one of these, the nitrate mixing factor, exclusively determines the nitrate concentration of the spring, but the nitrate mass transferred through the spring is sensitive to all of them. Four iterations of 1000 simulations of Latin Hypercube sampling are carried out to determine the uncertainty of the five model parameters that control karstic runoff. The parameters range is set to $\pm 0.38\%$ (see section 3.4.2). The range of the karstic flow for the period 2007–2017 is then calculated.

The final step is to quantify the parameter uncertainty of both SWAT and Karst-SWAT models. According to Taylor (1997), a good measurement of the uncertainty δx of variable x is the standard deviation σ_x . If variable x is measured with independent and random uncertainties σ_1, σ_2 , then the uncertainty σ_x is

$$\sigma_x = \sqrt{(\sigma_1)^2 + (\sigma_2)^2}. \quad (3.2)$$

Equation (3.2) can be used to estimate the “nitrate mass in total flow” uncertainty σ_x that results from (1) the uncertainty of nitrate mass in surface and karstic flow due to SWAT parameters, and (2) nitrate mass in karstic flow uncertainty due to Karst-SWAT parameters. The total uncertainty, due to the parameters from (i) SWAT and (ii) Karst-SWAT for the variable of the nitrate mass in the karstic flow alone (3), can be also calculated in a similar manner.

This framework is used for the uncertainty assessment of nitrate mass in the river. The framework could not be used for the case of suspended sediments in the Koiliaris River Basin, as the sub-basin for which the sediment data are available (a) has limited observed

data and (b) produces higher amounts of sediment (high erosion rate) compared to the rest of the sub-basins of the watershed. Therefore, we cannot assume uniform properties and, therefore, similar parameter ranges for the whole watershed, as we did for the case of nitrate mass, for the estimation of the non-observed variables (i.e. the sediment concentration at the basin exit, where no observed data are available).

3.3.4 Climate Change Scenarios

A sub-set of simulations is selected from the recent high resolution (12.5 km) climate model ensemble, the EURO-CORDEX (EUR-11) (Jacob et al., 2014). The Global Climate Models (GCMs) simulations of the EURO-CORDEX have been conducted within the Coupled Model Intercomparison Project Phase 5 (CMIP5) representing various scenarios of greenhouse gas emission pathways. The regional simulations downscale the global climate projections of CMIP5 (Taylor et al., 2012) and the RCPs (Moss et al., 2010; van Vuuren et al., 2007). EURO-CORDEX scenario simulations use the RCPs defined for the Fifth Assessment Report of the IPCC (Moss et al., 2010).

The RCM simulated temperature and precipitation data (for each emission pathway) are adjusted for biases against a thirty-year period between 1980 and 2009 that served as reference for the correction. The quantile mapping methodology known as multi-segment statistical bias correction (MSBC) is used (Grillakis et al., 2013). The bias correction of the RCM data is performed using point observations, hence the correction procedure also serves for the parameter downscaling.

The rainfall data for both reference (1979-2018) and projected period (2019-2098) for the selected models are analyzed. The future period is divided into two separate sub-periods corresponding to the years 2019-2058 and 2059-2098. This division was applied for two reasons: (1) the intensity of the precipitation and the duration of wet and dry periods changes significantly after 2060 and (2) at least 40 years of observed data are required to reliably calibrate the LARS-WG generator. Eventually, there is one time series for the reference period, and six time series referring to the projected time period (2019-2098), two per RCP, which are used as input for the LARS-WG.

3.3.5 Rainfall Simulation

The LARS weather generator (LARS-WG) is a single-site stochastic weather generator which simulates rainfall under present and future climate conditions (Semenov and Stratonovitch, 2010; Semenov et al., 1998; Racsko et al., 1991). LARS-WG is chosen in order to overcome the limitations of the Markov chain model of precipitation occurrence (Bailey et al., 1964; Richardson, 1981; Richardson and Wright, 1984). The latter considers two precipitation states, wet (non-zero rainfall) and dry (zero rainfall), and transitions based only on the conditions of the preceding day. This is not always sufficient to correctly

simulate the maximum dry spell length which is crucial for realistic assessment of water resources in semi-arid regions. LARS-WG has performed well compared to other weather generators by means of reproducing the statistical characteristics of observed rainfall (Mehan et al., 2017). The rainfall simulation technique followed by the latest version of the LARS-WG is described in detail in Semenov and Stratonovitch (2010). The LARS-WG utilizes semi-empirical distributions for the lengths of wet and dry day time series and for the intensity of daily precipitation. Precipitation occurrence WG is modelled as a sequence of alternating wet and dry series. The length of each series is chosen randomly from the wet/dry semi-empirical distribution for the month in which the series begins. The precipitation intensity for wet days is generated from the semi-empirical distribution of rainfall intensity on wet days for the particular month. The intensity value generated for each wet day is independent of the length of the wet series or the amount of precipitation on previous days.

LARS-WG is applied for the time-series of the Mouri station, which has the shortest period (one year) of missing data. Although located just outside the karstic watershed, Mouri is representative for the permanent springs flow and is the single station which is well correlated with the remaining 4 stations (Psichro, Samonas, Kalives and Askifou). Since LARS-WG cannot produce correlated time series at multiple locations, the remaining stations are “simulated” based on Mouri using the normal ratio methodology described in section 3.3.1. Thus, correlated time series are generated for the remaining four stations. The calibrated SWAT model was run using the Mouri-based rainfall time series. The results show that the fit between the predicted and observed flow values is satisfactory (see Figure 3.3 and section 3.4.1), which supports the selection of Mouri station as model input.

3.3.6 Assessment of Internal Variability

The input time series consist of the rainfall time series at Mouri station for the reference period (1979-2018) as well as the projected time series for the same station, based on three Representative Concentration Pathways (RCPs), i.e. RCP2.6, RCP4.5, and RCP8.5 of the CSC-REMO (Jacob et al., 2012) Regional Climate Model (section 3.3.4). The input time series from the RCPs are imported in the LARS-WG, and an ensemble of thirty time series (x30 in Figure 3.2) is generated for every initial time series. The generated time series are then used as input in the Karst-SWAT model. The model outcomes are surface runoff (provided by the classic SWAT model), spring flow (provided by the Karst-SWAT) model, nitrate concentration and sediment concentration at the basin exit (combination of classic SWAT and Karst-SWAT). The total flow of the basin is considered as the sum of the spring and karst flows. The sediment and nitrate mass of the surface flow are outputs of the SWAT model and the Karst-SWAT provides the nitrate and sediment mass through the spring. The methodology is schematically illustrated in Figure 3.2 and the stochastic

rainfall generator (LARS-WG) and the Karst-SWAT model are described in the subsections 3.3.5 and 3.3.2.

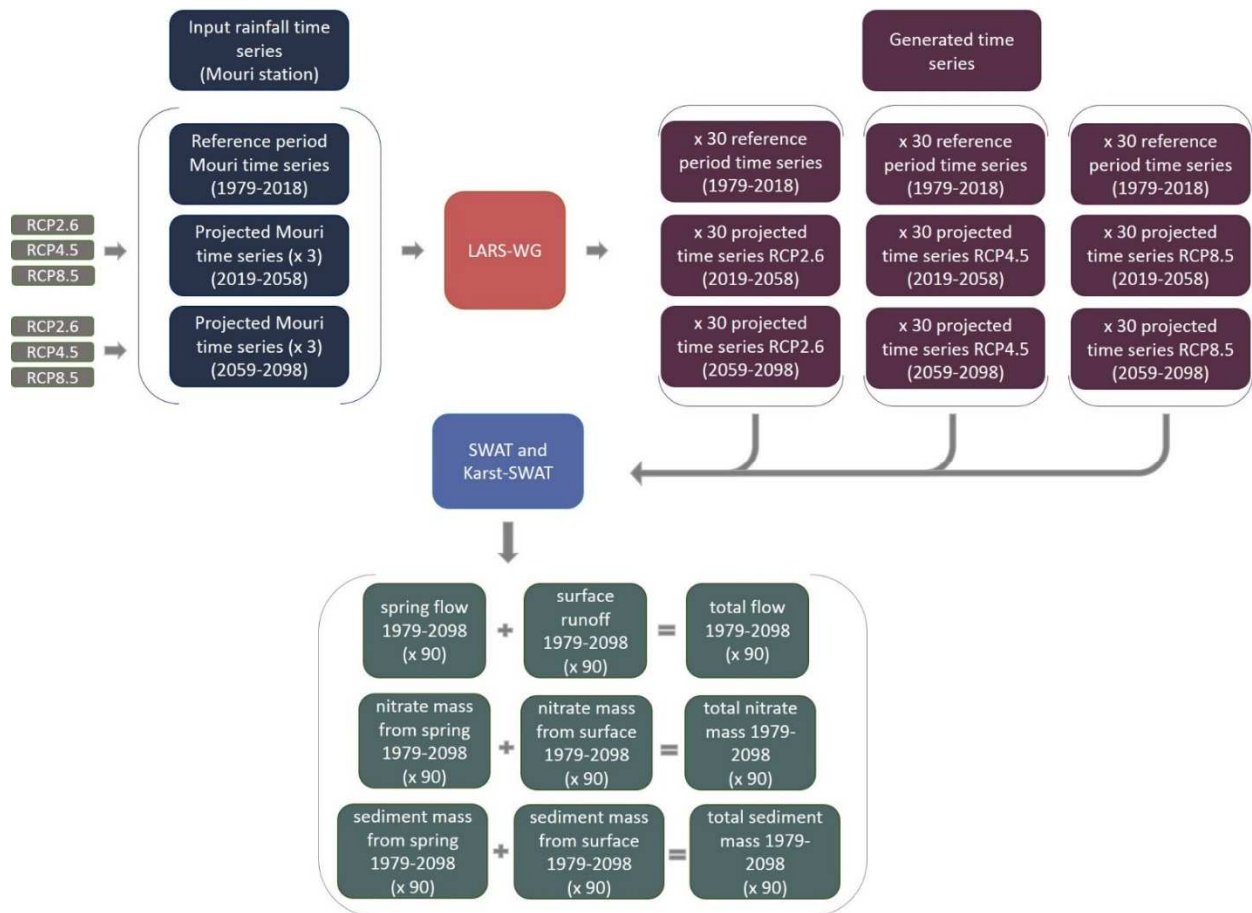


Figure 3.2 Schematic representation of the methodology followed to assess internal variability effect on the total flow, sediment and nitrate export of the Koiliaris River for the reference and future periods.

3.3.7 Monte Carlo Simulations

The six time series derived from the emission scenarios along with the reference period time series, are stochastically modeled using the LARS-WG. In order to select the optimum number of Monte Carlo simulations, we experiment with different numbers (10, 15, 30, 60, 90, 120, 170, and 220) of rainfall realizations and at the same time we check if the range of values of the simulated monthly time series contains at least 95% of the values of the original time series (Gilman, 1968). The respective percentage for each number of realizations is given respectively by 85.6%, 88.8%, 95%, 97.7%, 97.9%, 98.1%, 99.1%, and 99.4%. To reduce the overall computational time, the smallest number of realizations

meeting the 95% inclusion criterion, i.e., 30 realizations, is used in the analysis (as in Nerantzaki et al., 2020)

3.4 Results

3.4.1 Hydrologic Model Goodness of Fit

The agreement between the calibrated model (using SUFI2) for the reference period 2004-2013 (using the original rainfall time series at Mouri, and rainfall at the other four stations based on Mouri, see section 2.3) and the observed daily flow at the basin's exit is shown in Figure 3.3. The final P-factor was estimated at 0.58 and the R-factor was 1.20. The statistical indices suggested by Moriasi et al. (2007), namely the Nash-Sutcliffe Efficiency (NSE) which is the residual variance ("noise") compared to the measured data variance ("information"), the Percent Bias (PBias) which is the deviation of data being evaluated expressed as a percentage, and the standard deviation ratio (RSR), which is equal to the root mean square error (RMSE) divided by the standard deviation of the observations, were calculated leading to: NSE=0.59, PBias=-7.67% and RSR=0.64 for the daily values, and NSE=0.81, PBias=-3.67% and RSR=0.44 for the monthly values. A simulation is considered adequate if $NSE > 0.5$, $|PBias| < 0.25$ and $RSR < 0.7$ (Moriasi et al., 2007).

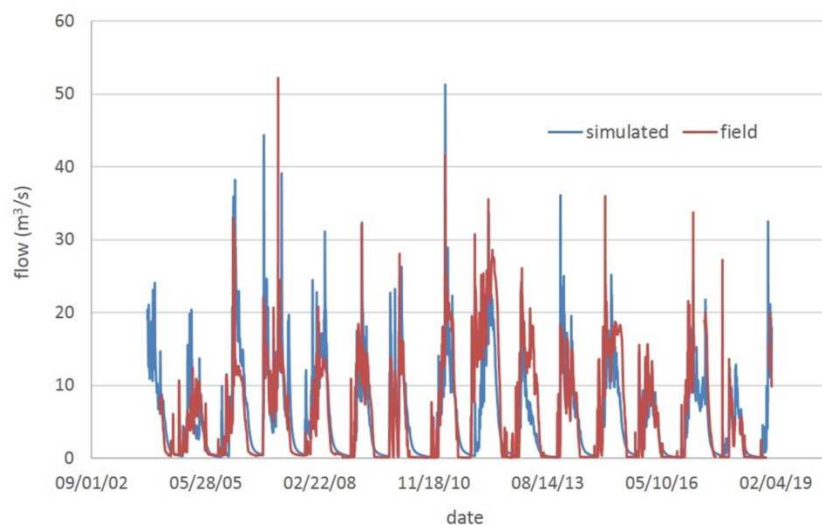


Figure 3.3. Comparison of observed daily flow at the basin's exit with the calibrated daily total flow (i.e., the simulation which gives optimal fit to the data) based on the SWAT model.

The model output (calibrated with the SUFI2) for nitrate and sediment concentration at the basin exit is presented in Figure 3.4 (again, the graphs are a result of the model which uses the original rainfall time series at Mouri, and rainfall at the other four stations based on Mouri). A simulation is considered adequate for water quality simulations if $NSE > 0.5$, $|PBias| < 70\%$ and $RSR < 0.7$. The nitrate simulation yielded NSE equal to 0.6, PBias 45.8

% and RSR 0.65. As far as the simulation of sediments is concerned, for the 2011–2014 period, the NSE is 0.97, the PBias is 53.0 % and RSR is 0.16 for the daily records.

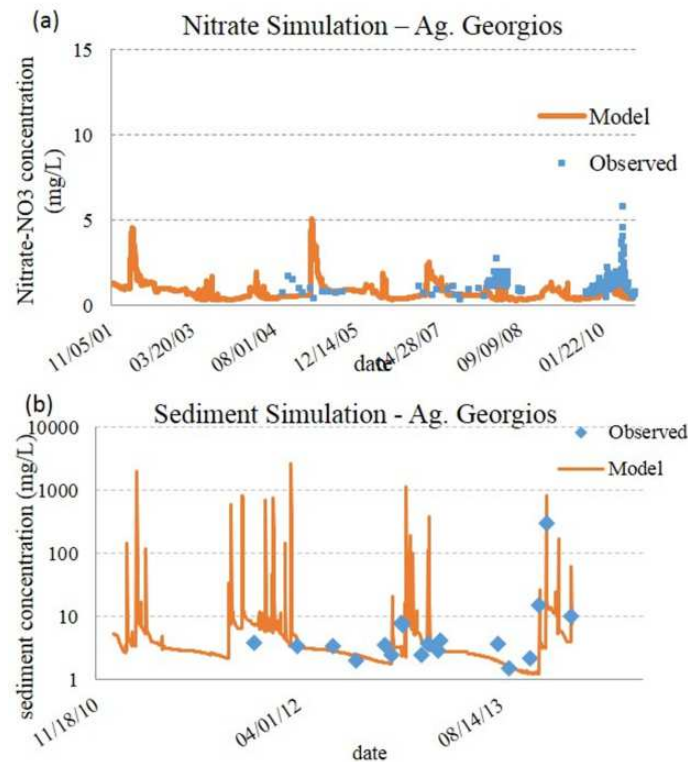


Figure 3.4 Validation of karst-SWAT model output, calibrated using the SUFI2 algorithm ((a) nitrate concentrations and (b) sediment concentrations), using rainfall input from Mouri and four other stations, with observed data at the basin’s exit.

3.4.2 Variability due to Hydrologic Model Parameters

The parameters used in SUFI2 are presented in Table 3.1 along with their final ranges. The classification of the parameters according to their sensitivity over nitrate mass (in the surface flow) is also indicated. These parameters yield a range of mean annual nitrate nitrogen mass at the basin exit equal to 77.0% (expressed as the standard deviation divided by the mean, i.e. Coefficient of Variation or CV). The mean annual nitrate mass leached in the groundwater has an uncertainty of 45.5%, which is equal to the uncertainty of the karstic flow due to the SWAT model parameters. The variability of the flow at the basin exit due to the uncertainty of parameters affecting the surface flow is equal to 17.1% (see Nerantzaki et al., 2020). In other words, 22.2% of the nitrate mass uncertainty is due to the parameters affecting the flow.

The Karst-SWAT model parameters range yielded an uncertainty in nitrate mass in karstic flow equal to 10.8%, using the @RISK software. The corresponding uncertainty for the karstic flow was estimated at 9.7% using the four karstic parameters defining karstic flow, according to Nerantzaki et al. (2020). Uncertainty analysis performed using the same program, revealed that the nitrate mixing factor is the most sensitive parameter,

followed by the lower reservoir recession parameter, the fraction of water moving from the upper to the lower reservoir, the fraction of the inflow to the upper reservoir and, finally, the upper reservoir recession constant.

With the use of Equation 3.2, the total uncertainty of the nitrate mass in the karstic flow is 93.2 t/year and the CV is equal to 46.8%. Using the same Equation, the total uncertainty in nitrate mass exported at the exit of the basin due to both SWAT and Karst-SWAT models is 113.6 t/year (CV equal to 40.1%).

Table 3.1. Definition and estimated range of SWAT model input parameters after four SUFI2 iterations. The first 10 parameters influence both flow and nitrate outputs, the last 6 parameters affect only nitrate outputs. The numbers in brackets indicate the sensitivity rankings for the nitrate flux at the entrance of the gorge, with “1” being the most sensitive parameter.

Parameter	Definition	Min	Max
(2) r_CN2.mgt	Initial SCS runoff curve number for moisture condition II	-0.95	-0.33
(5) r_CH_N1.sub	Manning's "n" value for the tributary channels.	-0.58	0.48
(10) r_CH_K2.rte	Effective hydraulic conductivity in main channel alluvium (mm/h)	-0.55	0.29
(3) r_SURLAG.bsn	Surface runoff lag coefficient.	-0.72	0.11
(13) r_OV_N.hru	Manning's "n" value for overland flow.	-0.67	-0.24
(4) r_ALPHA_BNK.rte	Baseflow alpha factor for bank storage (days)	-0.24	0.32
(15) r_SOL_Z().sol	Depth from soil surface to bottom of layer	0.56	1.21
(7) r_CH_N2.rte	Manning's "n" value for the main channel	-0.67	0.03
(8) r_GWQMN.gw	Threshold depth of water in the shallow aquifer	-0.92	-0.67
(1) r_SOL_K().sol	Saturated hydraulic conductivity (mm/hr)	-1.44	-0.86
(6) r_SHALLST_N.gw	Initial concentration of nitrate in shallow aquifer. (mg N/L).	-0.90	0.03
(14) r_RCN.bsn	Concentration of nitrogen in rainfall	-0.10	0.71
(9) r_N_UPDIS.bsn	Nitrogen uptake distribution parameter	-0.22	0.34
(11) r_CDN.bsn	Denitrification exponential rate coefficient	-0.89	0.04
(16) r_SDNCO.bsn	Denitrification threshold water content	-0.22	0.35
(12) r_SOL_NO3().chm	Initial concentration in soil layer	-0.04	0.89

3.4.3 Variability due to Climate Change Scenarios

The time series of rainfall and temperature of the 11 climate scenarios are used as input in the combined SWAT and Karst-SWAT model (calibrated using the optimal parameter set). The mean, range (maximum minus minimum value of mean flow), standard deviation (stdev) and Coefficient of Variation (CV) of the mean annual rainfall, total, karstic and surface flow for the 11 scenarios are presented in Table 3.2 for the two future periods. The values for rainfall and flows are given by Nerantzaki et al. (2020).

Following the patterns of flow, when comparing the future annual averages of the variables under the 11 scenarios, we have that the total nitrate mass increases during the period 2019-2058 (12.2%) and decreases after 2059 (23.7%). The nitrate mass transferred by the surface flow increases by 24.7% during the period 2019-2058 and continues to increase (10.1%) during the period 2059-2098. Conversely, the nitrate mass transferred through the spring increases slightly in the period 2019-2058 (4.8%) and decreases significantly after 2059 (37.5%). This occurs due to the fact that flash floods are expected to increase (despite the slight decrease in surface flow) thus favoring the flushing of nitrates. Analysis of the upper 10% quantile of the maximum nitrate concentrations in surface flow, revealed that most scenarios predict that there will be higher maximum concentrations in their time series compared to the reference period (Figure 3.5a). The Water Framework Directive (91/676/EEC – Nitrates Directive) for Nitrates has set a limit of maximum concentration equal to 50 mg/L for drinking waters, indicating good chemical status, which refers to total nitrate; when converted to nitrate nitrogen concentration, the maximum nitrate nitrogen concentration is equal to 11.3 mg/L. The World Health Organization guideline for drinking water is also less than 11.3 mg/L of NO₃-N. The mean annual concentration of nitrate nitrogen in the reference and future periods is very low compared to this limit (see Table 3.2). Regarding the daily concentrations of total nitrate nitrogen at the basin exit, these exceed the above mentioned limit 0.05% of the time during the 40 year reference period (1979-2018), and on average (based on the 11 climate change scenarios) 0.24% of the time during the 40 year period of 2059-2098 (ranging from 0 to 0.78%).

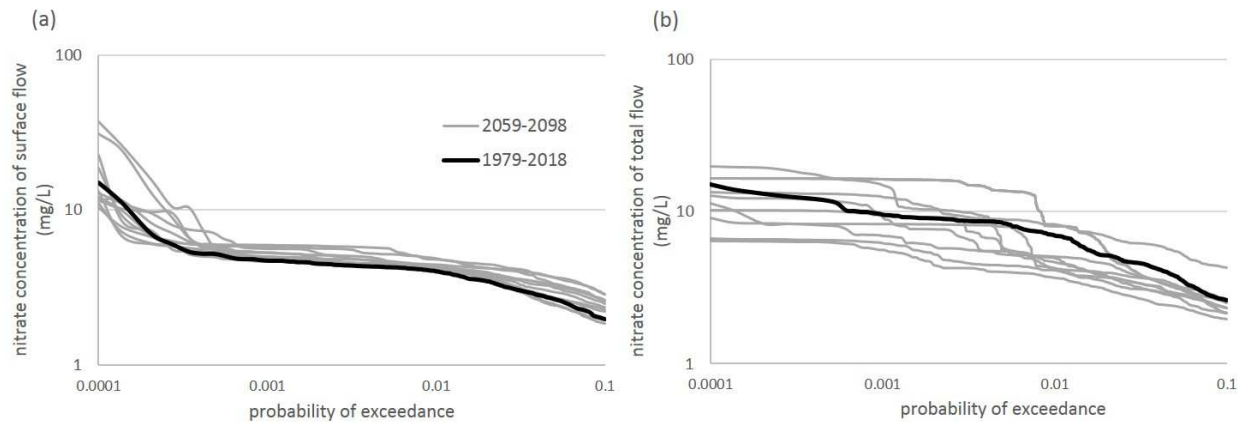


Figure 3.5. Probability of exceedance for the upper 10% quantile of the nitrate concentrations distribution of (a) total flow and (b) surface flow of the reference period 1979-2018 (black line) and the period 2059-2098 period based on the 11 scenarios (grey lines).

The total sediment mass decreases until 2059 (28.3%) and is stable after 2059 (low increase of 1.1%). For the case of sediments, the sediment mass delivered by the spring increases significantly after 2059 (740.6%) while the sediment mass of the surface flow decreases (38.2%), leading to stable total sediment mass at the basin exit. This difference between the progress of sediment and nitrate masses in the future is based on the spatial distribution of their sources. The nitrate production is homogeneous all over the Koiliaris River Basin, whereas the sub-basins of the watershed have different erodibilities. The majority of the sub-basins located inside the watershed are non-erodible, with the exception of the sub-basin of Keramianos. However, most of the sub-basins of the extended karst area are highly erodible, mainly due to their steep slopes. Therefore their sediment yield increases substantially due to the prevalence of torrent rain in the future, thus amplifying the sediment transport through the spring.

After 2059, the uncertainty range of the variables due to climate change scenario increases significantly, with the exception of the nitrate and sediment mass originating from the springs. Most scenarios agree that the sediment mass from the spring tends to increase and nitrate mass from the spring tends to decrease. Generally, nitrate follows the patterns of flow, therefore nitrate from the spring decreases as karstic flow decreases. Sediment, on the other hand, acts more independently. Due to the succession of longer dry periods and intense rainfall, sediment yield increases, especially in the erodible extended karstic area, due to the steep slopes. Therefore, the sediment input to the karstic spring increases too. The surface sediment mass decreases as the intermittent runoff does not last long enough to carry the produced sediment to the reach.

Table 3.2. Mean, range (maximum minus minimum value of mean variable) standard deviation (stdev), and coefficient of variation (CV) for rainfall, total, karstic, surface flow, nitrate and sediment mass originating from the spring and from the surface flow, and their concentrations, for the two future periods (2019-2058 and 2059-2098). The statistics are based on the temperature and rainfall projections according to the 11 selected scenarios (GCM, RCM and RCP combinations) which are used as input in the hydrological models (SWAT and Karst-SWAT with the SUFI2-based calibrated parameters).

variables	2019-2058				2059-2098			
variables	mean	range	stdev	CV (%)	mean	range	stdev	CV (%)
rainfall (mm/year)	1508.9	1309.3-1813.6	139.6	9.3%	1358.0	1067.9-1897.3	248.9	18.3%
total flow (mm/year)	845.9	693.4-1032.4	105.7	12.5%	724.8	480.7-1146.1	203.4	28.1%
karstic flow(mm/year)	543.4	462.1-622.8	55.1	10.1%	467.9	331.5-683.1	109.9	23.5%
surface flow (mm/year)	302.6	231.4-409.6	52.45	17.3%	256.9	147.1-463.0	94.2	36.7%
nitrate mass from surface (t/year)	105.0	75.0-162.0	24.8	23.5%	92.8	48.6-182.0	38.8	41.9%
nitrate mass from spring (t/year)	209.4	164.2-274.6	30.0	14.3%	124.8	92.8-147.6	17.8	14.3%
total nitrate mass (t/year)	316.6	239.0-436.6	51.4	16.3%	215.2	146.6-327.2	54.8	25.5%
total nitrate daily concentration (mg/L)	1.6	1.46-1.72	0.08	5.0%	1.46	1.22-1.72	0.18	12.9%
sediment mass from surface (t/year)	6527.4	4063.4-11700.9	2082.6	31.9%	6281.8	2878.3-13063.6	2925.9	46.6%
sediment mass from spring (t/year)	1145.0	480.9-3925.4	960.7	83.9%	4530.8	9989.2	3023.7	66.7%
total sediment mass (t/year)	7672.4	4544.3-15626.1	2972.4	38.7%	10812.6	4570.3-17165.5	4497.0	41.6%
total sediment daily concentration (mg/L)	10.9	7.3-22.4	4.1	37.9%	32.0	15.3-56.7	15.2	47.5%
variables	reference period							

rainfall (mm/year)	1460.3
total flow (mm/year)	833.4
karstic flow(mm/year)	559.8
surface flow (mm/year)	273.7
nitrate mass from surface (t/year)	84.2
nitrate mass from spring (t/year)	199.2
total nitrate mass (t/year)	282.2
total nitrate concentration (mg/L)	1.5
sediment mass from surface (t/year)	10258.2
sediment mass from spring (t/year)	546.1
total sediment mass (t/year)	10697.4
total sediment concentration (mg/L)	12.2

3.4.4 Uncertainty due to the Internal Variability of Rainfall

Thirty realizations of rainfall time-series were used as input in the SWAT model. The quantification of the uncertainty of the average 40-year nitrate and sediment mass export can be expressed as the CV over the 40-year period. The nitrate mass follows the patterns of flow (as in Nerantzaki et al., 2020), as the nitrate transfer is relatively proportional to runoff. The sediment amount, on the other hand, although follows the trends defined by precipitation and flow, has a more random behavior.

The internal variability of the karstic, surface and total flow (by Nerantzaki et al., 2020) along with the internal variability of spring, surface and total nitrate and sediment mass, and nitrate and sediment concentration are presented in Table 3.3. We only consider the present day variability in the Table, however, the variability over the future periods does not vary significantly compared to the reference period. The ranges of uncertainty for

flow and nitrate mass are similar (5.6-6.9%), however, this percentage is significantly higher for the case of sediment mass (18.5%), due to the complexity of the erosion process: sediment erosion and transport is affected by a greater number of factors, such as the duration of dry periods which make sediment more erodible and thus easily transferred during the subsequent wet period. The internal variability range for sediment and nitrate mass from the surface flow is slightly higher than the uncertainty for the corresponding masses transferred by the karstic flow.

The projected changes in total sediment and nitrate masses according to the scenario REMO (Table A1, Appendix A) under the RCPs 2.6, 4.5 and 8.5 are assessed. To the projected values, we have included the range of the possible outputs of sediment and nitrate values based on the estimation of the internal variability, and Figures 3.6 and 3.7 show these projected ranges for sediment and nitrate respectively. The period 2019-2058, is expected to be a transition period, during which the outcomes of different climate scenarios overlap due to the domination of internal variability, and the changes in nitrates (and flow, see Nerantzaki et al., 2020) are not as significant as the ones forecasted after 2060, when the choice of the emission scenario becomes more important. For the case of sediments, the uncertainty due to internal variability is higher, and even after 2059, the scenarios projections overlap.

Table 3.3. Mean, and coefficient of variation (within parentheses) for rainfall, total, karstic and surface flow (according to Nerantzaki et al., 2020) as well as for nitrate and sediment mass transferred through surface flow, spring flow, and total flow and their total concentrations for the two future periods (2019-2058 and 2059-2098) and the reference period (1979-2018). The statistics are based on the simulation of rainfall according to the internal variability for the reference period. The hydrological models (SWAT and Karst-SWAT) use the SUFI2-based calibrated parameters.

variables	Reference period (1979-2018)
rainfall (mm/year)	1446.1 (3.7%)
total flow (mm/year)	805.4 (5.6%)
karstic flow(mm/year)	543.8 (4.6%)
surface flow (mm/year)	261.6 (7.7%)
nitrate mass from surface (t/year)	75.4 (9.7%)
nitrate mass from spring (t/year)	188.0 (6.8%)
total nitrate mass (t/year)	263.4 (6.9%)
total nitrate concentration (mg/L)	1.56 (3.2%)
sediment mass from surface (t/year)	13966 (20.9%)
sediment mass from spring (t/year)	720.8 (18.8%)
total sediment mass (t/year)	17084 (18.5%)
total sediment concentration (mg/L)	23.7 (12.7%)

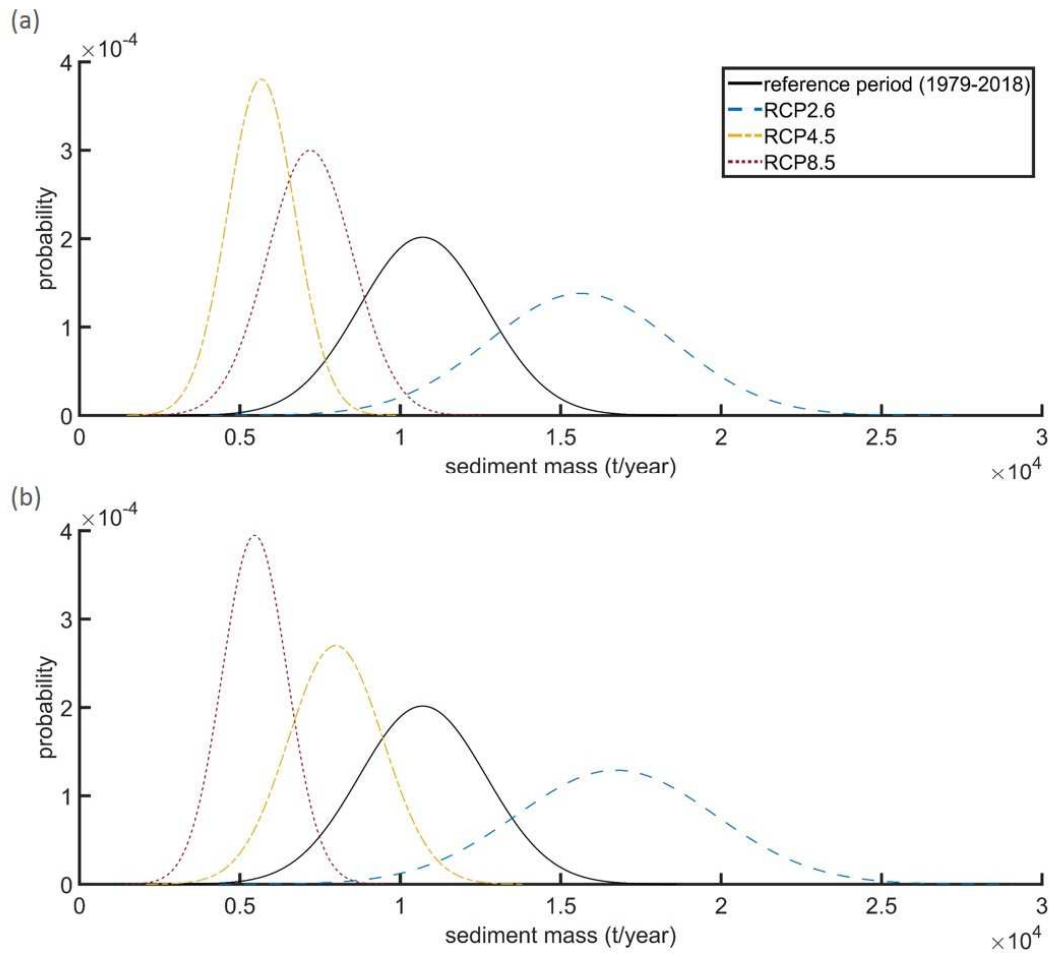


Figure 3.6. Probability density functions of the total exported sediment mass (based on the 30 realizations and the original time series for the respective climate change scenario) for the (a) 2019-2058 and (b) 2059-2098 period, plotted for the RCP2.6, RCP4.5 and RCP8.5 scenario

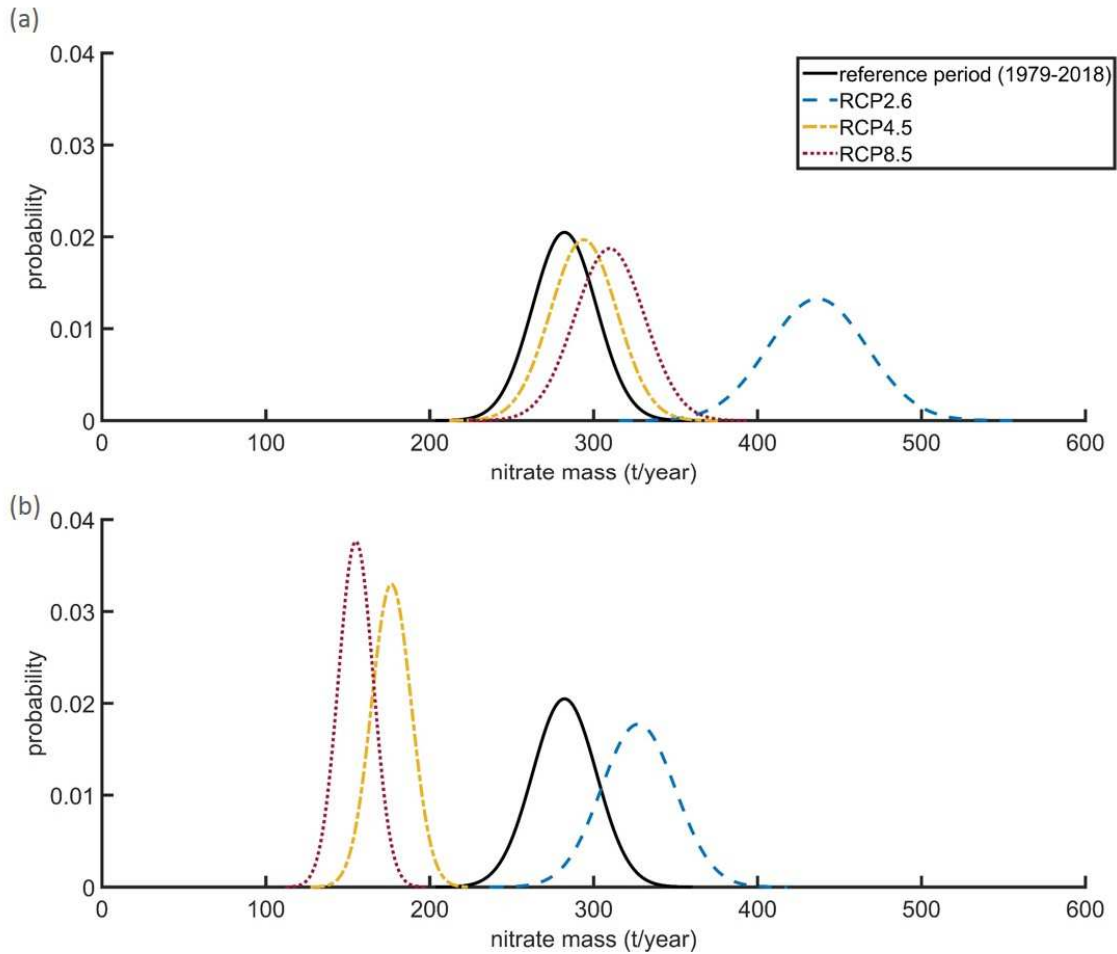


Figure 3.7. Probability density functions of the total exported nitrate mass (based on the 30 realizations and the original time series for the respective climate change scenario) for the (a) 2019-2058 and (b) 2059-2098 period, plotted for the RCP2.6, RCP4.5 and RCP8.5 scenario

3.4.5 Combining the Uncertainties of Nitrate Mass

The uncertainty of total exported nitrate mass due to both hydrologic model parameters and internal variability is estimated at 115.3 t/yr (CV equal to 40.7%). We use the Equation 3.2 and consider the standard deviation due to (1) hydrologic model parameters (standard deviation equal to 113.6 t/yr) and (2) internal variability of input (19.6 t/year). This combined parameter uncertainty is greater than the climate change uncertainty, even after 2059 (23.7%). The projected mean nitrate mass for the 2059-2098 period is 215.2 t/yr and ranges from 146.3 to 356.0 t/yr based on the 11 scenarios (from a decrease of 48.2% to an increase of 26.2%). When encompassing the rest of the uncertainties, the nitrate projections after 2059 vary from 27.2 to 935.6 t/yr. The uncertainty range in the mean annual nitrate mass projections is very high, but even when encompassing these uncertainties, the mean annual nitrogen nitrate concentration will never exceed the accepted limits.

3.5 Discussion and Conclusions

This study focuses on assessing the role of uncertainties on the flow and water quality estimates in a karstic Mediterranean watershed with semi-arid climate. In particular, we concentrate on the uncertainties stemming from the climate change scenario, the hydrologic model parameters (SWAT in combination with Karst-SWAT), and the model rainfall input time series (internal variability). The internal variability of temperature was not examined, as the temperature time series of the various climate change scenario present higher variability. Also, the internal variability of temperature has minimal effect on the flow outputs range (Nerantzaki et al., 2020).

The parameter uncertainty assessment framework has been applied for the quantification of the uncertainty in nitrate mass stemming from the SWAT and Karst-SWAT parameters. The total nitrate mass uncertainty due to model parameters is quite high (40.1%). This is partially due to limited observed nitrate data available. Also, the parameters of flow carry a big percentage of this uncertainty (10.0% in karstic flow and 17.1% in surface flow). Therefore, the proper assessment of the flow parameters uncertainty is necessary for the quantification of the uncertainty in water quality variables. In their study, Dakhlalla and Parajuli (2019) determined that parameter uncertainty was greatest for simulating the total nitrate load (r -factor = 1.25) compared to flow and sediment. According to Mehdi et al. (2018) the uncertainty simulated using non-unique behavioral parameter sets as determined by SUFI-2 depends on several factors, such as the objective criteria threshold chosen, the number of objective criteria, the number of variables being calibrated for at any one time and the number of gauges used during the calibration process. Schürz et al. (2019) identified climate change and model parametrization as being the most influential model inputs for the simulation of discharge and $\text{NO}_3\text{-N}$ loads in both case studies they studied in Austria.

The study reveals that the internal variability (or stochastic uncertainty) inherent in precipitation time series predicted by climate change time scenarios is propagated to the estimates of flow, sediment and nitrates. Taking the results presented in Nerantzaki et al. (2020) and the results of this study under consideration, the uncertainty due to the internal variability of rainfall, is on average 3.7% for rainfall, 5.6% for total flow, 6.9% for the exported nitrate mass, and 18.5% for the exported sediment mass. These values correspond to the Coefficient of Variation. The results do not vary significantly between the emission scenarios and the reference period. The rainfall uncertainty range is always lower compared to the range of the rest of the variables. The uncertainty in nitrate mass due to internal variability is slightly higher than the uncertainty of flow and the uncertainty in sediment mass is the highest, due to the complexity of the erosion process.

The results regarding the comparison of the distributions of the 40-year means (stemming from the 30 realizations) for the three REMO scenarios, point out that 2019-2058 will be a transition period, during which the outcomes of different climate scenarios overlap due to the domination of internal variability, and the changes in flow and nitrates

are not as significant as the ones forecasted after 2060, when the choice of the emission scenario becomes more important. Northrop and Chandler (2014) also came to a similar conclusion using Bayesian analysis on models obtained from phase 3 of the Coupled Model Intercomparison Project (CMIP3). The projected exported sediment mass, however, is very uncertain and scenarios overlap with each other and the distribution of sediment mass of the reference period even after 2059. After 2059, climate change scenarios suggest a wide envelope of projected mean annual sediment and nitrate masses, ranging from high decreases to high increases, according to the scenario realized. This statement is reinforced by Mas-Pla and Menció (2019) who studied the groundwater quality of several aquifers in Catalonia, Spain and state that there is no certainty that the overall groundwater nitrate content will likely be enriched, as high nitrogen inputs could counterbalance the effect of diminishing recharge. The same is true for the sediment projections (Bussi et al., 2014). The concentration of nitrate nitrogen in the river, though, is not expected to exceed the limits set by the Water Framework Directive, even when taking all the scenarios and uncertainties under consideration.

The methodology presented in this paper combines a fully integrated hydrologic model and a framework for the assessment of uncertainties in the estimation and forecast of water quality variables in karstic Mediterranean watersheds. The integration of surface and subsurface flow in the same model provides more realistic simulations of water and nitrate cycle and improved representation of groundwater recharge, which is important for impact assessment on groundwater resources. This is the first time, to our knowledge, that an assessment of water quality uncertainty in a composite karstic watershed is implemented and we believe that the framework introduced here can be applied at similar watersheds around the globe and incorporate different variables.

Acknowledgments

This research is co-financed by Greece and the European Union (European Social Fund-ESF) through the Operational Program «Human Resources Development, Education and Lifelong Learning» in the context of the project “Strengthening Human Resources Research Potential via Doctorate Research” (MIS-5000432), implemented by the State Scholarships Foundation (IKY).

The authors would also like to thank Dr. Grillakis M.G. for his contribution to bias correction of the climate dataset used in this article.

References

- American Society of Civil Engineers. Task Committee on Hydrology Handbook. Hydrology handbook (2nd ed). ASCE, New York (1996)
- Arnold, J.G., Srinivasan, R., Muttiah, R.S., Williams, J.R.: Large area hydrologic modeling and assessment Part I: Model development., *J. Am. Water Resour. As.*, 34(1), 73-89 (1998)
- Bailey, N. T. J.: *The Elements of Stochastic Processes with Applications to the Natural Sciences*. Wiley, New York (1964)
- Bangash, R.F., Passuello, A., Sanchez-Canales, M., Terrado, M., López, A., Elorza, F.J., Ziv, G., Acuña, V., Schuhmacher, M.: Ecosystem services in Mediterranean river basin: Climate change impact on water provisioning and erosion control. *Sci. Total Environ.* 458-460, 246-255 (2013)
- Box, G., Jenkins, G.: *Time Series Analysis: Forecasting and Control*. San Francisco: Holden-Day (1970)
- Bussi, G., Francés, F., Horel, E., López-Tarazón, J.A., Batalla, R.J.: Modelling the impact of climate change on sediment yield in a highly erodible Mediterranean catchment. *J. Soil Sediment.* 14, 1921-1937 (2014)
- Clauset, A., Shalizi, C., Newman, M.: Power-Law Distributions in Empirical Data. *SIAM Rev.* 51(4), 661-703 (2009)
- Dakhlalla, A.O., Parajuli, P.B.: Assessing model parameters sensitivity and uncertainty of streamflow, sediment, and nutrient transport using SWAT. *Inf. Process. Agric.* 6, 61-72. doi:10.1016/J.INPA.2018.08.007 (2019)
- Gilman, M. J.: A Brief Survey of Stopping Rules in Monte Carlo Simulations, *Proceedings of the Second Conference on Applications of Simulations (Winter Simulation Conference, 1968)*, 16-20. New York, New York, USA (1968)
- Grillakis, M.G., Koutroulis, A.G., Tsanis, I.K.: Multisegment statistical bias correction of daily GCM precipitation output. *J. Geophys. Res.-Atmos.*, 118(8), 3150-3162 (2013)
- Hartmann, A., Goldscheider, N., Wagener, T., Lange, J., Weiler, M.: Karst water resources in a changing world: Review of hydrological modeling approaches. *Rev. Geophys.* 52, 218-242 (2014).
- Jacob, D., Petersen, J., Eggert, B., Alias, A., Christensen, O.B., Bouwer, ... Yiou, P.: EURO-CORDEX: new high-resolution climate change projections for European impact research, *Reg. Environ. Change*, 14(1-2), 563-578 (2014)
- Jacob, D., Elizalde, A., Haensler, A., Hagemann, S., Kumar, P., Podzun, R., ... Wilhelm, C.: Assessing the transferability of the regional climate model REMO to different coordinated regional climate downscaling experiment (CORDEX) regions. *Atmosphere.* 3(1)181-199 (2012)
- Joseph, J., Ghosha, S., Pathak, A., Sahai, A.K.: Hydrologic impacts of climate change: Comparisons between hydrological parameter uncertainty and climate model uncertainty. *J. Hydrol.*, 566, 1-22. (2018)
- Lutz, S. R., Mallucci, S., Diamantini, E., Majone, B., Bellin, A., Merz, R.: Hydroclimatic and Water Quality Trends across Three Mediterranean River Basins, *Sci. Total Environ.*, 571, 1392-1406 (2016)

- Maas, G.S., Macklin, M.G.: The impact of recent climate change on flooding and sediment supply within a Mediterranean mountain catchment, southwestern Crete, Greece. *Earth Surf. Proc. Land.* 27, 1087–1105 (2002)
- Mas-Pla, J., Menció, A.: Groundwater nitrate pollution and climate change: learnings from a water balance-based analysis of several aquifers in a western Mediterranean region (Catalonia). *Environ. Sci. Pollut. R.* 26, 2184–2202 (2019)
- Mehan, S., Guo, T., Gitau, M.W., Flanagan, D.C.: Comparative Study of Different Stochastic Weather Generators for Long-Term Climate Data Simulation. *Climate*, 5(2), p. 26 (2017)
- Mehdi, B., Schulz, K., Ludwig, R., Ferber, F., Lehner, B.: Evaluating the Importance of Non-Unique Behavioural Parameter Sets on Surface Water Quality Variables under Climate Change Conditions in a Mesoscale Agricultural Watershed. *Water Resour. Manag.* 32, 619–639. doi:10.1007/s11269-017-1830-3 (2018)
- Moraetis, D., Efstathiou, D., Stamati, F., Tzoraki, O., Nikolaidis, N.P., Schnoor, J.L., Vozinakis, K.: High-frequency monitoring for the identification of hydrological and bio-geochemical processes in a Mediterranean river basin. *J. Hydrol.* 389(1-2), 127-136 (2010)
- Moriassi, D. N., Arnold, J. G., Van Liew, M. W., Bingner, R. L., Harmel, R. D., Veith, T. L.: Model evaluation guidelines for systematic quantification of accuracy in watershed simulations. *T. ASABE*, 50, 885–900 (2007)
- Moss, R.H., Edmonds, J.A., Hibbard, K.A., Manning, M.R., Rose, S.K., van Vuuren, D.P., ..., Wilbanks, T.J.: The next generation of scenarios for climate change research and assessment. *Nature*, 463, 747–56 (2010)
- Neitsch, S.L., Arnold, J.G., Kiniry, J.R., Williams, J.R.: Soil and Water Assessment Tool Theoretical Documentation Version 2009. Texas Water Resources Institute, Texas (2011)
- Nerantzaki, S.D., Nikolaidis, N.P., Hristopoulos, D.T.: Estimation of the uncertainty of climate change hydrologic predictions at a karstic Mediterranean watershed. *Science of the Total Environment*. In press (2020)
- Nerantzaki, S.D., Giannakis, G. V., Nikolaidis, N.P., Zacharias, I., Karatzas, G.P., Sibetheros, I.A.: Assessing the Impact of Climate Change on Sediment Loads in a Large Mediterranean Watershed. *Soil Sci.* 181, 306–314 (2016)
- Nerantzaki, S.D., Giannakis, G.V., Efstathiou, D., Nikolaidis, N.P., Sibetheros, I.A., Karatzas, G.P., Zacharias, I.: Modeling suspended sediment transport and assessing the impacts of climate change in a karstic Mediterranean watershed. *Sci. Total Environ.* 538, 288-297 (2015)
- Nikolaidis, N.P., Bouraoui, F., Bidoglio, G.: Hydrologic and Geochemical Modeling of a Karstic Mediterranean Watershed, *J. Hydrol.*, 477, 129–138 (2013)
- Northrop, P.J., Chandler, R.E.: Quantifying Sources of Uncertainty in Projections of Future Climate. *J. Climate*, 27, 8793–8808 (2014).
- O'Neill, B.C., Kriegler, E., Riahi, K., Ebi, K.L., Hallegatte, S., Carter, T.R., ... van Vuuren, D.P., (2013). A new scenario framework for climate change research: the concept of shared socioeconomic pathways. *Climatic Change*, 122(3), 387–400. doi:10.1007/s10584-013-0905-2
- Pachauri, R.K., Meyer, L.A... van Ypserle, J. P.: Climate Change 2014: Synthesis Report. Contribution of Working Groups I, II and III to the Fifth Assessment Report of the

- Intergovernmental Panel on Climate Change. Geneva, Switzerland, IPCC, 151 p. (2014)
- Racsko, P., Szeidl, L., Semenov, M.A. A serial approach to local stochastic weather models, *Ecol. Model.*, 57(1-2), 27–41 (1991)
- Richardson, C. W.: Stochastic simulation of daily precipitation, temperature, and solar radiation. *Water Resour. Res.* 17(1), 182-190 (1981)
- Richardson, C.W. Wright, D.A.: WGEN: A Model for Generating Daily Weather Variables. US Department of Agriculture, Agricultural Research Service, ARS-8, United States Department of Agriculture, Agricultural Research Services, Washington DC, p. 83 (1984)
- Sayama, T., Tachikawa, Y., Takara, K., Yamashiki, Y., Yamashiki, Y.: Assessing sources of parametric uncertainty and uncertainty propagation in sediment runoff simulations of flooding. *J. Flood Risk Manag.* 3, 270–284. doi:10.1111/j.1753-318X.2010.01077.x (2010)
- Semenov, M.A., Stratonovitch, P.: Use of multi-model ensembles from global climate models for assessment of climate change impacts. *Clim. Res.* 41(1), 1-4. (2010)
- Semenov, M.A., Brooks, R.J., Barrow, E.M., Richardson, C.W. Comparison of the WGEN and LARS-WG stochastic weather generators for diverse climates, *Clim. Res.* 10(2), 95–107 (1998).
- Singh, A., Imtiyaz, M., Isaac, R.K., Denis, D.M.: Assessing the performance and uncertainty analysis of the SWAT and RBNN models for simulation of sediment yield in the Nagwa watershed, India. *Hydrol. Sci. J.* 59, 351–364. doi:10.1080/02626667.2013.872787 (2014)
- Schürz, C., Hollosi, B., Matulla, C., Pressl, A., Ertl, T., Schulz, K., Mehdi, B.: A comprehensive sensitivity and uncertainty analysis for discharge and nitrate-nitrogen loads involving multiple discrete model inputs under future changing conditions. *Hydrol. Earth Syst. Sci.* 23, 1211–1244. doi:10.5194/hess-23-1211-2019 (2019)
- Taylor, K. E., Stouffer, R.J., Meehl, G.A.: An Overview of CMIP5 and the Experiment Design, *B. Am. Meteorol. Soc.*, 93(4), 485–98 (2012)
- Tzoraki, O., Nikolaidis, N. P.: A generalized framework for modeling the hydrologic and biogeochemical response of a Mediterranean temporary river basin. *J. Hydrol.*, 346(3), 112-121 (2007)
- van Vuuren, D.P., Lucas, P.L., Hilderink, H.: Downscaling drivers of global environmental change: Enabling use of global SRES scenarios at the national and grid levels. *Global Environ. Chang.*, 17(1), 114-130 (2007)
- Wang, C., Zeng, B., Shao, J.: Application of bootstrap method in Kolmogorov-Smirnov test. *International Conference on Quality, Reliability, Risk, Maintenance, and Safety Engineering 2011*, 287–291. Xi'an, China. (2011)
- Zhang, R., Corte-Real, J., Moreira, M., Kilsby, C., Birkinshaw, S., Burton, A., Fowler, H.J., Forsythe, N., Nunes, J.P., Sampaio, E., dos Santos, F.L., Mourato, S.: Downscaling climate change of water availability, sediment yield and extreme events: Application to a Mediterranean climate basin. *Int. J. Climatol.* 39, 2947–2963 (2019)

Chapter 4 The response of three Mediterranean karstic springs to drought and the impact of climate change

Sofia D. Nerantzaki ^{a*}, Nikolaos P. Nikolaidis ^a

^a*School of Environmental Engineering, Technical University of Crete, Chania, Greece*

**corresponding author, email: snerantzaki@isc.tiuc.gr, +306973475458*

Submitted to Journal: Journal of Hydrology, Special Issue: “Advances in Hydrology and the Water Environment in the Karst Critical Zone under the impacts of climate change and anthropogenic activities

4.1 Abstract

Karstic springs are the exclusive source of water during dry months for many Mediterranean regions. The impact of climate change on the hydrology of Mediterranean karstic springs has not received proper attention in the scientific literature. Specifically, the effect of climate change on the drought characteristics of karstic springs has not been studied. Here, the response to climate change of three Mediterranean karstic springs with different properties is examined, focusing on the frequency, duration and intensity of their drought events. The Karst-SWAT model is used to quantify the karstic springs flow. A set of representative climate change scenarios is used to assess the climate change impact on the springs and surface flow for the period 2019-2098. A non-parametric drought index is modified to estimate the future meteorological and hydrological drought characteristics in comparison to the reference period. Drought frequency, duration and intensity of karstic flows are expected to increase for all scenarios and karstic springs. The most adverse effects of climate change on the three karstic springs are expected to prevail after 2059. Depending on the spring, the mean annual karstic flow decreases from 14.2% to 25.1%, the mean number of drought events ranges from a decrease of 8.1% to an increase of 77.5%, the duration of drought events increases from 36.8% to 533% and the mean monthly water deficit increases from 27.3% to 83.6%. As the water detention time of the spring increases, the duration and intensity of the droughts are likely to increase more significantly. After 2059, multi-year droughts are forecasted for all springs under all scenarios. Both low and high flows will increase under all scenarios for most springs, with the former occupying even wet months. The next 40 years will be a transitional period during which adaptation measures should be planned to mitigate the adverse effects of climate change on the Mediterranean water resources.

Keywords: drought index, karstic springs, Mediterranean region, Karst-SWAT, climate change, semi-arid climate

4.2 Introduction

Karstic regions describe landscapes containing caves and extensive groundwater systems developed on soluble rocks (i.e. limestone, marble and gypsum). Karstic terrains have distinctive hydrology which stems from a combination of high rock solubility and well developed, fractured porosity. Usual hydrologic formations in these areas are sinking streams, caves, enclosed depressions and large springs. Karstic landscapes occupy approximately 20% of the planet's dry ice-free land and offer the partial or entire drinking supply of about one fourth of the global population (Ford and Williams, 2007). The Mediterranean basin is the cradle of karstic studies since ancient times (Ford and Williams, 2007) and it is estimated that at least 15% of the Mediterranean surface is covered by carbonate outcrops and that karstic aquifers supply at least 25% of domestic water supply, without taking industry, agricultural and tourism withdrawals under consideration (Bakalowicz, 2015). Seventy five percent of the total Mediterranean agricultural land is irrigated and it accounts for more than 60% of the total water abstractions (e.g. Spain 64%, Greece 88%, Portugal 80%) (Wriedt et al., 2009).

The Mediterranean region is identified as a prominent regional climate change hotspot that emerges in response to higher levels of forcing (Diffenbaugh and Giorgi, 2012). Future droughts are expected to greatly influence the Mediterranean region. According to literature, droughts can be categorized as meteorological, hydrological and agricultural (Wilhite and Glantz, 1985). Meteorological droughts refer to decrease in precipitation, hydrological droughts to deficit in surface water and agricultural droughts to drop in soil moisture. Orłowsky and Seneviratne (2012) found enhanced dryness (meteorological drought) on the annual time scale in the Mediterranean using the CMIP3 models. Lu et al. (2019) recently found statistically significant annual drying over the Mediterranean region (agricultural drought), with stronger drying as the strength of forcing increases, using the CMIP5 models.

Large scale hydrological drought studies do not take under consideration the effects of non-linearity in smaller scales, which is a result of specific hydrological processes, since many catchments do not have a tight hydrological budget and a rainfall-runoff response. An extensive bibliography of climate change assessment studies on several (regional scale) Mediterranean regions exists, however, the climate change impact research for karstic watersheds (Mediterranean or other), is limited. For example, Hartmann et al. (2012) used a multi-model approach to assess future water availability at a large Eastern Mediterranean karstic spring, and suggested that in the remote future (2068–2098), when variability of climate change decreases, a decrease of water availability of 15% to 30% is forecasted. Smiatek et al. (2013) used four dynamically downscaled and spatially highly resolved climate change datasets and predicted a decrease in discharge intensity in the range of –9% to –30% for the Fiegeh karstic spring in Syria in the middle and end of the century. Another example is the study of Nerantzaki et al. (2019), who used a combination of CMIP5 models to estimate the future hydrological budget of a karst-

dominated Mediterranean island (i.e. Crete) and found an average decrease of 16.5% for spring flow. This gap in literature needs to be filled, considering that water needs in the arid and semi-arid regions of the Mediterranean are exclusively covered by karstic springs and groundwater resources during the summer months, when there is no surface runoff. Several questions arise for Mediterranean karstic watersheds, such as whether climate change scenarios predictions suggest satisfactory available water supplies and how these water amounts are going to be distributed over the future years under the effect of hydrological droughts. It is crucial to acknowledge the importance of karstic springs, estimate the present and future response for these regions and plan water resources management accordingly.

The first step for reliable predictions of both surface and karstic flow is the robust hydrological modeling of the watershed of interest. The Soil and Water Assessment Tool (SWAT) has been extensively used for the simulation of surface runoff for a variety of watersheds. The SWAT model has been modified to account for the karstic springs flow by adding a karstic component, and the Karst-SWAT model (Nikolaidis et al., 2013) was developed for watersheds dominated by karstic sinkholes and spring flow. It has been implemented for the karstic watershed of Koiliaris, located in Chania, Crete, for the hydrological modeling of the composite surface and karstic flow (Nikolaidis et al., 2013), as well as for the simulation of sediment transport through the karstic springs (Nerantzaki et al., 2015). It was then scaled up for the hydrological modeling of the whole island of Crete (Malagò et al., 2016) and for the assessment of the effect of climate change on the hydrological budget of the island (Nerantzaki et al., 2019). Nerantzaki et al. (2020) also used it for the estimation of the projected average available water quantities and their uncertainties in the Koiliaris River Basin.

Here, in an attempt to assess the future variability of the Mediterranean karstic springs flow along with the effect of drought on their water reserve, we focus on three Mediterranean karstic springs located in Chania, Crete, with different hydrologic responses. We aim to (1) estimate the impact of climate change on the future water availability, (2) compare the frequency, duration and intensity of meteorological and hydrological drought events in future periods with the ones of the reference period (1979-2018), and (3) examine the frequency of extreme flows (high and low) in the reference and future periods. The efficiency of a meteorological index to describe hydrological droughts is also examined. The SWAT and Karst-SWAT models are used to simulate both the surface and the karstic runoff, emphasizing on the latter. A combination of eleven climate change scenarios is used to drive the hydrological model and the Standardized Drought Analysis Toolbox (SDAT) (Farahmand and AghaKouchak, 2015) is employed on both precipitation and karstic flow. The index proposed by Farahmand and AghaKouchak (2015) is modified to facilitate the comparison between future and reference drought characteristics. Future distributions of low flows are also compared to the ones of the reference period and the Mean Excess Function (Nerantzaki and

Papalexiou, 2019) is used for the analysis of the upper distribution tails of rainfall and flow.

4.3 Materials and Methods

4.3.1 Study Area and Data

The catchments under study are the Koiliaris River Basin and the Keritis River Basin (Figure 4.1), located in the prefecture of Chania, in Crete. These watersheds include karstic springs which discharge the broad karstic system of the White Mountains Range, located at the north (Figure 4.1) and they are the main contributors of water for the region of Chania.

The Koiliaris River Basin (Koiliaris RB) is a Critical Zone Observatory (Guo and Lin, 2016). The watershed is about 130 km², and includes two episodic streams (Keramianos and Anavreti) and the karstic springs of Stilos, which provide permanent flows throughout the year. The karstic springs of Stilos constitute a set of springs which share the same karstic system. As we consider a single common flow for the whole set of springs, hereafter they will be called the “Stilos karstic spring” (singular). The Stilos spring combined with the intermittent flow of Keramianos and Anavreti, form the Koiliaris River. The main geologic formations in the area are Plattenkalk limestones (karstic), Tripali units, crystalline Schists, Marls and marly Limestones and alluvial deposits (Figure 4.1). Stilos is fed from the karstic regions inside the basin but also from an area located outside of the watershed, i.e. the extended karstic area of Figure 4.1 (Moraetis et al., 2010; Nikolaidis et al., 2013). This karstic spring displays a relatively fast response with a detention time equal to 15 days and a slower response with a detention time of 100 days. The average annual karstic discharge is about 120hm³. Based on the Drought Resistance Indicator for Karstic Aquifers “DRIKA” (Orehova, 2004), which categorizes karstic aquifers into four classes of drought resistance, from weak to high, the Stilos spring belongs to the class of moderate drought resistance (DRIKA equal to 0.44). Altitudes in the watershed range from ±0 to +2120 m above mean sea level (a.m.s.l.). Rangeland covers 58% of the total area, while cultivated areas, forests, urban areas, and aquatic areas account for 29.4%, 8.5%, 2.8%, and 0.6% respectively.

The Keritis River Basin comprises of two river basins: the Therissos River Basin (60km²) and the Keritis River Basin (210km²). Since the Therissos River Basin is significantly smaller and some karstic parts of it feed the karstic springs of Keritis River Basin, the two basins are considered as one single basin, from now on called the “Keritis River Basin” or “Keritis RB”. The main geologic formations in the basin are similar to the ones found in the Koiliaris RB, but instead of the Crystalline Schists, this watershed has Phyllites. The main river of the Therissos RB is the intermittent Kladissos River. The Keritis River Basin includes the springs of Agia and Meskla, which, together with the intermittent surface runoff, form the Keritis River. As for the case of Stilos, Agia consists of a set of springs

which share the same karstic system. From now on, we will be referring to the Agia springs as “Agia spring” (singular), considering that these springs have a single common outflow. The springs of Agia and Meskla are fed by karstic regions within the watershed. The underground system of the particular watershed is more complex, as the underground reservoir of Meskla connects with the one of Agia, and transfers part of the stored water. The Meskla spring has a relatively fast response with detention time of 50 days and a slow response of 833 days (2.28 years). The Agia spring has a fast response of 5 days and a significant slow response of 2500 days (6.84 years). The mean annual flow of the Agia spring is 69hm³ and the mean annual flow of the Meskla spring is 30hm³. Based on the Drought Resistance Indicator for Karstic Aquifers “DRIKA” (Orehova, 2004) the Meskla spring belongs to the class of good drought resistance (DRIKA equal to 0.55) and the Agia spring has high drought resistance (DRIKA equal to 0.85). Altitudes in the Basin range from ±0 to +2100 m above mean sea level (a.m.s.l.). Rangeland covers 45% of the total area, while cultivated areas, olives, forests, and urban areas account for 23.6%, 17.7%, 11.3% and 2.1% respectively.

Precipitation data in the area are available from seven rainfall stations i.e., Psychro, Samonas, Kalives, Askifou, Mouri, Alikianos and Agrokipio. Psychro and Samonas also measure minimum and maximum temperature. Meteorological data are available for the period 1973-2018 on a daily time step. Monthly spring flow data are available for the Agia spring for the period 1978-1985 and for the Meskla spring for the period 1978-2005. The mean annual water needs covered by the spring of Agia are about 26.7 hm³ and the mean annual water needs covered by the spring of Meskla are about 5hm³ (Decentralized Administration of Crete, 2018). There are also two hydrometric stations measuring daily surface runoff along the Keramianos River (2013-2017) and one hydrometric station at the Koiliaris River Basin exit, measuring the combination of surface and karstic flow (daily flow for the period 2004-2018). Finally, the hydrometric station at the Keritis River Basin exit, measures the total flow (both springs and surface runoff) of the Keritis River (daily time step, 2014-2015).

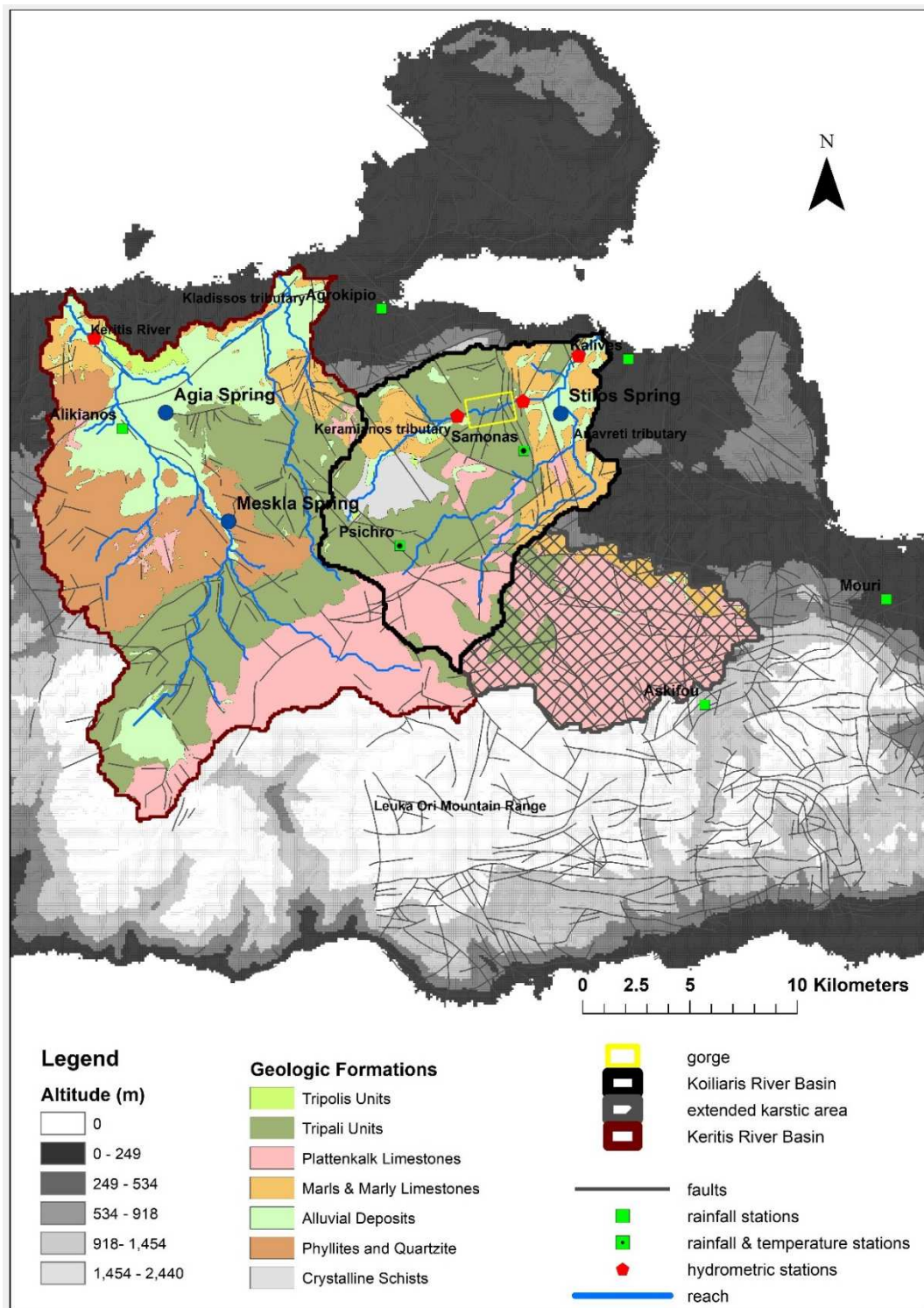


Figure 4.1. Map of Koiliaris River Basin, the modelled extended karstic area (shown with a hatched pattern), and the Keritis River Basin (Crete, Greece), showing the location of the three springs (blue circles), the seven rainfall and temperature stations (green squares), and the locations of the hydrometric stations (red hexagons).

4.3.2 Climate Change Scenarios

A sub-set of representative simulations is selected from the high-resolution (12.5 km) regional climate model (RCM) ensemble, the EURO-CORDEX (Jacob et al., 2014)(EUR-11) for a range of potential future climate scenarios. The General Circulation Models (GCMs) simulations of EURO-CORDEX have been conducted within the Coupled Model Intercomparison Project Phase 5 (CMIP5) and represent three scenarios of greenhouse gas emission pathways or Representative Concentration Pathways (RCPs): the “favorable” RCP2.6 (peaking radiative forcing within the 21st century at 3.0 W/m^2 and declining afterwards), the “intermediate” RCP4.5 (stabilization of radiative forcing after the 21st century at 4.5 W/m^2) and the “adverse” RCP8.5 (rising radiative forcing crossing 8.5 W/m^2 at the end of 21st century). The regional simulations (Regional Climate Models - RCMs) downscale the global climate projections of CMIP5 (Taylor et al., 2012) and the Representative Concentration Pathways (RCPs) (Moss et al., 2010; van Vuuren et al., 2007).

Five EUR-11 models were selected based on three criteria: (a) the range of driving Global Climate Models (GCMs), (b) the variety in model genealogy (institutions which develop the RCMs), and (c) the range of climate change signals (wet/dry and cold/warm responses). Based on these criteria and the methodology developed by Mendlik and Gobiet (2016), we use the same set of models as in the study of Nerantzaki et al. (2019), who assessed the climate change impact on the hydrological budget of Crete. The RCMs used in this study are presented in the Table B1 of Appendix B.

The RCM simulated temperature and rainfall data (for each emission pathway) have been adjusted for biases against a thirty-year period between 1981 and 2010 that served as reference for the correction. The quantile mapping methodology known as multi-segment statistical bias correction (MSBC) is used (Grillakis et al., 2013).

From the eleven RCMs of the ensemble, we depict some of the results focusing on the MPI-ESM-LR-r1_CSC-REMO (hereafter REMO). The selection of the REMO model is motivated by the fact that REMO includes the highest (RCP2.6) and the lowest (RCP8.5) rainfall projections among the selected 11 models; therefore, it is representative of the entire range of rainfall for the ensemble. In addition, REMO shows the satisfactory skill scores when tested against the observed droughts of the reference period (sub-section 3.1).

Based on the analysis of the rainfall and temperature data for both reference (1979-2018) and projected period (2019-2098), the projected period is divided into two non-overlapping segments which correspond to the intervals 2019-2058 and 2059-2098. This segmentation is driven by two factors. Firstly, the intensity of the rainfall and the duration of wet and dry periods change significantly around 2059. Secondly, by using this segmentation, we acquire three periods of equal duration so that we can perform comparative analysis: the reference period (1979-2018), the period 2019-2058 and the period 2059-2098.

4.3.3 The Karst-SWAT model

The SWAT model (Soil and Water Assessment Tool) is a well-known and widely used deterministic, watershed to river-basin scale, hydrological model, which operates on a daily time step. SWAT can assess the quality and quantity of surface and ground water and predict the environmental impacts of land use, land management practices, and climate change (Arnold et al., 1998; Neitsch et al., 2009). In the model, the watershed is divided into smaller sub-basins in order to separate the tributaries; these are further divided into hydrologic response units (HRUs) which constitute unique combinations of soil type, land use and slope value within the watershed. The land use classes for the Koiliaris and Keritis RBs are obtained by the Corine Land Use (2000), the soil types are defined using the European Soil Database (v2 Raster Library 1kmx1km), and the slopes are extracted from a Digital Elevation Model with 25 m pixel size (Bashfield and Keim, 2011), obtained from a Pan-European elevation data at 1 arc-second (EU-DEM).

The SWAT model uses the rainfall as input and simulates the surface hydrologic processes (snow accumulation and melt, surface runoff, infiltration to shallow groundwater and evapotranspiration) over the karstic HRUs. The surface water is then directed to the subsurface of the karstic area thus creating the deep groundwater discharge which feeds the spring flow. The deep aquifer recharge (DA_RCHG) is aggregated on a daily step and provides the input to the two-part reservoir karst model (see Nikolaidis et al. (2013) for the full description). The SWAT and Karst-SWAT combination has already been used in the Koiliaris RB and in the current study it is also applied to the Keritis RB. The equations used in the Karst-SWAT setup for the three springs are presented in the Appendix B section (Equations B1 to B13).

4.3.4 Methods used for the Analysis of the Results

4.3.4.1 Hydrological models Calibration and Goodness of fit

The calibration of the karstic flow of the Stilos spring is accomplished indirectly, since there are no measured data of the specific karstic spring. Instead, we calibrate the surface flow at the Keritis River (at the gorge exit), we then alter the SWAT parameters for the rest of the sub-basins in a similar manner in order to acquire an estimate of the surface runoff, and we adjust the four parameters of the Karst-SWAT (the detention time has been observed by experts in the area) so that we succeed the best possible calibration of the total flow (karstic flow plus surface runoff) at the basin exit. The procedure of calibration followed for the Keritis River Basin is different. The available monthly data of the Agia and Meksla flow are utilized for the calibration of the karstic flow for each spring. The SWAT parameters in the Keritis RB are then adjusted to attain a satisfactory calibration for the total flow at the Keritis basin exit. Every calibration stage for both basins is tested using the statistical indices proposed by Moriasi et al. (2007) for watershed simulations.

Specifically we use the Nash-Sutcliffe efficiency (NSE), the Percent Bias (PBIAS) and the RMSE-observations standard deviation ratio (RSR). The streamflow model simulation is judged as satisfactory if $NSE > 0.50$, $RSR < 0.70$, and $PBIAS \pm 25\%$.

2.4.2 Drought indices

The Standardized Drought Analysis Toolbox (SDAT) (Farahmand and AghaKouchak, 2015) is used for deriving nonparametric standardized drought indices for rainfall. To quantify the level of agreement between the climate change models and the rainfall observations, the index is applied on the rainfall time series of both the observed and the downscaled time series of the scenarios, over the reference period used for downscaling (1981-2010). In this framework, instead of the gamma (or any other parametric) distribution function, the marginal probability of precipitation and flow is derived using the empirical Gringorten plotting position.

$$p(x_i) = \frac{i-0.44}{n+0.12}, \quad (4.1)$$

where n is the sample size, i denotes the increasing rank of non-zero precipitation data, and $p(x_i)$ is the corresponding empirical probability. The outputs of Eq. (1) can be transformed into a Standardized Drought Index (SDI) as in:

$$SI = \phi^{-1}(p), \quad (4.2)$$

where ϕ is the standard normal distribution function, and p is probability derived from Equation (4.1).

We employ the index for an accumulation period of 6 months, which is commonly used for reduced streamflow and reservoir storage. According to McKee et al. (1993), three severity classes are defined: for index values lower than “-1” the drought is characterized as “moderate”, for values lower than “-1.5” the drought is “severe” and for values lower than “-2” the drought is “extreme”. A six-month period with an SDI value below these thresholds is considered as a 6-month drought. When n consecutive values lower than the above mentioned thresholds exist, the drought duration D is considered to be equal to $6 + n - 1$ months. Intensity is defined as the average monthly departure from the climatological mean during the drought event (Ukkola et al., 2018) and is expressed as:

$$I = \frac{\sum(\bar{x}_m - x_m)}{D}, \quad (4.3)$$

where x is the monthly value, \bar{x}_m the corresponding monthly mean, i is the drought start month, and j the end month. The duration and intensity can be calculated separately for each drought event and severity class.

Initially, we use the SDAT and the Relative Difference (RD) to quantify the level of agreement between the rainfall of the climate change models and the observed rainfall in terms of drought frequency, duration and intensity for the 1981-2010 period (according to Ukkola et al., 2018). The Relative Difference is defined as:

$$RD = \frac{(x_{model} - x_{obs})}{x_{obs}} \times 100, \quad (4.4)$$

where x_{model} is the mean value (mean frequency, mean duration and mean monthly intensity) for an individual climate change model, and x_{obs} is the corresponding mean value for the observations, during the period 1981-2010. The level of agreement is high for $|RD| \leq 10\%$, medium for $10\% < |RD| \leq 20\%$ and low for $|RD| > 20\%$.

The next step is to examine the droughts over the whole period of 1979-2098 and compare the drought characteristics (i.e. frequency, intensity and duration) of the future sub-periods (2019-2058 and 2059-2098) with the ones of the reference period (1979-2018). In this study, we modify the drought index in a way which facilitates this comparison. Previous assessments of drought indices examine each drought event of the time series based on the climatological mean of the whole time series. However, it is more substantial to investigate the relevant change of the future droughts in relation to the reference period alone. To achieve this, in the version proposed here: (a) the 6-month moving average of rainfall (or karstic flow) of the reference period (1979-2018) is subtracted from the 6-month moving average of the mean monthly rainfall (or karstic flow) of the reference period. (b) The time series of these differences is standardized using Equation (4.2). (c) Every successive 6-month average value in the reference and the future periods is associated with a standard score (or z-score) based on the Normal Distribution we acquired in step (b). We then apply the modified index on the rainfall and karstic flow for each climate change scenario over the 1979-2098 period. Essentially, the difference between the index proposed here and other indices is that the z-scores are not based on the entire time series under study, but they are estimated based on the reference period time series.

2.4.3 Analysis of Low and High Flows

We consider the 10th percentile (lowest 10% of ranked values) of the daily karstic flows distribution (of the three springs), during the reference period, as low flows. We examine the low flows probability of occurrence in each month during the reference and future periods according to selected climate change scenarios (REMO under RCPs 2.6, 4.5 and 8.5), the way the 10th percentile changes in the future periods, and whether the springs dry up in the future. .

For the high surface and karstic flows (as well as rainfall) we conduct an analysis on the upper part of the distributions of these variables. The upper part of a distribution, or the right tail, describes the magnitude and frequency of extreme events. Heavy-tailed

distributions (sub-exponential) characterize distributions with tails heavier than the exponential tail; this means that they present many outliers and frequent extreme events. Light-tailed distributions are those with similar (exponential) or thinner tails (hyper-exponential) than the Exponential distribution and they have less frequent extreme events. For the analysis of high flows (and rainfall), we use the Mean Excess Function (Nerantzaki and Papalexiou, 2019) on the upper 10% of the flows (and rainfall) distributions. The Mean Excess Function is a method for tail identification which discriminates between “sub-exponential” distributions and “light-tailed” or “exponential” distributions. For a random variable X with distribution function F_X the Mean Excess Function (MEF) is

$$e(x_p) = E(X - x_p | X > x_p) = \frac{1}{\overline{F}_X(x_p)} \int_{x_p}^{\infty} (x - x_p) f_X(x) dx, \quad x_p \geq 0 \quad (4.5)$$

where $x_p = F_X^{-1}(p)$ is the lower threshold value for probability p , $F_X^{-1}(p)$ is the quantile function, and $\overline{F}(x) = 1 - F(x)$ is the probability of exceedance. A property of $e(x_p)$ is that it is constant for distributions with exponential tails (due to the memoryless property of the Exponential distribution). Therefore, if the empirical value of $e(x_p)$ vs. x_p has a slope equal to zero, the graph indicates an exponential tail. If the plot slope is greater than zero, the graph suggests sub-exponential tails, as the MEF tends to infinity for such tails. Nerantzaki and Papalexiou (2019) constructed the 90% confidence interval (CI) of MEF slopes resulting from the Exponential tail (Figure B1, Appendix B). This graph facilitates the classification of tails based on their MEF slope value. Specifically, slope values higher than the CI limits signify sub-exponential tails, slope values inside the CI limits indicate exponential tails and values lower than the CI limits suggest hyper-exponential tails. The MEF function is applied on the time-series of interest (i.e. rainfall, karstic and surface flow) of the periods 1979-2018, 2019-2058 and 2059-2098 separately, for the RCM REMO to investigate the progress of the distribution tails in the future under different RCPs.

4.4 Results

4.4.1 Evaluation of Hydrologic and Climate Change Models.

The goodness of fit between observed and modeled values is presented in Figure 4.2. The calibration of the Agia spring (Figure 4.2a) based on the monthly observed values has unsatisfactory NSE and RSR indices (0.32 and 0.82 respectively) but is characterized by a satisfactory PBIAS index (0.5%) and manages to capture the mean monthly value of the Agia spring (modeled monthly flow equal to 2.22 m³/s and observed monthly flow equal to 2.21 m³/s). Generally the calibration succeeds in portraying the spring trend and periodicity but the NSE and RSR are unsatisfactory due to the limited observational data. The Meskla calibration (Figure 4.2b) has very good performance, with NSE equal to 0.84,

PBIAS equal to -5.0% and RSR equal to 0.40, and in combination with the Agia flow and the surface flow (adjusted in the SWAT model) gives a very good model performance for the daily total flow at the Keritis RB exit – Figure 4.2c (NSE=0.80, PBIAS=4.9%, RSR=0.44). The performance of the model for the total flow at the Koiliaris RB is also good (Figure 4.2d), with very good PBIAS (0.2%) and good NSE (0.67) and RSR (0.57).

We analyze the drought events of the downscaled rainfall time series of Psichro against the ones of the observed time series using the SDAT. All rainfall stations were examined using the SDAT for the reference period and the results of the index did not vary significantly (Appendix B, Table B2). Figure 4.3 shows the agreement (relative difference RD) between the time series in terms of mean frequency, duration and monthly intensity of droughts. The downscaled time series agree well with the observations for the mean duration for all drought intensities and scenarios, for the mean frequency for most scenarios, and for the mean monthly intensity for the extreme droughts. The REMO scenario has the most satisfactory scores compared to the rest of the scenarios and agrees with the drought characteristics of the reference period.

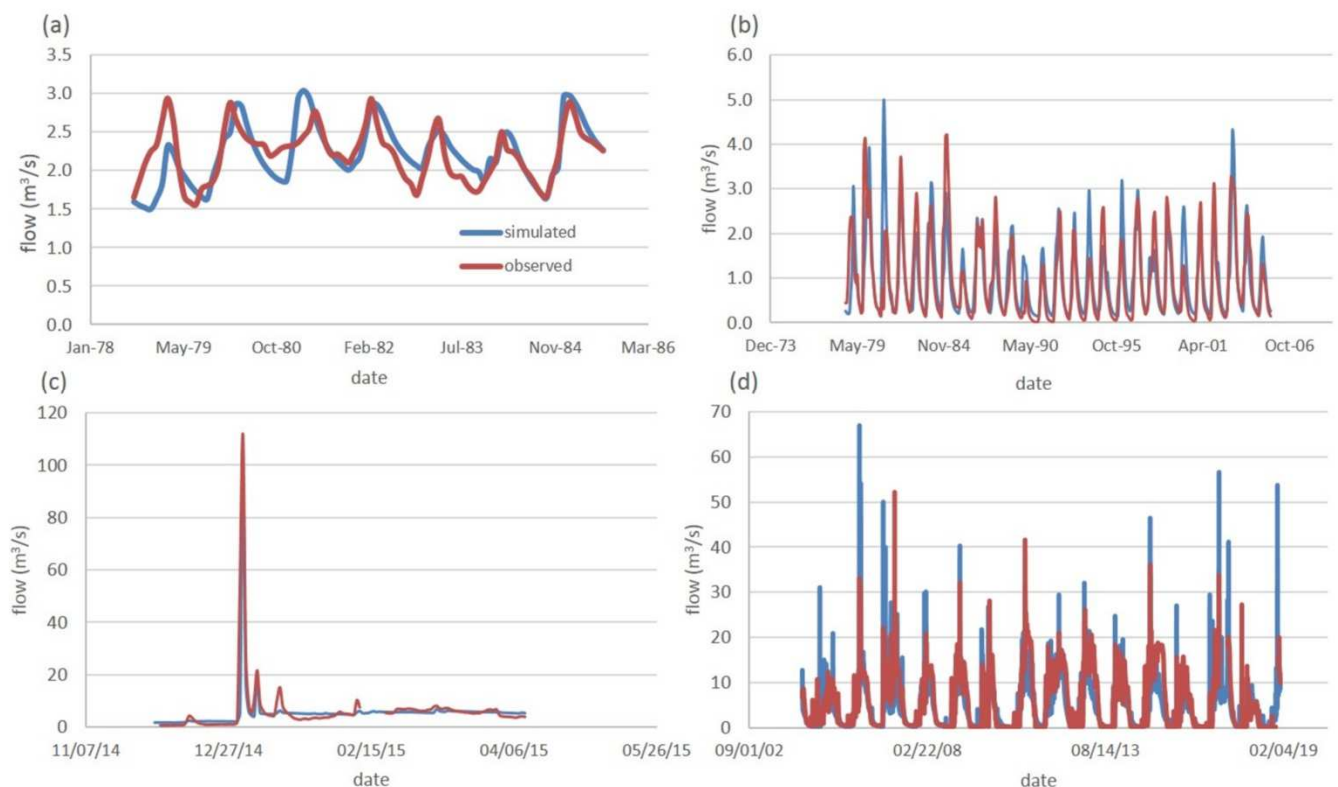


Figure 4.2. SWAT and Karst-SWAT performance for the (a) Agia spring, (b) Meskla spring, (c) total flow of the Keritis River at the Keritis RB exit, and (d) total flow of the Koiliaris River at the Koiliaris RB exit.

drought intensity	scenario	mean frequency	mean duration (months)	mean intensity (hm ³)
-1	observed	30	7.0	52.1
	EC-EARTH-r12 SMHI-RCA4 (2.6)	-0.2	0.1	0.0
	MPI-ESM-LR-r1 CSC-REMO (2.6)	-0.1	0.0	0.2
	EC-EARTH-r1 KNMI-RACMO22E (4.5)	-0.1	0.0	0.0
	EC-EARTH-r12 SMHI-RCA4 (4.5)	-0.2	0.1	0.1
	IPSL-CM5A-MR-r1 IPSL-INERIS-WRF331F (4.5)	-0.2	0.1	0.2
	HadGEM2-ES-r1 SMHI-RCA4 (4.5)	-0.1	0.0	0.3
	MPI-ESM-LR-r1 CSC-REMO (4.5)	-0.1	0.0	0.2
	EC-EARTH-r1 KNMI-RACMO22E (8.5)	0.0	0.0	-0.1
	EC-EARTH-r12 SMHI-RCA4 (8.5)	-0.2	0.1	0.1
	HadGEM2-ES-r1 SMHI-RCA4 (8.5)	-0.1	0.0	0.2
MPI-ESM-LR-r1 CSC-REMO (8.5)	-0.1	0.1	0.1	
-1.5	observed	16	6.5	63.4
	EC-EARTH-r12 SMHI-RCA4 (2.6)	0.1	0.0	0.2
	MPI-ESM-LR-r1 CSC-REMO (2.6)	-0.1	0.0	0.2
	EC-EARTH-r1 KNMI-RACMO22E (4.5)	-0.3	0.1	0.1
	EC-EARTH-r12 SMHI-RCA4 (4.5)	-0.1	0.0	0.2
	IPSL-CM5A-MR-r1 IPSL-INERIS-WRF331F (4.5)	-0.4	0.2	0.3
	HadGEM2-ES-r1 SMHI-RCA4 (4.5)	-0.1	0.0	0.3
	MPI-ESM-LR-r1 CSC-REMO (4.5)	-0.1	0.0	0.3
	EC-EARTH-r1 KNMI-RACMO22E (8.5)	-0.1	0.0	0.2
	EC-EARTH-r12 SMHI-RCA4 (8.5)	-0.1	0.0	0.3
	HadGEM2-ES-r1 SMHI-RCA4 (8.5)	0.0	0.0	0.2
MPI-ESM-LR-r1 CSC-REMO (8.5)	0.1	0.0	0.2	
-2	observed	7	6.7	78.1
	EC-EARTH-r12 SMHI-RCA4 (2.6)	0.3	-0.1	0.1
	MPI-ESM-LR-r1 CSC-REMO (2.6)	0.1	0.0	0.1
	EC-EARTH-r1 KNMI-RACMO22E (4.5)	0.1	0.0	0.0
	EC-EARTH-r12 SMHI-RCA4 (4.5)	0.0	0.0	-0.1
	IPSL-CM5A-MR-r1 IPSL-INERIS-WRF331F (4.5)	0.0	0.0	0.1
	HadGEM2-ES-r1 SMHI-RCA4 (4.5)	0.0	0.0	0.2
	MPI-ESM-LR-r1 CSC-REMO (4.5)	0.1	0.0	0.1
	EC-EARTH-r1 KNMI-RACMO22E (8.5)	0.0	0.0	0.0
	EC-EARTH-r12 SMHI-RCA4 (8.5)	0.6	-0.1	0.1
	HadGEM2-ES-r1 SMHI-RCA4 (8.5)	0.3	-0.1	0.1
MPI-ESM-LR-r1 CSC-REMO (8.5)	0.1	0.0	0.1	



Figure 4.3. Biases (relative difference) in individual climate change models relative to the observed mean for rainfall drought metrics: frequency, duration (months) and monthly intensity (hm³). The observed mean is noted on top of each column. Metrics were averaged across all drought events (denoted mean).

4.4.2 Impact of Climate Change on the Annual and Monthly Rainfall and Flow

The graphical depiction of the monthly rainfall, karstic and surface flow quartiles of the two basins for the reference period (1979-2018) is presented in the box-plots of Figure 4.4. The mean annual rainfall values of each watershed are estimated as the area weighted average of rainfall which falls over each sub-basin, since each sub-basin receives rainfall input from the rainfall station which is closest to it. The Koiliaris RB has higher precipitation records compared to Keritis RB, as a great percentage of its area lies over higher altitudes and the extended karstic area is also taken into account. The Stilos spring has higher flows during winter months compared to the Agia spring but presents high

monthly variability. The monthly variability of the Agia spring, however, is low, as a result of its high detention time. The Meskla spring demonstrates lower variability compared to Stilos spring, but the spring's flow is close to zero during dry months.

The mean annual values of rainfall, karstic and surface flow for both basins for the reference period (1979-2018) and for the two future periods (2019-2058 and 2059-2098), under the eleven scenarios, are presented in Table 4.1. The percentages of change, relative to the reference period values, are also presented in Table 4.1. As far as the period 2019-2058 is concerned, the eleven scenarios suggest a mean increase in rainfall, equal to 2.4% in Koiliaris and 3.6% in Keritis RB respectively. This increase induces a greater mean increase in surface flow for the Koiliaris River Basin (16.9%) and an even greater increase in the surface flow of the Keritis River Basin (28.1%). In addition, it is noteworthy that the mean increase in rainfall does not signify increase in karstic flow. On the contrary, the karstic flow decreases, especially for the case of Stilos spring (9.9%). The Meskla spring and Agia spring flows are not expected to change significantly during the 2019-2058 period (decrease of 0.7% and 0.8% respectively).

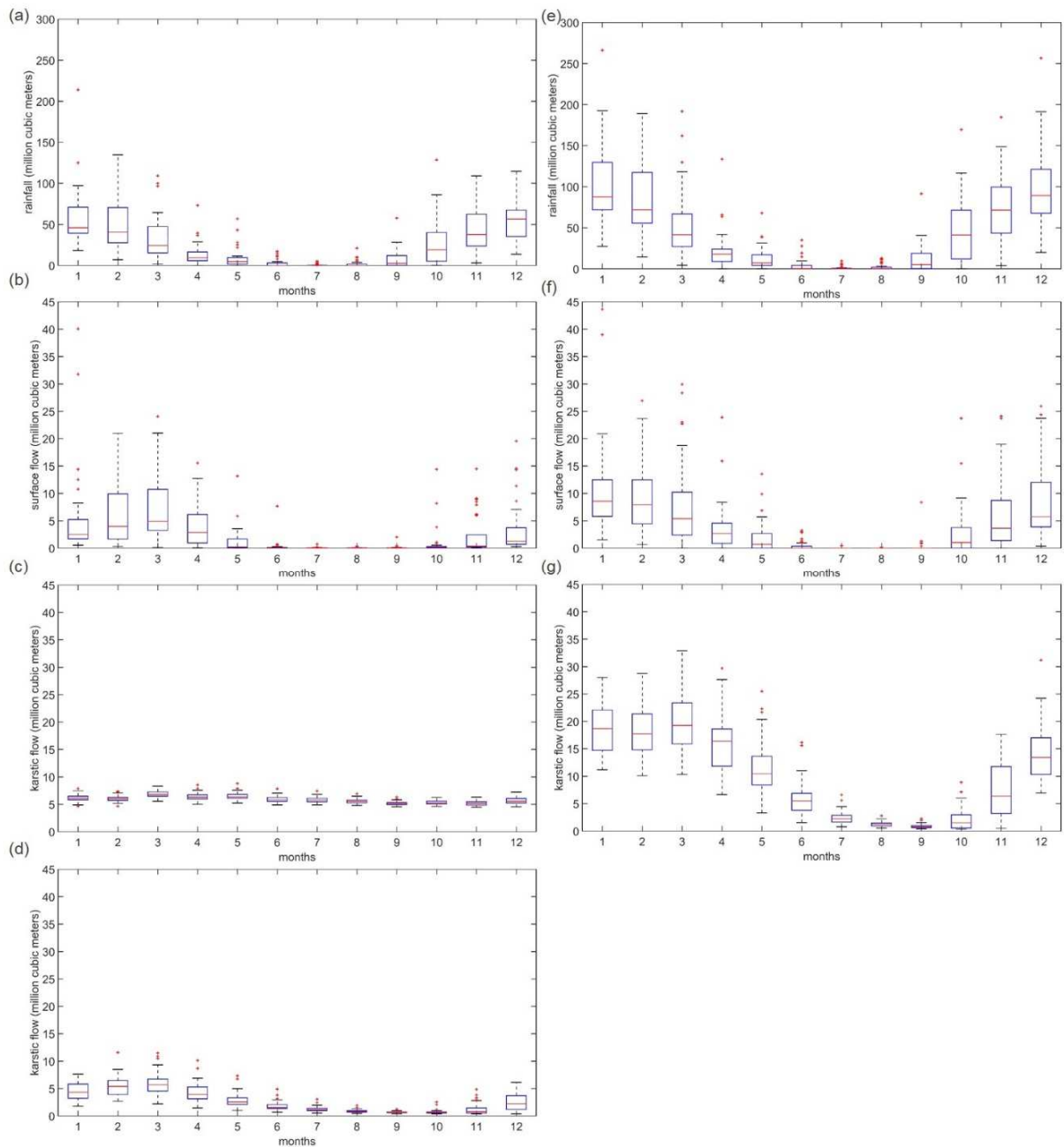


Figure 4.4. Box plots of monthly values of (a) rainfall in Keritis RB (b) surface flow in Keritis RB (c) karstic flow of Agia (d) karstic flow of Meskla (e) rainfall in Koiliaris RB (f) surface flow in Koiliaris RB (g) karstic flow of Stilos, for the reference period (1979-2018).

The greater increase in surface flow, compared to the increase in rainfall, can be explained by the frequency and intensity of daily rainfall in the future periods. The distribution of rainfall changes in the future, with higher probabilities of high daily rainfall and lower probabilities of low daily rainfall (Figure 4.9 and Tables 4.3 and 4.4). The high intensity rainfall favors the formation of surface flow at the expense of karstic flow, since the

rainfall intensity exceeds the infiltration rate (into the groundwater). This also explains the decrease in karstic flow.

After 2059, the mean annual rainfall decreases for both basins (9.0% and 6.5%) and induces a significant decrease in the mean annual karstic flow of Stilos spring (25.1%) and an important, but milder, decrease in the mean annual karstic flows of Meskla and Agia springs (18.7% and 14.2% respectively). The decrease is more eminent for Stilos spring compared to the Meskla and Agia springs, which respond better to adverse climate change due to their higher detention times, hence their more efficient water storage. Furthermore, the rainfall decrease in the Keritis RB is slightly milder compared to the one in Koiliaris RB, which partially explains the difference between the relative change of Stilos and Meskla springs. The mean annual surface flow is relatively stable for the Koiliaris RB (0.4%) and a relative increase is forecasted for the mean annual surface flow of the Keritis RB (8.0%).

Table 4.1. Mean annual values of rainfall, karstic and surface flows for the two basins for the reference period (1979-2018) and mean annual values of the same variables for two future periods (2019-2058 and 2059-2098) based on all eleven climate change scenarios under study. The percentage (%) change of the variables in the future periods in comparison with the reference period is also noted in brackets. Negative values suggest decrease of the variable of interest.

variable	1979-2018 (hm ³ /year)	2019-2058 (hm ³ /year)	2059-2098 (hm ³ /year)
rainfall	546.1	559.7 (2.4%)	496.8 (-9.0%)
rainfall	303.4	314.5 (3.6%)	283.7 (-6.5%)
Stilos spring	119.2	107.0 (-9.9%)	89.2 (-25.1%)
surface flow	52.0	60.8 (16.9%)	53.1 (0.4%)
Meskla	30.8	30.6 (-0.7%)	25.1 (-18.7%)
Agia spring	70.9	70.4 (-0.8%)	60.9 (-14.2%)
surface flow	30.2	38.7 (28.1%)	32.6 (8.0%)

The mean annual karstic flow values for the three springs along with their 90% confidence interval are presented in Figure 4.5. The descending trend of the mean is evident for the three springs. After 2059, the mean annual flow of the Agia spring (Figure 4.5a) is equal to the min of the reference period (about 34 hm³). However, the spring is expected to be able to cover the current water needs, even for the worst case scenario (min annual value equal to 30.1 hm³ and mean annual water needs equal to 26.7 hm³). The same stands for the Meskla spring (Figure 4.5b), for which the mean annual water needs are 5hm³. The Stilos spring (Figure 4.5c) is the most vulnerable spring, with the most adverse relative decrease, as a result of the lower water detention time.

As it is evident from the mean annual forecasts of the above mentioned variables, climate change has an adverse impact on karstic water resources after 2059. In order to depict the distribution of monthly karstic flow for the three karstic springs based on all eleven scenarios, the box plots of the monthly quartiles, taking into account the monthly karstic values of all the scenarios for the period 2059-2098, are depicted in Figure 4.6. The monthly flow of the Agia spring never falls under 1.9 hm^3 , while the minimum monthly flows of the Meskla spring and the Stilos spring are 94.7 dam^3 (0.0947 hm^3) and 20.1 dam^3 (0.0201 hm^3) respectively. It is notable that the Meskla and Stilos springs are expected to approach monthly values close to zero for all months, including the wettest months. During the reference period (Figure 4.4) this happens only for the dry months, especially for the case of the Stilos spring. In the next sections we will examine the temporal distribution of these low flows.

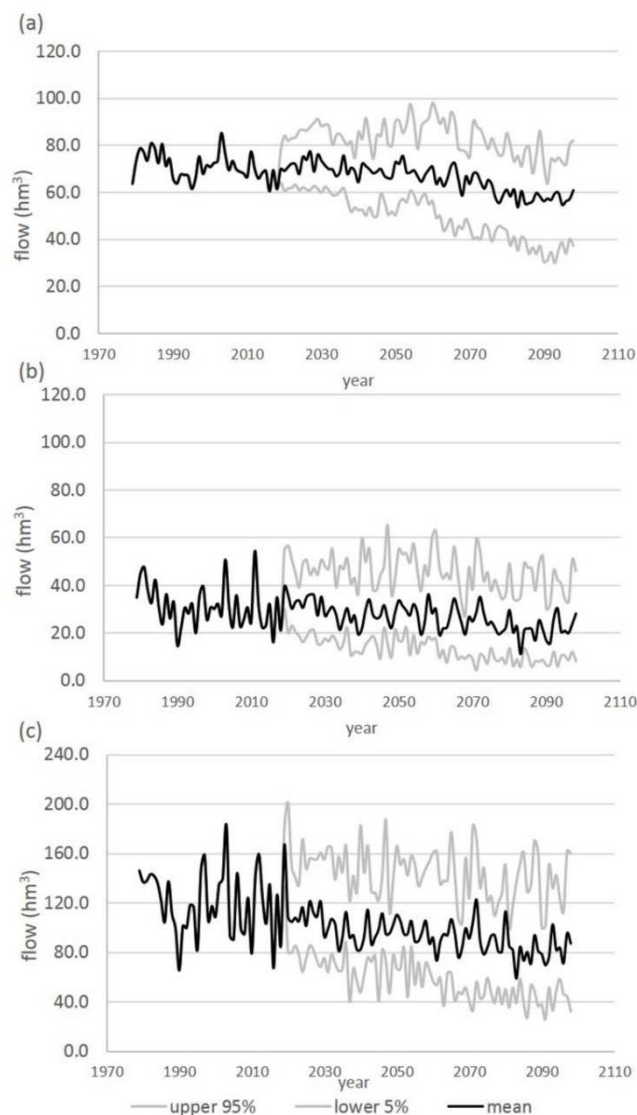


Figure 4.5. Mean annual karstic flow of the three springs (a) Agia, (b) Meskla and (c) Stilos for the reference (1979-2018) and the future period (2019-2098). Ninety percent confidence interval is marked with light grey lines.

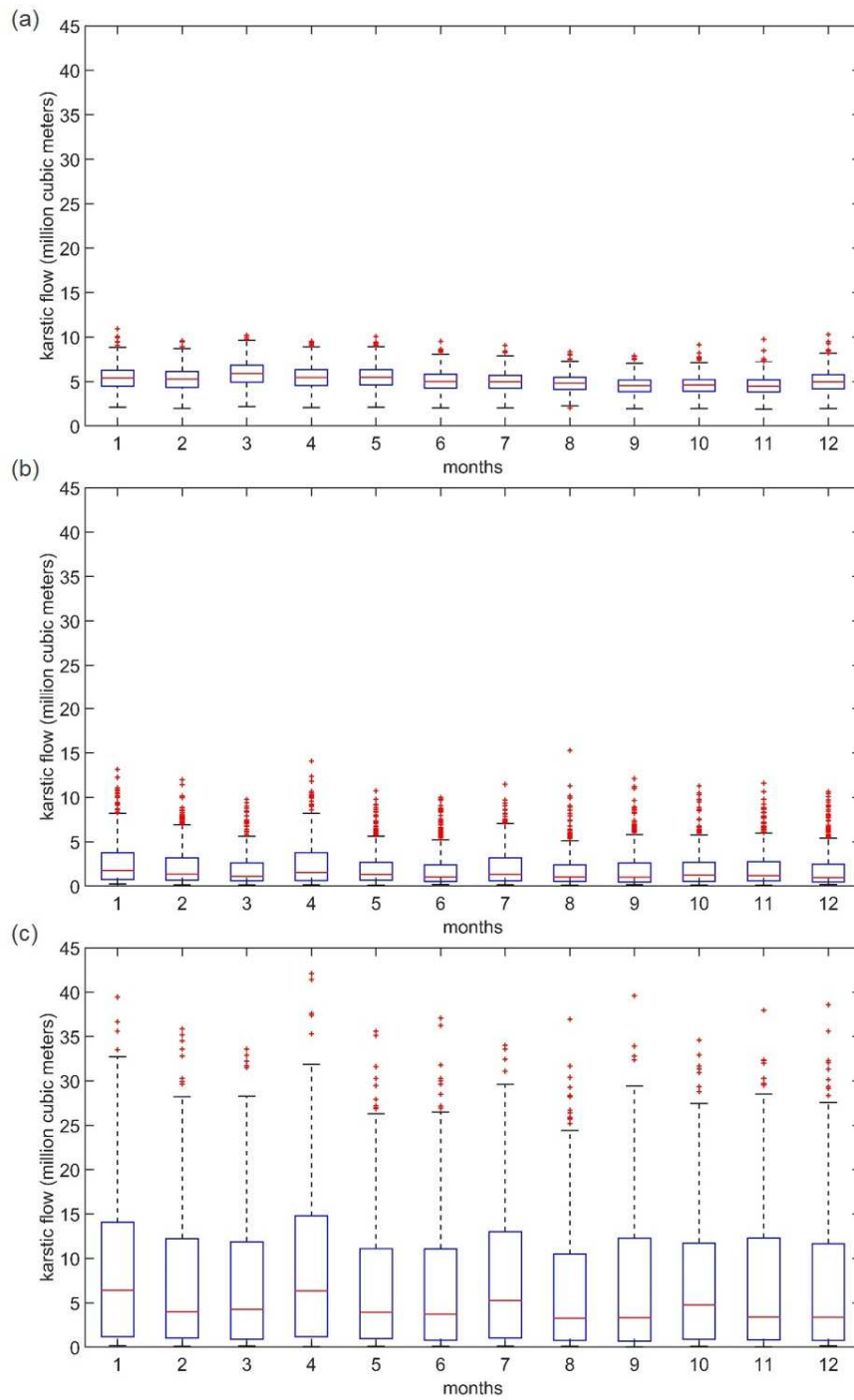


Figure 4.6. Box plots depicting the monthly quartiles of the flow of the three karstic springs (a) Agia, (b) Meskla and (c) Stilos for the 2059-2098 under the eleven scenarios of the study.

4.4.3 Impact of Climate Change on the Meteorological and Hydrological Drought Frequency, Intensity and Duration

We apply the modified drought index on the rainfall and karstic flows of the three springs under study. We choose the Psichro station for the analysis of the meteorological drought, since it is the only station which is used as input for both basins. Figure 4.7 depicts the mean number of drought events for (a) rainfall and (b) Stilos spring flow which occur during the reference period (1979-2018), and the two future periods (2019-2058, 2059-2098) under the (i) RCP2.6, (ii) RCP4.5 and (iii) RCP8.5 scenarios and Figure 4.8 is the same figure for the case of (a) Meskla spring flow and (b) Agia spring flow.

The first deduction from Figure 4.7 is that even for the favorable scenario RCP2.6, the meteorological drought index indicates more adverse conditions drought-wise, specifically for the frequency of severe and extreme droughts. The increased number of future meteorological droughts compared to the reference period droughts is obvious for scenarios RCP4.5 and RCP8.5. The frequency of the hydrological droughts of Stilos spring appear to mainly follow the trend of the frequency of the meteorological droughts. During the reference period, the frequency of Stilos hydrological droughts is lower than the meteorological droughts, however, during the future periods the number of occurring hydrological droughts is as high as the meteorological droughts, or even higher.

Even though the spring of Meskla (Figure 4.8a) has the same number of drought events with the Stilos spring during the reference period, the increase of the Meskla drought events in the future is milder. The frequency of the hydrological drought events of the Agia spring is low, compared to the other two springs. In addition, in many cases, the trend of the hydrological drought index of Agia does not conform to the trend of the meteorological drought. We should note that the cases where the “extreme” events outnumber the “severe to extreme” events (or the “moderate to extreme” events) for the same period, occur when a drought has a very long duration and “breaks” into multiple droughts when the index takes lower values (see for example Figure B2, Appendix B).

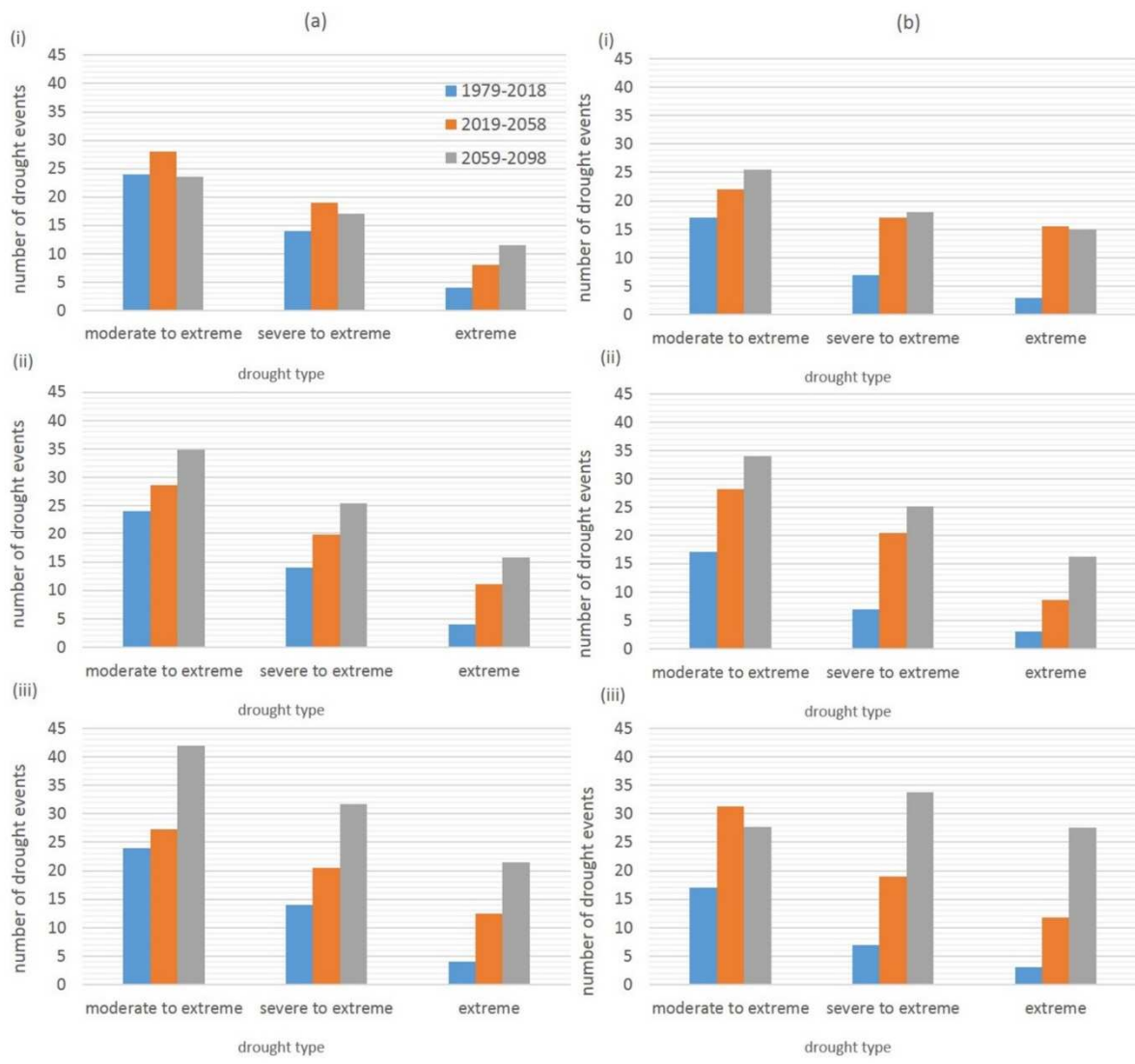


Figure 4.7. Bar charts depicting the mean number of drought events of (a) rainfall and (b) Stilos spring flow which occur during the reference period (1979-2018), the period 2019-2058 and the period 2059-2098 under the (i) RCP2.6, (ii) RCP4.5 and (iii) RCP8.5 scenarios.

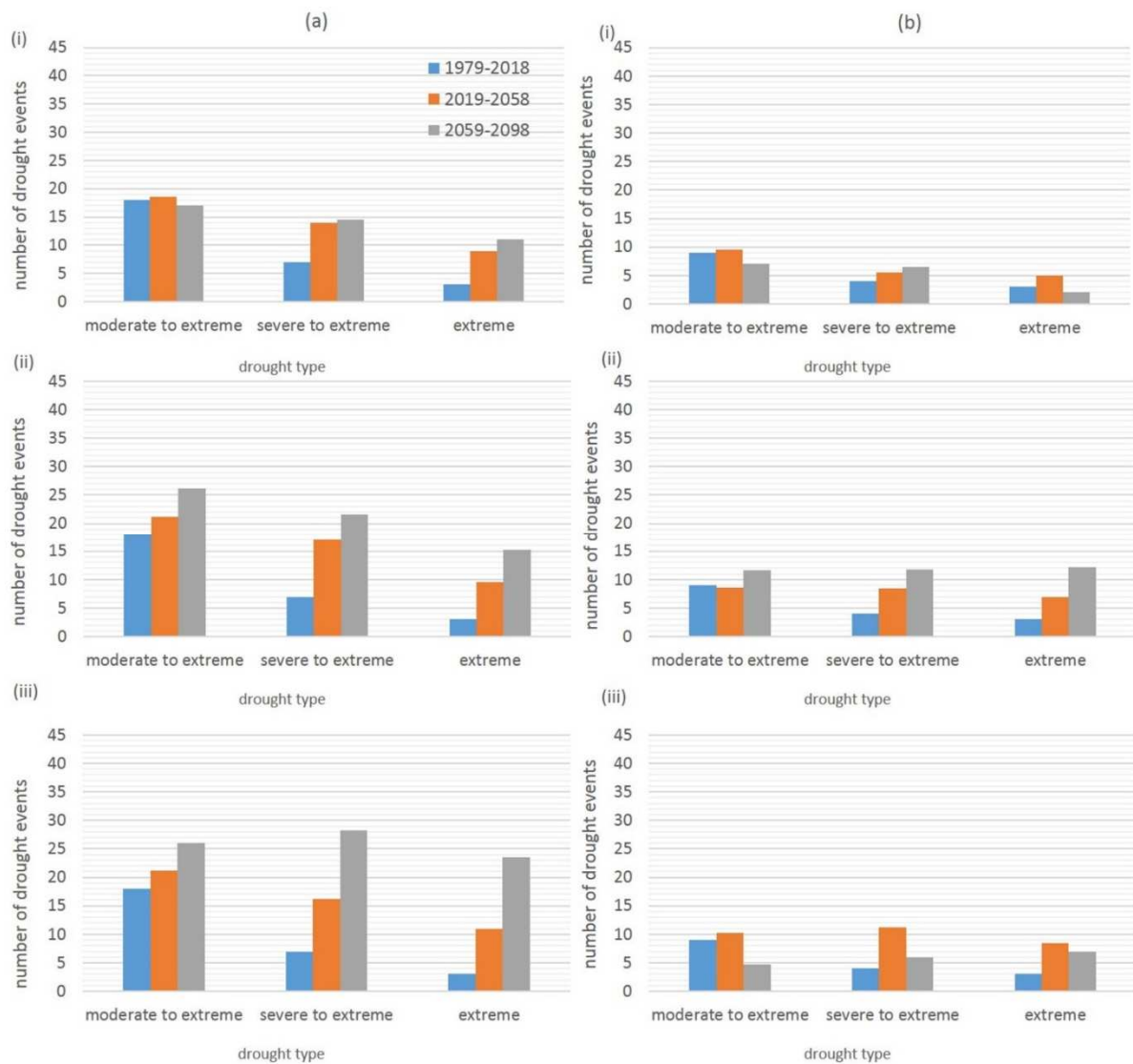


Figure 4.8. Bar charts depicting the mean number of drought events of (a) Meskla spring flow and (b) Agua spring flow which occur during the reference period (1979-2018), the period 2019-2058 and the period 2059-2098 under the (i) RCP2.6, (ii) RCP4.5 and (iii) RCP8.5 scenarios.

Table 4.2 presents the duration of the drought events characterized as “moderate to extreme”, i.e. the duration of events for which the modified (meteorological or hydrological) drought index is equal to or lower than -1. The values are in the form of ranges, since more than one RCM has been studied for each RCP. The index suggests that the meteorological droughts are expected to have a maximum duration of 15 months. The maximum duration of a hydrological drought is 97 months for the Stilos spring, 54 months for the Meskla spring and 480 months for the Agia spring flow (under RCP8.5 during the period 2059-2098). The duration of the drought event is the highest for the spring with the highest detention time and can last as long as 40 years (the whole period under study for the case of Agia). It is important to note that, for all springs, multi-year droughts are forecasted in the future, under most scenarios (even for the “favorable” RCP2.6), while

the longest hydrological drought lasts 14, 12 and 21 months for Stilos, Meskla and Agia respectively.

The combination of high frequency and duration of drought events in the future for the Stilos spring suggests that it is the most vulnerable spring to the adverse climate change impact. The Meskla spring, which has similar drought duration and frequency during the reference period, responds slightly better to climate change. Essentially, we cannot compare the response of the Stilos spring to drought with the response of the Meksla spring based on the detention time, as the Meskla spring has a different, more complex system and the water quantities of water are different. The Stilos mean annual discharge is 4 times higher than the Meskla mean annual discharge.

The Agia spring demonstrates very long periods of drought in the future. The frequency of the Agia drought events is lower after 2059 compared to the reference period (Figure 4.8b) because, essentially, the whole period of 2059-2098 tends to become a single drought period for this spring (under the RCP8.5). This increase in drought duration can be justified by the existence of many “short” meteorological droughts during the future period; these individual meteorological droughts which occur successively, accumulate over the long water detention time of Agia and are expressed as long drought periods by the spring. Figure B2 (Appendix B) depicts the 6-month modified drought index, applied on the time series of rainfall (Psichro) and the karstic flow of Agia under an adverse scenario (REMO under the RCP8.5 for the period 1979-2098). The figure shows the effect of the meteorological droughts on the hydrological droughts of Agia. After September 2073, there are many extreme meteorological droughts which cause a single extreme hydrological drought lasting until 2098. The trend of the 6-month meteorological drought index does not comply with the trend of the 6-month hydrological drought index for Agia. The trend of the 82-month moving average of the monthly rainfall time-series, though, follows the trend of the hydrological drought index and explains the long drought periods of Agia. The reason behind the choice of the 82-month moving average is that 82 months (or 6.84 years) equal the water detention time of Agia.

For the quantification of the water deficit (or intensity) during each drought event, we compare the total water volume during the drought event to the mean of the total water volume during the corresponding months of the reference period, as in Equation (4.3) (Table 4.3). We calculate both the mean total water deficit during all drought events of each sub-period, and the mean monthly water deficit based on all drought events of each sub-period. When comparing the mean monthly deficit of each spring with the mean monthly flow of each spring for the 2059-2098 period, the deficit constitutes the 47.9% of the mean monthly flow of the Stilos spring, the 53.1% of the mean monthly flow of the Meskla spring and the 18.1% of the mean monthly flow of the Agia spring. These percentages, for the reference period, are 28.3% for Stilos, 30.8% for Meskla and 8.5% for Agia. The spring with the highest detention time and the lowest variability has the lowest

deficit (relative to the monthly mean flow), but in the future, the relative deficit increases to a greater extent for Agia, then for Meskla and lastly for Stilos.

Finally, we compare the mean frequency, duration and intensity of the drought events for each of the springs during the reference period with those of the two future periods (2019-2058 and 2059-2098), based on all the climate change scenarios. The results are shown in Table 4.4. It is evident that climate change will have an adverse impact on the frequency, duration, and intensity of drought events. Overall, the meteorological drought index is far more conservative than the hydrological drought index for all three springs. Between the Stilos and Meskla spring, the former is expected to have more frequent and longer drought events but the latter is forecasted to have higher drought intensities (compared to its mean monthly flow). The frequency of drought events is relatively stable for the Agia spring but the intensity and duration of the spring's drought events present a dramatic increase in the future.

Table 4.2. Mean duration (and range in parenthesis) of moderate to extreme drought events in months (drought index lower than -1) of rainfall (Psichro station), Stilos spring flow, Meskla spring flow and Agia spring flow for the reference period (1979-2018), and the future periods 2019-2058 and 2059-2098, under the RCP2.6, RCP4.5 and RCP8.5 scenarios.

Variable	1979-2018 drought duration mean and range (months)	2019-2058 drought duration mean and range (months)	2059-2098 drought duration mean and range (months)
RCP2.6			
rainfall	8.1 (6-12)	7.8 (6-14)	8.5 (6-13)
Stilos flow	9.4 (6-14)	11.2 (6-27)	10.9 (6-23)
Meskla flow	9.2 (6-12)	11.1 (6-15)	11.4 (6-17)
Agia flow	11.9 (6-21)	16.4 (7-48)	11.9 (6-19)
RCP4.5			
rainfall	8.1 (6-12)	8.0 (6-13)	8.5 (6-15)
Stilos flow	9.4 (6-14)	11.3 (6-28)	12.4 (6-38)
Meskla flow	9.2 (6-12)	11.1 (6-24)	11.9 (6-26)
Agia flow	11.9 (6-21)	23.6 (6-128)	42.0 (6-64)
RCP8.5			
rainfall	8.1 (6-12)	8.5 (6-15)	8.9 (6-15)
Stilos flow	9.4 (6-14)	11.5 (6-75)	16.6 (6-97)
Meskla flow	9.2 (6-12)	11.0 (6-15)	14.0 (6-54)
Agia flow	11.9 (6-21)	22.2 (6-89)	172.0 (6-480)

Table 4.3. Mean intensity (i.e. mean total water deficit during drought) of moderate to extreme drought events in million cubic meters (drought index lower than -1) of Stilos spring flow, Mekska spring flow and Agia spring flow for the reference period (1979-2018), and the future periods 2019-2058 and 2059-2098, under the RCP2.6, RCP4.5 and RCP8.5 scenarios. The mean monthly deficit is shown in the parentheses.

Variable	1979-2018 mean total water deficit during drought and mean monthly deficit (hm³)	2019-2058 mean total water deficit during drought and mean monthly deficit (hm³)	2059-2098 mean total water deficit during drought and mean monthly deficit (hm³)
RCP2.6			
Stilos flow	28.9 (2.8)	42.9 (3.1)	40.4 (3.2)
Meskla flow	6.9 (0.8)	11.8 (1.0)	12.8 (1.1)
Agia flow	7.3 (0.5)	11.0 (0.6)	5.6 (0.5)
RCP4.5			
Stilos flow	28.9 (2.8)	38.8 (2.9)	53.5 (3.5)
Meskla flow	6.9 (0.8)	10.3 (0.9)	14.2 (1.1)
Agia flow	7.3 (0.5)	21.1 (0.6)	54.7 (0.8)
RCP8.5			
Stilos flow	28.9 (2.8)	47.5 (3.2)	74.7 (3.9)
Meskla flow	6.9 (0.8)	11.4 (1.0)	21.7 (1.2)
Agia flow	7.3 (0.5)	18.4 (0.6)	377.4 (1.4)

Table 4.4. Percentages of change of the drought events frequency, duration and intensity (mean monthly intensity) in the two future periods (2019-2058 and 2059-2098) compared to the reference period (1979-2018)

2019-2058 compared to 1979-2018			
variable	Frequency	Duration	Intensity
rainfall	16.7 %	0.2 %	14.9 %
Stilos flow	65.8 %	20.4 %	8.6 %
Meskla flow	15.2 %	20.2 %	20.5 %
Agia flow	4.0 %	83.0 %	20.0 %
2059-2098 compared to 1979-2018			
variable	Frequency	Duration	Intensity
rainfall	47.3 %	6.7 %	22.9 %
Stilos flow	77.5 %	45.0 %	27.3 %
Meskla flow	35.9 %	36.8 %	38.6 %
Agia flow	-8.1 %	533 %	83.6 %

The correlation between the 6-month modified drought index applied (1) on the rainfall of Psichro and (2) the karstic flows of (i) Stilos, (ii) Meskla and (iii) Agia is also examined, in order to test the efficacy of the meteorological index to depict the hydrological droughts. The coefficient of determination (r^2) between the meteorological and hydrological index is (on average, based on the 11 scenarios) 0.54 for the Stilos flow, 0.48 for the Meskla flow and 0.18 for the Agia flow. A coefficient of determination of at least 0.5 is considered satisfactory (Moriassi et al., 2007). As it is evident, the 6-month meteorological index cannot provide a satisfactory representation for the hydrological droughts of a karstic spring with high detention time, and its performance is mediocre even for the springs with lower detention times. Fiorillo and Guadagno (2010) found that the best correlation between the Standard Precipitation Index (SPI) and the discharges of the karstic springs they studied (located in Italy) occurs for a time scale of 9 or 12 months. Therefore we also apply the modified drought index for a time scale of 9 and 12 months on the monthly rainfall and karstic flows time series. The average r^2 between the meteorological and hydrological 9-month index (based on the 11 scenarios) is 0.64, 0.66 and 0.23 for the flows of Stilos, Meskla and Agia respectively. The corresponding r^2 values are 0.72, 0.74 and 0.35 when the index is applied with the 12-month time scale. The correlation between the meteorological and hydrological index (for karstic flow) is improved with the increase in the time scale, and the meteorological index can satisfactorily describe the trend of the hydrological droughts of Stilos and Meskla for a time scale of 9 and 12 months but cannot reproduce the drought conditions of the Agia spring, even for large time scales. A meteorological drought index of 82 months would provide a satisfactory correlation with the hydrological index of Agia (Figure B2).

4.4.4 Impact of Climate Change on the Flow Extremes

The flow value which corresponds to the 10th percentile of the daily karstic flow for Stilos and Meskla is 0.278 m³/s and 0.132 m³/s respectively, for the 40-year reference period (1979-2018). According to Table 4.5, based on all three RCPs of the RCM REMO, the percentage of daily flow values which are lower than the reference period's 10th percentile threshold increases for all scenarios in the future for Stilos and Meskla, ranging from 12.7% to 31.9% for Stilos and 10.5% to 37.9% for Meskla. For the case of the Agia spring, the percentage of daily flow values lower than the reference period's 10th percentile threshold increases under the RCPs 4.5 and 8.5 (ranging from 25.7% to 71.7%) but decreases under the RCP2.6 (ranging from 1.7% to 7.1%). On average, based on the three RCPs, the low flows of Stilos increase by 61.3% during the period 2019-2058 and 126.5% during the period 2059-2098, the low flows of Meskla increase by 62.0% and 129.6% respectively, and the low flows of Agia increase by 61.8% and 73.4%. The highest percentage corresponds to the period 2059-2098 of the RCP8.5 scenario, and the lowest corresponds to the RCP2.6 scenario. Even for the favorable scenario RCP2.6, though, the

number of low flows increases in the future for both future periods and for Stilos and Meskla springs.

The distribution of the low flows frequency is presented in Figure 4.9. This figure reveals that all three scenarios suggest a shift of the low flows towards wetter months, especially after 2059. The Stilos spring low flows of the reference period take place from July to November, with the majority of the low flows happening during October. During the 2019-2058 period, the majority of low flows still occurs during October (except for the RCP4.5 with the peak during September), but there are also low flows during June and December and more low flows during the July-November period. After 2059, under the RCP8.5, September is the month with the most of the low flows and there are low flows throughout the year. Under the RCP4.5 and RCP2.6, low flows take place from May to December.

Most of the low flows of the Meskla spring occur during October and there are low flows from July to January, during the reference period. During the period 2019-2058, low flows exist from June to January (RCP8.5) and from May to January for the other RCPs. After 2059, during the two future periods, low flows are present throughout the year for all scenarios. Also, it is noteworthy that for the RCP8.5 and the 2059-2098 period, the Meskla flows are equal to zero, i.e. the spring is completely dry for 10.7% of the days in this 40-year period, and the zero flows occur throughout the year.

The low flows of Agia occur from June to January during the reference period. The peak of Agia low flows occurs during October for the reference and future periods. The forecasted low flows for Agia present high variability; the favorable RCP2.6 scenario predicts decreased frequency in low flows, whereas scenarios RCP4.5 and RCP8.5 predict great increase in low flows which are expected to take place throughout the year.

Table 4.5. Number of days with low flow for the Stilos and Meskla springs and their percentage on the total 14610 days of each 40-year period: the reference period and the two future periods (2019-2058 and 2059-2098), under the Regional Climate Scenario REMO and the Representative Concentration Pathways RCP2.6, 4.5 and 8.5

scenario/period	number of low flow days of Stilos (percentage on total days)	number of low flow days of Meskla (percentage on total days)	number of low flow days of Agia (percentage on total days)
reference period	1461 (10.0%)	1461 (10.0%)	1461 (10.0%)
REMO2.6/2019-2058	1851 (12.7%)	1941 (13.3%)	1030 (7.1%)
REMO2.6/2059-2098	1910 (13.1%)	1541 (10.5%)	248 (1.7%)
REMO4.5/2019-2058	2794 (19.1%)	2913 (19.9%)	6691 (45.8%)
REMO4.5/2059-2098	3360 (23.0%)	2986 (20.4%)	5757 (39.4%)
REMO8.5/2019-2058	2423 (16.6%)	2246 (15.4%)	3758 (25.7%)
REMO8.5/2059-2098	4656 (31.9%)	5535 (37.9%)	10384 (71.7%)

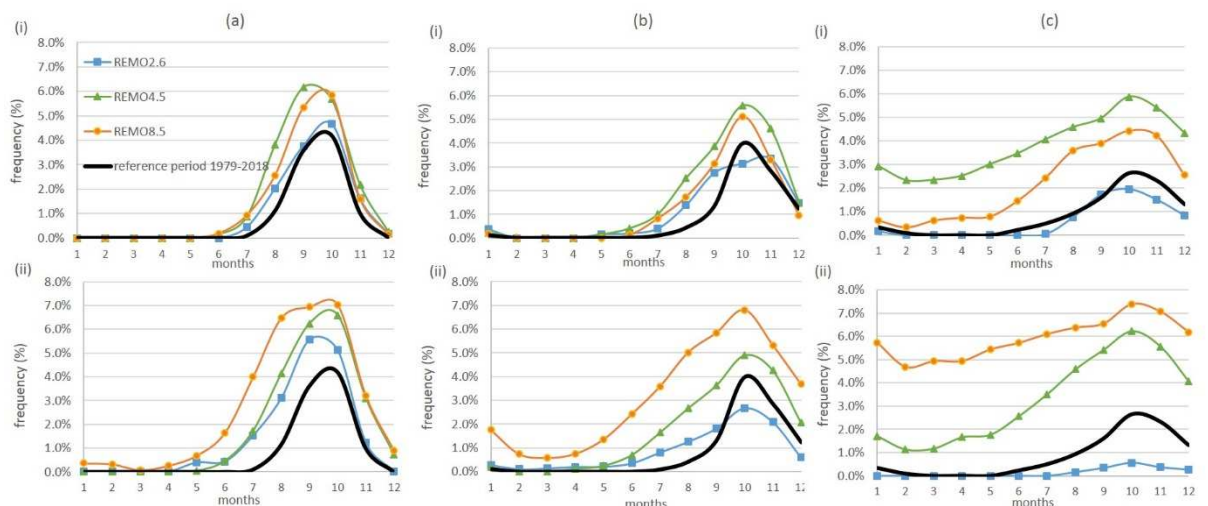


Figure 4.9. Frequency of low daily karstic flows (10th percentile of reference period) of (a) Stilos (b) Meskla and (c) Agia corresponding to every month (days with low flows divided by the total 14610 days of each 40-year period), for the reference (1979-2018) and the two future periods: (i) 2019-2058 and (ii) 2059-2098) under the Regional Climate Scenario REMO and the Representative Concentration Pathways RCP2.6, 4.5 and 8.5.

The Mean Excess Function is applied on the time series of rainfall, surface flow of Koiliaris and Keritis RBs, and the karstic flows of Stilos, Meskla and Agia under the scenario REMO and the RCPs 2.6, 4.5 and 8.5 (future periods) as well as the reference period. The distributions of rainfall and both surface flows have generally heavy tails (Table 4.6)

(according to Figure B1 of Appendix B, the tails are sub-exponential), whereas the distributions of karstic flows have light tails (hyper-exponential). During the future periods, the rainfall distribution tail becomes heavier under the RCP2.6 (both future periods) and the RCP8.5 (period 2059-2098), while the rainfall tail is relatively the same for the RCP4.5 scenario. The surface flows display even heavier tails compared to the rainfall tails. The surface flow distribution tails in the future are always heavier than the ones of the reference period and the Keritis RB surface flow distribution tail of is always heavier than the one of Koiliaris RB. This explains the more intense increase in the surface flow of Keritis compared to the surface flow of Koiliaris, due to climate change. The hyper-exponential tails of the karstic flows of Stilos and Agia are still hyper-exponential during the future. The distribution tail of the Stilos spring becomes heavier as time progresses, but the distribution tail of the Agia spring is relatively stable with time. The tail of the Meskla karstic flow distribution converts to exponential and even sub-exponential (for the case RCP8.5 and the period 20598-2098), indicating more frequent high flows for the Meskla spring.

Table 4.6. Mean Excess Function slopes for the time series of rainfall at Psichro, surface flow at the Koiliaris and Keritis River Basins, and karstic flow of Stilos, Meskla and Agia springs, under the Regional Climate Model REMO and the Representative Concentration Pathways 2.6, 4.5 and 8.5, for the reference period (1979-2018) and two future periods (2019-2058 and 2059-2098).

variable	MEF slope 1979-2018	MEF slope 2019-2058	MEF slope 2059-2098
REMO RCP2.6			
rainfall	0.78	1.05	0.93
Surface flow	1.27	2.28	2.26
Surface flow	1.61	4.17	3.23
Stilos flow	-0.37	-0.29	-0.28
Meskla flow	-0.16	-0.04	-0.08
Agia flow	-0.37	-0.31	-0.36
REMO RCP4.5			
rainfall	0.78	0.71	0.72
Surface flow	1.27	1.87	2.15
Surface flow	1.61	4.74	3.69
Stilos flow	-0.37	-0.26	-0.28
Meskla flow	-0.16	-0.03	-0.11
Agia flow	-0.37	-0.31	-0.28
REMO RCP8.5			
rainfall	0.78	0.67	0.91
Surface flow	1.27	1.92	2.73
Surface flow	1.61	3.06	6.83
Stilos flow	-0.37	-0.031	-0.13
Meskla flow	-0.16	-0.12	0.15
Agia flow	-0.37	-0.33	-0.38

4.5 Discussion and Conclusions

The study focuses on three Mediterranean karstic springs with different hydrologic responses and, specifically, different karstic systems and water detention times. The results in this study mainly focus on the low flows of the three karstic springs, but they also deal with the upper tails of the distributions of rainfall and flow, as they facilitate the interpretation of the results. The climate change impact study suggests that more intense changes in flow are observed after 2059, when a mild decrease in the mean annual rainfall (based on the eleven scenarios under study), leads to a substantial decrease in the mean annual karstic flow. Specifically, the Stilos spring is expected to decrease significantly after 2059 (25.1% on average, based on the eleven scenarios), and the decrease is considerable but less intense for the karstic flow of Meskla (18.7%) and Agia (14.2%) springs. A high detention time of the spring secures more efficient water storage and better response to climate change. The projected changes for the karstic springs flow in this study are in accordance with the studies of Hartman et al. (2012) and Smiatek et al. (2013) who conducted climate change impact analyses for Mediterranean karstic springs. The mean annual surface flow demonstrates a slight increase after 2059 (0.4% for Koiliaris and 8.0% for Keritis RB), due to the increase in the frequency of extreme rainfall. High intensity rainfall favors the generation of surface runoff at the expense of karstic flow, since rainfall intensity exceeds the infiltration rate. The Agia spring, which is the main source of water supply and irrigation for the city of Chania, is forecasted to have lower flows after 2059, but the spring will be able to cover the current water needs of the area even for the worst case scenario (although marginally). These water needs will definitely increase in the future since the local authorities have already started discussing and proposing actions for more intensive exploitation of the spring (Decentralized Administration of Crete, 2018). In light of these new data and the estimation of the future water resources in this study, the water management actions for the area should be cautiously designed.

The effect of the springs' detention time is also evident in the analysis of present and future droughts. The frequency of future drought events is higher in karstic springs with lower water detention time (i.e. Stilos) and lower in karstic springs with higher detention time (i.e. Agia). Conversely, the duration of individual drought events is higher for karstic springs with high detention time. Also, the correlation between the meteorological and hydrological drought index decreases as the spring's detention time increases. All the above mentioned results indicate that the droughts of a spring with flashy discharge are more in accordance with the patterns of meteorological droughts compared to a spring with higher storage capacity. In addition, a long hydrological drought of a Mediterranean karstic spring with high detention time is a result of many individual meteorological drought events situated close to each other in time for a long period, rather than one long meteorological drought.

Nerantzaki et al. (2020) have reported that after 2059, the variability of karstic flow due to the climate change scenario is significant (23.5% expressed as Coefficient of Variation). Even with this high uncertainty scores, the most adverse impacts on the hydrological-karstic droughts are expected to take place after 2059, independently of the climate change scenario realized. The Stilos spring is the most vulnerable spring under the impact of climate change, with an increase of 77.5% in frequency, 45% in duration and 27.3% in the mean monthly intensity of drought events. The Meskla spring is projected to have an increase of 35.9% in frequency, 36.8% in duration and 38.6% in mean monthly intensity of droughts. Finally, the drought frequency of the Agia spring decreases 8.1% after 2059, as the duration of drought events increases remarkably (533%), and the mean monthly drought intensity increases (83.6%). The mean deficit to mean monthly flow ratio increases for all springs, especially for the Agia spring, for which it doubles. In addition, for all springs, multi-year droughts are forecasted after 2059, under all scenarios.

The analysis of the extreme low and high flows of the springs and surface flow demonstrates that there will be an increase in the variability of flow values, with increasing high and low flows in frequency and intensity, a statement also supported by Asadieh and Krakauer (2017) for the Mediterranean region. The increase in the extreme high flows and torrential rain will be accompanied by the inflation of flood events, erosion and crop disaster (Papalexioiu and Montanari, 2019). The future distributions of (high) rainfall extremes do not facilitate the water storage of the springs and the increasing frequency of meteorological droughts lead to increasing low flows during the whole year, and especially during the dry months, deteriorating an already challenging situation. Specifically, for both Stilos, Meskla and Agia springs, the low flows will increase 126.5%, 129.5%, and 73.4% after 2059, based on the three REMO scenarios.

These results provide an illustration of the conditions which are expected to prevail for Mediterranean karstic springs in the future. The drought status is anticipated to deteriorate, especially after 2059, regardless of the scenario realized for all springs and the results of this study can be used as a guide for competent bodies to adapt their management practices for the prevention of the negative repercussions of karstic spring droughts. A 40-year period is offered for adaptation measures to be prepared and planned for the improved management of the springs' water resources without running the risk of their drying up.

Acknowledgments

This research is co-financed by Greece and the European Union (European Social Fund-ESF) through the Operational Program «Human Resources Development, Education and Lifelong Learning» in the context of the project “Strengthening Human Resources Research Potential via Doctorate Research” (MIS-5000432), implemented by the State Scholarships Foundation (IKY).

The authors would also like to thank Dr. M.G. Grillakis for his contribution to bias correction of the climate dataset used in this article.

References

- Arnold, J.G., Srinivasan, R., Muttiah, R.S., Williams, J.R., 1998. LARGE AREA HYDROLOGIC MODELING AND ASSESSMENT PART I: MODEL DEVELOPMENT. *J. Am. Water Resour. Assoc.* 34, 73–89. doi:10.1111/j.1752-1688.1998.tb05961.x
- Asadieh, B., Krakauer, N.Y., 2017. Global change in streamflow extremes under climate change over the 21st century. *Hydrol. Earth Syst. Sci.* 21, 5863–5874. doi:10.5194/hess-21-5863-2017
- Bakalowicz, M., 2015. Karst and karst groundwater resources in the Mediterranean. *Environ. Earth Sci.* 74, 5–14. doi:10.1007/s12665-015-4239-4
- Bashfield, A., Keim, A., 2011. Continent-wide DEM creation for the European Union. 34th Int. Symp. Remote Sens. Environ.
- Decentralized Administration of Crete, 2018, Special Management Plan for the Readjustment of Agia Springs, Chania, Technical Report, (In Greek).
- Diffenbaugh, N.S., Giorgi, F., 2012. Climate change hotspots in the CMIP5 global climate model ensemble. *Clim. Change* 114, 813–822. doi:10.1007/s10584-012-0570-x
- Farahmand, A., AghaKouchak, A., 2015. A generalized framework for deriving nonparametric standardized drought indicators. *Adv. Water Resour.* 76, 140–145. doi:10.1016/J.ADVWATRES.2014.11.012
- Fiorillo, F., Guadagno, F.M., 2010. Karst Spring Discharges Analysis in Relation to Drought Periods, Using the SPI. *Water Resour. Manag.* 24, 1867–1884. doi:10.1007/s11269-009-9528-9
- Ford, D. (Derek C., Williams, P.W. (Paul W., 2007. Karst hydrogeology and geomorphology. John Wiley & Sons.
- Grillakis, M.G., Koutroulis, A.G., Tsanis, I.K., 2013. Multisegment statistical bias correction of daily GCM precipitation output. *J. Geophys. Res. Atmos.* 118, 3150–3162. doi:10.1002/jgrd.50323
- Guo, L., Lin, H., 2016. Critical Zone Research and Observatories: Current Status and Future Perspectives. *Vadose Zo. J.* 15, vzt2016.06.0050. doi:10.2136/vzt2016.06.0050
- Hartmann, A., Lange, J., Vivó Aguado, À., Mizyed, N., Smiatek, G., Kunstmann, H., 2012. A multi-model approach for improved simulations of future water availability at a large Eastern Mediterranean karst spring. *J. Hydrol.* 468, 130–138. doi:10.1016/j.jhydrol.2012.08.024
- Jacob, D., Petersen, J., Eggert, B., Alias, A., Christensen, O.B., Bouwer, L.M., Braun, A., Colette, A., Déqué, M., Georgievski, G., Georgopoulou, E., Gobiet, A., Menut, L., Nikulin, G., Haensler, A., Hempelmann, N., Jones, C., Keuler, K., Kovats, S., Kröner, N., Kotlarski, S., Kriegsmann, A., Martin, E., van Meijgaard, E., Moseley, C., Pfeifer, S., Preuschmann, S., Radermacher, C., Radtke, K., Rechid, D., Rounsevell, M., Samuelsson, P., Somot, S., Soussana, J.-F., Teichmann, C., Valentini, R., Vautard, R., Weber, B., Yiou, P., 2014. EURO-CORDEX: new high-resolution climate change projections for European impact research. *Reg. Environ. Chang.* 14, 563–578. doi:10.1007/s10113-013-0499-2
- Lu, J., Carbone, G.J., Grego, J.M., 2019. Uncertainty and hotspots in 21st century projections of agricultural drought from CMIP5 models. *Sci. Rep.* 9, 4922. doi:10.1038/s41598-019-41196-z

- Malagò, A., Efstathiou, D., Bouraoui, F., Nikolaidis, N.P., Franchini, M., Bidoglio, G., Kritsotakis, M., 2016. Regional scale hydrologic modeling of a karst-dominant geomorphology: The case study of the Island of Crete. *J. Hydrol.* 540, 64–81. doi:10.1016/j.jhydrol.2016.05.061
- Mckee, T.B., Doesken, N.J., Kleist, J., 1993. THE RELATIONSHIP OF DROUGHT FREQUENCY AND DURATION TO TIME SCALES.
- Mendlik, T., Gobiet, A., 2016. Selecting climate simulations for impact studies based on multivariate patterns of climate change. *Clim. Change* 135, 381–393. doi:10.1007/s10584-015-1582-0
- Moraetis, D., Efstathiou, D., Stamati, F., Tzoraki, O., Nikolaidis, N.P., Schnoor, J.L., Vozinakis, K., 2010. High-frequency monitoring for the identification of hydrological and biogeochemical processes in a Mediterranean river basin. *J. Hydrol.* 389, 127–136. doi:10.1016/j.jhydrol.2010.05.037
- Moriasi, D.N., Arnold, J.G., Van Liew, M.W., Bingner, R.L., Harmel, R., Veith, T.L., 2007. Model evaluation guidelines for systematic quantification of accuracy in watershed simulations. *Trans. ASABE* 50, 885–900. doi:10.13031/2013.23153
- Moss, R.H., Edmonds, J.A., Hibbard, K.A., Manning, M.R., Rose, S.K., van Vuuren, D.P., Carter, T.R., Emori, S., Kainuma, M., Kram, T., Meehl, G.A., Mitchell, J.F.B., Nakicenovic, N., Riahi, K., Smith, S.J., Stouffer, R.J., Thomson, A.M., Weyant, J.P., Wilbanks, T.J., 2010. The next generation of scenarios for climate change research and assessment. *Nature* 463, 747–756. doi:10.1038/nature08823
- Neitsch, S.L., Arnold, J.G., Kiniry, J.R., Williams, J.R., 2009. Soil and Water Assessment Tool Theoretical Documentation—Version 2009. Temple.
- Nerantzaki, S.D., Efstathiou, D., Giannakis, G. V., Kritsotakis, M., Grillakis, M.G., Koutroulis, A.G., Tsanis, I.K., Nikolaidis, N.P., 2019. Climate change impact on the hydrological budget of a large Mediterranean island. *Hydrol. Sci. J.* 64, 1190–1203. doi:10.1080/02626667.2019.1630741
- Nerantzaki, S.D., Giannakis, G.V., Efstathiou, D., Nikolaidis, N.P., Sibetheros, I.A., Karatzas, G.P., Zacharias, I., 2015. Modeling suspended sediment transport and assessing the impacts of climate change in a karstic Mediterranean watershed. *Sci. Total Environ.* 538, 288–297. doi:10.1016/j.scitotenv.2015.07.092
- Nerantzaki, S.D., Hristopoulos, D.T., Nikolaidis, N.P., 2020. Estimation of the uncertainty of hydrologic predictions in a karstic Mediterranean watershed. *Sci. Total Environ.* 137131. doi:10.1016/j.scitotenv.2020.137131
- Nerantzaki, S.D., Papalexiou, S.M., 2019. Tails of extremes: Advancing a graphical method and harnessing big data to assess precipitation extremes. *Adv. Water Resour.* 134, 103448. doi:10.1016/j.advwatres.2019.103448
- Nikolaidis, N.P., Bouraoui, F., Bidoglio, G., 2013. Hydrologic and geochemical modeling of a karstic Mediterranean watershed. *J. Hydrol.* 477, 129–138. doi:10.1016/j.jhydrol.2012.11.018
- Orehova, T., 2004. Comparative estimate of resistance to drought for selected karstic aquifers in Bulgaria. *Int. J. Speleol.* 33, 73–79. doi:10.5038/1827-806x.33.1.7
- Orlowsky, B., Seneviratne, S.I., 2012. Global changes in extreme events: regional and seasonal dimension. *Clim. Change* 110, 669–696. doi:10.1007/s10584-011-0122-9

- Papalexiou, S.M., Montanari, A., 2019. Global and Regional Increase of Precipitation Extremes under Global Warming. *Water Resour. Res.* 2018WR024067. doi:10.1029/2018WR024067
- Smiatek, G., Kaspar, S., Kunstmann, H., 2013. Hydrological Climate Change Impact Analysis for the Fiegh Spring near Damascus, Syria. *J. Hydrometeorol.* 14, 577–593. doi:10.1175/JHM-D-12-065.1
- Taylor, K.E., Stouffer, R.J., Meehl, G.A., Taylor, K.E., Stouffer, R.J., Meehl, G.A., 2012. An Overview of CMIP5 and the Experiment Design. *Bull. Am. Meteorol. Soc.* 93, 485–498. doi:10.1175/BAMS-D-11-00094.1
- Ukkola, A.M., Pitman, A.J., De Kauwe, M.G., Abramowitz, G., Herger, N., Evans, J.P., Decker, M., Ukkola, A.M., Pitman, A.J., Kauwe, M.G. De, Abramowitz, G., Herger, N., Evans, J.P., Decker, M., 2018. Evaluating CMIP5 Model Agreement for Multiple Drought Metrics. *J. Hydrometeorol.* 19, 969–988. doi:10.1175/JHM-D-17-0099.1
- van Vuuren, D.P., Lucas, P.L., Hilderink, H., 2007. Downscaling drivers of global environmental change: Enabling use of global SRES scenarios at the national and grid levels. *Glob. Environ. Chang.* 17, 114–130. doi:10.1016/J.GLOENVCHA.2006.04.004
- Wilhite, D.A., Glantz, M.H., 1985. Understanding: the Drought Phenomenon: The Role of Definitions. *Water Int.* 10, 111–120. doi:10.1080/02508068508686328
- Wriedt, G., Van der Velde, M., Aloe, A., Bouraoui, F., 2009. Estimating irrigation water requirements in Europe. *J. Hydrol.* 373, 527–544. doi:10.1016/J.JHYDROL.2009.05.018

Chapter 5 Summary and Conclusions

5.1 Summary of aims and methodology

The thesis addresses three main topics: (a) the quantification of the uncertainty of hydrologic predictions in karstic Mediterranean watersheds, (b) the quantification of nitrate mass (and suspended sediment) predictions in karstic Mediterranean watersheds, and (c) the assessment of the climate change impact on karstic Mediterranean springs with different properties. This research intended to “fill” some gaps in the scientific literature, regarding the hydrologic and hydrochemical projections of karstic Mediterranean watersheds and the quantification of their uncertainties. In that regard, a modeling framework is introduced, for the assessment of the uncertainty of composite flow projections, i.e. flows which combine karstic and surface flow. This framework can be also employed for the uncertainty assessment of water quality projections of complex karstic watersheds. It, ultimately, aims to evaluate the impact of climate change on karstic springs, which are valuable and vulnerable Mediterranean water resources, a topic which has not received proper attention in scientific literature, emphasizing on the frequency, duration and intensity of their hydrologic droughts.

Regarding the quantification of the hydrologic predictions uncertainty for karstic Mediterranean watersheds, the research focuses on the uncertainties related to the hydrologic model parameters, the internal variability of input, and the climate change scenarios. The methodology is applied on the karstic Mediterranean watershed of Koiliaris. The hydrologic model used in this study is the SWAT model, modified to account for the karstic spring flow (Karst-SWAT). The SUFI-2 interface in combination with the @RISK software are used to quantify the uncertainty of the surface and karstic flow parameters respectively. Input to the hydrologic models is provided by eleven combinations of five Regional Climate Models (RCMs) and three Representative Concentration Pathways (RCPs). Representative rainfall time series for certain of these scenarios are stochastically modeled with the LARS weather generator. Monte Carlo simulations are used to investigate the effect of input internal variability on the flow output. The uncertainties stemming from different sources are combined. The same framework, with some adjustments, is used for the quantification of the nitrate fluxes uncertainty in the Koiliaris River Basin.

The Karst-SWAT model is applied at a larger scale, i.e. the Koiliaris and Keritis River Basins, in order to quantify the hydrologic response of three karstic springs with different properties in the Mediterranean island of Crete. The same set of representative climate change scenarios is used to assess the climate change impact on the springs and surface flow for the period 2019-2098. A non-parametric drought index is modified within the context of this study, with the intention of estimating the future frequency, duration and intensity of meteorological and hydrological droughts in comparison to the reference

period. The progress of the lowest and the highest flows in the future is analyzed, the latter using an algorithm of the Mean Excess Function.

5.2 Conclusions

5.2.1 On the quantification of hydrologic predictions uncertainty of karstic Mediterranean watersheds

5.2.1.1 Quantification of uncertainties from different sources

The uncertainty of total flow at the basin exit due to hydrological model parameters is estimated at 6.6% (Coefficient of Variation, CV), based on the combination of both SWAT and Karst-SWAT model parameters. Specifically, the uncertainty of surface flow is 17.1% and of karstic flow 10.0% (CV). The uncertainty due to internal variability is on average 3.9% for rainfall, 5.6% for total flow, 4.9% for karstic flow and 7.1% for surface flow. The range due to climate change uncertainty is 12.5%, 10.1% and 17.3% for total, karstic and surface flow for the period 2019-2058 and 28.1%, 23.5% and 36.7% for the period 2059-2098 respectively.

The rainfall range due to internal variability propagates to higher uncertainty ranges for the total and surface flow, and the uncertainty range of karstic flow is always lower than that of the surface flow, due to the higher stability of the karstic system. For the case of karstic flow, the range due to model parameters uncertainty (10.0%) is equally important as the range due to climate change scenario (10.1%) until 2058; however, the latter more than doubles after 2059 (23.5%). The uncertainty due to internal variability for the total flow (5.6%) is similar to the uncertainty due to model parameters in the basin of Koiliaris (6.6%). Again, the value of the latter, more than doubles after 2059 (28.1%) due to climate change scenario uncertainty.

5.2.1.2 Importance of methodology and results

In our study, the comparison of the future 40-year means for all scenarios reveals that 2019-2058 is a transition period, during which the outcomes of different climate scenarios overlap due to the dominant role of internal variability. In addition, during this period changes in flow are not as significant as those forecasted after 2060, when the particular realization of the emission scenario becomes more important. The projected impact of climate change at the Koiliaris River, and the island of Crete in general, changes significantly as a function of the scenario that will be realized after 2059 and ranges from significant flow increases (37.5% for RCP2.6) to significant decreases in flow (42.3% for RCP8.5). The climate change ensemble mean, however, indicates a significant decrease in the mean annual total flow (13.0%) and karstic flow (16.4%) after 2059. The worst case scenario (REMO RCP8.5) predicts a mean karstic flow of 347.7 mm/yr (decrease of 37.9%). Furthermore, by taking the uncertainties of model parameter and internal

variability into consideration, the predicted karstic flow can be as low as 271.5 mm/yr (decrease of 51.5%).

The methodology combines the advantages of climate change impact analysis with those of a fully integrated hydrologic model. The integration of surface and subsurface flow in the same model provides more realistic simulations of water cycle and improved representation of the dominant hydrologic process of groundwater recharge interaction, which is important for impact assessment on groundwater resources. This is the first time, to our knowledge, that a combined assessment of surface and karstic flow model parameter uncertainty and internal variability is applied to a karstic Mediterranean watershed. Our analysis shows that the parameter uncertainty of the hydrologic model and the internal variability of the climate change scenarios should be considered in planning water resources adaptation and mitigation measures that aim to alleviate climate change impacts in watersheds of semi-arid or arid climates, especially for the 2019-2058 period. After 2059, the climate change scenario is the most important uncertainty factor. The case of the Koiliaris River Basin provides a benchmark for comparative studies in other similar regions of the globe, where water needs during the summer are exclusively covered by the flow originating from karstic springs. Accurate estimates of the overall uncertainty are necessary for planning purposes and may reveal possible water deficits that cannot otherwise be identified.

5.2.2 On the quantification of nitrate (and sediment) fluxes predictions uncertainty in karstic Mediterranean watersheds

5.2.2.1 Impact of climate change on nitrate and sediment fluxes

Following the patterns of flow, when comparing the future annual averages of the variables under the 11 climate change scenarios, we predict that the total nitrate mass decreases after 2059 (23.7%). The nitrate mass transferred by the surface flow increases by 10.1% during the period 2059-2098. This occurs due to the fact that flash floods are expected to increase (despite the slight decrease in surface flow) thus favoring the flushing of nitrates. The total sediment mass is stable after 2059 (low increase of 1.1%).

5.2.2.2 Quantification of uncertainties from different sources

As in the case of flow, after 2059, the uncertainty range of nitrate and sediment fluxes, due to climate change scenario, increases significantly, with the exception of the nitrate and sediment mass originating from the springs. The uncertainty due to climate change scenario, after 2059, is estimated at 23.7% (CV) for the mean annual total nitrate mass exported to the sea and at 41.6% for the mean annual total sediment mass exported to the sea. The uncertainty of the same variables due to internal variability is 6.9% (nitrate)

and 18.5% (sediment), which is significant, but lower than the uncertainty due to climate change scenario.

The parameter uncertainty estimation of nitrate fluxes revealed that the total parameter uncertainty is 40.1% on the annual mean nitrate mass exported to the sea, taking both SWAT and Karst-SWAT parameters under consideration. When the uncertainty due to internal variability is added to the parameter uncertainty, the total uncertainty in the exported nitrate mass is 40.7%. This uncertainty is significant and greater than climate change scenario uncertainty. The high parameter uncertainty of nitrate fluxes is owed mainly to the limited observational data and also to the uncertainty of flow parameters which define the nitrate masses.

5.2.2.3. Importance of study

The watershed under study (Koiliaris River Basin) is not expected to undergo significant changes in water quality according to the scenarios under study. The increase in nitrate concentration does not constitute a problem for the water quality of the basin, as the climate change analysis suggests that it is never going to exceed the limits established by the Water Framework Directive, even when considering the estimated uncertainties.

The framework for the quantification of nitrate fluxes uncertainty introduced in this study can be applied on other complex karstic watersheds with water quality issues, for the quantification of nitrate and sediment fluxes, with the condition that observational data are adequate. The methodology can be expanded to any water quality variable in karstic watersheds.

5.2.3 On the estimation of the impact of climate change on three karstic springs with different properties

5.2.3.1 Impact of climate change on annual means and drought frequency, intensity and duration

The climate change impact study suggests that more intense changes in flow are observed after 2059, when the mean annual karstic flow of the Stilos spring is expected to decrease significantly (25.1% on average, based on the eleven scenarios). This decrease is less intense for the karstic flow of Meskla (18.7%) and Agia (14.2%) springs. A mild decrease in the mean annual rainfall (based on the eleven scenarios under study), induces a slight increase in the mean annual surface flow (0.4% for Koiliaris and 8.0% for Keritis RB), due to the increase in the frequency of extreme rainfall. High intensity rainfall favors the generation of surface flow at the expense of karstic flow, since rainfall intensity exceeds the infiltration rate.

Considering each spring under study separately, we get the following results regarding the characteristics of drought for the 2059-2098 period: Stilos spring is the most

vulnerable spring under the impact of climate change, with an increase of 77.5% in frequency, 45% in duration and 27.3% in intensity of drought. Meskla spring has an increase of 35.9% in frequency, 36.8% in duration and 38.6% in intensity (mean monthly water deficit) of droughts. Finally, the drought frequency of the Agia spring decreases 8.1% after 2059, as the duration of drought events increases remarkably (533%), and the drought intensity increases (83.6%). The mean deficit to mean monthly flow ratio increases for all springs, especially for the Agia spring, for which it doubles. However, even for the worst case scenario, the Agia spring manages to address the annual water needs of the area, considering they do not change in the future.

5.2.3.2 Impact of climate change on extreme flows

The analysis of the extreme low and high flows of the springs and surface flow demonstrates that there will be an increase in the variability of flow values, with increasing high and low flows in frequency and intensity. The increase in the extreme high flows and torrential rain may be accompanied by the inflation of flood events, erosion and crop disaster. The future, heavier tailed, distributions of rainfall extremes do not facilitate the water storage of the springs and the increasing frequency of meteorological droughts lead to increasing low flows during the whole year, and especially during the dry months, deteriorating an already challenging situation.

5.2.3.3 Response to climate change based on different spring characteristics

The mean annual karstic flow of the Stilos spring is expected to decrease significantly after 2059 (25.1% on average, based on the eleven scenarios), and this decrease is less intense for the karstic flow of Meskla (18.7%) and Agia (14.2%) springs. A high detention time secures a more efficient water storage. The effect of the springs' detention time is also evident in the analysis of present and future droughts. The frequency of future drought events is higher in karstic springs with lower water detention time (i.e. Stilos) and lower in karstic springs with higher detention time (i.e. Agia). Conversely, the duration of individual drought events is higher for karstic springs with high detention time. Also, the correlation between the meteorological and hydrological drought index decreases as the spring's detention time increases. All the above mentioned results indicate that the droughts of a spring with low storage capacity are more in accordance with the patterns of rainfall droughts compared to a spring with higher storage capacity. In addition, a long hydrological drought of a spring with high detention time is a result of many individual meteorological drought events situated close to each other in time, rather than one long meteorological drought.

5.2.3.4 Other remarks

The analysis of the meteorological and hydrological drought indices indicates that the meteorological drought index alone cannot be used for the assessment of hydrologic droughts in karstic watersheds as it severely underestimates the drought status of the springs, especially for the case of springs with high detention times.

In addition, within the context of this study, a non-parametric drought index was modified, and a new index is introduced, which is able to assess the future frequency, duration and intensity of meteorological and hydrological droughts in comparison to the reference period. The new index can be applied on the time series of observed and projected flow (or rainfall) at once and provide a comparison of the drought conditions across the time series.

5.2.3.5 Importance of results

According to Chapter 2, after 2059, the variability due to climate change scenario is very high for karstic flows (23.5%). Even with this high uncertainty scores, the most adverse impacts on karstic water resources are expected to take place after 2059, independently of the climate change scenario.

The Agia spring, which is the main source of water supply and irrigation for the city of Chania, is forecasted to have lower flows after 2059, but the spring will be able to cover the current water needs of the area even for the worst case scenario (although marginally). These water needs, however, will definitely increase in the future since the local authorities have already started discussing and proposing actions for more intensive exploitation of the spring.

These results provide an illustration of the conditions which are expected to prevail for Mediterranean karstic springs in the future. The drought status is anticipated to deteriorate, especially after 2059, regardless of the scenario realized for all springs and the results of this study can be used as a guide for competent authorities to adapt their management practices for the prevention of the negative repercussions of karstic spring droughts. A 40-year period is offered for adaptation measures to be prepared and planned for the improved management of the springs' water resources.

5.3 General Remarks

The modeling framework proposed here can be expanded and improved. The methodology has been applied on karstic watersheds located in Chania but can be extrapolated to the whole island of Crete. In their study, Malagò et al. (2016) used the hydrological similarity approach to validate flow gauging stations all over Crete and proved that the sub-basins of Crete have similar to identical properties. Likewise, this methodology can be used for the quantification of the uncertainty of hydrologic and

geochemical predictions and the estimation of the characteristics of present and future hydrological droughts for the whole island of Crete. The relative uncertainty is not expected to vary significantly among different areas of the island, whereas the hydrological drought characteristics are expected to vary according to the properties of the springs studied.

A representative sub-set of climate change scenarios has been used here, but the methodology could be improved with the addition of a wider range of climate change scenarios which would account for the full spectrum of uncertainty. Several downscaling methods could also be tested to investigate the most appropriate one and also account for the uncertainty stemming from the downscaling methodology. In addition, the weather generator used here underestimated the variance of the rainfall; this underestimation is because of the underlying stationarity assumption of the weather generator. Other approaches which preserve the variance and autocorrelation properties of precipitation processes could be chosen to quantify the uncertainty due to internal variability more efficiently. Finally, the uncertainty assessment could benefit from the acquisition of more observed data which could more accurately describe the uncertainty ranges.

The study introduced, for the first time, a modeling framework for the quantification of the hydrologic predictions uncertainty in karstic Mediterranean watersheds. This framework provided uncertainty ranges for the forecasted flows, and revealed new minimum flows which should be used as the design flows for water resources management. The methodology can also be employed for the uncertainty assessment of other variables (e.g. water quality) and can be applied to different regions around the globe with similar hydrologic systems. In the context of this study, the hydrological drought characteristics of different karstic springs were examined under present and future conditions, providing a guide for competent authorities to adapt their management practices for the prevention of the negative repercussions of karstic spring droughts. The study provides a benchmark for comparative studies in other similar arid and semi-arid regions with karstic formations.

Publications

Publications in Scientific Journals based on the Thesis

Nerantzaki, S.D., Hristopoulos, D.T., Nikolaidis, N.P. 2020. Estimation of the uncertainty of hydrologic predictions in a karstic Mediterranean watershed, *Science of the Total Environment*. <https://doi.org/10.1016/j.scitotenv.2020.137131>

Nerantzaki, S.D., Nikolaidis, N.P. 2020. The response of three Mediterranean karstic springs to drought and the impact of climate change. *Journal of Hydrology* (Under Review)

Publication in Conference Proceedings based on the Thesis

Nerantzaki S.D., Nikolaidis N.P., Hristopoulos D.T., 2019. Evaluation of the uncertainty of the impact of climate change on flow, sediment and nitrate predictions at the Koiliaris Critical Zone Observatory. ADAPTtoCLIMATE Conference Proceedings, June 24-25, Heraklion, Crete.

Conference Presentations based on the Thesis

Nerantzaki, S.D., Nikolaidis, N.P., Estimation of the uncertainty of the hydrologic predictions due to climate change at the Koiliaris Critical Zone Observatory. TERENO International Conference, Oct 8-12 2018, Berlin, Germany (poster presentation).

Publications in Scientific Journals related to the Thesis

Nerantzaki, S.D., Papalexiou, S.M., 2019. Tails of extremes: Advancing a graphical method and harnessing big data to assess precipitation extremes. *Adv. Water Resour.* 134, 103448. doi:10.1016/J.ADVWATRES.2019.103448

Nerantzaki, S.D., Efstathiou, D., Giannakis, G. V., Kritsotakis, M., Grillakis, M.G., Koutroulis, A.G., Tsanis, I.K., Nikolaidis, N.P., 2019. Climate change impact on the hydrological budget of a large Mediterranean island. *Hydrol. Sci. J.* 64, 1190–1203. doi:10.1080/02626667.2019.1630741

Nerantzaki, S.D., Giannakis, G.V., Efstathiou, D., Nikolaidis, N.P., Sibetheros, I.A., Karatzas, G.P., Zacharias, I., 2015. Modeling suspended sediment transport and assessing the impacts of climate change in a karstic Mediterranean watershed. *Sci. Total Environ.* 538, 288–297. doi:10.1016/J.SCITOTENV.2015.07.092

Appendix A

A1 Tables and Figures

Table A1. EURO-CORDEX (Jacob et al., 2014) (EUR-11) regional climate models (RCM) and their driving realization of global climate models (GCM). X denotes the scenario runs considered in this study for each RCM. RCP: representative concentration pathway.

Driving GCM	RCM	Scenario			Reference
		RCP2.6	RCP4.5	RCP8.5	
EC-EARTH-r1	KNMI-RACMO22E		X	X	Van Meijgaard et al. (2012)
EC-EARTH-r12	SMHI-RCA4	X	X	X	Kjellström et al. (2016)
IPSL-CM5A-MR-r1	IPSL-INERIS-WRF331F		X		Skamarock and Klemp (2008)
HadGEM2-ES-r1	SMHI-RCA4		X	X	Kjellström et al. (2016)
MPI-ESM-LR-r1	CSC-REMO	X	X	X	Jacob et al. (2012)

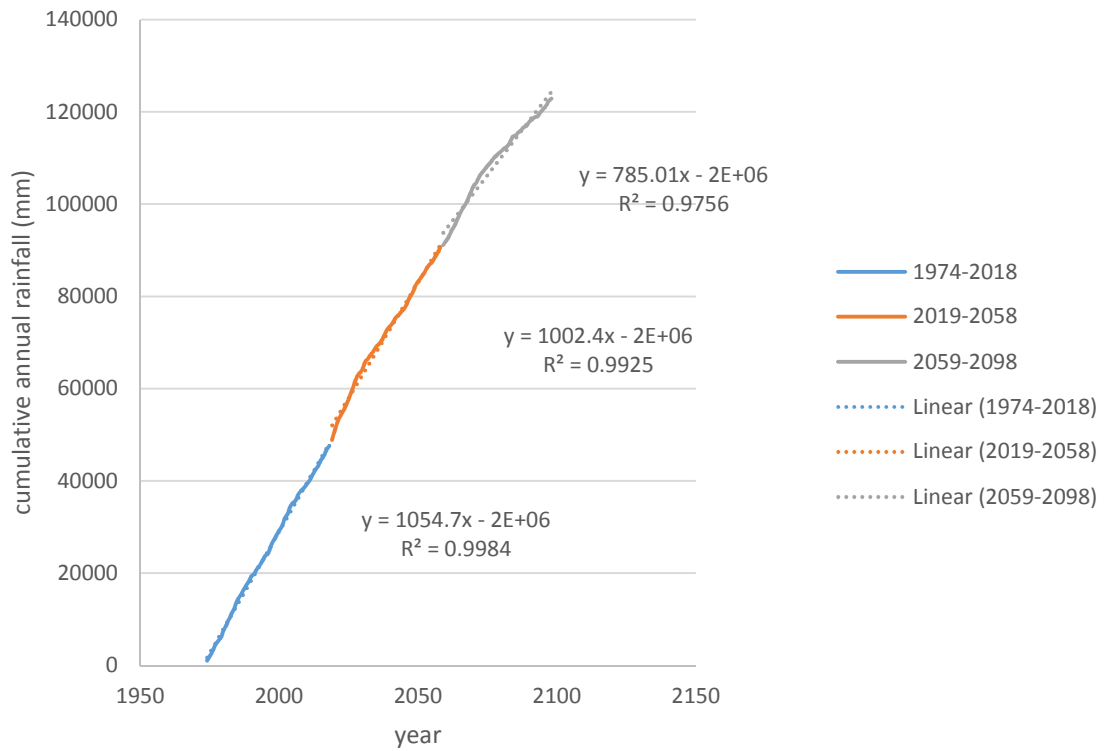


Figure A1: Cumulative distribution of annual rainfall for the 1974-2098 period and applied trend-line for each sub-period: 1974-2018, 2019-2058 and 2059-2098.

Table A2: Sensitivity analysis of parameters used for uncertainty analysis. A low P-value denotes high sensitivity

Parameter Name	explanation	P-Value
R_SOL_K(..).sol	Saturated hydraulic conductivity (mm/hr)	0.00
R_SOL_Z(..).sol	Depth from soil surface to bottom of layer	0.00
R_ALPHA_BNK.rte	Baseflow alpha factor for bank storage (days)	0.00
R_CH_N2.rte	Manning's "n" value for the main channel	0.02
R_CH_K2.rte	Effective hydraulic conductivity in main channel alluvium (mm/h)	0.22
R_CH_K1.sub	Effective hydraulic conductivity in tributary channel alluvium (mm/hr)	0.26
R_OV_N.hru	Manning's "n" value for overland flow.	0.31
R_SURLAG.bsn	Surface runoff lag coefficient.	0.37
R_REVAPMN.gw	Threshold depth of water in the shallow aquifer for "revap" or percolation to the deep aquifer to occur (mmH2O)	0.42
R_CH_N1.sub	Manning's "n" value for the tributary channels.	0.44
R_ALPHA_BF	Baseflow alpha factor (days)	0.48
R_SOL_AWC(..).sol	Available water capacity of the soil layer (mm H2O/mm soil)	0.50
R_CN2.mgt	Initial SCS runoff curve number for moisture condition II	0.51

A2 Simulation of minimum and maximum temperature using the Box-Jenkins methodology

Data for temperature were available from two stations: Psichro Pigadi and Samonas, which also provide daily minimum and maximum temperatures for the period 1974-2013. Daily minimum and maximum temperatures are considered as stochastic processes characterized by variable daily means and standard deviations. The Box-Jenkins methodology is used to simulate the time series. The seasonal cycles of means and standard deviations are modelled by a sum of five sinusoidal terms and the residuals are approximated by the Student's t distribution (also known as t location-

scale distribution.) The sinusoidal series for the mean is fitted to the observed daily values. The residuals, obtained by removing the periodic term from the observed data, are used to analyze a time autocorrelation for minimum and maximum temperatures. Occasionally, the simulated minimum temperature is greater than the simulated maximum temperature. In this case the minimum and maximum temperatures are interchanged. The temperature model can be defined by: i) the mean temperature "m", ii) the sinusoidal model "model", iii) regression parameters "beta", iv) autocorrelation lags "lags", v) the residual probability distribution "PD" (t Location-Scale Distribution).

For the validation of the temperature model, the residuals of regression for serial correlation were analyzed and were found to be serially uncorrelated for all scenarios and time periods, as seen in Figure A2 for the 2019-2058 period for the maximum temperature of Samonas station. The rest of the temperature variables (minimum temperature of Samonas and maximum and minimum temperature of Psichro Pigadi) have also uncorrelated residuals.

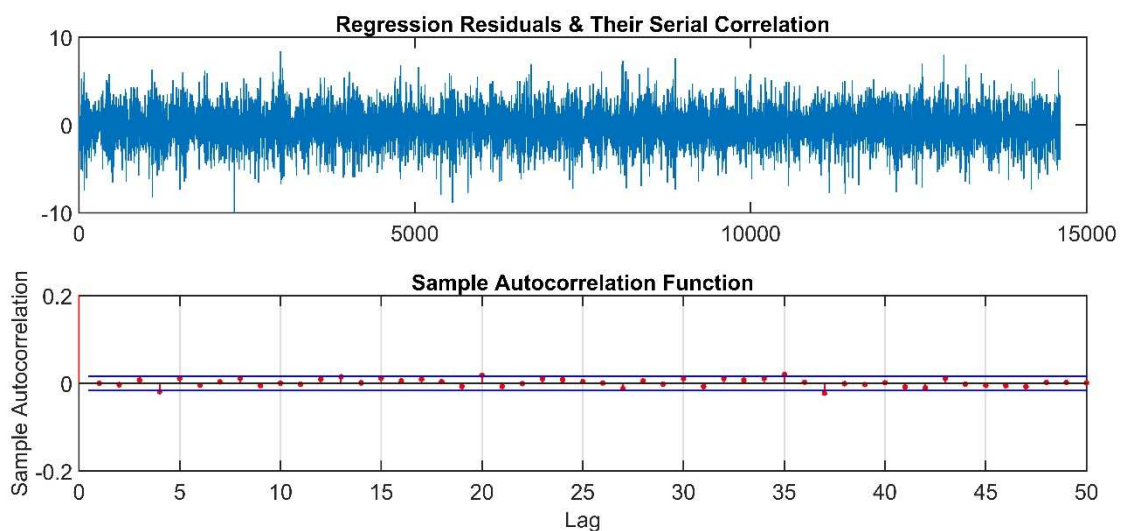


Figure A2: Residuals of regression (top) and serial correlation function (bottom) for the maximum temperature of Samonas for the 2019-2058 period.

Thirty alterations of the temperature input were run for each scenario while the precipitation input of the original time series was kept constant for each simulation. Results suggested that, for every realization, the outcome of flow was not differentiated more than 5% compared to the original flow outcome. Therefore, for the purposes of assessing the effect of input uncertainty in the hydrological outcome, only precipitation was considered to cause variations on the flow outcome, and the variable of temperature was not taken under consideration. The mean annual temperatures of the original time series along with the 95% confidence interval (CI) of the realizations of every future year are presented in Figure A3.

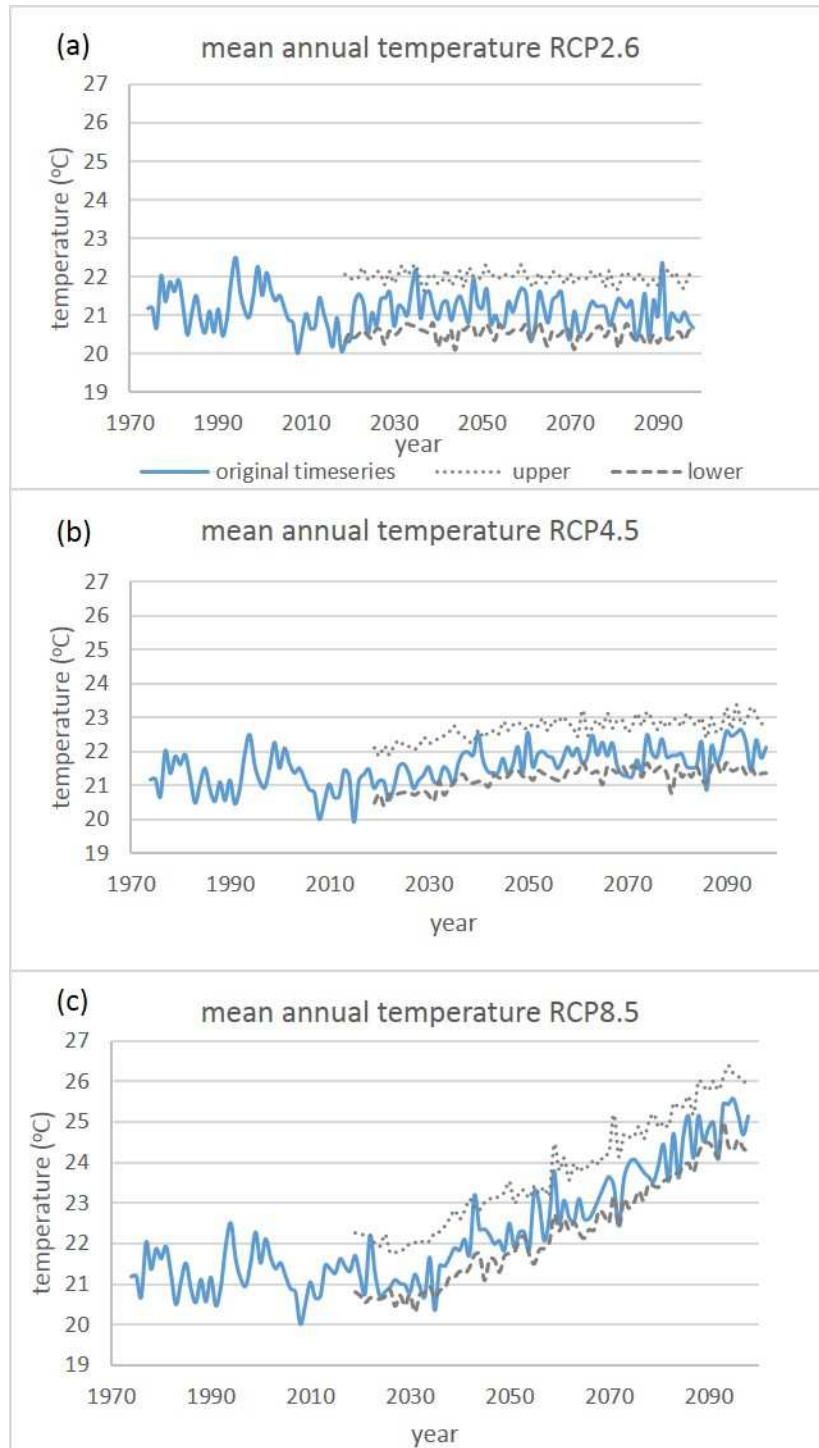


Figure A3: Monte Carlo simulation of temperature for three climate change scenarios: original time series (continuous blue line) and 90% range (dash and dot lines) based on 30 realizations for the following scenarios: (a) RCP2.6, (b) RCP4.5 and (c) RCP8.5. The plots include the observed data from the reference period (up to 2018).

A3 Adjustment of LARS-WG

In order to investigate the variability of the LARS-WG simulations, box-plots of the standard deviations for each month and all scenarios are constructed. Results suggest that the LARS-WG simulations in certain months do not satisfactorily reproduce the inherent variability of the rainfall. In order to rectify the variability underestimation problem, a linear transformation is applied to those time series that are not adequately simulated by the LARS generator. The transformation generates corrected time series with the same properties (mean and variance) as the original sample.

First, the empirical probability distributions are fitted to several probability distribution models (we use the FBD - "Find the Best Distribution" tool of Matlab which includes a wide range of probability distributions). All the original and simulated samples are adequately described by the Generalized Extreme Value (GEV) distribution, based on the Akaike information criterion (AIC) along with the AIC with small-sample correction (AICc), and the Bayesian information criterion (BIC). The GEV distribution belongs to the location–scale family of distributions. This family is parametrized by a location parameter and a non-negative scale parameter. If X is a random variable in this family, the random variable $Y = a + bX$, where a , and b are real numbers and $b > 0$ also belongs to the same family. Therefore, the following transformation is applied to the simulated rainfall time series (for the months showing low variability):

$$Y = m_2 + (X - m_1) * \frac{s_2}{s_1} \quad (A1)$$

where X is the generated monthly value per year (for each scenario and time period), m_1 and s_1 are respectively the simulation-based average and standard deviation, and m_2 , s_2 are mean and standard deviation correcting factors. The variable m_2 is a random realization from the normal distribution with a mean equal to the average rainfall of the original sample and standard deviation equal to the standard deviation (over a set of thirty values) of the monthly simulated means (calculated over the respective 40 year period). The variable s_2 is a random realization from the normal distribution with mean equal to the standard deviation of the original sample and standard deviation equal to the standard deviation of the monthly simulated standard deviations (again over the respective 40-year period).

For each scenario and time window, the mean and standard deviation of the observed and simulated monthly values (by LARS-WG) are shown in Figure A4. The model succeeds in portraying the monthly means; however, in some cases the standard deviation of the rainy months is underestimated by the simulations.

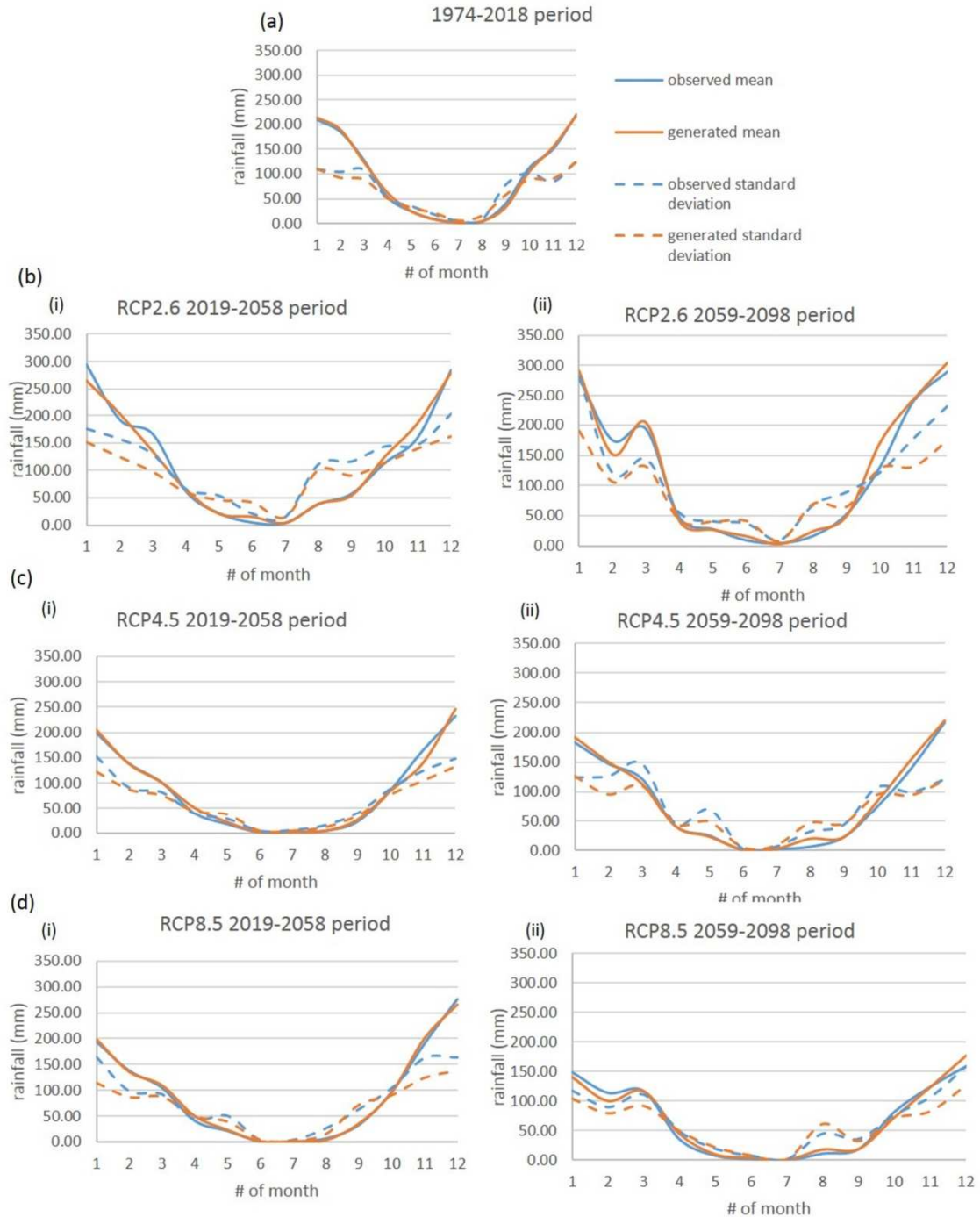


Figure A4. Mean and standard deviation of observed (reference period) and predicted (RCP projection periods) rainfall versus simulated monthly rainfall (produced by LARS-WG) for the (a) reference period 1974-2018, (b) RCP2.6 scenario, (c) RCP4.5 scenario, (d) RCP8.5 scenario. The first column, denoted by (i), corresponds to the 2019-2058 period, while the second column, denoted by (ii) refers to the 2059-2098 period.

The box-plots of the standard deviations for each month and all scenarios above are shown in Figures A5-A10. These figures reveal that the LARS-WG simulations in certain months do not satisfactorily reproduce the inherent variability of the rainfall. More specifically, for the RCP2.6 scenario during the period 2019-2058 (Figure A5), the LARS-

WG simulations underestimate the variability for the months of January, February, March and December. For the same scenario, the variability of January, November and December is underestimated for the next period (2059-2098). Similarly, for the RCP8.5 scenario the variability is underestimated in January and November for the period 2019-2058 and in November and December for the period 2059-2098. For the RCP4.5 scenario the variability is adequately simulated for both periods (Figures A7, A8). This underestimation effect has also been observed in other works (Semenov et al., 1998) and the transformation proposed here is applied to overcome this problem.

To ensure that the probability distributions, after the transformation, do not significantly differ from the initially generated (by LARS-WG) distributions for the respective months, we compare the cumulative distribution functions before and after the transformation. Similar results are obtained for all months. For example, the CDFs are compared for the month of January in the period 2059-2098 in Figure A11. As this figure shows, the transformation does not significantly affect the CDF (both the initial and the transformed CDFs are equally well approximated by a GEV distribution). However, the samples generated from the transformed CDF have the correct standard deviations (Figures A12-A15).

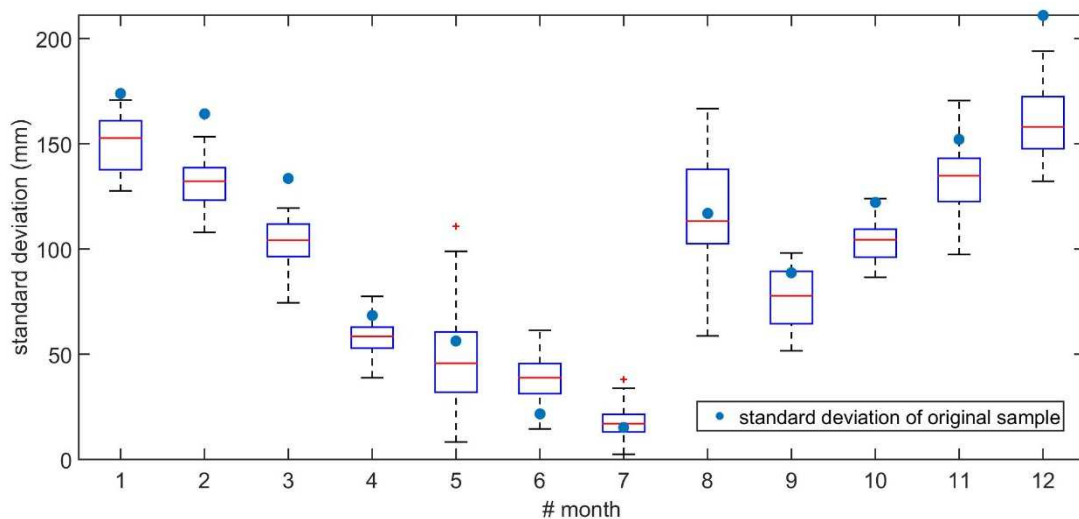


Figure A5: Box plots of the standard deviation of simulated monthly rainfall for the RCP2.6 scenario during the 2019-2058 period and the standard deviation of the monthly rainfall of the original sample (measurements and projected rainfall). The box-plots are based on 30 values of standard deviations, each one calculated from the rainfall values over a period of forty years. The markers (circles) represent the sample standard deviation for the respective time period.

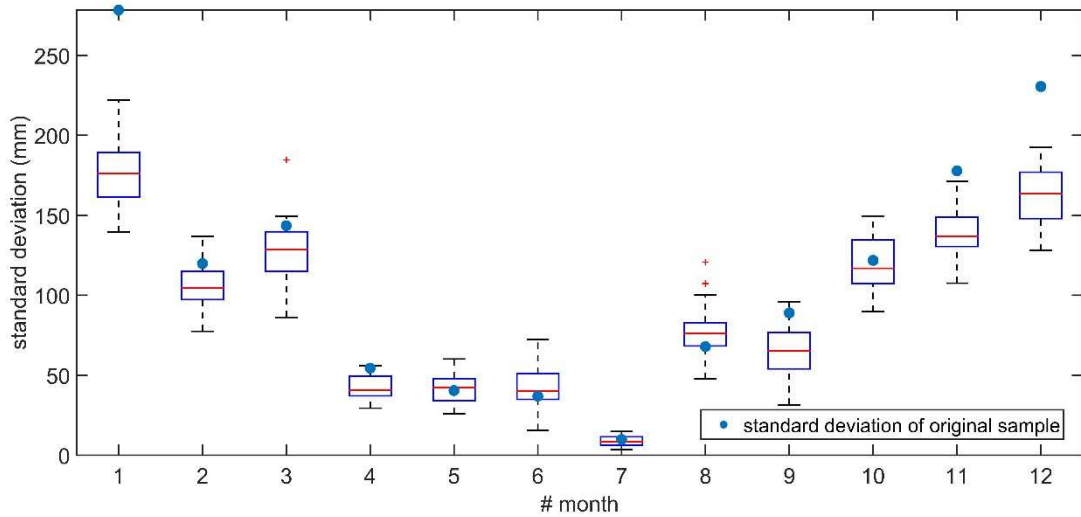


Figure A6: Same as Figure A5 for the RCP2.6 scenario but for the 2059-2098 period.

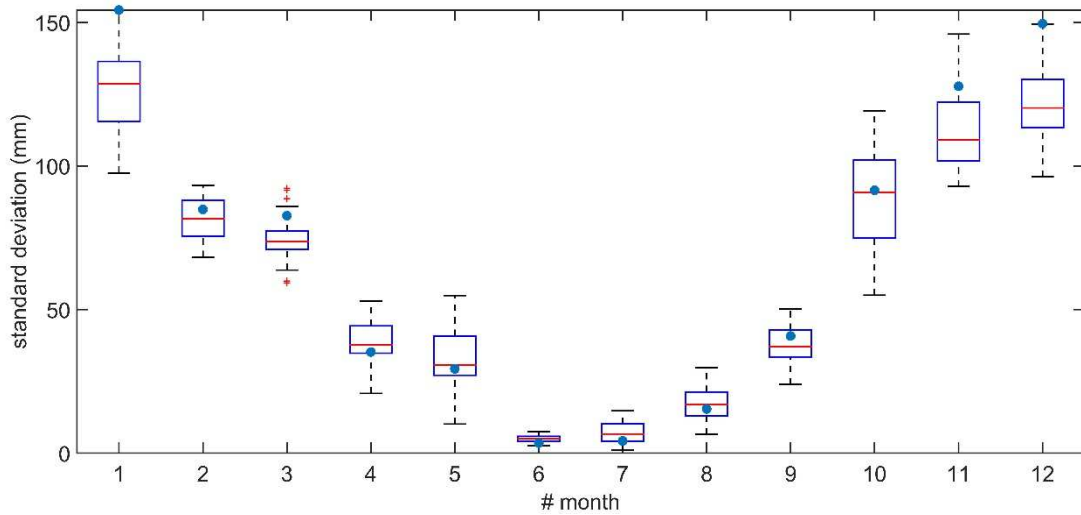


Figure A7: Same as Figure A5 but for the RCP4.5 scenario (2019-2058 period).

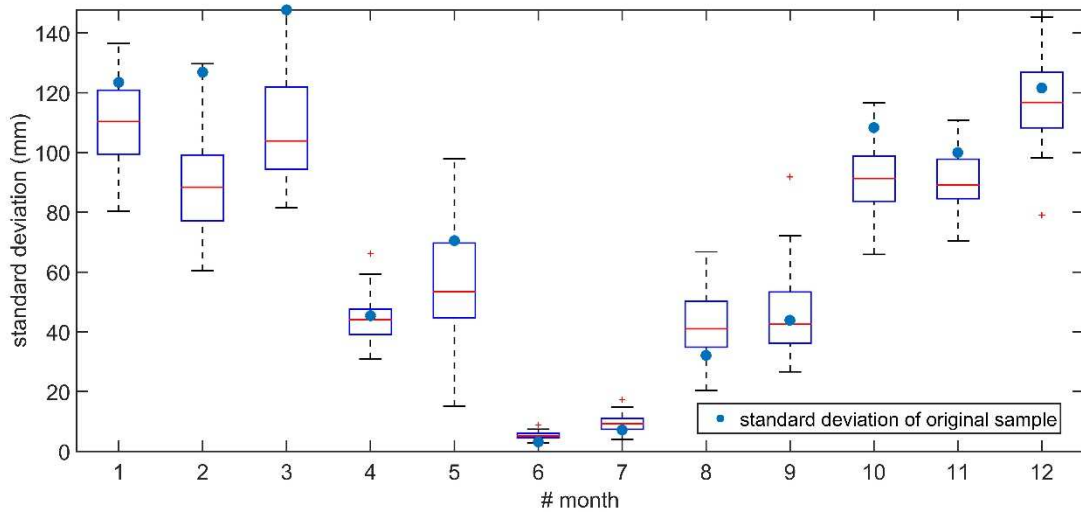


Figure A8: Same as Figure A5 but for the RCP4.5 scenario and the 2059-2098 period.

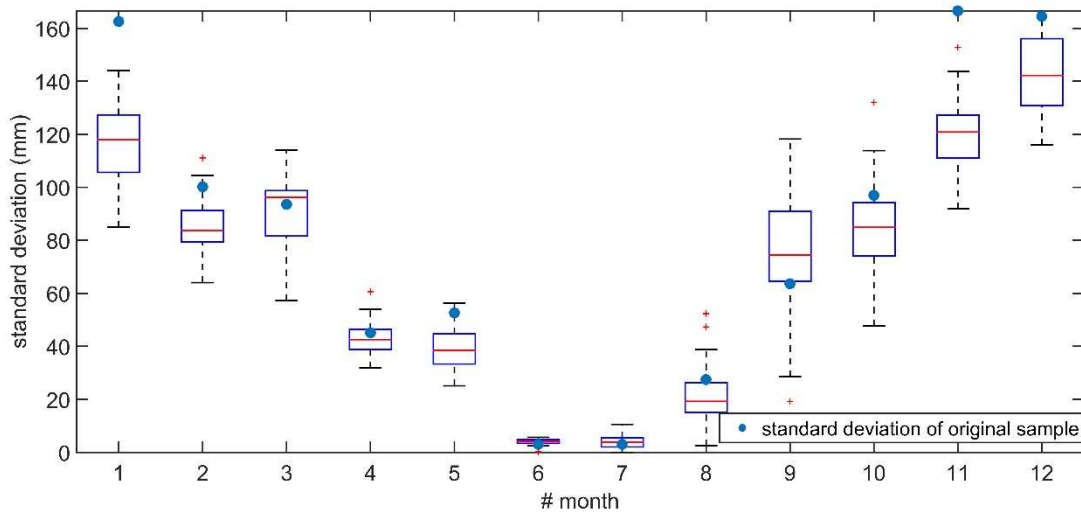


Figure A9: Same as Figure A5 but for the RCP8.5 scenario (2019-2058 period).

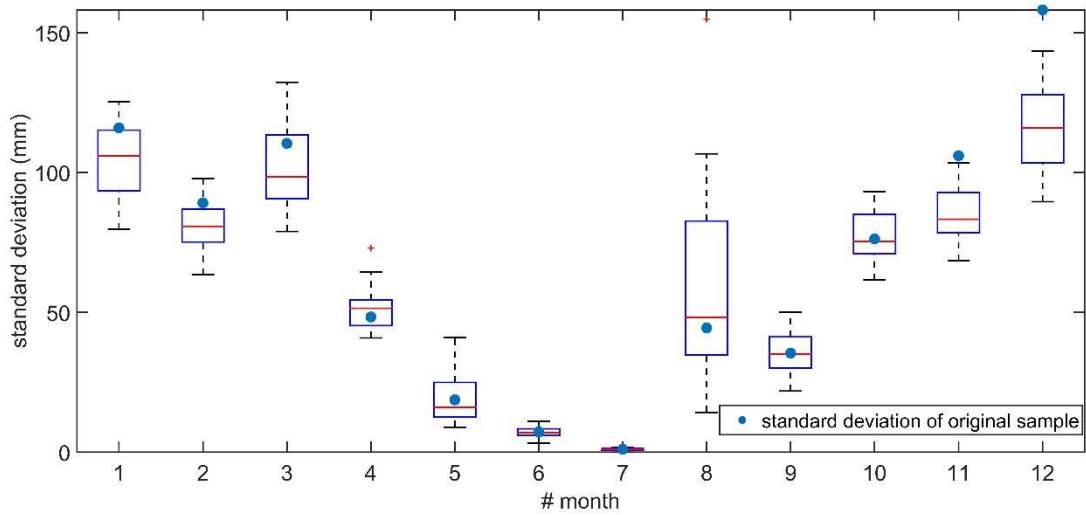


Figure A10: Same as Figure A5 but for the RCP8.5 scenario and the 2059-2098 period.

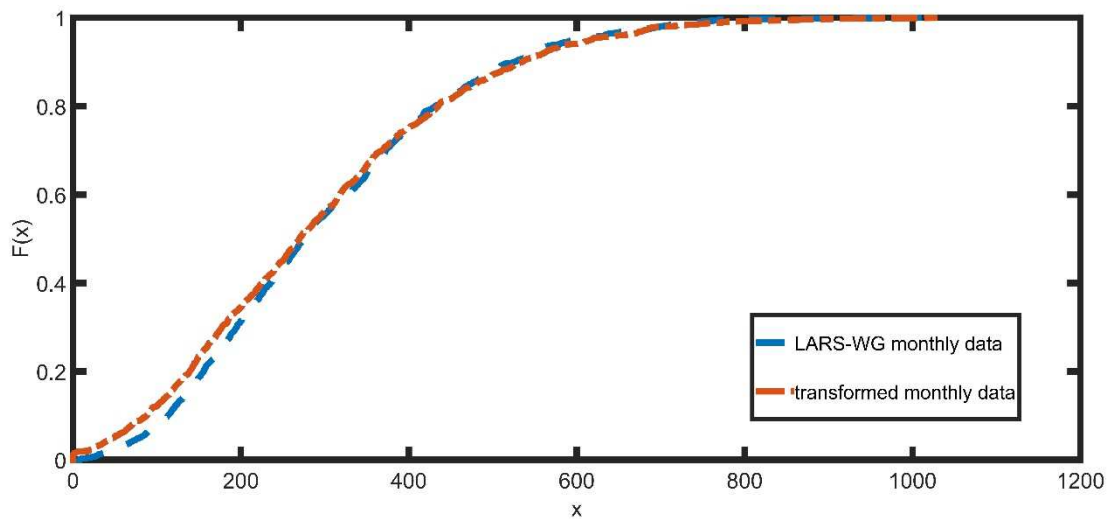


Figure A11: Cumulative Distribution Functions of the month of January generated by LARS-WG and as they are transformed for the correction of variation (30 realizations of 40 years for the 2019-2058 period, 1200 values)

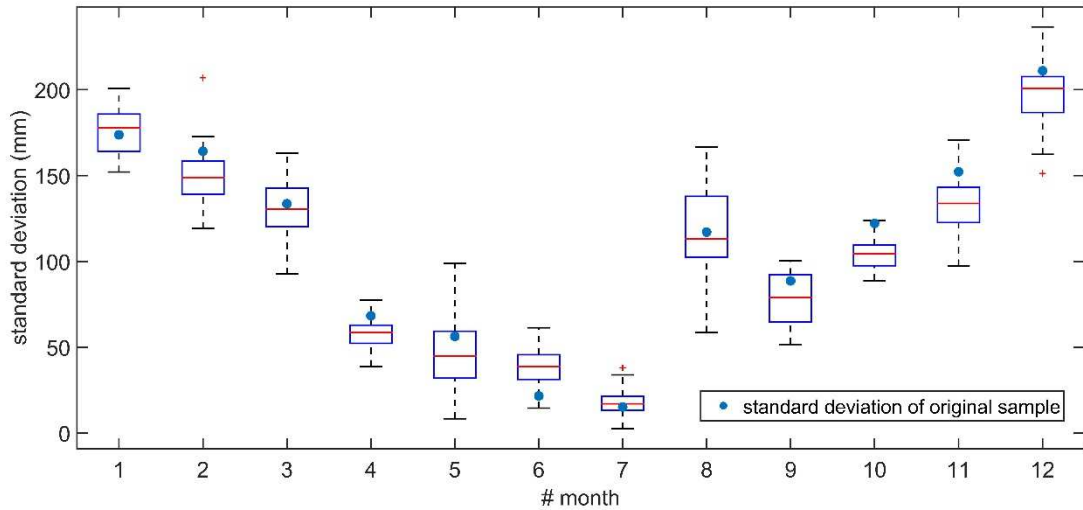


Figure A12: Box plots of the standard deviation of simulated monthly rainfall for the RCP2.6 scenario during the 2019-2058 period and the standard deviation of the monthly rainfall of the original sample (measurements and projected rainfall) after the transformation. The box-plots are based on 30 values of standard deviations, each one calculated from the rainfall values over a period of forty years. The markers (circles) represent the sample standard deviation for the respective time period.

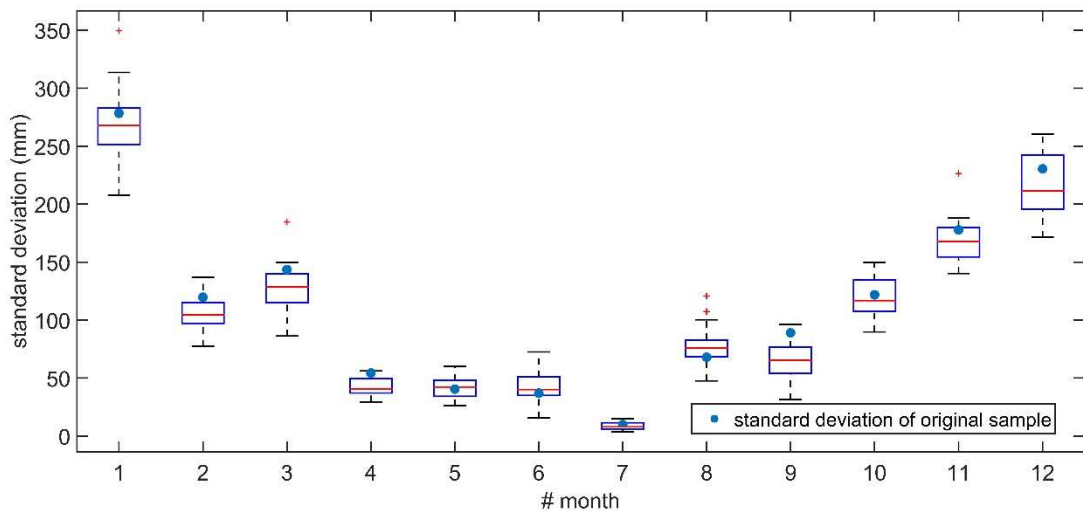


Figure A13: Same as Figure A10 for the RCP2.6 but the 2059-2098 period

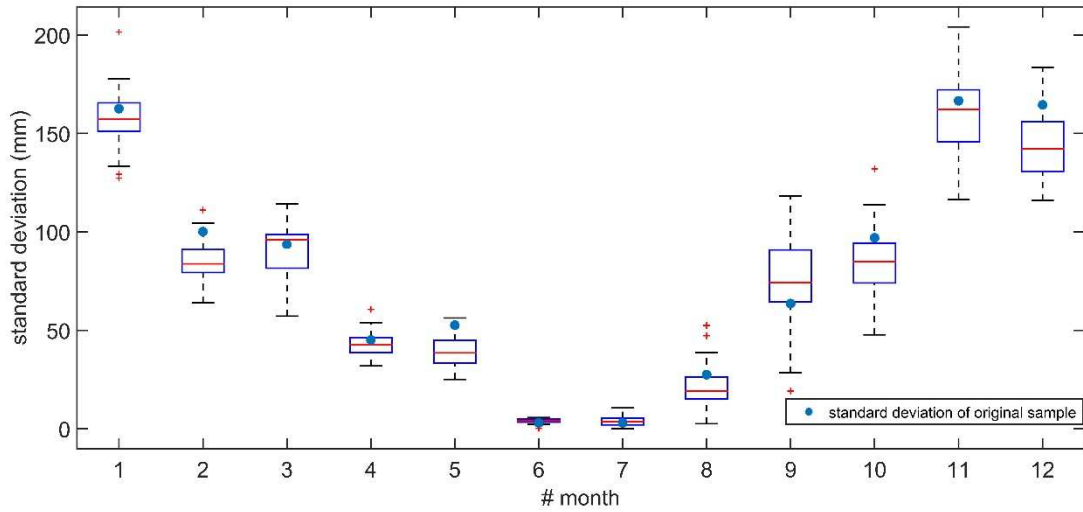


Figure A14: Same as Figure A10 but for the RCP8.5 (2019-2058 period)

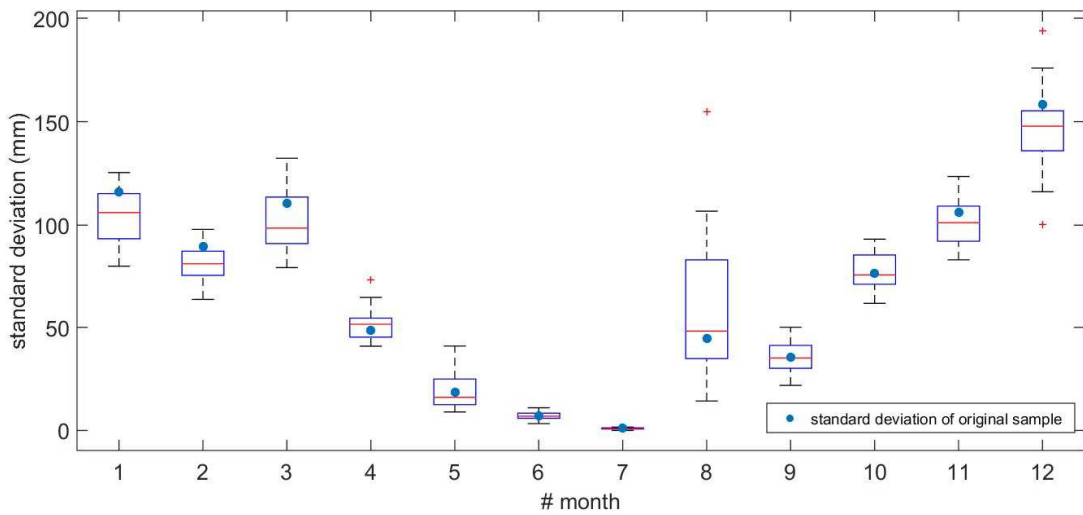


Figure A15: Same as Figure A12 for the RCP8.5 but for 2059-2098 period

References

- Jacob, D., Petersen, J., Eggert, B., Alias, A., Christensen, O.B., Bouwer, L.M., Braun, A., Colette, A., Déqué, M., Georgievski, G., Georgopoulou, E., Gobiet, A., Menut, L., Nikulin, G., Haensler, A., Hempelmann, N., Jones, C., Keuler, K., Kovats, S., Kröner, N., Kotlarski, S., Kriegsmann, A., Martin, E., van Meijgaard, E., Moseley, C., Pfeifer, S., Preuschmann, S., Radermacher, C., Radtke, K., Rechid, D., Rounsevell, M., Samuelsson, P., Somot, S., Soussana, J.-F., Teichmann, C., Valentini, R., Vautard, R., Weber, B., Yiou, P., 2014. EURO-CORDEX: new high-resolution climate change projections for European impact research. *Reg. Environ. Chang.* 14, 563–578. doi:10.1007/s10113-013-0499-2.
- Jacob, D., Elizalde, A., Haensler, A., Hagemann, S., Kumar, P., Podzun, R., Rechid, D., Remedio, A.R., Saeed, F., Sieck, K., Teichmann, C., Wilhelm, C., 2012. Assessing the Transferability of the Regional Climate Model REMO to Different COordinated Regional Climate Downscaling EXperiment (CORDEX) Regions. *Atmosphere (Basel)*. 3, 181–199. doi:10.3390/atmos3010181
- Kjellström, E., Bärring, L., Nikulin, G., Nilsson, C., Persson, G., Strandberg, G., 2016. Production and use of regional climate model projections – A Swedish perspective on building climate services. *Clim. Serv.* 2–3, 15–29. doi:10.1016/J.CLISER.2016.06.004
- Skamarock, W.C., Klemp, J.B., 2008. A time-split nonhydrostatic atmospheric model for weather research and forecasting applications. *J. Comput. Phys.* 227, 3465–3485. doi:10.1016/J.JCP.2007.01.037
- Van Meijgaard, E., Van Ulft, L. H., Lenderink, G., De Roode, S. R., Wipfler, L., Boers, R., Timmermans, A. 2012. Refinement and application of a regional atmospheric model for climate scenario calculations of Western Europe, *Climate changes Spatial Planning* publication: KvR 054/12 (44 pp.). *Climate changes Spatial Planning*.

Appendix B

B.1 Karst-SWAT equations

Stilos spring

The model equations describing the karst component include the upper reservoir mass balance, i.e.

$$\frac{dV_1}{dt} = Q_{in,1} - Q_2, \quad (B1)$$

and the lower reservoir mass balance, i.e.,

$$\frac{dV_2}{dt} = Q_{in,2} - Q_2, \quad (B2)$$

where

$$Q_{in,1} = a_1 \cdot Q_{in,deepGW}, \quad (B3)$$

$$Q_{in,2} = (1 - a_1) \cdot Q_{in,deepGW} + a_2 \cdot Q_1 \quad (B4)$$

$$Q_1 = k_u \cdot V_1 \quad (B5)$$

$$Q_2 = k_l \cdot V_2, \quad (B6)$$

and $Q_{in,deepGW}$ is the deep groundwater discharge from SWAT (the corresponding variable from SWAT is DA_RCHG, or deep aquifer recharge), a_1 is the fraction of flow entering the upper reservoir, a_2 is the fraction of flow from the upper reservoir discharge entering the lower reservoir and k_u and k_l are recession constants (in units of 1/day) for the upper and lower reservoir. For constant $Q_{in,1}$ and $Q_{in,2}$ the analytical solutions of (B1) and (B2) are:

$$Q_1 = Q_{1,0}e^{-k_u t} + Q_{in,1} \cdot (1 - e^{-k_u t}), \quad (B7)$$

$$Q_2 = Q_{2,0}e^{-k_l t} + Q_{in,2} \cdot (1 - e^{-k_l t}). \quad (B8)$$

The total karstic flow is then calculated as

$$Q_{karstic} = (1 - a_2) \cdot Q_1 + Q_2 \quad (B9)$$

The karst model parameters are calibrated, and the resulting karstic flow time series is used as point source input at the spring location (Equation B9).

The sediment mass balance of the karst is calculated in a similar manner as the nitrate — N mass balance presented by Nikolaidis et al. (2013)

$$\frac{d(V_1 \cdot C_1)}{dt} = a_1 \cdot Q_{in,1} \cdot C_{in,1} - Q_1 \cdot C_1 \quad (B10)$$

$$\frac{d(V_2 \cdot C_2)}{dt} = (1 - a_1) \cdot Q_{in,1} \cdot C_{in,1} + a_2 \cdot Q_1 \cdot C_1 - Q_2 \cdot C_2 \quad (B11)$$

for the upper and lower reservoir respectively, where $C_{in,1}$ is the concentration of water entering the karst and C_1, C_2 are the suspended sediment concentrations of the upper and lower reservoirs respectively.

Meskla and Agia springs

The equations for Meskla are constructed in a similar manner:

$$Q_{1m} = Q_{1,0m}e^{-k_{um}t} + Q_{in,deep,GW,m} \cdot a_{1m} \cdot (1 - e^{-k_{um}t}) \quad (B12)$$

$$Q_{2m} = Q_{2,0m}e^{-k_{lm}t} + ((1 - a_{1m}) \cdot Q_{in,deep,GW,m} + a_{2m} \cdot Q_{1m}) \cdot (1 - e^{-k_{lm}t}) \quad (B13)$$

where $Q_{in,deepGW,m}$ is the deep groundwater discharge from SWAT which enters the Meskla system (the corresponding variable from SWAT is DA_RCHG, or deep aquifer recharge), $a_{1,m}$ is the fraction of flow entering the upper reservoir of Meskla, a_{2m} is the fraction of flow from the upper reservoir discharge entering the lower reservoir and k_u and k_l are recession constants (in units of 1/day) for the upper and lower reservoir. For the case of Agia, we get:

$$Q_{1a} = Q_{1,0a}e^{-k_{ua}t} + (Q_{in,deep,GW,a} \cdot a_{1a} + a_{3m} \cdot Q_{2m}) \cdot (1 - e^{-k_{ua}t}) \quad (B14)$$

$$Q_{2a} = Q_{2,0a}e^{-k_{la}t} + ((1 - a_{1a}) \cdot Q_{in,deep,GW,a} + a_{2a} \cdot Q_{1a}) \cdot (1 - e^{-k_{la}t}) \quad (B15)$$

where a_{3m} is the fraction of flow from Meskla, which enters the upper reservoir of Agia.

B.2 Tables and Figures

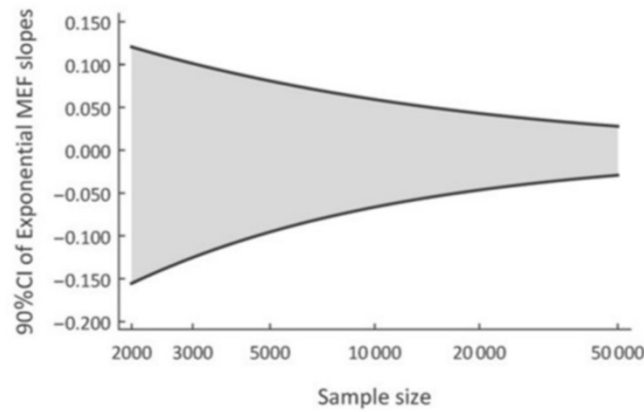


Figure B1. 90% confidence interval (CI) of MEF slopes resulting from the Exponential tail. Slope values higher than the CI are characterized as sub-exponential, slope values inside the CI are exponential and values lower than the CI are hyper-exponential.

Table B2. The relative difference (RD) between the drought index of Psychro and the rest of the six rainfall stations. The drought is index applied on the rainfall time series of Psychro (x_{obs} according to Equation (4.4)) and the six stations (x_{model} according to Equation (4.4)) listed in this Table for the 1979-2098 period and the REMO4.5 scenario. The duration and frequency of Psychro drought events (drought index lower than -1) are compared to the duration and frequency of the drought events of the rest of the stations for each sub-period.

Rainfall station	reference period		2019-2058		2059-2098	
	duration	frequency	duration	frequency	duration	frequency
Samonas	1.4%	0.0%	-4.1%	2.9%	0.0%	0.0%
Kalives	-9.5%	5.9%	4.1%	2.9%	-2.6%	0.0%
Askifou	0.0%	-5.9%	0.0%	8.6%	-2.6%	-4.9%
Mouri	4.1%	0.0%	0.0%	5.7%	-3.9%	0.0%
Agrokipio	-8.1%	11.8%	-2.7%	-5.7%	3.9%	0.0%
Alikianos	-6.8%	5.9%	-2.7%	-5.7%	1.3%	2.4%

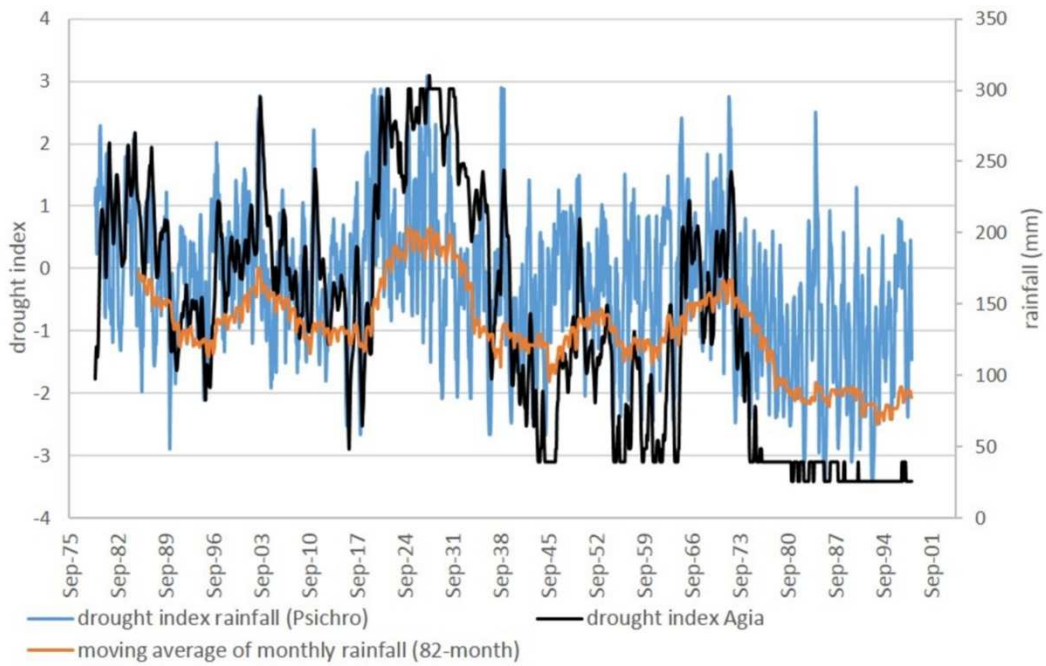


Figure B2. Modified drought index (6-month) applied on the rainfall (blue line) and the Agia flow (black line) and moving average of rainfall (82 month moving average – orange line).